Department of Nuclear Engineering

University of California, Berkeley

Preliminary study of the Pebble-Bed Advanced High Temperature Reactor

Report UCBTH-06-001

EV1 François-Paul Fardin and EV1 Fabien Koenig

August 2006

ACKNOWLEDGMENTS

We would like to thank Dr Per F. Peterson for his warm welcome in his lab. Thanks also go to Dr Ehud Greenspan for his precious advices and experience on neutronic.
Special thanks to Dr Haihua Zhao for is availability and comprehensive explanations.
Very special thanks to Massimiliano Fratoni for his continuous support on MCNP5, and his patience for my numerous questions. See you on next world cup!
Vielen Danken zür Björn Becker für seine Hilfe.
Grand merci au Dr Philippe Bardet pour son enthousiasme, à Alain Griveau pour ses connaissances en "scaling analysis" et MatLab.
Finally we would like to say how grateful we are to all the staff and students of the Department of Nuclear Engineering for their friendly welcome and support all along our project.

Preliminary study of the Pebble-Bed Advanced High Temperature Reactor

Elèves : EV **FARDIN** et EV **KOENIG**, EN. 00

Organisme d'accueil : Department of Nuclear Engineering
University of California, Berkeley

Abstract :

Our project, performed at the University of California, Berkeley, was intended to take part into the preliminary studies of the PB-AHTR. The work was completed in two domains: neutronics and thermal hydraulics.

The neutronic study relied on the MCNP5 code that required as prior work, consequent training before the modeling of a fuel element. The complexity of the pebble fuel element raised problems that have to be solved before moving to the full core analysis. From there, the project was focused on the definition of an adapted method, using the tools available to address the question of the equilibrium core. Again unexpected issues raised and were solved to end up with a depletion analysis method that will provide the basis for a complete parametric study of the core. Then with a better knowledge of the core, choices in the design of the core will be allowed and further work will bring the PB-AHTR to a new step.

The thermal-hydraulics part was focused on the writing of a preliminary phenomena identification and ranking table, a valuable tool in the licensing process of advanced reactors. First, the delimitation of the purpose and scope of this study, first of a kind for a reactor at a pre-conceptuel stage, required a certain amount of literature review. Then, using simple modeling methods to define and quantify the phenomena, a ranking has been proposed for the full power mode, which should provide a framework in terms of experiments needs. Finally, a first-cut work has been completed for the loss of forced circulation scenario, representative of AHTR passive safety features.

Résumé - Présentation du projet (buts - cahier des charges - solutions) :

Etude préliminaire du réacteur avancé à haute température à chargement par boulet

Notre projet réalisé à l'Université de Californie, Berkeley avait pour but de participer aux études préliminaires du PB-AHTR. Notre travail c'est scindé en une étude de neutronique et une étude aux aspects majoritairement thermo hydrauliques.

L'étude de neutronique s'est appuyée sur le code MCNP5 qu'il a d'abord fallu apprendre pour développer un modèle d'élément combustible. Une fois les problèmes de modélisation de cet élément réglés, le travail s'est concentré sur la mise au point d'un outil de calcul de la composition du cœur à l'équilibre. Le système complexe d'un cœur à chargement continu a une fois de plus soulevé des difficultés qu'il a fallu résoudre. Le temps pris par les nombreux problèmes de modélisation de ce système innovant n'a pas permis de compléter une étude paramétrique complète du cœur. Néanmoins, il a été montré qu'une méthode associant les différents outils de calcul du département permet d'accéder aux informations recherchées. Les résultats d'une étude complète permettront la prise de choix dans le développement du PB-AHTR pour aborder une nouvelle étape de conception.

La partie thermo hydraulique s'est développée autour de la rédaction d'une table préliminaire d'identification et de classement des phénomènes, outil d'importance croissante dans la démonstration de sûreté des réacteurs avancés aux Etats-Unis. La définition du besoin et la forme précise du travail, jusqu'à présent jamais menées au stade pré-conceptuel, a nécessité un effort significatif de documentation. Puis, utilisant des méthodes simples pour identifier et quantifier ces phénomènes, un classement a été proposé pour la marche en puissance et doit servir de toile de fond pour guider les futures recherches. Par ailleurs, une ébauche a été dressée pour le scénario de perte de pompage primaire, très illustratif de la grande sûreté passive du AHTR.

CONTENTS

INTRODUCTION

The 2005 Energy Bill authorized in the United States the construction by 2017 of the Next Generation Nuclear Plant (NGNP), aimed at electricity production as well as high temperatures industry applications (hydrogen production particularly). This national program sponsored by the Department of Energy, fits in the requirements of the Generation IV forum of enhanced economics and safety. The main candidate is a gas-cooled reactor, known as the Very High Temperature Reactor (VHTR). Part of this program is an innovative concept using clean liquid fluoride salts as a coolant instead of helium, called the Advanced High Temperature Reactor (AHTR). The development of this reactor is lead by the Oak Ridge National Laboratory (ORNL) and includes other national partners (Idaho and Argonne National Laboratories), industry (AREVA NP) and the University of California, Berkeley (UCB).

Liquid salts provide numerous advantages compared to helium coolant in high temperature reactors. Their large volumetric heat capacity reduces the pumping power and adds significant thermal inertia, during transients. This inertia combined to the ability to achieve effective cooling of the core by natural circulation helps to reduce considerably the peak temperature reached during loss of forced cooling transients. Thus the power density can be increased and the output power also.
This technology benefits from the knowledge accumulated in 50 years of Molten Salt Reactor Experiment (MSRE) program at ORNL. Clean liquid salt fluoride salts show very low corrosion rates with graphite and nickel-based alloys at fairly high temperatures, by using appropriate chemistry control. Some alloys have already been developed at ORNL and are qualified by ASME, such as Hastelloy N and could provide a base for AHTR materials choice. Moreover, the transparency of liquid salts allows optical inspection in service, as technology already exists for high temperature environments. The main candidate for coolant is Flibe ($^{7}LiF_2BeF_4$) with a high level of ^{7}Li enrichment that combines the best neutronic and thermal hydraulic characteristics.
The disadvantages of such coolants are their high freezing points and their corrosiveness when mixed with fuel, as in the MSRE. The AHTR bypasses these issues by using solid fuel and working at high temperatures when at full power (in shut-down conditions, auxiliary heating would be supplied if necessary to supplement decay heat).

The fuel to be used has been developed in past gas cooled reactor programs and is similar to the one envisioned for the VHTR: TRISO particles sustaining high temperatures, embedded in matrix of graphite and adapted in prismatic blocks (as in Fort Saint Vrain or Gas Turbine Modular High Temperature reactors) or pebbles (as in the Pebble Bed Modular Reactor).

The UCB, as partner in the AHTR program, proposed a closed primary loop design, instead of the early pool design. The primary loop is immersed in a tank containing a separate, inexpensive sodium fluoroborate buffer salt, thus reducing the amount of primary salt (which is expensive if Flibe is used) and increasing the thermal inertia of the reactor. This design has been retained as the baseline design for the AHTR program. In May 2006, positive buoyancy issues of prismatic fuel blocks that may complicate the refueling operations caused the program to envision other types of fuel. The UCB took the lead in a pebble-bed version (PB-AHTR), whereas prismatic blocks and stringers fuels were developed in parallel by the other laboratories.

PB-AHTR DESCRIPTION

I. Primary loop main characteristics

The PB-AHTR is currently designed for an output power of 2400 MW(t). The outlet temperatures considered range from 700°C to 1000°C, making the reactor suitable for electricity production (lower outlet temperature) and for hydrogen production (higher outlet temperature). The current temperature difference through the core is 100°C.
The core is a cylinder delimited by a graphite reflector on the top and sides and by a liquid salt reflector at the bottom. It is loaded with pebble fuel elements. They do not include any technological change; current designs have modest positive buoyancy in the primary salt at any operating temperature. Pebbles will be continuously fed into the core from the bottom throughout multiple injection points, to allow eventually a radial control of the pebble distribution in the core. Experimentations are currently in progress to demonstrate the feasibility of this design. The objective is to create a two zones core, with a central, high burn-up area at the center that should flatten the power profile and limit the peak fuel temperature.
This, added to a very low neutron leakage (contrary to annular cores for modular gas cooled reactors), should allow very high burn-up (over 100MWd/tHM). The pebbles are recovered at the top of the core through four exit points. Once out, their burn-up is checked and they are either discarded or reinserted into the core. After a start-up phase, the core should be continuously fed with fresh and used pebbles to allow the core to operate with very small excess of reactivity, this excess being kept to address power reduction transients and the Xenon peak associated. Control rods should be inserted directly in the bed or in holes designed in the side reflector. Cruciform-shaped control rods are envisioned to prevent pebbles floating up into the control rod entry ports in the top reflector. In case of SCRAM without control rods insertion, the reactor should automatically shut down under Doppler effects, as well as having a reserve shutdown option based on injection of lithium fluoroborate salt.

The coolant flows upward through the bed and exits through the reactor vessel through 4 hot legs. The bed is hold down by an upper graphite reflector, drilled with thousands of coolant exit channels and four de-fueling chutes for pebble recirculation, as shown in.. The hot salt flows through an outlet plenum towards the 4 hot legs.
The high volumetric heat capacity and the reduced pressure drop allow the use of primary pumps with characteristics similar to, but smaller in size than classic pressurized water reactor pumps. These 4 pumps are equipped with level equalizing lines to maintain the same free surface level in the four pumps.
At full power, the heat is removed by compact heat exchangers of Heatric type (Figure 0-1), defined as the Intermediate Heat Exchangers (IHX). These components can achieve a high heat removal rate in a limited volume which is much smaller than would be typical for the intermediate heat exchangers of a sodium fast reactor or the volume of a typical PWR steam generator. Their design is not fully definitive as different channels geometries are available (Figure 0-2), as well as the materials (ceramic, diffusion bonded metals). Moreover, their design is strongly dependent of the final purpose of the AHTR as working temperatures greatly influence stress mechanisms. This issue is intensively studied at UCB, as this technology is also relevant for hydrogen production, with helium cooled VHTR using a Flinak intermediate loop. The advantage of these exchangers is their modular use: they can be sized independently and then be installed in parallel clusters (Figure 0-3 and Figure 0-4), optimizing the space available and minimizing the size of the surrounding structures.

Figure 0-1 Photo of a cutaway-model of a typical Heatric heat exchanger showing multiple inlet and outlet manifolds and slices across various plates and flow channels.

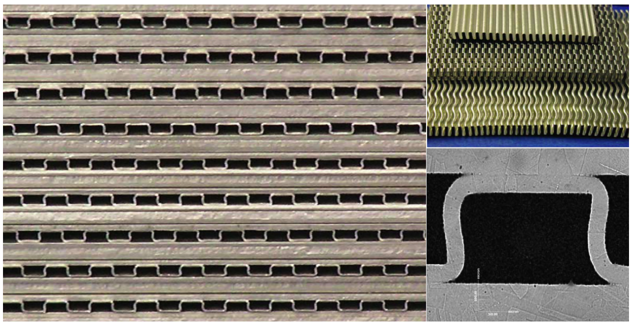

Figure 0-2 Diffusion bonded formed plate heat exchanger (FPHE).

The cold salt exiting from the IHX is collected in 32 cold legs (compared to 4 hot legs), to provide multiple ports for injecting pebbles into the bottom of the reactor vessel. Pebbles re-circulated from the top of the core are tested for burn-up and then are injected in these ducts, entrained by the primary flow and then released in the inlet plenum, upwards to the bottom of the bed. A small amount of the cold flow is by-passed to cool the radial reflector, in order to minimize the temperature gradient through the reactor vessel.

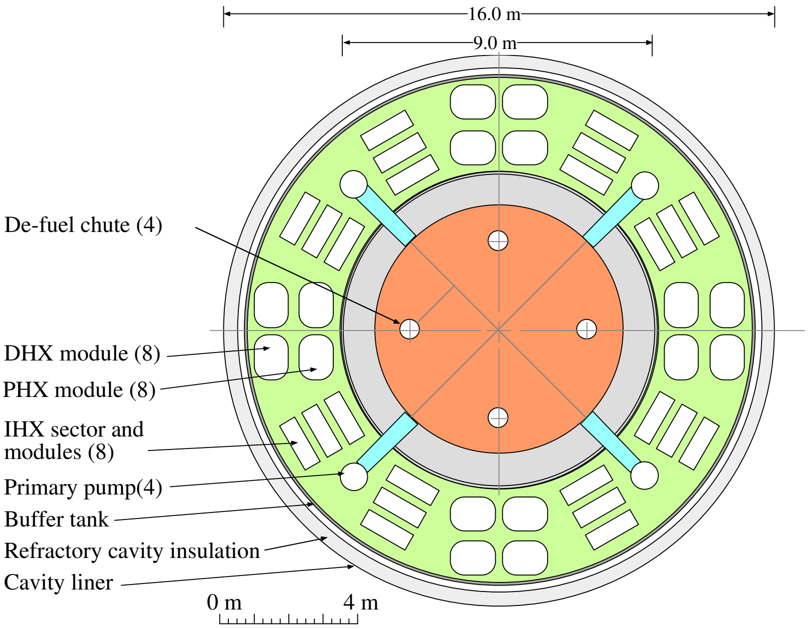

Figure 0-3 Top view of the PB-AHTR design

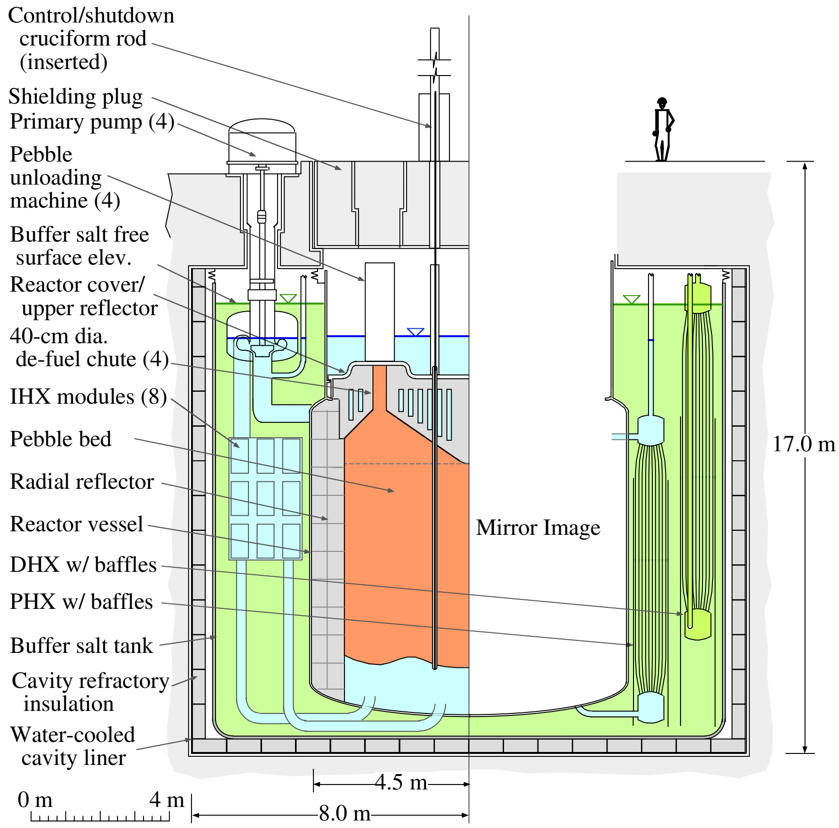

Figure 0-4 Side view of the PB-AHTR design

II. <u>Buffer salt pool and passive heat removal systems</u>

As shown in Figure 0-4, the reactor vessel and the whole primary loop are immersed in a cooler buffer salt pool. When the IHX cannot perform their role of main heat sink (reactor shutdown, accidental loss of cooling), the heat is removed from the core through the Pool Reactor Auxiliary Cooling Systems (PRACS) heat exchangers.

The hot primary salt flows, by natural circulation, upwards through the core, then downwards through the PHX and back to the core, via the inlet plenum. The PHX are cooled by the buffer salt flowing along the bundles (shrouded by a baffle to enhance the buffer salt natural circulation).

At full power, to prevent the inlet flow to pass through PHX, fluidic diodes are included at the bottom of each PHX. These passive devices oppose a large flow resistance in one way that prevents any significant leakage of the normal operational flow.

The PRACS are modular systems, and are sized to match decay heat after a significant time of an order of 1 hour (roughly 2% of the nominal power).

The heat is removed from the buffer salt by modular Direct Reactor Auxiliary Cooling Systems (DRACS) heat exchangers. These systems are liquid salts loops that cool the buffer salt pool, and release the heat through external passive heat sinks such as water or air. Similar systems were used in Super-Phenix and EBR-II sodium reactors. DRACS are sized to match decay heat after several hours. These passive systems, combined to the large thermal capacity of the components involved, yield to temperatures increase far from the TRISO fuel failure threshold. These intrinsic safety characteristics allow designing higher power density than other gas-cooled high temperature reactors.

III. CAVITY, BUILDING AND POWER CONVERSION SYSTEM

The tank containing the buffer salt pool is embedded in an insulated cavity. This tank that must sustain the horizontal loads imposed during seismic motions is equipped at its bottom with a pin to transfer these constraints to cavity.

The liner surrounding the tank is cooled by the Reactor Cavity Cooling System (RCCS). The RCCS uses forced circulation of water through pipes to maintain the cavity at acceptable temperatures.

During severe accidents conditions, when buffer salt tank could rupture, heat is still removed by the boiling of RCCS water. Moreover, leaks of salt through concrete silo are limited due to its high freezing point. Thus, the reduced potential for direct containment heating of the AHTR allows selecting a simple filtered confinement building.

This reactor, coupled to an advanced power conversion system, as a multiple reheated Brayton cycle would finally result in a plant size that presents more compactness than other types of high temperature facilities, as shown in Figure 0-5.

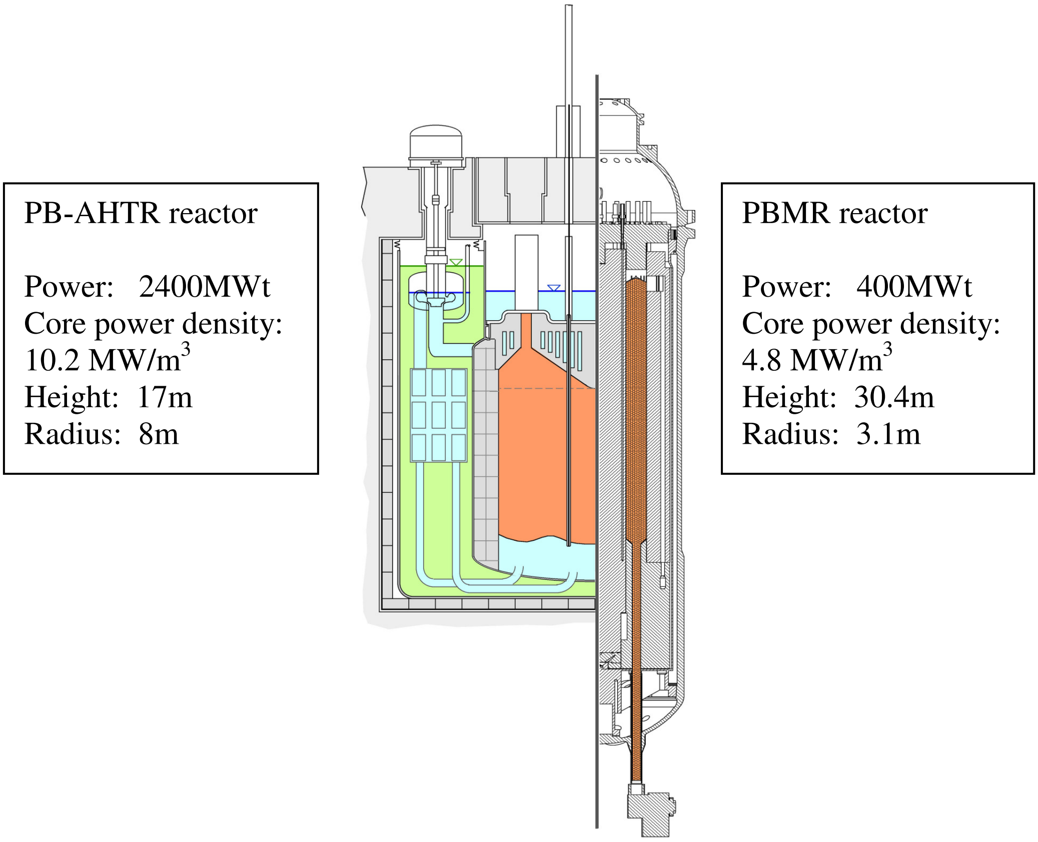

Figure 0-5 Comparison between the PB-AHTR and the PBMR reactor

PART I :
PIRT STUDY

A. PRELIMINARY WORK

This chapter provides the necessary preparative work for further development of a definitive and detailed Phenomena Identification and Ranking Table (PIRT) of the AHTR. It describes the purpose of this process in AHTR case and defines a general comprehensive approach to describe the system. It finally highlights issues that should be fully addressed later by the process.

I. PURPOSE

In 1989, the US National Regulatory Commission (NRC) authorized the use of best-estimate methods in safety analysis within the reactor licensing process, as an alternative to the previous practice of using deterministic, bounding analysis. To apply best estimate methods, however, the NRC required that reactor vendors provided a quantification of the resulting uncertainty in the best estimate analysis. For this reason, the NRC sponsored research to develop a systematic approach to properly assess the uncertainty. The resulting methodology, called the Code Scaling, Applicability and Uncertainty (CSAU) method, has been demonstrated and applied in many cases, for example in the assessment of a Large Break and Loss of Coolant Accident (LBLOCA) in a pressurized water reactor [1]. This methodology includes a systematic method to identify the set of relevant phenomena that the code must properly model, based upon their importance in affecting the safety criteria established for the system. The results are referred to as a Phenomena Identification and Ranking Table (PIRT).

Since the generation of a PIRT tackles various topics (further understandings of the plant behavior, systematic survey of phenomena knowledge), PIRTs have proven to be valuable tools not only to demonstrate the adequacy of modeling codes, but also to establish the separate effect test (SET) and integral effect test (IET) experiments required to validate these codes. These aspects have been highlighted in recent papers [2, 3].

A complete PIRT is prepared only after an initial, “umbrella” PIRT is completed, as recommended by the NRC [8]. In the past, most applications of PIRTs have been to reactor designs that are quite complete, and for well defined transients. However, the early development of an umbrella PIRT is a valuable activity early in the conceptual design of any reactor, as with the current work to develop the design of the AHTR-MI. The relevance and efficiency of a PIRT are strongly dependent of the precision of the background data (design features, modelisations of several transients, survey of existing literature, etc…). Referencing to the previous works done on this subject, this report presents a preliminary PIRT for the AHTR-MI.

This work follows the simplified PIRT process [3], and is mainly focused on the initial steps of the process.

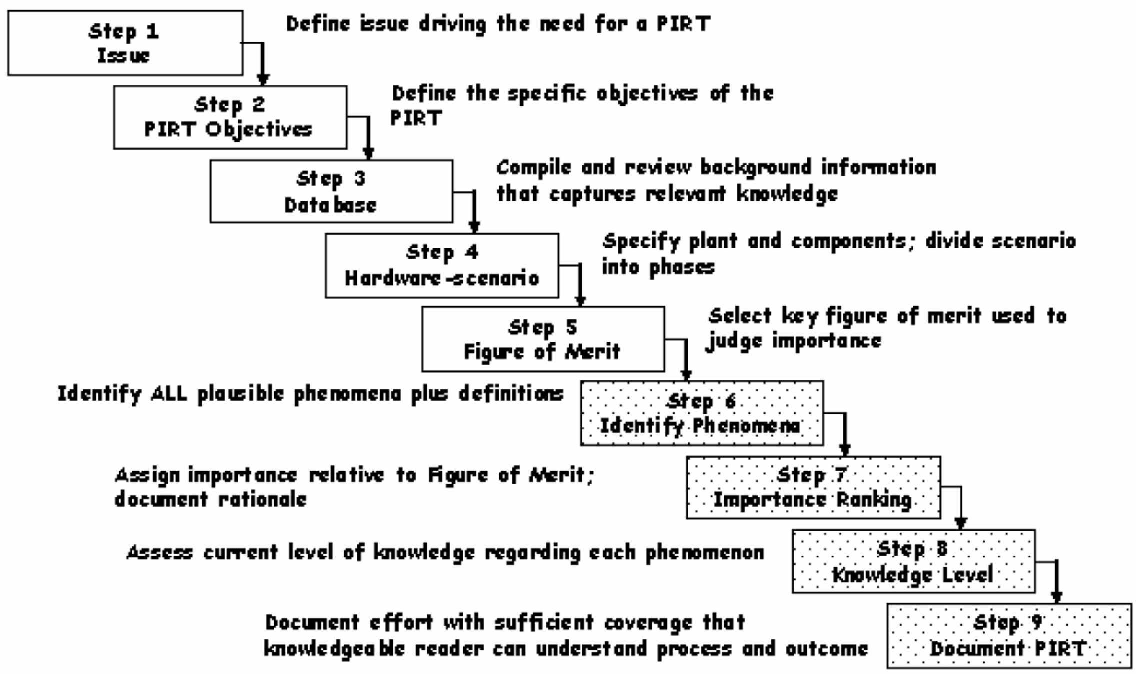

Figure A-1: Simplified nine-step process.

The LS-VHTR program and especially the AHTR-MI are still at a pre-conceptual design stage: the selection, improvement of modeling tools and database are essential prior to the beginning of the licensing process. The motivation for a preliminary PIRT include:

- To create a better understanding of plant's response to normal and off-normal scenarios,
- To identify requirements for separate effects test (SET) and integral effects test (IET) experiments,
- To verify and improve the adequacy of codes that would be used for modeling these scenarios.

Creating a PIRT requires the availability of detailed background information about the system being studied. The AHTR-MI is a conceptual design that shares attributes with high temperature gas-cooled reactors, pool-type sodium fast reactors, and pressurized water reactors, but which also has significant differences. While major attributes of the primary, intermediate, and decay heat removal systems have been defined, design information is still not complete and no detailed thermal hydraulics simulations have been performed yet. However, the following materials can provide some background:

- Previous LS-VHTR reports since 2004, including the U.C. Berkeley 2006 ICAPP paper [10] describing the AHTR-MI,
- VHTR reports as they provide a great amount of data on fuel and graphite performances. Some VHTR projects are now at a pre-licensing stage (like the Pebble Bed Modular Reactor).

II. HARDWARE DESCRIPTION

This step is relevant in the sense that it ensures that no constituent of the plant is missed.
The general design is the one early defined by UCB, which differs from AHTR 2004 baseline

design mainly by its use of a closed primary loop with a separate buffer salt pool and a direct reactor auxiliary cooling system (DRACS). The closed loop design has been selected as the new baseline configuration by ORNL [10], however the passive decay heat removal system has not yet been finally decided [11].

Some features of the AHTR-MI are flexible:
- Type of core: the fuel may be pebbles, stringers, or prismatic blocks (and the associated neutron control and refueling methods). The design is most advanced for prismatic fuel blocks, however, issues with positive block buoyancy causing difficulty for refueling have prompted investigation into pebble and stringer fuel geometries that would permit online refueling.
- Working temperatures, whether the reactor will be optimized for hydrogen or electricity production,
- Total thermal power, as the very preliminary calculations showed that it could exceed the 2400 MW currently used as the base line value.

These three major variables drive the following uncertainties:
- Design and number of the intermediate heat exchangers (IHX),
- Number of intermediate loops,
- Choice of materials and alloys for the various components,
- Sizing of the passive decay heat removal systems: Pool Reactor Auxiliary Cooling Systems (PRACS) and Direct Reactor Auxiliary Cooling Systems (DRACS).
- Design of the confinement building and type of heat sinks (water, air) for the DRACS and Reactor Cavity Cooling System (RCCS).

For the convenience of the study, the plant (system) is divided in sub-systems and components (called modules [9]). This top-down hierarchy has been used in previous complete PIRT studies [12] and is required to study complex systems, where phenomena can be local (limited to a component) or integral (interactions between components) [2, 13].

Due to the conceptual design level, a detailed division in components is not possible at this stage. The efforts have to be focused on the primary loop and buffer salt sub-systems, as the others are subject to uncertainties in their design. However, some components retained for the study have not yet been fully designed, and instead are treated by specifying functional requirements.
- **Primary**: this includes every component wetted by the primary coolant salt.
- **Intermediate**: this includes components wetted by the intermediate salt that transports heat to the hydrogen plant or electricity power conversion system. We assume that we encounter only one type of intermediate loop and that one unique heat sink is linked to these loops. Actually, this heat sink could be decomposed in several independent ones (helium loop linked to a power turbine, Hydrogen thermo-chemical generator, water cooler for shutdown transients). For this study, the intermediate sub-system is limited to the IHX itself.
- **Buffer**: delimited by the buffer salt tank.
- **Tertiary**: Includes all others components, this sub-system includes the direct surroundings of the reactor and buffer salt tank (the reactor cavity and associated containment building) and the outside of the plant. The salt loops of the DRACS are included, but are not described in detail.
- In term of completeness, one may also consider the **secondary** sub-system, which is composed of the power conversion system or hydrogen plant. Nevertheless, to simplify the model, this sub-system is treated as a simple heat sink for the intermediate system.

The detailed description of AHTR components is given in Appendix II.

The safety assessment of a plant identifies the components that are required to maintain plant safety during off-normal situations.

The components are ranked regarding to their contribution to the safety of the plant. We use the IAEA simple classification (described in Appendix I) that defines two classes: operational systems and safety systems [14, 15]. The safety systems are the systems that ensure the three basic safety functions [17] listed below are maintained during off-normal scenarios:

- Control reactivity
- Remove heat from the core
- Confine radioactive materials and shield radiation

Hence the following safety systems can be defined:

Table A-1: Safety systems of the AHTR-MI.

Safety system	Related safety function	Description
Coating of the TRISO particle	- Confine radioactive materials	This entirely passive system (class A) is the first boundary.
Fuel, reflectors, primary coolant	- Provide thermal inertia - Confine radioactive materials	The large mass of graphite in the core and reflectors provides large thermal inertia that reduces the rate of core temperature rise. The primary coolant is effective in absorbing and confining fission products. These are entirely passive (class B) functions.
Primary system boundary	- Confine radioactive materials	This system is the second boundary. It can be considered as passive (class A) only in power.
Reactor cavity and building	Confine radioactive materials	This system is partly active as vents and isolating flaps (air loops) and valves (pressurized loops) require power and signals to shut and isolate this third and last boundary. The need of a confinement (no pressure boundary), against a containment (pressure boundary) is a current US regulatory issue [18].
PRACS	- Transport heat from core to buffer salt - Confine radioactive materials	This system is entirely passive (class B). By preventing heat up from the core and then fuel or metallic components failure, it participates in the confinement protection.
Buffer salt	- Provide thermal inertia - Transport heat from PRACS to DRACS - Provide negative reactivity upon	The very large mass of buffer salt provides large thermal inertia. The sodium fluoroborate provides effective reactor shut down upon breach of the primary boundary. These are entirely passive (class B) functions.

	primary loop breach	
DRACS	- Remove heat from the core - Confine radioactive materials	This system is passive (D class). During an accident, flaps or valves must open wide after receiving a control system signal.
RCCS	- Remove heat from the reactor cavity - Maintain cavity concrete within acceptable temperature limits	Under normal operation the RCCS is active, the water flow through tubes is driven by external forces (pumps). Under loss of pump power, the system is passive and removes heat by boiling of water.
Protection Systems	- Control reactivity - Trip primary pumps - activate DRACS decay heat removal	The Instrumentation and Control (I&C) system detects an upset and commands: - SCRAM system - Trip of the power conversion system (Turbine, hydrogen generator, intermediate loops) - Trip of 4 primary pumps - Activation of the other safety systems (passive cooling, confinement).

Additional safety systems could be discussed but are not taken into account in this work:
- Use of reserve reactivity control (in addition to safety and control rods), like the addition of a soluble poison (lithium fluoroborate) to the primary salt.

The set of actions controlled by the I&C system include:
- Reactor SCRAM,
- Turbine trip
- Primary pumps trip: required to activate the PHX by removing the pressure differential across the PHX fluidic diode.

For the construction of scenarios, discussed in the next section, the single failure criterion principle is applied to these safety systems: the additional failure of one safety system is assumed and taken to be the most demanding. Systems not considered as safety-related are not used. PRACS and DRACS are modular, passive systems. Then, the single failure criterion assumes failure of one of the modules to operate. The protection system is required to reach a safe state: assuming the total, long-term failure of the I&C will drive the system to beyond design basis conditions. Partial failure of the actions ordered by the I&C will be retained as an application of the single-failure criterion.

In new licensing processes of the US NRC [19,18, 20], safety systems are defined after the results of preliminary Probability Risk Assessments are available. These safety systems will be the Systems, Structures and Components (SCC) that will be found essential to meet the safety criteria for Design Basis Events (Annual frequency per plant between 10^{-2} and 10^{-4}). It is illustrated by the process in licensing the PBMR [19].

III. DEFINITION OF SCENARIOS OF INTEREST

To perform phenomena identification and ranking for a reactor system design, the specific scenario to be modeled must be defined. In general, safety analysis requires analysis of a range of steady-state, operating transient, and accident scenarios. To do this, a systematic process is required to identify all relevant scenarios, and to select a representative set to be studied in detail. At the conceptual design level, it is valuable to focus on a smaller subset of scenarios, to provide early information on requirements for modeling and experiments, and to provide early feedback into the design to select options the facilitate modeling and simplify experimental requirements.

No well defined systematic process exists to identify scenarios for new reactor designs. In fifteen years, PIRTs have been developed mainly to address well-known complex problems from well understood reactor types such as LWRs and HTGRs (e.g. LBLOCA or TRISO fuel behavior). Therefore this study developed and applied a systematic approach to identify the key steady-state, operating transient, and accident scenarios that could be of importance to the AHTR-MI. From these, a small subset was selected for use in developing PIRT tables and for early safety analysis for the AHTR-MI concept.

The staff of the NRC Advanced Research Reactor Plan [8] requires the use of two different types of PIRTs in the licensing process for advanced reactors. NRC staff will first draw an “umbrella” PIRT, built after scenarios selected among the Licensing Basis Events (LBEs) proposed by the pre-applicant and, if necessarily, for additional scenarios identified by the NRC. A second formal PIRT should be performed within schedule and resource constraints. The use of PRA and risk-informed methods to identify and rank scenarios is closely linked to this process to help to ensure that correct events are treated.

The present study does not use the risk-informed method, because the design is not yet sufficiently complete for data on component reliability to be available. Our approach steps between the three approaches detailed above: we mix general considerations for selection of initiating events and “classical” simplified construction of licensing scenarios. This “first-cut” work has to be improved by PRA studies as soon as the AHTR-MI design will allow it and will be subject to modifications when progress in the understanding of the plant will highlight unexpected issues. As the NRC [8] points out, the process to identify scenarios is iterative.

We will build scenarios in that way (more details are given below):

1- We list the general Postulated Initiating Events (PIE) and normal operating conditions;
2- We reduce the list of the PIE and normal operating conditions: we find a PIE which could reasonably bound the severity of the consequences. We estimate a conservative frequency of occurrence;
3- We build a bounding scenario and a “PIRT interesting” scenario for each PIE. For that purpose, we lay the emphasis on simple within-design basis scenarios, as they present “a priori” a sufficient large scale of phenomena, and are simpler than Beyond-Design Basis Accidents (BDBA). Moreover, these scenarios have highest priority by the NRC for a PIRT process [8]. These scenarios are simple and based on a “safety analysis looking” method, as they only include:
    - Initial conditions (which normal operations state, what conditions external to the plant?)
    - One PIE
    - Single failure criterion [17, 22] application

  - Conservative timing of protection actions
4- Some BDBAs presenting particular phenomena are proposed. There is no systematic method applied for this selection.

This process provides a small set of useful scenarios to use in the development of a set of “first-cut” PIRTs, and to aid in the detailed design of the plant. Specifically:

- We do not address all the off-normal scenarios, as we consider only a PIE and not a combination of a PIE and all possible additional failures (as built in an events tree, in many national approaches to deterministic safety analysis). This simple method is adopted by the Russian safety authority to analyse the common PIEs [14].
- Rare phenomena could be generated by combining in the same scenario a PIE and particular additional failures. As we do not use a software tool to generate all possible scenarios, we artificially broaden the space of generated phenomena with the single failure criterion.

The normal operation states are the different operating conditions, typically called operating modes, that occur routinely in a nuclear power plant during its life. Plant operating modes are standardized for light-water reactors [15]. Some adaptations must be performed for the AHTR to identify the major operating modes.
These scenarios, given in Appendix I, are simplified in chapter V.1, for the purpose of conceptual design.

IV. OFF-NORMAL EVENTS

IV.1. Postulated initiating events

External initiating events are independent from the design of the reactor itself and can generate simultaneous internal initiating events [15] (common cause failures). They can result from human errors or natural hazards. These hazards are typically specified by the national and international standards (Appendix I). Their frequencies and intensity are site-dependent.

In this preliminary study for the AHTR, these external PIEs are not considered, and instead PIEs based on internal events are considered. However, that the consequences generated by some of these external PIEs are covered by the internal PIE cases considered. We assume that selected DBA and BDBA, constructed with internal PIEs, address a sufficient list of phenomena for a “first-cut” PIRT.

The various existing standards give several types of classifications for the PIEs (regarding to their consequences, their frequency or their nature). They are summarized in [23]. Internal PIEs used for the safety assessment of the LWRs are nowadays quite accurately addressed. Moreover, systematical and accurate methods can be used to draw an exhaustive list of PIEs [20]. They are based on computational approaches and require a fine knowledge of the plant’s design and data on components reliability. Examples include Failure Modes and Effects Analysis (FMEA) and Hazards and Operability Studies (HAZOP). However, for a conceptual design like the AHTR-MI, it is necessary to find PIEs a simple and general way, one cannot rely on LWR experience or component reliability data.

The AHTR is composed of several sub-systems. The steady behavior of each sub-system (composed of fluid and materials and limited by a boundary) is ruled by equations of conservation of mass (fluids), momentum (fluids) and energy (solids and fluids).

Table A-2: Families of Postulated Initiating Events (PIE).

Balance	Variable	Practical translation of the variable
Mass	Changes in inventory and nature	Break or opening in the sub-system boundary
Momentum	Changes in flow characteristics	Flow blockage / run-down
		Flow run-up
		Flow instability, oscillations
Energy	Changes in heat source and sink	Heat source: decrease / increase of the capacity
		Heat sink: decrease / increase of the capacity

Thus we propose the variables that specifically upset the balances shown in Table 4.1.
For each sub-system the possible events are specified that **directly** alter the balances shown in Table A-2. These initiating events are detailed in Appendix III.

For example, we don't have considered void (if there is any neutronic positive void coefficient) as an initiating event in "heating increase" family, as void is not created by it-self but is generated necessarily by another PIE (gas entrainment, or consequences of a particular LOCA).

We focus in this work on the very events that generate upsets: thus, we neglect hazards that generate simultaneously several of these PIEs. We have only cited hazards that would generate phenomena unexpected otherwise (shaking of the fluids and components by seismic motions for instance).

IV.2. Sequence construction

We retain only the **internal** initiating events and ignore the few particular hazards highlighted (those with complexity not consistent with a preliminary study: e.g. seismic motion). We also suppress events that can be judged to be **beyond design basis** (e.g. rupture of the reactor vessel) or present similarities with other bounding events (e.g. primary pump trip bounded by a flow blockage in the leg).

We suppress also local events that are bounded by more general ones (e.g. flow blockage in one intermediate loop bounded by a flow blockage in all the intermediate loops). This simplification puts aside local phenomena (e.g. mixing of the un-cooled flow with the colder ones in the inlet plenum, in the latter case) and would require more investigations later in a matter of completeness.

The simplified list is given in Appendix IV.

The single failure criterion is applied to the safety systems defined above, after each PIE defined, regarding a particular topic arisen with the PIE. Realism must be conserved: a failure with a very low probability (estimations are given in Appendix II) is not applied after a PIE with also a very low probability.

The main issues of a sequence considered for the failure selection are:

- Neutronics: ability to shut-down if the reactivity increases or forced cooling is interrupted
- Heat removal: ability to sustain in the passive cooling phase of the sequence an extra heat to remove, due to an increase of the decay heat (feedbacks have not limited enough the neutronic power increase) or more energy stored in the primary system (increase of the average temperature in salt and core)
- Temperature distribution: local hot point, important ΔT core or important drop in temperature elsewhere.
- Void reactivity: gas entrained in the core causes an increase of reactivity (here the single failure criterion is systematically applied to the primary pumps to increase the effects of gas suction)
- Mixture of different salts: heat removal characteristics of one loop are modified (especially here the primary loop), chemical reactions are small.

V. NORMAL AND WITHIN DESIGN BASIS EVENTS RETAINED

V.1. Normal operation

The AHTR PIRT should retain the following operational scenarios:

- Normal reactor start-up from shutdown through criticality to power,
- Full power operation (100 %), for which a preliminary PIRT will be proposed in this project,
- Reactor shut-down from full power operation,
- Shut-down state (no particular shut-down state is retained, as we assume that the addressed safety issues remain the same: avoid salt freezing)

The other following scenarios have been eliminated from consideration, at the conceptual design stage, because we expect that the phenomena they address are included in the other scenarios selected.

- Initial approach to reactor criticality: phenomena expected are similar as those addressed in a classical start-up. The risk in safety terms for an initial approach is more important (possible excess of reactivity, as all the fuel is fresh), but the mechanisms of the transient itself are similar. The whole start-up scenario is more interesting as it includes the whole range of powers;
- Power operation low (40 %) power: steady phenomena are expected to present more significant consequences at a higher power;
- Changes in the reactor power level including load follow modes if employed: these changes are including in the high power level phase of start-up and shut-down scenarios;
- Handling and storage of fresh and irradiated fuel: this scenario is not developed in order to reduce the arena of the study. Moreover, it’s not specific to the AHTR-MI as the possible fuel designs have already been experienced at an industrial scale (FSV, AVR, AGR).

V.2. Within design-basis scenarios

Among the sequences built in Appendix V, few are selected for PIRT purpose, as they present particular features, in terms of severity or particular phenomena:

- Reactivity insertion without SCRAM,
- Loss of off-site power when shutdown (heating system failure), with a DRACS rise in efficiency,
- Load increase with a PRACS failure,
- Loss of cooling with a PRACS failure,
- Loss of forced circulation without SCRAM,
- Partial flow blockage in the core with a PRACS failure,
- Primary pump shaft seizure, the other pumps fail to trip,
- Flow blockage in one PRACS in shut-down state, with a failure of one DRACS,
- Flow blockage in RCCS, in early stage of shut-down state, with a failure of one DRACS,
- Flow blockage in one DRACS, in shut-down state, with a failure of one DRACS,
- Flow run-up of one primary pump, without SCRAM,
- Vibration in core during a start-up, without SCRAM,
- Vibration in RCCS during a start-up, without SCRAM,
- Primary break up-stream the pump, no pumps trip,
- Primary break down-stream the pump, before IHX, no pumps trip,
- Primary break on the cold leg, no pumps trip,
- Primary break on a PRACS, no pumps trip,
- Pinhole in IHX between intermediate/primary side, without SCRAM,
- Primary break on an auxiliary loop, to the outside, no pumps trip.

Additional studies may show that some of the scenarios proposed are bounded in severity and interest by other scenarios (for instance in the cases of breaks down-stream the primary pump, a single scenario might be relevant). Studies of external events may also encompass some of the scenarios proposed (vibration issues).

For conceptual design, the University of California at Berkeley will then focus on the two scenarios that include most of the phenomena of importance to the AHTR-MI response to internal PIE's:

- Loss of forced circulation, which will be succinctly studied in this project,
- Primary break.

VI. BEYOND DESIGN BASIS EVENTS RETAINED

Beyond design basis events are characterized by major failures in components (boundaries) and a deficient operation of safety systems. They can drive a reactor to a severe accident (core is totally or partially damaged).

Regarding AHTR-MI design and in search of particular phenomena, we can select these beyond design scenarios for a PIRT.

- Rupture of buffer salt tank (heat transfer by conduction instead of radiation in the reactor cavity, phenomena expected if primary loops are not totally flooded, cooling of buffer salt by boiling water in the RCCS),

- Rupture of buffer salt tank and of reactor vessel, partial PRACS and DRACS failure (effective shut-down of the core by the buffer salt, heat removed by conduction and boiling in the cavity),
- Failure of all DRACS (external hazard: fire, explosion): heat removed by RCCS
- Core overheating and release of fission products into primary salt,
- Severe reactivity events (void, uncontrolled CR withdrawal, flux pitching, pebble bed shaking from seismic motion) in the operational states where feedbacks are not established (start-up, shut-down, first approach to criticality).

VII. PHENOMENA AND CRITERIA FOR RANKING

Previous PIRTs for gas-cooled reactors show that a great flexibility is used to define the phenomena judged of interest. These phenomena, taken out the previous PIRT experiences and liquid salt reactors analyses, can be ranked in families [12] and are given in Appendix II.
To perform a ranking of the phenomena occurring, criteria have to be defined, taking into account economical and safety aspects. A proposal of detailed criteria is also given in Appendix II.

Providing the tools (criteria and previous experienced phenomena) is the last stage before the beginning of the very PIRT study. Since a preliminary framework has now been set, further studies are conceivable. This project will propose a preliminary PIRT for the "full power" operational scenario and then provides elements for a PIRT concerning the "Loss of Forced Circulation" (LOFC) scenario.

B. FULL POWER

I. INTRODUCTION

In this chapter, the phenomena expected to be important in each module of the AHTR system are identified and studied for the case of the full-power, steady-state operating mode. This study is relevant since it provides a first and simple example of a full application of the PIRT process to an innovative system.
The phenomena identified here differ somewhat from the first list given in Appendix II (Table A.II.6.). The precise definition of a phenomenon is flexible and PIRTs sometimes give different names for identical phenomena. One may note that the emphasis is laid on the pebble-bed version of the AHTR.

Here are some preliminary comments about the following work:

1- Gamma heating is neglected compared to heat transferred by convective flows.

2- Flow distribution and heat transfer are important in the critical places of the system (modules where differential temperatures are the highest: hot pipes in contact with cold buffer salt, heat exchangers, mixing locations for cool core bypass flow): we need to accurately model these kinds of phenomena to accurately predict gradients of temperatures (and therefore the thermal stresses generated in structures).

3- Some components, with auxiliary functions, are not precisely designed at this stage. Only general comments are then proposed since precise PIRT would not be relevant considering the large uncertainties. In particular, those systems where design is incomplete:
- Chemistry control systems for primary, buffer and intermediate salts,
- Drain tank for intermediate salt,
- Volume control/expansion tanks for primary and buffer salts,
- Intermediate loops.

4- Simplification: Some phenomena are common to all components, but have different levels of importance for these components. For simplicity, they are not considered in the following presentation. These include:

Fouling: the fluids (primary, buffer, intermediate or water of RCCS) are fouled by impurities. These impurities can be generated by **erosion** and **corrosion** phenomena.
Some elements mitigate these phenomena, compared to other known reactor designs:
- Liquid salts don't wet the graphite. Graphite erosion may occur by rubbing of graphite blocks due to fluid mechanics forces, and due to pebble motion and rubbing in the PB-AHTR.
- Corrosion of metallic alloys by liquid salts is known to be limited and is driven by the redox potential of the salt, itself influenced by the temperature and the presence of species, such as fluorine (F2) or tritium (TF). However these mechanisms can be limited by adapted chemistry control [27, 28, 29]. Moreover, experiments performed at Oak Ridge National Laboratory demonstrate very little corrosion rates with candidate materials up to temperatures of 850°C [29].

However, the attention on these phenomena should be focused on the most critical components:

- Core:
  - In pebble-bed version, pebble bed motion and interactions with flowing fluids may generate rubbing and graphite dust.
  - If the buffer salt is not particularly concerned with the temperature induced corrosion, the primary and intermediate loops (especially for the hydrogen version), working at significantly higher temperatures, may experience significant corrosion rates and require efficient chemistry control systems. Material removed from hot parts of the system by solubility induced corrosion will then deposit on low-temperature parts of the system, in particular, deposition may occur on the primary side of the IHX.
- Intermediate heat exchangers: important stresses (important pressure differences and high temperatures) are expected in these components that could be made of metallic or ceramic materials.
- Cold cover-gas-space components where condensation (or sublimation) could occur. The salts are chosen to present the lowest vapor pressure to minimize the release of gas in the cover. However, condensation layer could alter local chemical conditions and maybe enhance corrosion mechanisms (TF gas for instance in the primary pool).
- RCCS: cool water is flowing in metallic pipes embedded below the cavity liner; classical issues of corrosion arise.

Mechanical loads: the AHTR is working at near atmospheric pressure (the maximum pressure in the primary loop could reach 6 bar). **Mechanical stresses** are then limited in the primary, buffer and tertiary sub-systems. The stresses are found in the power conversion system components as they work at a highest pressure (turbine, intermediate-to-helium heat exchangers for instance).
One of the most important components (except of course the intermediate components) is the buffer tank, because it must sustain substantial hydrostatic and thermal stress loads. Moreover, a pin will be used to transfer the horizontal loads (during seismic motion, a portion of horizontal acceleration is passed through the cavity base isolation system) to the bottom of the cavity. This pin will have normally to transfer the entire horizontal loading of the buffer and primary sub-systems through a pin of limited size, where temperature gradients will be high. Thus, the design of this component will be challenging as it will see important mechanical and thermal stresses.

Radiation issues:
Neutron and high-energy gamma rays damage the components. The most concerned components are those contained in the reactor vessel: core and reflectors and vessel.
The following elements are of interest:

- High temperature anneals part of the radiation damage effects.
- These effects of radiations at high temperature are subject to discussions and may be responsible of an enhanced Wigner effect [30].

Particular concerns draw the attention on the de-fueling systems for the pebble version of the core. The small space available in the upper part of the reactor implies that pebble handling machines must accommodate substantial radiation doses, including some high-energy neutron irradiation from sub-critical fission from pebbles in the de-fueling chute.

To be consistent with the simplification of phenomena list and taking into account the comments above, the following simplified list of criteria (after Table A.II.3.) is used for the ranking:

Table B-1: Ranking criteria for "full-power" scenario.

Investment protection	Stresses (this could also be put in safety category)
	Heat losses
	Pumping power
	Fuel operational performance
Safety	Initials conditions for transients
	Radioprotection

5- Method:

Step 1: The study is first performed at a module level. Different criteria can pull towards different rankings. Hence just a relative ranking is made at this stage. A phenomenon is ranked of high, medium or low importance (noted respectively by **H**, **M** or **L** in tables). More detailed PIRTs may strive to get more precise by defining up to 5 ranks. This preliminary study will remain based on a simpler 3 ranks approach.

Step 2: The first results are then used in to identify the relative importance of modules in the whole system (system level analysis). Finally, the proposed ranks per module take into account:
- The criterion found to be the most relatively relevant in the module,
- The relevance of the module after a system approach.

It might be noted that the rankings proposed in Appendix VI are the final rankings and therefore take already into account the system-level comparisons.

II. STEP ONE: MODULE LEVEL ANALYSIS

In this paragraph is illustrated the systematic analysis performed for the components identified in chapter A. For that purpose, summarized examples of studies of two very different components of the AHTR are provided here (core and cavity). Complete studies are given in Appendix VI, for all the components.
Using the initial list of phenomena given after a literature review on liquid-salts and high-temperatures reactor, their influence on the main criteria is assessed. For that purpose, simple tools have been used: 1-D calculations with Microsoft Excel or Mathcad software. Each study results in a preliminary relative ranking of the phenomena that will be modified after a system-level analysis. An example of a Mathcad worksheet is provided in Appendix X.

II.1. <u>Primary sub-system, Core</u>

Whatever the design finally retained (prismatic blocks or pebble-bed), the following phenomena are encountered and are of high importance as they all combine to bring about the issue of fuel operational temperature and the steady peak coolant temperature:
- Power:
    - o Steady state neutronics has to be accurately predicted to assess the fuel performance achievable (burn-up, k-effective, radioactive materials to be released in accidents conditions)
    - o Gamma heating is expected to be the most important in the fuel zone, however, it is often neglected in steady-state calculations [31].
- Flow:

- Flow distribution, linked to the pressure drop, convective heat transfer and power profile, drives the peak fuel temperature and the peak exit coolant temperature (that might creates hot jet impinging structures in the outlet plenum and also thermal striping that could affect critical components as IHX). In the particular case of prismatic core, it is considered as one-dimensional ($\frac{L}{D} >> 1$).
- Pressure drop is a relevant phenomenon as it affects the pumping power and the flow distribution.

Comments concerning the prismatic core:

The pressure loss by friction is estimated, assuming a constant flow speed and density through core and using the Blasius relation for the friction factor. Liquid Salts don't wet graphite; therefore, even rough surface for salt is smooth, precise values for roughness are not relevant. Pressure drop calculations will assume smooth surfaces.

The total value of pressure drop (singular and regular) is an order of 10^5 Pa, which represents the third of the IHX pressure drop.

Comments concerning the pebble-bed core:

Different correlations to get the frictional pressure loss in a packed bed of spheres are available in literature. Rough calculations are done for 3 correlations, considering the simplification of a one-dimensional core (with theoretical power profile in sinus and a constant mass flow rate).

The resulting pressure drops are fairly reduced (order of 75 % of the prismatic core values). The average porosity (Figure B-1) and the working temperature do not affect much the total contribution of the core in the total pressure drop in the primary loop.

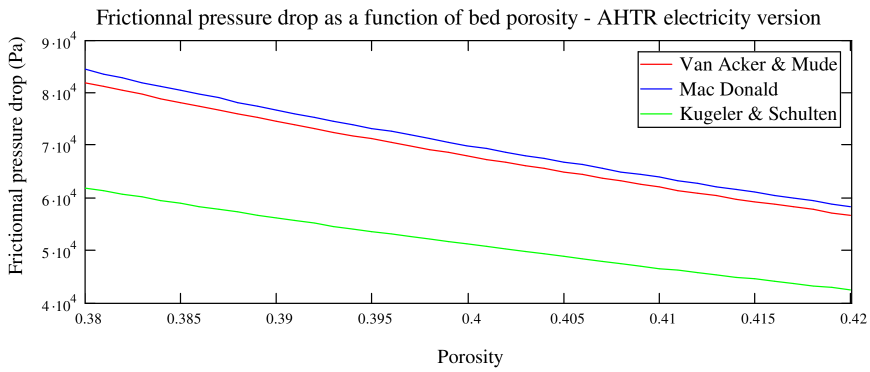

Figure B-1: Influence of porosity on frictional pressure drop through the pebble-bed core (low temperature version).

- Heat transfer:

Conduction issue is important in fuel materials (spherical TRISO particles, cylindrical compacts, hexagonal graphite blocks or spherical pebbles). Graphite conductivity has been well studied and data are available. However, since AHTR works at a higher power density than gas-cooled reactors, fuel conductivity values have great importance to predict the peak fuel temperature. More detailed information (results of ORNL studies) is available concerning the graphite conductivity in [31]. TRISO conductivities are not clearly known, however, this is not particularly relevant due to the small size, leading to small temperatures differences within a TRISO particle (less than 5°C).

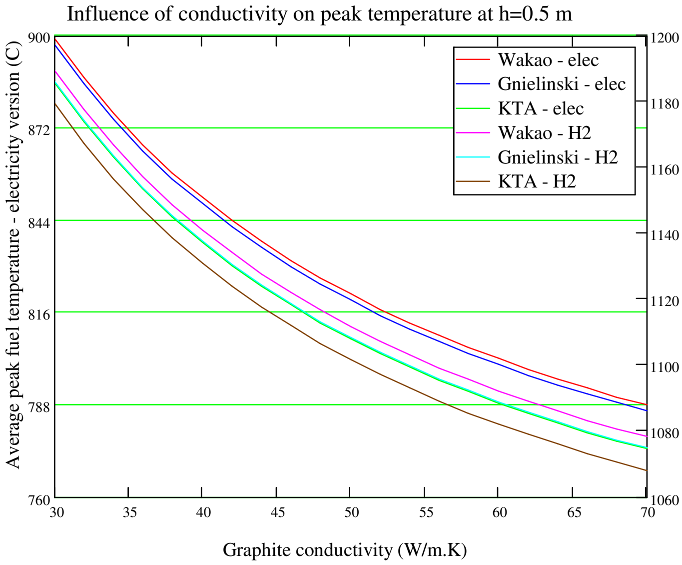

Figure B-2: Fuel conductivity effect on peak temperature (1-D model).

This importance is illustrated by estimations of peak fuel temperature in the pebble-bed AHTR. A one–dimensional calculation (Figure B-2) shows that, in the range we are interested in (fuel temperatures superior to 900 K, where conductivity is between 30 and 70 $W.m^{-1}.K^{-1}$), conduction modifies the peak core temperature of an order of 100 K, whatever the correlation used or the average core temperature.

The second important heat transfer mechanism is the forced convection in coolant channels or around pebbles.

Comments concerning the prismatic core:

Estimations have been done of the possibility of mixed convection. It has been found that, whatever the criterion retained (Metais and Eckert flow chart or A. Bejan criterion), the flow is turbulent and forced convection is the heat transfer mechanism, rather than mixed convection.

Comments concerning the pebble-bed core:

Numerous studies have been conducted around heat transfer in packed bed of spheres, however the literature shows a great scattering in the available known reliable correlations, especially when it comes to high Prandtl fluids (Appendix VIII). Three correlations are used to assess the convection and have been selected because of the large experimental database they rely on. Convection importance is illustrated by the contribution to the peak fuel temperature: temperature difference within the boundary layer ranges from 30 to 50°C (Figure B-3).

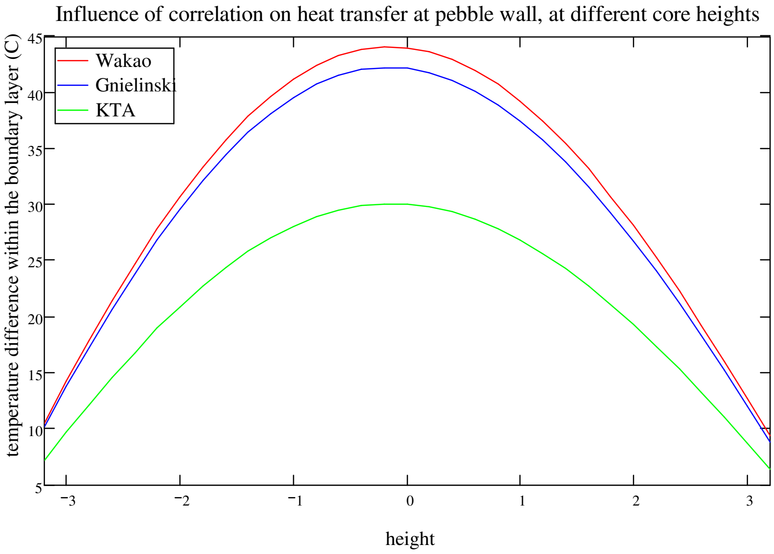

Figure B-3: Heat transfer at the pebble wall.

The resulting (conduction and convection) uncertainty in fuel temperature prediction might be relevant for a neutronic calculation and also for the prediction of initial conditions during transients (amount of stored heat in the graphite, instantly released in the salt).
However, 1-D calculations considering a conservative conductivity (30 $W.m^{-1}.K^{-1}$) showed that for the low temperature version of AHTR, the peak fuel temperatures are extremely low (below 900°C). It has been confirmed by some preliminary 3-D modeling with RELAP5 that showed a peak fuel of an order of 950°C. The high temperature version of AHTR shows significantly higher values (Figure B-4).

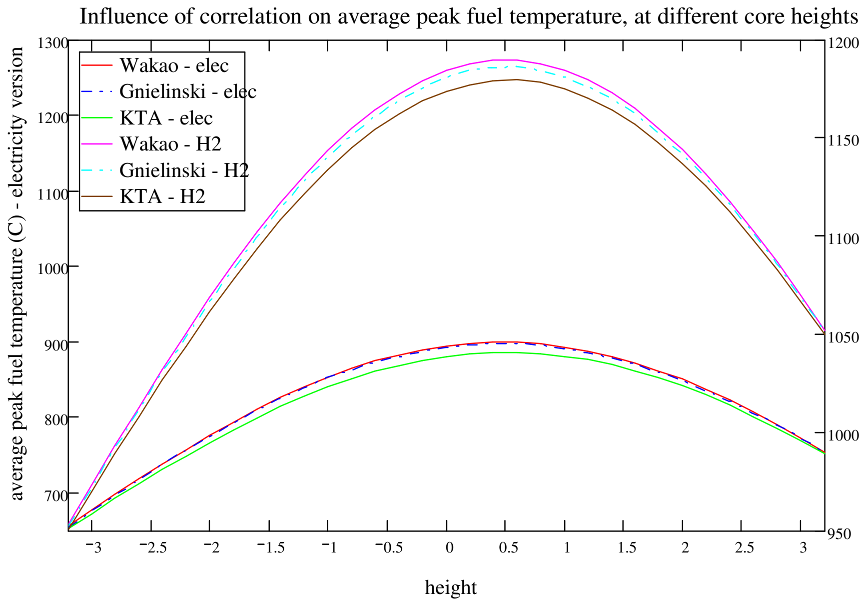

Figure B-4: Radialy-averaged peak fuel temperature as a function of height.

Other phenomena of importance are expected:

- Thermal stresses generated by gradients of temperatures throughout components, especially in the TRISO particles (this has been intensively studied in different VHTR programs).
- Kernel migration due to over pressure of CO2 in the TRISO particle. This phenomenon is important at the edge of the core where the temperature gradient is steep. The cylindrical shape of the core is likely to amplify the temperature gradient, compared to annular cores.

- Pebbles distribution is not uniform through the bed. The average porosity of a randomly packed bed in gas-cooled reactor is given by the formula:

$$\varepsilon = 0.375 + 0.34 \cdot \frac{d_{pebble}}{D_{bed}}$$

Where d_{pebble} and D_{bed} are respectively the diameters of a pebble and the bed. It gives the theoretical value: $\varepsilon = 0.378$. Buoyancy will alter these values. Important porosity changes are also observed near the walls [32], on a 4 pebbles thick layer.
The flow velocity and so the pressure drop will certainly be lower near the walls than in the center (due to a higher porosity near the walls). However, the small buoyancy of pebbles and the limited friction (roughness becomes relative issue when it comes to liquid salts as a coolant) may limit the scattering in porosity distribution.
Finally, the influence of the total average porosity in a short range of values (around 0.4) on the peak fuel temperature is not important, as shown on Figure B-5. However, porosity remains an important issue to predict the k effective and local distortions could also have significant local effects on the fuel temperature.

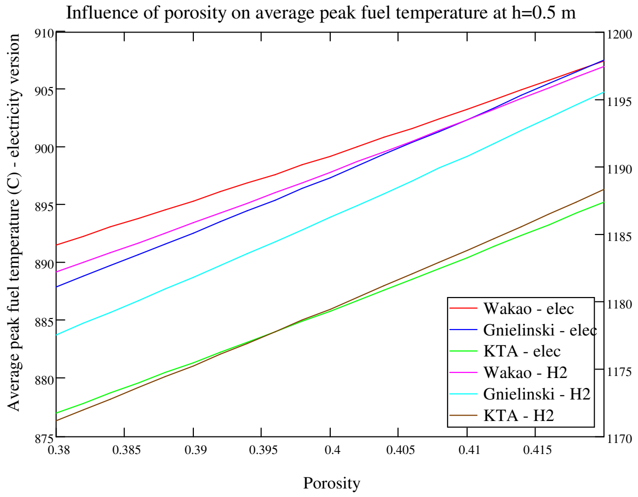

Figure B-5: Influence of average porosity on peak fuel temperature (Radially-averaged at h=0.5m)

As a conclusion, the phenomena highlighted in this simple study show all some important impact on at least one of the different criteria proposed. Already, one may presume that a system level study won't modify the proposed ranking.

Table B-2: Initial ranking of phenomena in the core.

Rank - PBR	Rank - PMR	Phenomena	Criteria
H	H	Flow distribution	Fuel operational performance (FOP)
H	H	Forced convection	FOP
H	H	Pressure drop – forced convection	FOP – Pumping power
H	H	Conduction (including gaps)	FOP - Stresses
H	H	Thermal stresses	Radioprotection
H	H	Kernel migration	Radioprotection
M	M	Gamma heating	All
H	/	Pebble distribution	FOP

II.2. Tertiary sub-system, Cavity

Here is studied a module that obviously has limited influence on the core behavior. This module, where the free space is likely to be filled with argon, houses the buffer salt tank and is cooled. The bottom of the buffer salt tank lays on an insulation layer, downwards heat transfer calculations are not presented here, only transfers to the sides.

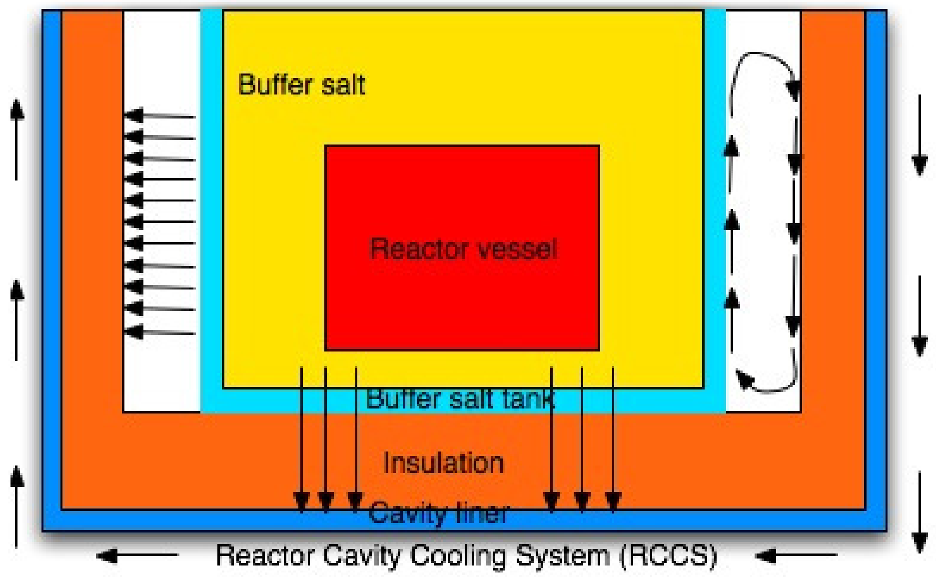

Figure B-6: Schematic of the cavity.

The argon gas, the only fluid constituent, of this component can flow in its cavity, driven by a natural circulation, created along the inner hot and outer cold walls by external free convection mechanisms. The gas far from these zones could stratify vertically.
Heat is transferred by conduction through buffer salt tank, argon (expected to be negligible), graphite insulation, liner and then RCCS tubes. In the argon filled gap, radiation and convection compete to transfer heat.

Convective and radiation heat transfer is estimated by considering that the situation in argon gap is similar to a situation with two plates at different temperatures (the curvature of the large tank allows this simplification).

The main issues arisen are the heat losses and the temperature gradient though the buffer salt tank. Two parameters can be used to minimize this: insulation and emissivity of the walls of the gap. In some high temperature reactors designs, the cavity is one of the main systems used for heat removal, thus cavity design is optimized for radiation heat transfer (emissivity of 0.4 for air or 0.8 for argon are commonly used [33], [34] and [31]). In AHTR, emissivity can be reduced to help to insulate the buffer tank and then reduce temperature differences, as other systems are used for heat removal.

The use of low emissivity surfaces has the same consequences in terms of heat losses and temperature gradient than an insulating layer of 0.3m, as shown in Figure B-7. Heat losses (order of several hundreds of kW) become inferior by far to the estimated primary heat losses (several MW) and temperature gradients are inferior of those within the reactor vessel.

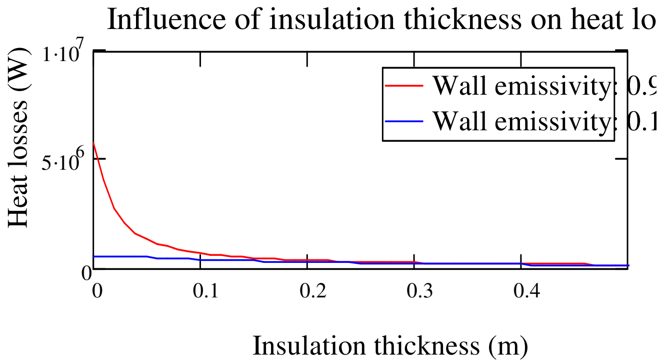

Figure B-7: Effect of insulation on heat losses (high and low emissivity cases).

Low emissivity surfaces induce a higher temperature difference through the argon gap, thus increasing the internal free convection mechanisms. This phenomenon is reduced by the insulation. Then, convection mechanisms are found to transfer up to 50 % of the heat transferred by radiation (Figure B-8), in low emissivity walls cases, with little insulation (still 10 % with important insulation layer).

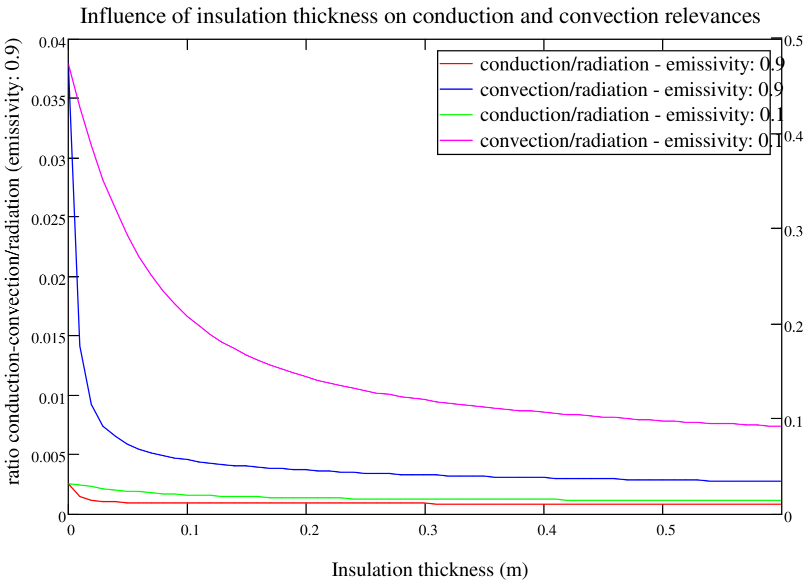

Figure B-8: Ratios of heat transferred by conduction (or convection) over heat transferred by radiation, as functions of insulation thickness. Effect of emissivity on these ratios.

Conduction through insulation and radiation through argon are the most important phenomena. Changes in the boundary conditions (linked for instance to free convection mechanisms of the buffer salt along the tank, or forced circulation of water in the RCCS) don't affect much the temperature gradients, the heat losses or the relative importance of convection. The buffer salt temperature influence is illustrated by Figure B-9.

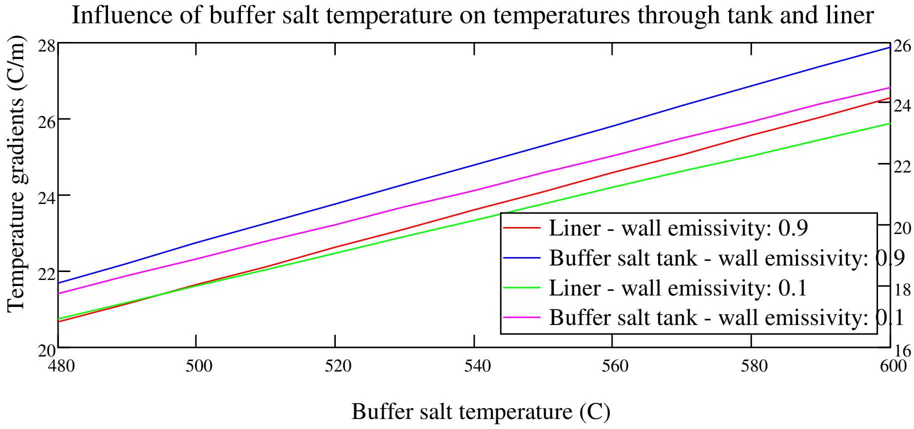

Figure B-9: Influence of buffer salt temperature on temperature gradients through metallic constituents (insulated cavity).

The following initial ranking can be proposed. It can be presumed that their importance will be lowered, considering the small values of temperature gradients and heat losses compared to other obvious critical modules (PHX or DHX).

Table B-3: Initial ranking of phenomena in the cavity.

Rank	Phenomena	Criteria
H	Radiation (including emissivity issues)	**Stresses** – Heat losses – Initial conditions
H	Conduction (including gaps)	**Stresses** – Heat losses – Initial conditions
M	Natural convection (in argon)	**Stresses** – Heat losses – Initial conditions
L	Stratification (in argon)	**Stresses** – Heat losses – Initial conditions
L	Thermal stresses	**Stresses**

III. STEP TWO: SYSTEM LEVEL ANALYSIS

At the system level analysis, the relative relevancies of modules are compared, regarding their impact on the different criteria. If a component is found to have a secondary influence, whatever the criteria, it results in a down review of the initial phenomena ranking.

Fuel operational performance is affected by few modules: the plena, the core and the reflector. Convective heat transfer in the core is by far more important that heat transfers through the reflector. Hence, the latter's influence on core and its working temperature is secondary. The plena (especially the inlet plenum) impact the flow distribution in core and then are relevant modules.

Pumping power is also affected by few modules: the IHX (mainly), the core and the plena (pipes contribution is very secondary).

Heat losses economics issues shares the same background with prediction of buffer salt temperature for the determination of initial conditions in transient calculations. Thus one single comparison table is proposed.

Table B-4: Heat losses comparison table (in order of decreasing importance)

Sub-systems	Main heat transfer direction	Components involved (driving component in bold face)	Driving phenomenon	Estimation order	Comments
Primary towards Buffer	PHX	**PRACS pipes**, PHX, Buffer salt region.	Pressure drop in vortex diode.	From 10 MW (Elec) to 80 MW (H2)	The value of the diode K is a relevant parameter.
	Legs	**Hot and cold legs**, Buffer salt region	Conduction through leg insulation	From 1 MW to 5 MW (Elec) From 2 MW to 20 MW (H2)	Insulation is needed to reduce the temperature difference through the metal, so are the heat losses. These values are multiplied by 4 if 32 cold legs are used.
	Side of reactor	**Reflector**, Reactor vessel, Buffer salt region	Convection in by-pass flow	From 300 kW to 1.5 MW (Elec) From 800 kW to 3 MW (H2)	The fraction of by-pass flow is a flexible parameter. Insulation can be added to the vessel.
	Bottom of reactor	Inlet plenum, Reactor vessel, **Buffer salt region, Cavity**	Conduction through insulation in the cavity	4 kW (Elec) 6 kW (H2)	A minimum insulation is required in the cavity. Thickness of salt is a relevant also.
Buffer towards Tertiary	DHX	**Buffer salt region, DRACS system,**	Convection in heat exchangers	From 5 MW to up to 50 MW (in the worst case)	The buffer salt must be kept at constant temperature.
	Side of tank	Buffer salt region, **Cavity**, RCCS	Conduction through cavity insulation and Radiation in argon gap	6MW (normal emissivity, no insulation) less than 1MW (if low emissivity	Insulation or low emissivity are needed to reduce the concrete temperature, so are the heat losses.

				insulation)	
	Bottom of tank	See losses from the bottom of the reactor	See losses from the bottom of the reactor	See losses from the bottom of the reactor	See losses from the bottom of the reactor
Primary towards tertiary	Top of reactor	Outlet plenum, **Reactor cover and pool**, Concrete silo	Conduction through pool insulation	From 50 kW to 100 kW (Elec)	Insulation is needed to reduce the concrete temperature, so are the heat losses.

Hence, it can be concluded that the PHX are by far the main contributors to heat losses and heating of the buffer salt. By proper design, losses through others modules can be reduced to become negligible. Then phenomena involved in heat transfer mechanism in the PHX region will be more important than heat transfer phenomena in other modules (regarding the heat losses and buffer salt temperature prediction criteria).

Temperature differences through the metallic constituents of the system could help to get an idea of the relative importance of stresses. However, this question depends also of numerous other parameters, such as the working temperature, the constraints at the boundary of the materials or the capacity to have free thermal expansion (which is the same issue).

Table B-5: Temperature gradients through sensitive components estimation table (in order of decreasing importance).

Constituent - Component	Estimation order	Driving phenomenon	Comments
Hot leg	From 600 C/m (Elec insulated) to 10^4 C/m (H2 non insulated).	Conduction through leg insulation	Insulation is needed to reduce the temperature difference through the metal.
PHX pipes	Up to 1000 C/m (Elec) and 5000 C/m (H2)	Pressure drop in core, and Fluidic diode.	Flexibility of diode design.
Reactor vessel	From less than 200 C/m (with by-pass) to 250 C/m (Elec) to 600 C/m (H2)	Conduction and Convection in the reflector	The by-pass flow is a flexible relevant parameter.
Buffer salt tank	From less than 100 C/m (if insulation) to 600 C/m (if no insulation)	Conduction through pool insulation and emissivity of surfaces	Insulation is needed to reduce the concrete temperature, so the liner is isothermal.
Cavity liner	Less than 50 C/m	Conduction through pool insulation and emissivity of surfaces	Insulation is needed to reduce the concrete temperature, so the liner is isothermal.
Primary pool liner	Less than 20 C/m	Conduction through pool insulation	Insulation is needed to reduce the concrete temperature, so the liner is isothermal.

This table showed that the PHX and the hot legs should be subject to important temperature gradients. However, using insulating materials that can withstand liquid-salts environment would solve the hot leg issue. The temperatures gradients through other modules are fairly reduced.

As a practical example of this system-level analysis application, the phenomena in the cavity have been ranked as low or medium importance. The cavity is affected by few criteria (heat losses, stresses) and do not show any other issue. Thus the driving phenomena (radiation and conduction) have been put down from “high” to “medium-low”, whereas the others have been ranked as “low”.

IV. FULL POWER SCENARIO PRELIMINARY PIRT CONCLUSIONS

A definitive table is provided in Appendix VII and emphasizes some particular points that must be recalled:

- Important parameters in the design must be tackled: insulation of the legs, the cavity and primary pool and exact design of the PHX.
- Important phenomena have been identified and then required particular attention in code development. Integral experiments have already been envisioned to respond to some of these issues.

Here is a summary of the important phenomena identified (except thermal stresses).

Table B-6: Summary of important phenomena.

	Inlet plenum	Core	IHX	DRACS	Diode	Outlet plenum
Flow distribution	X	X	X	X		
Forced convection		X	X	X		
Pressure drop		X	X	X	X	
Conduction		X	X			
Pebble distribution		X				
Mixing						X

The integral experiments are:

- PREX experiments will assess the pebbles movements in the inlet plenum, the coolant local velocity and the pebble distribution in the core.
- Scaled Integral Effect Test Experiments (IET) may be useful to assess the heat transfer, and pressure drop through a bed of heated spheres, as correlations available show significant differences.
- IET are needed to assess the mixing effects in the complex outlet plenum, as done for GT-MHR.
- Conduction issues have already been solved in the HTR long experience. No additional tests are required. Conduction issue in IHX could be bypassed by tackling general heat transfer issue in an IET. Ceramic heat exchangers are currently in fabrication for full-scale testing.

- Pressure drop through Vortex diode value could be determined by the vendor on test benches.
- IET may be needed to assess heat transfer, pressure drop and flow distribution in a bundle of tubes (DHX type exchanger simulation).

This preliminary systematic study has cleared the way towards a more detailed PIRT work that would be supported by Computational Fluid Dynamics simulations, such as RELAP5-3D for instance.

C. LOSS OF FORCED CIRCULATION

I. DESCRIPTION OF THE TRANSIENT

The Loss of Forced Circulation (LOFC) transient has a high probability of occurrence and thus deserves particular attention. That is why a PIRT is expected to be an important tool to fully demonstrate AHTR ability to cope with this event. This chapter will provide initial discussions that could be used in a later more comprehensive work. It offers an early glance at some of AHTR safety performances.

The most conservative case of a four pumps trip is considered, as it minimizes the amount of heat removed in the very first instants of the transient, where scram and trip of the power conversion system have not yet occurred.
The transient can be decomposed in the following stages (to be detailed below):

- Stage one: coast-down,
- Stage two: natural circulation establishment,
- Stage three: quasi-steady heat removal.

The attention is drawn on:

- Peak salt temperature (affects metallic components)
- Peak fuel temperature (affects TRISO particle integrity)
- Temperature changes within fuel (affects k effective)

This discussion is focused on the following modules affected:

- Core,
- Full power primary loop (including the IHX) at the beginning,
- PRACS loop (including the PHX), in a second time,
- The buffer salt (DHX and PHX regions concerned),
- The DRACS loop.

The full power results showed that heat losses through others modules were negligible, it is still true, compared to the amount of the decay heat to remove (tens of MW).

I.1. Stage one: Coast-down

1-D calculations have been performed with Mathcad to describe this stage. The detailed model is given in Appendix X.

The four primary pumps still spin on their inertia; this time is reduced compared to the light-water reactor to allow the PHX to operate. This time is taken to be 10 seconds (used in LS-VHTR preliminary calculations [72]).
Regarding this timing, it is clear that the few primary loop modules are relevant in this stage, as the massive amount of the “insulating” buffer salt allows to consider that others components have no influence.

Moreover, the inlet temperature is not affected by the phenomena upstream, as a long time is required to empty the large volumes of salt enclosed in the upstream modules.

If a longer coast-down time (order of 20 seconds) is retained in design, the IHX will play an important role in the core response. However, the large salt volume between the IHX and the bottom of the core, combined with a low mass flow rate at that time, reduces this effect (heat up or over-cooling of salt).

Forced convection is then assumed to be the preponderant heat transfer mechanism. During this stage, reactor scram occurs and the intermediate heat exchangers still remove heat from the primary loop as the Power Conversion System (PCS) trip could occur in the later time than scram. This stage is studied below in more details.

I.1.a. <u>Before scram and power conversion system trip</u>

These two protective actions occur very early (order of 1 second), compared to the long inertia of pumps.

The graphite thermal diffusivity (α=10^{-5}) gives time constant of temperature redistribution within the pebbles of few tens of seconds. Thus, considering the short time of this stage, temperature distribution is not really affected in pebble and a very reduced increase of the temperature and the stored energy will occur. Meanwhile, the heat transferred to salt will very slowly decrease. The convective heat transfer coefficient h is roughly proportional to $Re^{0.5}$, hence the decrease in h will follow the square root of the mass flow rate.

1-D calculation shows that the peak fuel temperature rise is negligible (less than a few degrees) if scram occurs after 1 second. It is illustrated by Figure C-1.

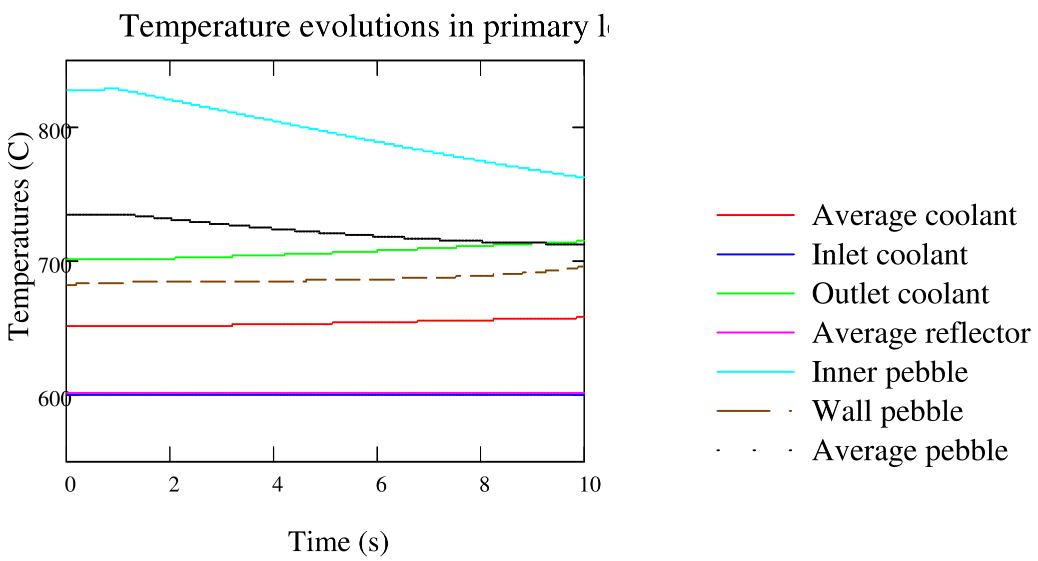

Figure C-1 Temperatures in core during a 10 seconds coast-down, scram after 1 second

Following these remarks, the reflector will not play an important role here due to the characteristic time of the graphite, even if it stores some power by conduction.

I.1.b. After scram

The main result of scram is the decrease of inner pebble temperature. The reactivity feedback following this change is balanced by the anti-reactivity of the control rods. The energy stored in the pebbles is slowly released to the salt, because of the graphite diffusivity that smoothes the dynamics.

During the scram, the PCS is tripped. The shutdown time of this loop will be voluntary reduced, to minimize the possibilities of thermal shock on the sensitive heat exchangers. The intermediate loop has a reduced volume of salt, because of space constraints and is not designed for any natural circulation. Thus a rapid heat up of the Flinak salt will occur.

The peak pebble temperature decreases gently to reach an equilibrium ruled by the decay heat generation and the buoyancy driven flow with the coolant, as shown in Figure C-2. It is simulated in the calculations by a mass flow at the end of the coast-down of 1 % of the steady state value.

The severity of the same transient without scram (and temperature feedbacks) is somewhat balanced by a better convective heat transfer to the salt (higher temperature difference between pebble wall and salt); the pebble center temperature rise after 10 seconds is an order of 30°C. It has to be noted that these results are for 1-D model, where no radial peaking factor is taken into account. Hence it might be reasonably enhanced by a factor of 2, which remains reasonable, knowing that this peaking factor is 1.6.

Temperature distribution in average pebble

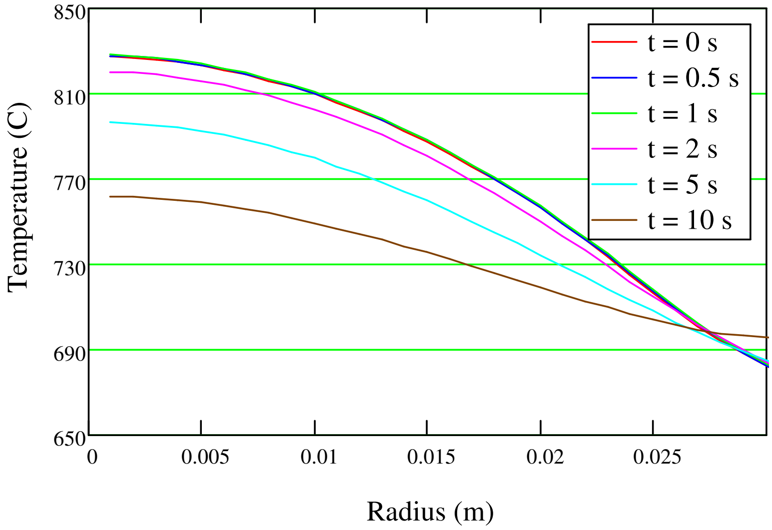

Figure C-2: Temperature distribution in average pebble during a 10 seconds coast down, scram after 1 second.

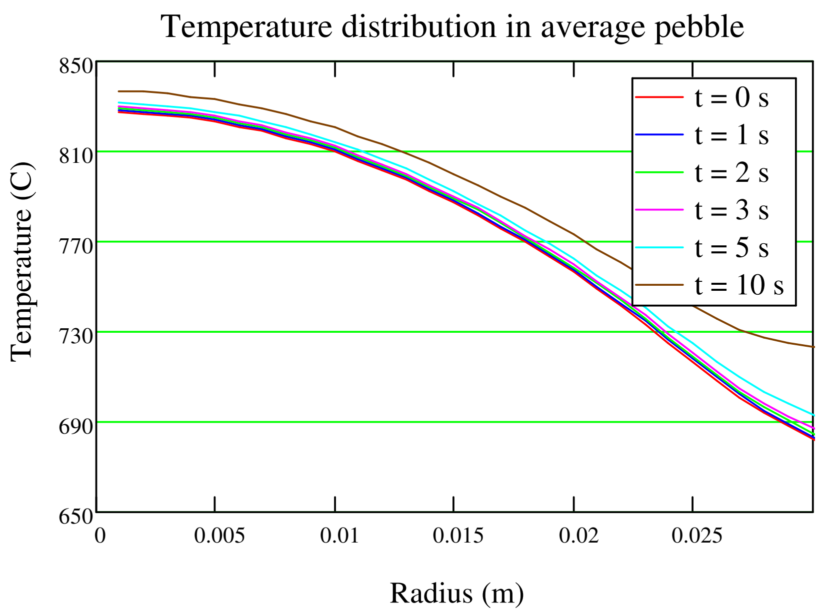

Figure C-3: Temperature distribution in average pebble during a 10 seconds coast down, without scram.

At the end of the coast-down, the salt outlet temperature of the core will see a very small increase if scram has occurred (order of 15°C). If scram failed, this rise would be of 25°C.

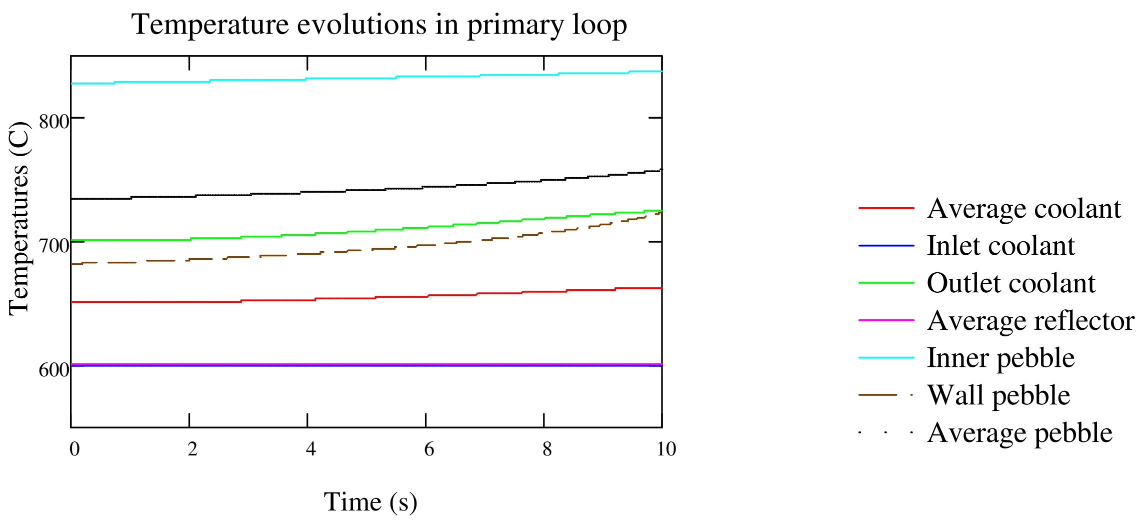

Figure C-4 Temperatures in core during a 10 seconds coast-down, without scram

Thus the effect of the stored energy in pebble, released in the salt by convection, on the salt outlet temperature is perfectly balanced by the reflector and salt thermal inertias.
It is not clear that whether salt or reflector is more important Indeed, calculations of heat transferred from salt to reflector have been done assuming a temperature at the interface equal to the salt one. On the one hand, the efficiency of the reflector might be altered by a heat resistance due to the thermal boundary layer. On the other hand, pebbles directly contact side annual reflector, the salt is transparent, so the contact conduction heat transfer and radiation heat transfer may enhance the heat transfer between pebble bed and reflector.

Figure C-5 shows the importance of the heat transfer by convection that remains dominant, compared to the inertia of reflector. The important time constants of these latter components, compared to the speed of the transient, explain the initial rise in heat storage in theses constituents.
When temperatures are beginning to significantly be modified (order of 8 seconds), the heat storage in salt finally decreases. However, at the end of the stage natural circulation effects will be effective, which is not illustrated by these calculations.

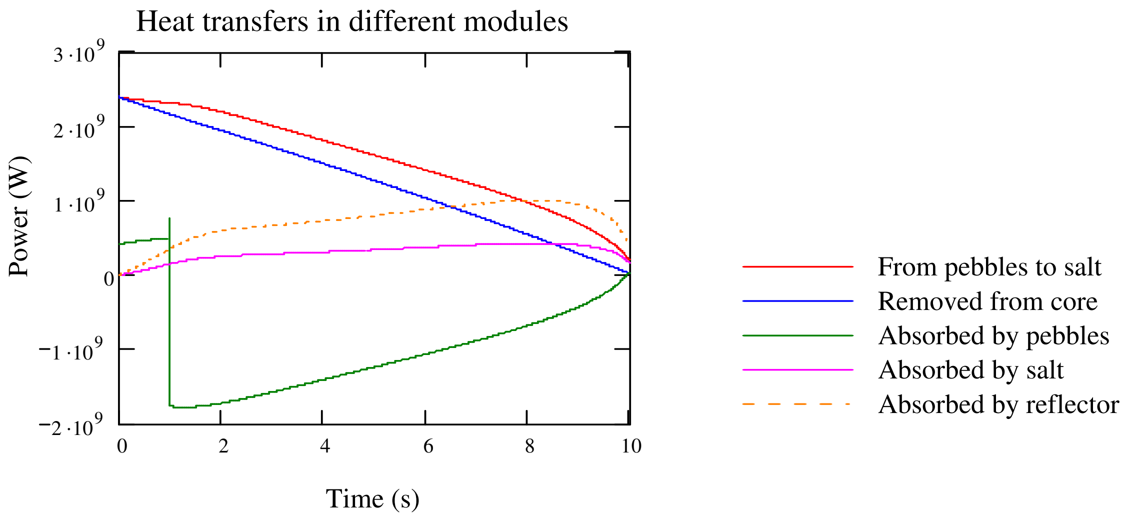

Figure C-5 Heat transferred between main core constituents, during a 10 seconds coast-down, with scram after 1 second

The increasing power absorbed by the fuel (Figure C-6) if no scram or feedbacks are available let presume the following rise in pebble temperature in the following stage.

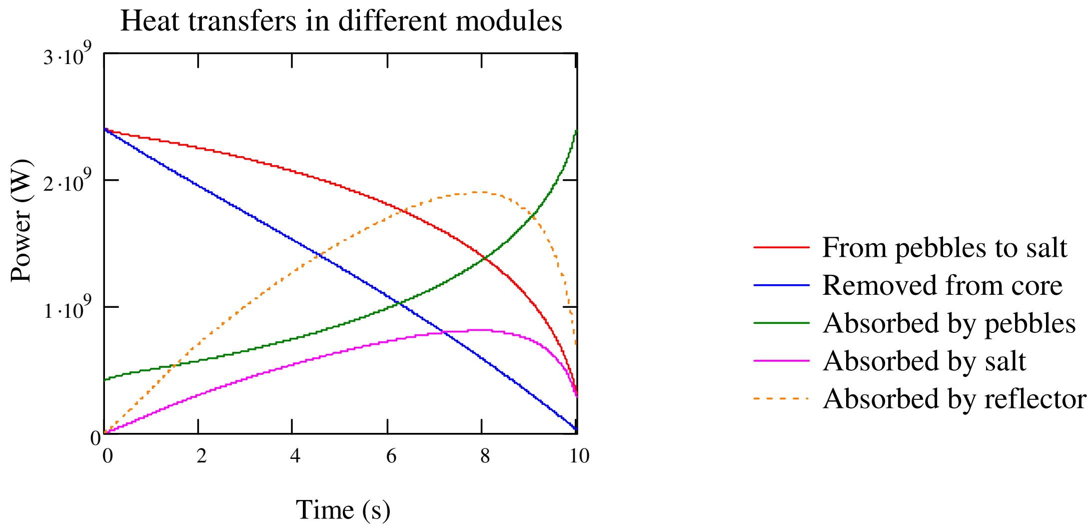

Figure C-6 Heat transferred between main core constituents, during a 10 seconds coast-down, without scram

I.1.c. Coast-down preliminary conclusions

The large mass of fluids and solids involved in the core prevent from an important temperature rise of the coolant. The design of the pump (short coast-down) and the large inlet plenum volume reduces the risk of interference with IHX. This stage is not likely to influence the following stage, as the initial conditions are not far from the steady states conditions.
It might be noted that the average pebble temperature is closed to the surface one (if scram). This observation allows considering the simplification for the next stage calculations that the pebble temperature can be assumed uniform. The peak pebble temperature is not a relevant parameter, since the temperature peaking within a pebble (order of 50°C) is reduced: the flibe boiling temperature (1400°C) sets the pebble failure threshold far beyond (1600°C). Thus the coolant temperature is the only relevant parameter.

I.2. Stage two: Natural circulation establishment

This stage begins as soon as the flow driven by the natural circulation mechanism becomes preponderant on the flow forced by pumps. Since the maximum natural circulation flow is of an order of few hundreds kg per second (to be discussed below), thus it can be assumed that it properly begins when the forced flow reach zero. It ends when a quasi-steady mass flow rate is reached.

I.2.a. Description of the model

A simple 1-D model of the natural circulation mechanism has been used in Matlab. The following assumptions are made:
- The pebble temperature is assumed to be uniform.
- The initial temperature distributions in the PHX and in the core are taken out the steady states calculations (for the PHX) and the coast-downs simulations (for the core).
- The plena and the reflector are not modeled. These large masses, compared to the mass in the primary loop would greatly reduce the outlet temperature increase. Here, the natural circulation loop is composed

- The heat generation in the core is assumed to be uniform linearly,
- The buffer salt is treated as a lump mass,
- The DHX (sized to remove 2% of the full power with a 100°C temperature difference) are assumed to be heat sinks at 500°C and the thermal power is assumed to be linear with the temperature difference between the hot and cold fluids.

The behavior of the primary coolant (temperature and velocity) is ruled by the following system, composed of:
- The momentum conservation equation in the loop composed of the core, the PRACS pipes and the PHX tubes:

$$\rho_f \sum_i L_i \frac{dU_i}{dt} = -\sum_i \int_i \rho_f g \, dz - \sum_i \left(\frac{f_i L_i}{D_i} \frac{\rho_f U_i^2}{2} + K_i \frac{\rho_f U_i^2}{2} \right) \quad (1)$$

Where:
- ρ_f is the density of flibe salt,

- L_i is the length of the module *i* (core, PRACS pipe or PHX tube),
- U_i is the fluid speed,
- *g* is the gravity acceleration,
- f_i is the friction coefficient (given by the Blasius, Poiseuille or Ergun relation)
- D_i is the hydraulic diameter (to be modified if the Ergun relation is used)
- K_i is the singular pressure loss coefficient.

A scaling [73] analysis of (1) showed that the turbulent pressures losses due to the orifices (PRACS pipes and PHX tubes) are preponderant on the others losses (laminar and turbulent terms of the Ergun relation in the core, laminar losses in the PHX tubes). It yields the following relation:

$$\dot{m} = \sqrt{coef \cdot \overline{\Delta T}} \quad (2)$$

Where:
- $\dot{m}$ is the mass flow rate in the loop,
- $\overline{\Delta T}$ is the temperature difference between the hot and cold parts of the loop (at the same height), averaged on the height of the core,
- *coef* is a coefficient depending on the design parameters and physical properties of the coolant.

- The energy conservation equation in the primary loop

$$A_p(x)\rho_f c_f\left(\frac{\partial T_p}{\partial t} + U(x)\frac{\partial T_p}{\partial x}\right) = h_p(x)L_p^w(x)(T_{ext}(x) - T_p(x)) \quad (3)$$

Where:
- $A_p(x)$ is the cross-section area at the position *x* in the loop,
- c_f is the heat capacity of flibe salt
- T_p is the coolant temperature
- $T_{ext}(x)$ is the external temperature (pebble in the core or inner wall of the tube in the PHX)
- h_p is the convective heat transfer coefficient (given by the Wakao correlation in the core, or the *Nu*=3.66 in the PHX, as the flow is laminar, fully developed)
- L_p^w is the wetted perimeter

- The energy conservation in the fuel

$$(1-\varepsilon)A_c\rho_c c_c\frac{\partial T_c}{\partial t} = h_c L_c^w(T_p - T_c) + (1-\varepsilon)A_c q''' \quad (4)$$

Where:
- ε is the porosity of the bed
- A_c is the core cross-section area
- ρ_c is the density of the pebbles
- c_c is the heat capacity of the pebbles
- T_c is the pebble temperature
- h_c is the convective heat transfer coefficient given by the Wakao correlation,
- L_c^w is the actual wetted perimeter in the core (taking into account the porosity)
- q''' is the power density in the pebble (the decay heat function is given by the ANS 79 curve)

The energy conservation in the buffer salt

$$M_{buffer} \cdot c_{buffer} \cdot \frac{dT_{buffer}}{dt} = \left(\int_{phx} h_{buffer}(x) L_p^w(x)(T_{wall}(x) - T_{buffer}) \cdot dx \right) - P_{dhx} \cdot \frac{T_{buffer} - T_{flinak}}{\Delta T_{dhx}} \quad (5)$$

Where:
- M_{buffer} is the mass of buffer salt,
- c_{buffer} is the heat capacity of the buffer salt,
- T_{buffer} is the bulk buffer salt temperature
- h_{buffer} is the convective heat transfer coefficient given by the natural free convection correlation: $Nu = 0.53 \cdot (Gr \cdot 5.938)^{0.25}$, where Nu is the Nusselt number and Gr the Grashoff number, taken with characteristic length of the diameter of the tube.
- T_{wall} is the temperature of the outer wall of the PHX tube
- P_{dhx} is the maximum power that the DHX are designed to remove
- T_{flinak} is the DRACS flinak temperature
- ΔT_{dhx} is the temperature difference at which the DHX are designed to operate.

I.2.b. Results

The mechanism has a slow dynamics, compared to the fastness of the coast-down. Temperatures and mass flow change slowly to reach a quasi-steady state (extremely slowly evolutive) after a time of an order of ten minutes. It is illustrated by Figure C-7 and Figure C-8. It can be concluded that:
- Assumption of steady-state PHX temperatures as initial conditions is valid, as it won't be much affected during the fast coast-down.
- Assumption of a uniform pebble temperature is valid as long as the decay power is small, the effect of thermal diffusivity of graphite is not relevant and the parabolic shape of the temperature distribution within a pebble is very flat.

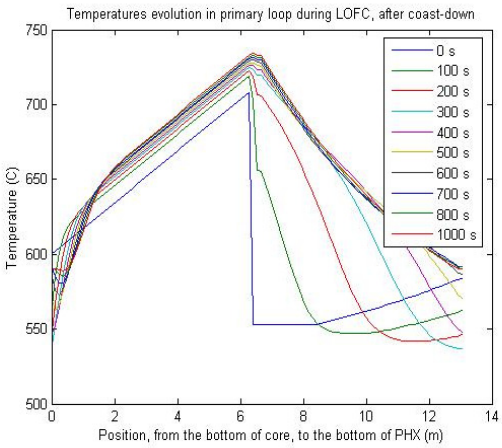

Figure C-7: Temperature distribution in the primary loop

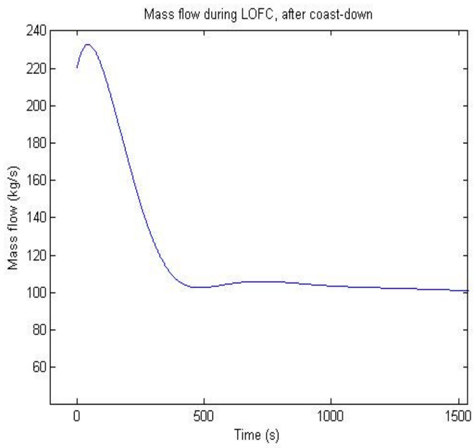

Figure C-8: Mass flow rate, during the establishment of natural circulation

Considering the very low mass flow rate, the residence time of the fluid in the core is an order of ten minutes. Thus, during this stage, the coolant has not enough time to travel through the whole core.

The following temperature profiles are obtained and displayed in Figure C-9. The very low values for the inlet temperatures correspond to the cold mass of salt enclosed in the PHX flowing downward to the core. This does not affect the average core temperature since the residence time is extremely long (a small amount of cold salt is introduced, compared to the large mass of salt heated, already present).

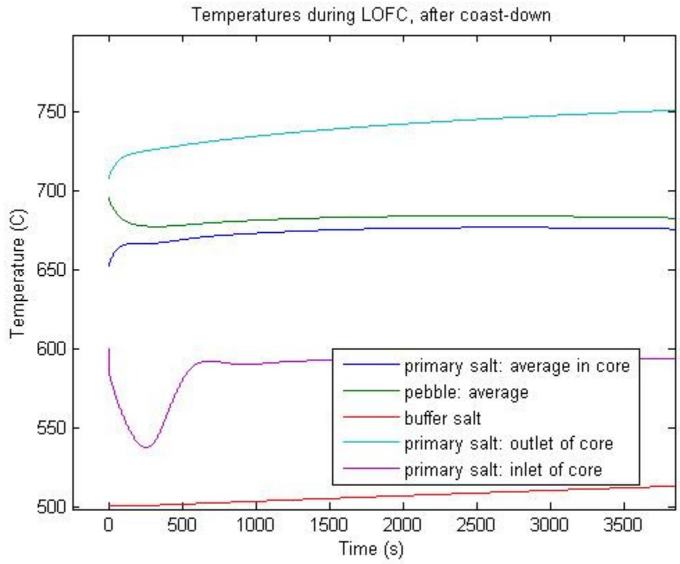

Figure C-9: Characteristic temperatures in the natural circulation loop, during the establishment of natural circulation.

In the beginning of this stage, the convection phenomena at the surface of the pebbles are still more important than the decay heat (Figure C-10), thus reducing the fuel temperature, creating a steep rise of the outlet temperature. Meanwhile, the PHX thermal power remains very limited, as long as some cold salt remains in the PHX tubes. The buoyancy forces are enhanced, thus creating a temporary increase of the mass flow rate, as long as some cold salt remains in the PHX (Figure C-7). At this time, the heat is stored by the primary salt (Figure C-11). The large heat transfer area in the core, compared to the reduced area in the PHX is an influent parameter.

When the PHX is sufficiently hot (order of 2 minutes), the circulation forces are reduced and the flow definitely decreases. This phenomenon reduces the heat transfer at the surface of the pebble, whereas the PHX thermal power is increased (rise of temperature). Finally, the pebbles are heated by the residual power and not efficiently cooled. The main results are a smoother increase in the outlet and average temperature (the short time of average steady temperature after 3-4 minutes could be explained by the effect of the slow “dilution” in the core of the mass of initially cold salt in the PHX). The other effect is the end of the pebble temperature decrease. In this period, the heat stored by the buffer salt is comparable to the one stored in the primary salt. At the end of this stage, the temperature profile in the PHX reaches its final shape as shown in Figure C-7.

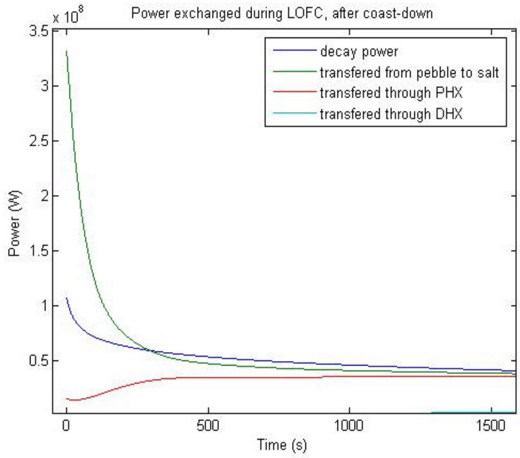

Figure C-10: Power transferred between the constituents, during the establishment of natural circulation.

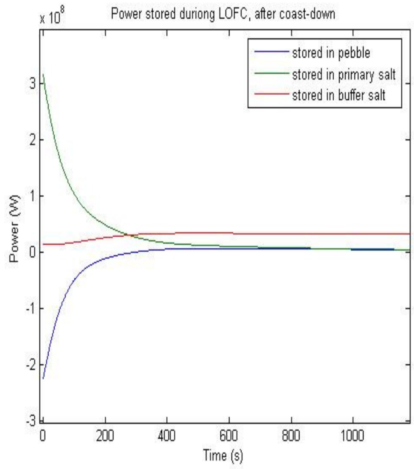

Figure C-11: Power stored by the constituents, during the establishment of natural circulation.

I.2.c. Preliminary conclusions

The temperature of the coolant gained roughly 20°C, which is significant compared to the final rise (order of 60°C).
In this stage, the buffer salt plays a secondary role compared to the primary salt, as its role becomes relevant at the end. Thus the amount of heat transferred to the primary salt is of the order of stored energy in it.
It might be noted that the dynamics of this stage is slower than the coast-down and graphite response to the temperature variations would be sufficiently fast: the assumption of a flat profile in pebble could be still valid.
A very important comment must be added: the temperatures rises found are not taking into account the presence of a reflector and plena. Thus, these rises displayed are extremely conservative.
In this stage, the reflector is slowly heated: this heat sink could generate cells of natural circulation, within the reactor vessel. Moreover, it would be enhanced by the high porosity along the walls of the bed (low pressure drop and heat generation).

I.3. Stage three: quasi-steady heat removal

After a time of an order of tens of minutes, a quasi-steady flow is reached (Figure C-12) and the temperature distribution in the primary loop will not experience any important shape variation (Figure C-7).

I.3.a. Heat up

The heat-up of the core and the primary loop (resulting from the misbalance between the heat removed by the PHX and the convection heat transfer in the core) increases the PHX power, since the buffer salt temperature increases more slowly (larger mass, order of 4 times the primary salt one). The peak coolant temperature corresponds to the time where the PHX match the heat delivered by the core. The resulting effective cooling of the primary salt

reduces then the power of the PHX. This characteristic time is reached after a long time of 1 hour. The peak temperature is 760°C as shown in Figure C-13.
The buffer salt is the main heat sink of the system, as shown in Figure C-11 and Figure C-15. The influence of the stored energy in the salt and the pebbles is secondary, compared to the energy absorbed by the buffer salt (Figure C-11 and Figure C-15) and the amount exchanged between the constituents by convection (Figure C-14).
In these times, the reflector would be at the same temperature as the coolant.

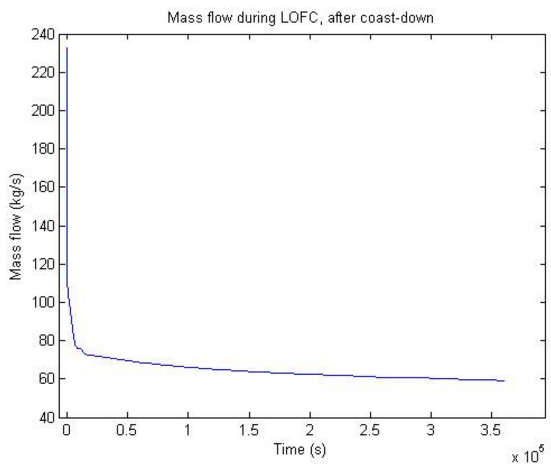

Figure C-12: Mass flow rate, during LOFC

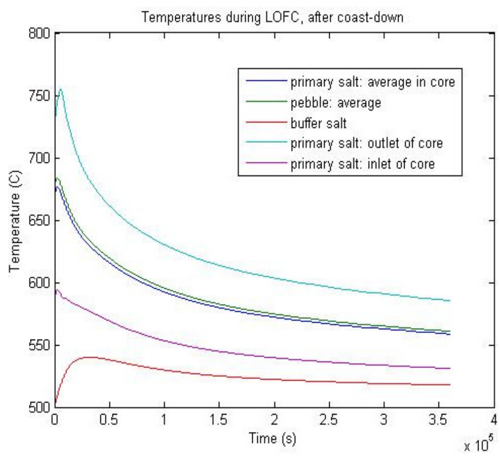

Figure C-13: Characteristic temperatures in the natural circulation loop, during LOFC.

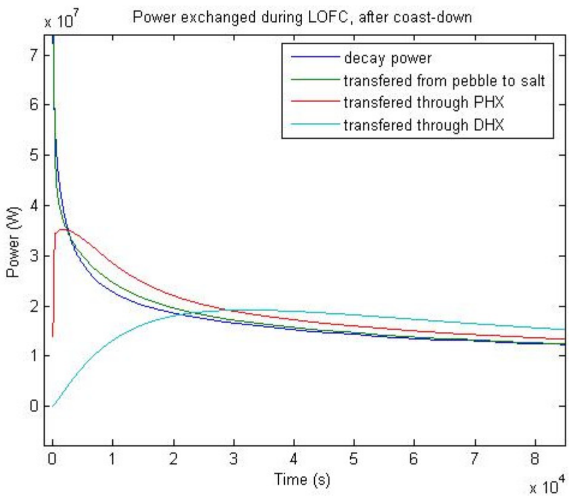

Figure C-14: Power transferred between the constituents, during LOFC.

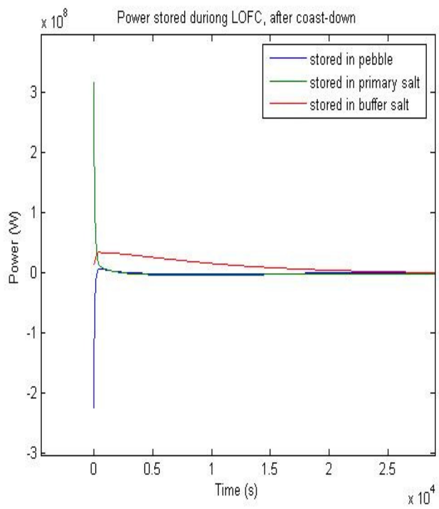

Figure C-15: Power stored by the constituents, during the establishment of natural circulation.

I.3.b. <u>Cooling</u>

The heat removed by the PHX remains superior to the heat transferred by convection in the core. The buffer salt heating is correlated to the increasing heat removal by the DHX. The

buffer salt temperature finally rises a maximum after a long time (order of 10 hours), corresponding to the time where DHX match the PHX heat removal.
During this stage the convective heat transfers regulate the temperature and the heat capacities of the constituents play a secondary role (especially for the core), as shown by Figure C-14 and Figure C-15.
In terms of PIRT, this stage is not relevant has it does not contribute to the peak temperature, which was reached before…

I.3.c. Preliminary conclusions.

An important conclusion of this stage is that the large thermal inertia of the buffer salt allows considering the phenomena linked to the DHX as not relevant. Thus the approximated model of the PHX is valid.
The influence of the convective heat transfer in the PHX region of the buffer salt has been found to be a relevant issue. The AHTR design may retain the addition of baffles around the bundle of PHX tubes. Then forced convection will be studied, rather than natural convection. However, the heat transfer coefficient would not be too much affected, as the Nusselt numbers may remain close. The previous results would still be applicable.

I.4. General conclusions

These calculations showed that the only relevant criterion is the peak coolant temperature (if scram occurs) since the average fuel temperature remains close to the coolant one. The temperature at the center of the fuel will remain also limited with scram.

Additional calculations (see Appendix IX) showed that the initial temperatures profile in the core and in the DHX (using temperatures difference of 50°C) don't influence much the dynamics of the mechanism, as well as the peak coolant temperature. That is why phenomena occurring during the coast-down stage of the transient are not really relevant. This might not be true for the second stage, as its contribution to the peak coolant temperature is important.

The effects of the very large thermal inertia, combined with the efficiency of cooling by natural convection of the liquid salts yield to limited temperature increase. Alloys already developed, as Hastelloy N, can sustain these situations.
However, the values given can only provide an order of estimation of the characteristics of AHTR behavior. Using a real radial power profile in the core increases the maximum outlet temperature at the center of the cross-section area, but still well under the metal failure threshold values.
The design of the natural circulation loop can greatly influence the results: reducing the height of the PHX by keeping the same heat transfer area could result in a higher mass flow rate (higher buoyancy forces) and a smaller temperature drop within the core. The diameter of the PRACS pipes orifices, as the main source of pressure loss, is a key parameter also.

A simplified PIRT that takes into account this comment is proposed in Appendix VII.

Most of the requirements in terms of IET may encompass those proposed for the full power scenario. Some issues have already been found such as convective heat transfer at low Reynolds number in the bed (correlations are uncertain at low Peclet, as highlighted in Appendix VIII) or in the PHX.

APPENDIX I

ADDITIONAL INFORMATIONS ON THE CSAU METHOD AND SAFETY REFERENCES USED

1. IAEA ranking of passive systems.

The IAEA [14, 15] ranks the passive safety systems of a power plant as follows:

Table A.I.1: Categories of Passive systems.

	A	B	C	D
Instrumentation & Control Signal	/	/	/	X
Stored Energy	/	/	/	Battery, or compressed fluid or gravity driven injection
Moving Mechanical Parts	/	/	X	X
Moving Working Fluids	/	X	X	X

2. More about PIRT and the CSAU Method.

PIRTs have mostly been developed in the US for light water reactors and for loss of coolant accidents, as these transients present a complex set of two-phases phenomena. In Europe, PIRTs have begun to rise in importance with the 2002 EURSAFE initiative, but have been focused primarily on the severe accidents (especially phenomena associated with core meltdown) [4].

Fitting in the objectives of Generation IV roadmap, best estimate methods are required to reach better economics while increasing safety. That is why PIRTs are naturally expected to take an important role in the design and licensing of the future advanced nuclear reactors. In the US, this has been illustrated by the efforts of national laboratories [5] and vendors [6] in the Very High Temperature Reactor (VHTR) program, also known as the Next Generation Nuclear Plant (NGNP) initiative. The NRC, through its processes to define new policies for licensing non-light water reactors [7] and research on advanced reactors [8], has also considered this approach in its policy for licensing the new non-water-cooled reactors.

One may note that the CSAU methodology is an illustration of a more general approach defined by the NRC in its recent Regulatory Guide [9], called Evaluation Model Development and Assessment Process (EMDAP), taking part in the safety analysis of a nuclear plant. Contrary to the CSAU methodology, the EMDAP does not necessarily provide formal uncertainty quantification.

The Advanced High Temperature Reactor (AHTR-MI), as an advanced candidate for hydrogen and electricity production, will be licensed following the CSAU methodology. The first 3 steps of this 14 steps process correspond to the PIRT development itself.

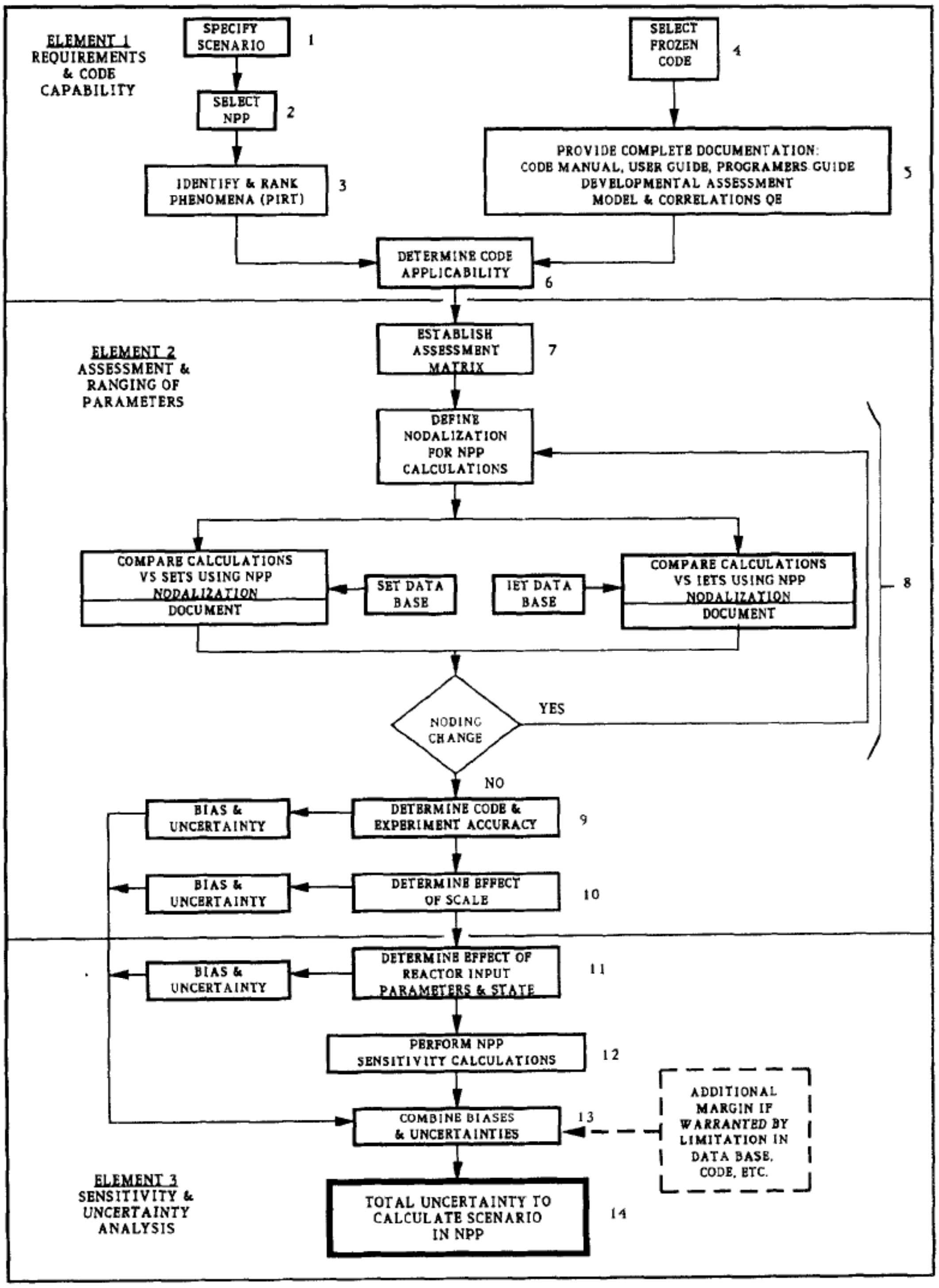

Figure A.I.1: Code scaling, applicability and uncertainty evaluation methodology [2].

3. Vocabulary used for off-normal events

Since the first safety analysis reports were created for nuclear power plants, safety vocabulary has constantly evolved, reflecting the concerns of the national regulatory agencies. This section reviews the vocabulary, to provide context for the subsequent discussion.

For off-normal transients and accidents, the initiator of the transient is referred to as a Postulated

Initiating Event (PIE) and can arise from an internal or external source. A PIE, combined with defined initial conditions and sometimes with other actions (operator, operational or safety-related component failure or spurious action) then generates to off-normal events scenarios.
These off-normal scenarios can be divided into two main categories:

- Within design-basis events (when studied during a licensing process, called by the US NRC the Licensing Basis Events):
  - Anticipated operational occurrences (AOO) (or transients), with an annual frequency of occurrence of the sequence greater than 10^{-2}, per plant. These off-normal events are expected to have significant probability of occuring once or more in plant's life.
  - Design basis accidents (DBA or DBE), with an annual frequency of occurrence of the sequence between 10^{-2} and 10^{-5} (or 10^{-4} for the US NRC) per plant. These events are expected to be unlikely to occur in plant's life, but are expected to have significant probability of occurring within an entire fleet of reactors.
- Beyond design basis accidents (BDBA) (very low probability). Among these are severe accidents which result in a partial damage of the core.

DBAs are always assessed by safety analysis reports (SAR), BDBAs are not systematically treated in SARs; this depends on the country. Often analysis for BDBAs does not consider the initiating event, but rather hypothesizes that substantial core damage does occur, and considers the subsequent plant response.

For LWRs, the case of the Anticipated Transients Without Scram (ATWS) must be considered apart: they are sometimes considered as a BDBA [14] or as AOO [23]. The ATWS transient is also of interest for the AHTR-MI.

4. Classical operation modes as defined by the IAEA.

- 1 Initial approach to reactor criticality (once in plant's lifetime);
- 2 Normal reactor startup from shutdown through criticality to power (once every 18 month is the goal);
- 3 Power operation (the availability is expected to be greater than 90%) including both:
  - 3.1. Full power (100 %);
  - 3.2. Low power (40 %);
- 4 Changes in the reactor power level including load following modes if employed;
- 5 Reactor shutdown from power operation (once every 18 month is the goal);
- 6 Shutdown (10 % of the lifetime) in:
  - Hot standby mode (it is not relevant to define an equivalent state to the PWR cold shutdown state, as the temperature and pressure conditions of the primary coolant will remain within the same range);
  - Refueling mode for the prismatic and stringer version of the AHTR.
  - Reflector replacement mode
  - Equivalent maintenance mode that opens major closures in the reactor primary coolant boundary (primary pump replacement);
- 7 Shutdown in other modes or plant configurations with unique temperature, pressure or coolant inventory conditions (one may envision maintenance on buffer salt wetted components for instance);
- 8 Handling and storage of fresh and irradiated fuel (100 % of the lifetime, except the first power production cycle).

5. Classical external events as defined by the IAEA.

Hazards internal to the site include:

- Pipe whipping;
- Impingement forces;
- Internal flooding, spraying, chemical reactions, vapor generation, and gas heating due to leaks or breaks of pipes, pumps, valves;
- Internal missiles;
- Load drop;
- Internal explosion from hydrogen or other combustible gases;
- Fire;
- Loss of off-site power.

Hazards external to the site include:

- Natural external events such as:
    - Extreme weather conditions, resulting in:
        - Extreme wind loading,
        - Extreme atmospheric temperatures,
        - Extremes of rainfall and snowfall,
        - Extreme cooling water temperatures and icing,
        - Extreme amounts of sea vegetation.
    - Earthquakes;
    - External flooding;
- Human generated events such as:
    - Aircraft crashes.
    - Hazards arising from transportation and industrial activities (fire, explosion, missiles, release of toxic gases).

6. IFR approach to determine PIEs.

An example of a general approach to identify the PIEs is given in [21], for the Integral Fast Reactor. A balance of reactivity shows that reactivity is ruled by:

- External reactivity insertion (driven by reactivity control elements)
- Inlet and outlet temperatures of coolant (driven practically by flow and heat sink capacity)
- Void coefficient (if void generation is physically possible)

Hence the following families of PIEs were identified for the IFR:

- Reactivity insertion
- Flow run-up/run-down
- Overcooling/loss of load

Void reactivity is indirectly linked with the other PIE families (e.g., boiling).

7. Different approaches for the definition of PIRT scenarios.

The literature provides two very different approaches to identify a complete set of scenarios:

- Argonne laboratory conducted an initial study [5] to identify the needs in terms of research and code assessment for the VHTR safety analysis program, following the CSAU approach. The objectives of this work are the closest to those for the ATHR-MI. This work relies on the assumption that scenarios can be subsumed in 5 families of events (plus “loss of coolant”), with possibly failure to SCRAM. These event families are directly transitioned in general “operating regimes” (OR) (combination of basic TH parameters), event-independent. Finally, each OR is studied through a component-phenomena decomposition. This structural and simplified method is suitable for a PIRT applying to a pre-conceptual design. However, this assumption that 6 classes of events relies on work for gas cooled reactors [21] that neglects loss of coolant and void fraction issues.

- A detailed investigation has been conducted for the MHTGR [12]. Here 100 potentially interesting scenarios have been constructed and ranked regarding their frequency of occurrence. This number suggests that a risk-informed method has been used. Among the credible scenarios, a few (13) have been selected to address surely the whole space of phenomena. This practical approach produces useful results similar to those from detailed Probability Risk Assessment (PRA), but reduces the resources required.

APPENDIX II

AHTR PIRT SPECIFIC INFORMATIONS

1. AHTR systematic description in sub-systems and components.

Table A.II.1: Detailed description of the components.

Sub-systems		
Components	**Nb**	**Comments**
Primary		
Inlet plenum	1	The inlet plenum extends axially from the lower core region boundary to the outer surface of the reactor vessel. The radial boundary is given by the outer surface of the reactor vessel. The lower reflector is included in the inlet plenum component. For a pebble bed core, the lower reflector is created by the liquid salt in the gap between the bed and the bottom of the reactor vessel.
Core	1	The core is enclosed axially by the two plenums and radially by the inner surfaces of the radial reflector.
Radial reflector	1	This component, annulus-shaped, is radially enclosed by the core and the outer surfaces of the reactor vessel, and is cooled by bypass flow from the core.
Outlet plenum (with control rods)	1	The outlet plenum extends axially from the top core region to the outer surface of the reactor vessel. The radial boundary is given by the outer surface of the reactor vessel. The upper reflector, the control rods and the pebble recirculation system (four 40-cm diameter defueling chutes) are included in this component.
Reactor cover and primary salt pool	1	This section begins at the bottom at the outer surface of the reactor vessel and on the other sides by the outer boundaries of the insulation materials. It includes a liner, the reactor cover, defueling machines, and control rod drives.
Cover gas chemistry control system	1	This component comprises the system for recirculation and chemistry control of the argon cover gas above the primary salt pool
Reactor vessel	1	This component comprises the metallic vessel that contains the reactor reflector, inlet and outlet plenums, cover, and core, and provides the primary structural element supporting these components and transferring horizontal seismic loads through a pin system at the bottom of the buffer salt tank into the reactor cavity structure.
Hot leg (Up-stream pump)	4	These components are pipes which extend from the outer plenum to the primary pumps, and include siphon-break standpipes and high-point gas vents.
Primary pump	4	This region is limited on the top by the shaft bearing.
Primary pump seal bowls and level equalizing lines	4	This region is limited on the bottom by the shaft bearing and also includes the lines between the seal bowls and the primary pool.
Cross-over leg (Down-stream pump)	4	These components extend from the primary pumps (4) to the IHX modules (72). The design of the flow distribution pipes (Christmas tree shaped) is not yet defined. To simplify, 4 cross-over legs are

		assumed.
IHX	72	These components are limited to the primary volume and part of the solid structures (primary manifolds). The spatial arrangement of the IHX modules is flexible and dependent of the design working temperatures. The actual design is 72 IHX modules, grouped in 8 clusters. The flow coming from one cross-leg will divide towards 2x8 parallel IHXs.
Cold leg (Down-stream IHX)	4-16-32	These components extend from the outlet of the IHX to the inlet plenum. As for the cross-over legs design, the link between the numerous IHX and the reduced number of inlet pipes is not yet defined. The prismatic and stringer fuel core designs require 4 cold legs. The pebble-bed version would use more cold legs (likely 32), as these pipes would also be used to inject pebbles at different locations around the inlet plenum, and each cold leg includes a pebble injection and in-service inspection standpipe.
PRACS Heat Exchanger (PHX)	8	These components include an inlet plenum with an in-service inspection standpipe, the tube bundle and the outlet plenum. Metal is also part of the HX.
PRACS pipe	16	Each PHX is linked to the reactor vessel by two pipes (cold and hot). The cold at the bottom of the PHX pipe includes a fluidic diode. Pipes extend from the plenums of the reactor.
Chemistry and volume control system and pebble injection system)	1	This component gathers different systems that extend from the cold legs (highest density), to more complex systems that are not defined yet (e.g. argon filled pebble inspection/injection hot cell).
Intermediate		
Cold leg (up-stream IHX)	4	It extends from the outlet of the secondary-intermediate heat exchanger to the inlet of the IHX, with electrical trace heating and insulation outside the buffer salt tank. It excludes the intermediate pumps. As for the primary pipes, particular shapes for pipes division arrangement have to be defined.
IHX	72	It includes the intermediate salt and part of the solid structures (intermediate salt inlet and outlet manifolds)
Hot leg (down-stream IHX)	4	It extends from the outlet of the IHX to the inlet of the secondary-intermediate heat exchanger, with electrical trace heating and insulation outside the buffer salt tank. As for the primary pipes, particular shapes for pipes division arrangement have to be defined.
Intermediate pumps	4	This component is self-inclusive.
Secondary-Intermediate Heat Exchangers	4	It includes the intermediate salt and part of the solid structures (intermediate manifolds)
Expansion tank to control inventory and pressure	4	This system is linked to the cold leg (highest density). It includes pipe and tank. One system is required for each loop to prevent pollution transmission to other loops in case of leak.
Drain tank	2	This component includes the drain pipes and the tank. 2 components are necessary to deal with clean and contaminated salts in the same time, during maintenance.

Chemistry and volume control system	4	This component is defined in the same way than one of the primary sub-system. The separation of the 4 loops and their associated active systems is a constraint and drives to the need of 4 control systems.
Buffer		
PHX region	8	This region is determined by the outer surface of the baffle that shrouds the PHX bundle to enhance vertical mixing of the buffer salt, and excludes the primary tube bundle itself.
DRACS Heat Exchanger (DHX) region	8	This region is determined by the outer surface of the baffle that shrouds the DHX tube bundle and excludes the tertiary bundles itself.
Reactor vessel region	1	This region is defined by the closeness of the reactor vessel, where natural convection is expected that maintains the reactor vessel at the buffer salt temperature.
Free space	1	This region features the whole buffer salt cavity (delimited by the tank), except the immerged primary objects and the regions defined above.
Cover gas chemistry control system	1	This component comprises the system for recirculation and chemistry control of the argon cover gas in the buffer tank free space, and the system for maintaining $NaBF_3$ partial pressure above the sodium fluoroborate buffer salt
Tank	1	This component includes the metallic tank and the top liner with equipment maintenance and in-service inspection ports over the buffer salt pool.
Tertiary		
Liner / Refractory insulation system / Centering pin / Cavity	1	This region is delimited on the side and bottom (radially and axially) by the outer surface of the buffer salt tank and by the outer surface of the reactor cavity liner. It includes the refractory insulation blocks that line the cavity and reduce heat losses from the buffer tank to the water-cooled cavity liner. It also includes the centering pin system that transfers horizontal seismic loads from the buffer tank to the reinforced concrete structure of the reactor cavity.
DHX	8	These components include an inlet plenum, the tubes bundle and the outlet plenum of the DRACS heat exchangers.
DRACS external exchangers	8	These critical components have not been definitely designed and several options are envisioned (external air or water cooling). It is expected that heat transfer from these heat exchangers will be regulated by external dampers (air) or valves (water) to control heat losses during normal reactor operation.
DRACS hot and cold legs	8	These ducts connect the two heat exchangers.
RCCS	1	The reactor cavity cooling system (RCCS) is composed of an embedded water cooling system under the reactor cavity liner, interconnecting pipes, pumps and the heat exchangers (design not yet defined)
Concrete silo / Containment	1	This region includes the seismically base isolated surrounding structures, around and over the reactor cavity.

2. Estimated reliability of AHTR safety-related components.

Table A.II.2: Elements of judgment for the single failure criterion application.

Failure	Proposed average frequency	Reference	Comments
Failure to SCRAM	10^{-6}	[24]: 10^{-6}, [17]: 1 to 5 10^{-6}	ATWS are often considered as BDBA.
Failure to trip one pump	10^{-3}	[25]: 10^{-3}(feed-water pump during earthquake), [26]: order of 10^{-3} (failure of a pump at solicitation at start-up)	This value is a very conservative one, as the primary pump trip is essential to achieve safety function. This probability will be lowered as much as possible by design and maintenance efficiencies.
Failure to trip the Power Conversion system	10^{-6}	None	Uncouple the alternator from the electrical network is done by simple electrical systems. The trip of the power conversion system is very reliable.
Failure of one DRACS	10^{-2}	[26]: order of 10^{-2} (opening of a pneumatic valve)	This system is not totally passive. A spurious closure/opening of a damper could occur very likely, but a steady failure is not credible, since a long time is available to activate the damper and it can be done manually if required.
Failure of PRACS	10^{-6}	None	This system is totally passive and essential to achieve the safety function. The failure likely to happen would be a break due to high temperatures reached during a heat-up accident, however, to remain with simple sequences, we assume a simple blockage for the failure.
Failure of RCCS	10^{-6}	[24]: 10^{-6} (RCCS is an active water cooled system under normal operation, but is passive (boiling) under accident conditions)	With boiling heat transfer, the RCCS performance is completely passive, and depends only upon maintaining the inventory of replacement water.

3. Criteria for phenomena ranking.

Table A.II.3: Issues arisen in full power scenario.

ISSUE	CRITERIA	PARAMETERS OF INTEREST
ECONOMICS	Long term behavior reliability: which means minimize: - Steady stresses (temperatures gradients, differential pressures, hydrostatic heads), - Corrosion and erosion, - Gas generation, (what is this?) - Irradiation damages (LS, components) - Failure of coatings	- Temperatures distribution - Pressures distribution - Flow velocity - Neutrons flux
	Minimize heat losses	- Temperature distribution
	Achieve high burn-up and long fuel cycles	- Fuel evolution
	Minimize pumping power	- Pressures distribution
SAFETY	Radioprotection: minimize (ALARA principle: 10 CFR 50. Appendix I) the dose to workers (40 CFR 90) and public (and 10 CFR 20).	- Neutrons flux - Gamma flux
	Predict accurate initial conditions for transient's response assessment, particularly: - Temperature of buffer salt (ability to remove heat) - Temperature of fuel (effective Doppler effect and stored energy) - Neutronics performance (temperature, void coefficients)	- Temperatures distribution - Fuel evolution

Table A.II.4: Issues arisen in loss of forced circulation scenario.

ISSUE	CRITERIA	PARAMETERS OF INTEREST
ECONOMICS	Long term behavior reliability: which means minimize the mechanical and thermal cycles.	- Temperatures variation as a function of time, - Pressures variation as a function of time - Peak metal temperature - Peak TRISO particle temperature

SAFETY	Avoid: - Release of radioactive materials (10 CFR 50. Appendix I), - Failure of boundaries (TRISO: 1600 °C, alloy: refers to ASME code up to 950°C), - Primary salt boiling (FLIBE: 1400°C).	- Peak TRISO particle temperature - Peak metal temperature - Peak primary salt temperature
	Sub-criticality	- k_{eff}

Table A.II.5: Criteria for other normal operating mode scenarios.

SCENARIOS	SAFETY ISSUES	PARAMETERS OF INTEREST
Normal reactor startup from shutdown through criticality to power	- No feedbacks: prumpt criticity - Reactivity management, stability of PB (changes in buoyancy and hypothetic movements) - Fatigue	- Rho - temperature gradients evolution
Reactor shutdown from power operation	- No feedbacks: prumpt criticity - Reactivity management, stability of PB (changes in buoyancy and hypothetic movements) - Fatigue - Poisons	- rho - temperature gradients evolution
Shutdown	- Avoid local freezing of coolant	- Temperature distribution

4. Overwiew of Phenomena in AHTR.

This comprehensive list has been drawn after a review of different PIRTs specific to high temperature reactors.

Phenomena are usually ranked in flexible families.

Table A.II.6: Phenomena expected.

Phenomena	Description and Particularities
Power	
Neutronics	Power distributions are functions of time and space. Feedback phenomena are included in this topic (among them, interaction between reactivity and pebble movement, poisoning, Doppler effect). It applies only to transients.
Decay heat	Heat produced after SCRAM. Tables or codes have to predict this heat source.
Steady state	Power distributions are function of space. Coupled neutronics and TH code will have to predict the distribution of power. It applies only to the "power" operating regime.
Gamma heating	Gamma rays generate heat when hitting structures (graphite in fuel for instance). Could be ignored for a lump PIRT.
Flow:	
Forced one dimensional	Pumps force flow in one direction path. Equation of momentum simpler, Pressure drop to be calculated.
Forced multi-dimensional	Pumps force flow in 2 or 3 directions. 3-D flow in a pebble bed may need a very important work of code's applicability verification. Plenums are also concerned.
Natural circulation (loop)	One dimensional, closed loop, flow driven by gravity forces.
Natural circulation (pool/cavity)	Multi-dimensional flow driven by gravity forces. Some "dead" ends pipes are described that way. See also comments about 3-D forced flow in PB.
Transition in flow nature	Flow characteristics are modified (e.g. from turbulent to laminar) and mixed flow occurs. This transition zone, which can be steady, has impact on prediction of accurate heat transfer coefficients (difficulties in the particular case of mixed convection, in the transition zone)
Multiphase	2 phases are coexisting in a sub-system. The issue is to measure the impact on neutronics, pressure drop, and heat transfer characteristics of this void ingress. This point is linked with pump cavitation and multi-component issues, as we do not expect boilings.
Multi-component	A fluid is composed of different fluids. It can also include the case of cover gas entrainment. The issue is to measure the impact on neutronics, pressure drop, heat transfer characteristics and possible chemistry reactions.
Heat transfer	
Mixing	Fluid can be not perfectly mixed and some hot streaks occur. It is possible for an AHTR, however the high Prandtl number of liquid salts will help reduce resulting thermal stresses in materials
Radiation	Heat is transferred from a solid surface through a intermediate medium
Forced convection	Heat transfer coefficient is dictated by the nature of flow, which is driven by external force.
Mixed convection	External and buoyancy forces are comparable and heat transfer coefficient is modified.
Natural convection	Heat transfer coefficient is dictated by a buoyancy-driven flow.
Conduction	Heat transfer by conduction through a solid sub-system. Does not

	address pipe walls?
Stratification	Temperatures are distributed in layers in sub-systems where circulation is negligible.
Boiling	Coolant boils. Rare, situation studied in BDBA
Gas release	Coolants release gases (activation, decomposition) which modify heat transfer characteristics.
Condensation	Some of released gases condensate
Stored energy	Thermal capacities of some components permit energy storage. Energy can be released during transients phases and can modify conduction mechanisms. Phenomena of interest during transient, where conduction plays a major part of heat removal.
Others	
Fouling	Coolant is fouled by impurities: graphite dust, corrosion products, oxidation in particular cases. Components walls are fooled by these impurities, forming an insulating layer and imbedding heat transfer. Oxidation in RCCS (water)
Change in mechanical stresses (mechanical fatigue)	During transients, pressures are modified, changing also the mechanical stresses. Fatigue. The AHTR is working at near atmospheric pressures, thus this phenomenon is expected to remain limited. We can study the changes on loads due to hydrostatic head changes with temperature.
Changes in temperature gradients in components thickness (thermal stresses-induced fatigue)	During transients, temperatures gradients are changing, generating fatigue in materials where these stresses occur.
Steady mechanical stresses	Stresses created by differential pressures are altering the long-term reliability of components. Intermediate heat exchangers are the components to be concerned as AHTR is mainly working at near atmospheric pressure.
Steady thermal stresses	Stresses created by differential temperatures are altering the long-term reliability of components. This phenomena is of important significance has AHTR is working at high temperatures, however, design is studied to minimize these differences within the components. IHX are subject to complex stresses.
Cavitation	Due to a low level of fluid, pump cavitation occurs, resulting in a possible 2-phase fluid injection. The issue is to define the behavior of the pump in a 2-phases flow and quantify the volume of void injected in the loop. Only for DBA
TRISO failure	Migration of the kernel within the TRISO particle due to non-uniform creation of CO_2. This is influenced by temperature gradient. Phenomena important at the edge of the core. Mostly found for TRISO particles loaded with Pu. The motion (even slight) of pebbles through the salt flow could help to mitigate this phenomenon.
Irradiation	Neutrons and gamma flux alter mechanical behavior of components and modify composition of coolant (activation)

Specific to helium loops	
Compression	Compressibility of helium (and its phenomena associated, like détente or blow-down) drives its TH characteristics.
Abrupt change in flow nature	A brutal change in flow nature occurs when a fast-response safety system stops circulation in a loop (safety valve).

APPENDIX III

GENERAL LIST OF POSTULATED INITIATING EVENTS

Primarely affected general parameter	Class of the Postulated Initiating Event (PIE)	Sub-class of the PIE (if necessary)	Postulated Initiating Events							
			Primary	P	Intermediate :	I	Buffer	B	Tertiary	T
ENERGY	Heat source	Increase	Reactivity insertion (withdrawal of one group of control rods).	P11-1	Spurious heating by the stand-by heaters	I11	Spurious heating by the stand-by heaters	B11	Fire (hazard).	T11-1
			Power distribution anomaly (errors in fuel position,spurious CR insertion and flux pinching)	P11-2					Spurious heating by the stand-by heaters	T11-2
			Spurious heating by the stand-by heaters	P11-3						
		Decrease	Heating system failure when stand-by.	P12-1	Heating system failure when stand-by.	I12	Heating system failure when stand-by.	B12	Heating system failure when stand-by.	T12
			Spurious scram.	P12-2						
	Heat sink	Increase	*The primary sub-system does not contain any heat sink.*	/	Load increase.	I21	*The buffer sub-system does not contain any heat sink.*	/	Decrease of outside temperatures (hazard).	T21
		Decrease	*The primary sub-system does not contain any heat sink.*	/	Load decrease	I22-1	*The buffer sub-system does not contain any heat sink*	/	Increase of outside temperatures (hazard).	T22
					Loss of load	I22-2				
MOMENTUM	Flow properties	Flow blockage / run-down	Loss of forced circulation (the motor stops, due to a loss of power, human error, the shaft breaks, etc...). Natural circulation occurs as cooling is still active.	P31-1	Loss of forced circulation (the motor stops or the shaft breaks).	I31-1	*The buffer sub-system does not contain any pump.*	/	*The tertiary sub-system may require pumps only for the RCCS. But this point is not yet defined.*	/
			Flow blockage : channels/pipes are blocked by migrant impurities. Natural circulation is hindered or non-existent. The main possible affected regions are:	P31-2	Flow blockage : pipes or IHX are blocked by migrant impurities or by the spurious closure of a valve.	I31-2	Flow blockage : insulating layer of impurities on buffer salt side. The main possible affected regions are:	B31	Flow blockage: pipes are blocked by migrant impurities or by the spurious closure of a valve (water cooling system) or a damper (air cooling system). The main systems possibly affected are:	T31
			o pipes external to the core vessel, but regarding their diameter, this event can be ignored.				o DRACS HX		o RCCS	
			o core (fuel blocks, stringer, pebbles bed)				o PRACS HX		o DRACS HX	
			o reflector o IHX o PRACS						o DRACS loops but regarding their diameter, this event can be ignored.	
		Flow run-up	Flow run-up. Primary pump speed increases anormally (cavitation occurs, or automatic shutdown, or breakdown). Spurious start-up of an inactive pump.	P32	Flow run-up. Intermediate pump speed increases anormally. Cavitation occurs, or automatic shutdown, or breakdown.	I32	*The buffer sub-system does not contain any pump or regulating valve.*	/	Flow run-up : storm (hazard), floodings (hazard). It can also be induced by the spurious wide opening of a regulated valve or damper on the cooling systems.	T32
		Flow instabilities and oscillations	Off-normal fuel motion (pebbles, blocks, stringers) or component vibration (pipe) induced by a vibratory mode (mechanical interaction between materials and fluid due to error in design and sudden failure of some materials). This event will occur preferencially during non steady state mode, where flow speed will change.	P33-1	Off-normal component vibration (pipe) induced by a vibratory mode (mechanical interaction between materials and fluid due to error in design and sudden failure of some materials). This event will occur preferencially during non steady state mode, where flow speed will change.	I33-1	*The buffer sub-system is design to work with natural circulation. No vibration would occur due to low speeds.*	/	Off-normal component vibration (RCCS pipe) induced by a vibratory mode (mechanical interaction between materials and fluid due to error in design and sudden failure of some materials). This event will occur preferencially during non steady state mode, where flow speed will change.	T33-1
			Shaking of fluid and material due to seismic motion (hazard).	P33-2	Shaking of fluid and material due to seismic motion (hazard).	I33-2	Shaking of fluid and material due to seismic motion (hazard).	B33	Shaking of fluid and material due to seismic motion (hazard).	T33-2

Note: the break in a sub-system boundary are represented by colors.
The following code is used:

Green for Primary-Buffer break
Red for Primary-Intermediate break
Orange for Intermediate-Buffer break
Yellow for Buffer-Tertiary break
Blue for breaks towards air or atmosphere.

Primarely affected general parameter	Class of the Postulated Initiating Event (PIE)	Sub-class of the PIE (if necessary)	Postulated Initiating Events							
			Primary	P	Intermediate :	I	Buffer	B	Tertiary	T
MASS	Break in containment : changes in coolant inventory and nature		Size of Loss Of Coolant Accident (LOCA): small (pinehole), moderate break, large break, spurious opening of a valve. Studies should adress these different cases. The main different possible regions are:	P4-1	Size of LOCA: small (pinehole), moderate break, large break, spurious opening of a valve. Studies should adress these different cases.	I4-1	Size of LOCA: small (pinehole), moderate break, large break, spurious opening of a valve. Studies should adress these different cases.	B4-1	Size of LOCA: small (pinehole), moderate break, large break, spurious opening of a valve. Studies should adress these different cases.	T4-1
			o Primary pipe (up-stream pump). o Primary pipe (down-stream pump). o IHX primary side.				o Primary pipe (up-stream pump). o Primary pipe (down-stream pump). o IHX primary side.			
			o IHX intermediate side.		o IHX intermediate side. o Intermediate pipe/HX (inside the buffer tank).		o Intermediate pipe/HX (inside the buffer tank).			
			o Primary loop extruding from core vessel to outside (inside the buffer tank) (chemistry control, pebbles injector)				o Primary loop chemistry and activation control system (inside the buffer tank)			
			o PRACS (especially the PHX as thin tubes are used)				o PRACS (especially the PHX as thin tubes are used)			
			o Core vessel.				o Core vessel.			
							o DRACS (especially the DHX as thin tubes are used)		o DRACS (especially the DHX as thin tubes are used)	
			o Primary loop extruding from core vessel to outside (outside the buffer tank, at the atmosphere) (chemistry control, pebbles injector)		o Intermediate loop (at the atmosphere)		o Buffer tank (in the argon filled cavity).		o Other loops used for passive cooling (RCCS, DRACS)	
							o Buffer loop extruding to outside, at the atmosphere (chemistry control)			
			Intrusion / Extrusion of gases via normal connections: gas entrainment (in pebble injection system for instance), loss of argon of the primary pool, or spurious pressurization of the argon cover.	P4-2	Intrusion / Extrusion of gases via normal connections (gas of expansion tank for instance)	I4-2	Intrusion / Extrusion of gases via normal connections (loss of argon of the buffer salt tank cover, for instance)	B4-2	Intrusion / Extrusion of gases via normal connections (introduction of air in the DRACS Flinak loop via the chemistry control system)	T4-2
			Failure of coatings in a fuel particle	P4-3					Failure in the tertiary boundary (concrete containment, spurious opening of a valve or damper)	T4-3

Note: the break in a sub-system boundary are represented by colors.
The following code is used:
Green for Primary-Buffer break
Red for Primary-Intermediate break
Orange for Intermediate-Buffer break
Yellow for Buffer-Tertiary break
Blue for breaks towards air or atmosphere.

Primarely affected general parameter	class of the Postulated Initiating Event (PIE)	sub-class of the PIE (if necessary)	Postulated Initiating Events							
			Primary	P	Intermediate :	I	Buffer	B	Tertiary	T
ENERGY	heat source	increase	Reactivity insertion (withdrawal of one group of control rods).	P11-1	Spurious heating by the stand-by heaters	I11	Spurious heating by the stand by heaters	B11	Fire (hazard).	T11-1
			Power distribution anomaly (errors in fuel position,spurious CR insertion and flux pinching)	P11-2					Spurious heating by the stand-by heaters	T11-2
			Spurious heating by the stand-by heaters	P11-3						
		decrease	Heating system failure when stand-by.	P12-1	Heating system failure when stand-by.	I12	Heating system failure when stand-by.	B12	Heating system failure when stand-by.	T12
			Spurious scram.	P12-2						
	heat sink	increase	*The primary sub-system does not contain any heat sink.*	/	Load increase.	I21	*The buffer sub-system does not contain any heat sink.*	/	Decrease of outside temperatures (hazard).	T21
		decrease	*The primary sub-system does not contain any heat sink.*	/	Load decrease	I22-1	*The buffer sub-system does not contain any heat sink*	/	Increase of outside temperatures (hazard).	T22
					Loss of load	I22-2				
MOMENTUM	Flow properties	flow blockage / run-down	Loss of forced circulation (the motor stops, due to a loss of power, human error, the shaft breaks, etc...). Natural circulation occurs as cooling is still active.	P31-1	Loss of forced circulation (the motor stops or the shaft breaks).	I31-1	*The buffer sub-system does not contain any pump.*	/	*The tertiary sub-system may require pumps only for the RCCS. But this point is not yet defined.*	/
			Flow blockage : channels/pipes are blocked by migrant impurities. Natural circulation is hindered or non-existent. The main possible affected regions are: o pipes external to the core vessel, but regarding their diameter, this event can be ignored. o core (fuel blocks, stringer, pebbles bed) o reflector o IHX o PRACS	P31-2	Flow blockage : pipes or IHX are blocked by migrant impurities or by the spurious closure of a valve.	I31-2	Flow blockage : insulating layer of impurities on buffer salt side. The main possible affected regions are: o DRACS HX o PRACS HX	B31	Flow blockage: pipes are blocked by migrant impurities or by the spurious closure of a valve (water cooling system) or a damper (air cooling system). The main systems possibly affected are: o RCCS o DRACS HX o DRACS loops but regarding their diameter, this event can be ignored.	T31
		flow run-up	Flow run-up. Primary pump speed increases anormally (cavitation occurs, or automatic shutdown, or breakdown). Spurious start-up of an inactive pump.	P32	Flow run-up. Intermediate pump speed increases anormally. Cavitation occurs, or automatic shutdown, or breakdown.	I32	*The buffer sub-system does not contain any pump or regulating valve.*	/	Flow run-up : storm (hazard), floodings (hazard). It can also be induced by the spurious wide opening of a regulated valve or damper on the cooling systems.	T32
		Flow instabilities and oscillations	Off-normal fuel motion (pebbles, blocks, stringers) or component vibration (pipe) induced by a vibratory mode (mechanical interaction between materials and fluid due to error in design and sudden failure of some materials). This event will occur preferencially during non steady state mode, where flow speed will change.	P33-1	Off-normal component vibration (pipe) induced by a vibratory mode (mechanical interaction between materials and fluid due to error in design and sudden failure of some materials). This event will occur preferencially during non steady state mode, where flow speed will change.	I33-1	*The buffer sub-system is design to work with natural circulation. No vibration would occur due to low speeds.*	/	Off-normal component vibration (RCCS pipe) induced by a vibratory mode (mechanical interaction between materials and fluid due to error in design and sudden failure of some materials). This event will occur preferencially during non steady state mode, where flow speed will change.	T33-1
			Shaking of fluid and material due to seismic motion (hazard).	P33-2	Shaking of fluid and material due to seismic motion (hazard).	I33-2	Shaking of fluid and material due to seismic motion (hazard).	B33	Shaking of fluid and material due to seismic motion (hazard).	T33-2

Note: the break in a sub-system boundary are represented by colors.
The following code is used:
Green for Primary-Buffer break
Red for Primary-Intermediate break
Orange for Intermediate-Buffer break
Yellow for Buffer-Tertiary break
Blue for breaks towards air or atmosphere.

Primarely affected general parameter	class of the Postulated Initiating Event (PIE)	sub-class of the PIE (if necessary)	Postulated Initiating Events							
			Primary	P	Intermediate :	I	Buffer	B	Tertiary	T
MASS	Break in containment : changes in coolant inventory and nature		Size of Loss Of Coolant Accident (LOCA): small (pinehole), moderate break, large break, spurious opening of a valve. Studies should adress these different cases. The main different possible regions are:	P4-1	Size of LOCA: small (pinehole), moderate break, large break, spurious opening of a valve. Studies should adress these different cases.	I4-1	Size of LOCA: small (pinehole), moderate break, large break, spurious opening of a valve. Studies should adress these different cases.	B4-1	Size of LOCA: small (pinehole), moderate break, large break, spurious opening of a valve. Studies should adress these different cases.	T4-1
			o Primary pipe (up-stream pump). o Primary pipe (down-stream pump). o IHX primary side.				o Primary pipe (up-stream pump). o Primary pipe (down-stream pump). o IHX primary side.			
			o IHX intermediate side.		o IHX intermediate side.					
					o Intermediate pipe/HX (inside the buffer tank).		o Intermediate pipe/HX (inside the buffer tank).			
			o Primary loop extruding from core vessel to outside (inside the buffer tank) (chemistry control, pebbles injector)				o Primary loop chemistry and activation control system (inside the buffer tank)			
			o PRACS (especially the PHX as thin tubes are used)				o PRACS (especially the PHX as thin tubes are used)			
			o Core vessel.				o Core vessel.			
							o DRACS (especially the DHX as thin tubes are used)		o DRACS (especially the DHX as thin tubes are used)	
			o Primary loop extruding from core vessel to outside (outside the buffer tank, at the atmosphere) (chemistry control, pebbles injector)		o Intermediate loop (at the atmosphere)		o Buffer tank (in the argon filled cavity).		o Other loops used for passive cooling (RCCS, DRACS)	
							o Buffer loop extruding to outside, at the atmosphere (chemistry control)			
			Intrusion / Extrusion of gases via normal connections: gas entrainment (in pebble injection system for instance), loss of argon of the primary pool, or spurious pressurization of the argon cover.	P4-2	Intrusion / Extrusion of gases via normal connections (gas of expansion tank for instance)	I4-2	Intrusion / Extrusion of gases via normal connections (loss of argon of the buffer salt tank cover, for instance)	B4-2	Intrusion / Extrusion of gases via normal connections (introduction of air in the DRACS Flinak loop via the chemistry control system)	T4-2
			Failure of coatings in a fuel particle	P4-3					Failure in the tertiary boundary (concrete containment, spurious opening of a valve or damper)	T4-3

Note: the break in a sub-system boundary are represented by colors.
The following code is used:

Green for Primary-Buffer break
Red for Primary-Intermediate break
Orange for Intermediate-Buffer break
Yellow for Buffer-Tertiary break
Blue for breaks towards air or atmosphere.

APPENDIX IV

SIMPLIFIED LIST OF POSTULATED INITIATING EVENTS

Family	S-System	Postulated Initiating Event	Reference IRSN (LWR)	Reference INPRO 2005 (LWR)	Reference PBMR	Judgement of the PIE	Probability
increase	P	Reactivity insertion (withdrawal of one group of control rods).	steady withdrawal: AOO, ejection DBA-BDBA			We retain only a steady withdrawal, as no excessive pressure in the primary system could eject a control rod.	AOO
	P	Power distribution anomaly (errors in fuel position, spurious CR insertion and flux pinching)	AOO-DBA			The uncertainties regarding the pebble behavior in the bed, and errors I fabrication could lead to have distortions in reactivity through the bed.	AOO
	PIBT	Spurious heating by the stand-by heaters				At full power, we may assume that this event is negligible regarding the total power and forced flow at stake.	Neglected
decrease	PIBT	Heating system failure when stand-by (it could be generated by a loss of off-site power)				Freezing issues are often criticized. Reliability must be demonstrated. Loss of off-site power are relevant issues.	AOO
	P	Spurious scram.	AOO	5. 10^{-1}		This "safe" event is frequent.	AOO
increase	I	Load increase.	AOO				AOO
decrease	I	Load decrease	AOO	Turbine/by-pass malfunctonning: 1. 10^{-1}		Transient bounded in severity by a total loss of load	Neglected
	I	Loss of load. One could assume that some heat can still be removed from primary salt as long as some circulation remains in the intermediate loop.	AOO	loss of heat sink: 3. 10^{-1}	loss of power conversion system: 3.5 10^{-2}	This transient (AOO) bounded in severety by a total flow blockage in intermediate loop (DBA).	Neglected
flow blockage / run-down	P	Loss of forced circulation (the motor stops, due to a loss of power, human error, the shaft breaks, etc...). Natural circulation could occur as cooling is still active.	partial: AOO (one pump: 7. 10^{-2} two pumps: 1. 10^{-2}), total: DBA (it appears not consistent with the frequency of a loss of off-site power)	Loss of off-site power: 2. 10^{-2}		Two PIE should be studied: all pumps trip (loss of off-site power) and partial trip. A partial trip is bounded in severity by a primary pump seizure (the transient is more "steep").	AOO
	P	Flow blockage : channels/pipes are blocked by migrant impurities. The flow area is reduced. Natural circulation is hindered or non-existent. The main possible affected regions are:	partial: DBA, total (e.g. pump rotors seized: BDBA				
	P	o pipes external to the core vessel.				We retain only a primary pump shaft seizure. Blockages of pipes can be ignored, regarding their diameter.	DBA
	P	o core (fuel blocks, stringer, pebbles bed)				One may only retain a partial blocage of the core, total blockage is not realistic.	DBA
	P	o reflector				One may only retain a partial blocage of the reflector, total blockage is not realistic.	DBA
	P	o IHX (few on one loop to remain realistic)				One retain a partial blocage of one IHX (narrow channels), total blockage is not realistic. Partial blockage of several IHX could be possible (blockage in a division of cross-over legs)	one: AOO several: DBA
	P	o PRACS (one, more wouldn't be unrealistic)				One may only retain a partial blocage of one PRACS (few tubes blocked by impurities), total blockage is not likely to occur (for instance, blockage of the upper pipe linked to the outlet plenum, by a piece of reflector, broken away when natural circulation establishes and flow reverses).	total : DBA partial : AOO
	I	Loss of forced circulation (the motor stops or the shaft breaks). If the design allows it, some natural circulation could be possible.	total: AOO	loss of feed water: 2. 10^{-1}	loss of power conversion system: 3.5 10-2	Transient bounded by a loss of load. Consequences for the core are similar to a loss of load, but are limited locally to an IHX. Heat is still removed, but much slowly.	Neglected
	I	Flow blockage : pipes or IHX are blocked by migrant impurities or by the spurious closure of a valve. No circulation. This event is a loss of cooling event. No heat removal through IHX, except by conduction.	total: AOO	loss of feed water: 2. 10^{-1}	loss of power conversion system: 3.5 10-2	The blockage of the flow in all the loops would be a DBA (spurious closure of valves). In one loop could be more frequent.	total : DBA partial : AOO
	B	Flow blockage : insulating layer of impurities on buffer salt side. The main possible affected regions are:					
	B	o DRACS HX				The deposition of an insulating layer is prevented by inspection. Impurities could block partially the flow through the bundles. Blockage by freezing of the salt is not tackled because it is induced by another PIE.	DBA
	B	o PRACS HX				The geometry is similar than DRACS one, so the risks are the same than for DRACS HX	DBA
	T	Flow blockage: pipes are blocked by migrant impurities (vegetal, etc...) or by the spurious closure of a valve (water cooling system) or a damper (DRACS air cooling system). The main systems possibly affected are:					
	T	o RCCS				This partly passive system is safety related: a failure could be a DBA. Its design is not modular, thus a failure, could be significant.	DBA
	T	o DRACS loops but regarding their diameter, this event can be ignored.					Neglected
	T	o DRACS (air cooling, liquid alt DRACS HX)	Valve failure: order of 10^{-2}			We consider a total blockage of one DRACS system: a spurious closure of a damper could occur.	DBA
flow run-up	P	Flow run-up. Primary pump speed increases anormally (cavitation occurs, or automatic shutdown, or breakdown). Spurious start-up of an inactive pump.				We retain an increase for one pump.	AOO
	I	Flow run-up. Intermediate pump speed increases anormally. Cavitation occurs, or automatic shutdown, or breakdown.		Overfeeding: 2. 10^{-1}		Consequences for the core are similar to an increase of load. This phenomenon would be locally limited to a bunch of IHX.	AOO
	T	Flow run-up : storm (hazard), floodings (hazard). It can also be induced by the spurious wide opening of a regulated valve or damper on the cooling systems.	spurious opening of a pneumatic valve: 10^{-2}			We retain this event for one DRACS.	AOO

Family	S-System	Postulated Initiating Event	Reference IRSN (LWR)	Reference INPRO 2005 (LWR)	Reference PBMR	Judgement of the PIE	Probability
Flow instabilities and oscillations	P	Off-normal fuel motion (pebbles, blocks, stringers) or component vibration (pipe) induced by a vibratory mode (mechanical interaction between materials and fluid due to error in design and sudden failure of some materials). This event will occur preferencially during non steady state mode, where flow speed will change (small probability).				These events are external in case of seismic motion. The internal events are due to error design and early failure. Only internal events are retained and are assumed to occur once in plant's life time (vibration during the first start-up after a badly managed maintenance). Classify this event as an AOO is not too pessimistic (e.g. british AGRs suffered from these issues).	External: Neglected, Internal: AOO
	I	Off-normal component vibration (pipe) induced by a vibratory mode (mechanical interaction between materials and fluid due to error in design and sudden failure of some materials). This event will occur preferencially during non steady state mode, where flow speed will change (small probability).				These events are external in case of seismic motion. The internal events are due to error design and early failure. Only internal events are retained and are assumed to occur once in plant's life time (vibration during the first start-up after a badly managed maintenance)	External: Neglected, Internal: AOO
	T	Off-normal component vibration (RCCS pipe) induced by a vibratory mode (mechanical interaction between materials and fluid due to error in design and sudden failure of some materials). This event will occur preferencially during non steady state mode, where flow speed will change (small probability).				These events are external in case of seismic motion. The internal events are due to error design and early failure. Only internal events are retained and are assumed to occur once in plant's life time (vibration during the first start-up after a badly managed maintenance)	External: Neglected, Internal: AOO
Break in containment : changes in coolant inventory and nature		Size of Loss Of Coolant Accident (LOCA): small (pinhole), moderate break, large break, spurious opening of a valve. Studies should adress these different cases. One break is studied, more wouldn't be realistic. The main different possible regions are:	Large break: BDBA	Large break: 10^{-7}, Medium: 9. 10^{-6}, Small: 3. 10^{-5}		All events presenting estimated frequencies for AOO or DBA should be assessed.	
	P-B	o Primary pipe (up-stream pump). (one, more wouldn't be unrealistic)	small break or valve (if any) opening: DBA				DBA
	P-B	o Primary pipe (down-stream pump). (one, more wouldn't be unrealistic)					DBA
	P-B	o IHX primary side.(one, more wouldn't be unrealistic)					DBA
	P-I	o IHX intermediate side, (intermediate pressure is high)					medium break : DBA pinhole : AOO
	I-B	o Intermediate pipe/HX (inside the buffer tank), (intermediate pressure is high, high risks in the IHX, due to thermal stresses)					break : DBA pinhole (HX): AOO
	P-B	o Primary loop extruding from core vessel to outside (inside the buffer tank) (chemistry control, pebbles injector)					DBA
	P-B	o PRACS (especially the PHX as thin tubes are used)					DBA
	P-B	o Core vessel.				This event is a beyond design basis event.	Neglected
	B-T	o DRACS (especially the DHX as thin tubes are used)					DBA
	P-T	o Primary loop extruding from core vessel to outside (outside the buffer tank, at the atmosphere) (chemistry control, pebbles injector)					DBA
	I-T	o Intermediate loop (at the atmosphere)	spurious opening of a valve: AOO				DBA
	B-T	o Buffer tank (in the argon filled cavity).				This event is a beyond design basis event.	Neglected
	B-T	o Buffer loop extruding to outside, at the atmosphere (chemistry control)					DBA
	T-T	o Other loops used for passive cooling (RCCS, DRACS)					DBA
	PIBT	Intrusion / Extrusion of gases via normal connections					AOO
	P	Failure of coatings in a fuel particle (small release)					AOO (misconception)
	T	Failure in the tertiary boundary (concrete containment, spurious opening of a valve or damper)				The failure of the concrete containment is a beyond design basis event. A spurious opening of a valve is common.	AOO

Family	S-System	Postulated Initiating Event	Reference IRSN (LWR)	Reference INPRO 2005 (LWR)	Reference PBMR	Judgement of the PIE	Probability
flow run-up	P	Flow run-up. Primary pump speed increases anormally (cavitation occurs, or automatic shutdown, or breakdown). Spurious start-up of an inactive pump.				We retain an increase for one pump.	AOO
	I	Flow run-up. Intermediate pump speed increases anormally. Cavitation occurs, or automatic shutdown, or breakdown.		Overfeeding: 2. 10^{-1}		Consequences for the core are similar to an increase of load. This phenomenon would be locally limited to a bunch of IHX.	AOO
	T	Flow run-up : storm (hazard), floodings (hazard). It can also be induced by the spurious wide opening of a regulated valve or damper on the cooling systems.	spurious opening of a pneumatic valve: 10^{-2}			We retain this event for one DRACS.	AOO
Flow instabilities and oscillations	P	Off-normal fuel motion (pebbles, blocks, stringers) or component vibration (pipe) induced by a vibratory mode (mechanical interaction between materials and fluid due to error in design and sudden failure of some materials). This event will occur preferencially during non steady state mode, where flow speed will change (small probability).				These events are external in case of seismic motion. The internal events are due to error design and early failure. Only internal events are retained and are assumed to occur once in plant's life time (vibration during the first start-up after a badly managed maintenance). Classify this event as an AOO is not too pessimistic (e.g. british AGRs suffered from these issues).	External: Neglected, Internal: AOO
	I	Off-normal component vibration (pipe) induced by a vibratory mode (mechanical interaction between materials and fluid due to error in design and sudden failure of some materials). This event will occur preferencially during non steady state mode, where flow speed will change (small probability).				These events are external in case of seismic motion. The internal events are due to error design and early failure. Only internal events are retained and are assumed to occur once in plant's life time (vibration during the first start-up after a badly managed maintenance)	External: Neglected, Internal: AOO
	T	Off-normal component vibration (RCCS pipe) induced by a vibratory mode (mechanical interaction between materials and fluid due to error in design and sudden failure of some materials). This event will occur preferencially during non steady state mode, where flow speed will change (small probability).				These events are external in case of seismic motion. The internal events are due to error design and early failure. Only internal events are retained and are assumed to occur once in plant's life time (vibration during the first start-up after a badly managed maintenance)	External: Neglected, Internal: AOO
Break in containment : changes in coolant inventory and nature		Size of Loss Of Coolant Accident (LOCA): small (pinhole), moderate break, large break, spurious opening of a valve. Studies should adress these different cases. One break is studied, more wouldn't be realistic. The main different possible regions are:	Large break: BDBA	Large break: 10^{-7}, Medium: 9. 10^{-6}, Small: 3. 10^{-5}		All events presenting estimated frequencies for AOO or DBA should be assessed.	
	P-B	o Primary pipe (up-stream pump). (one, more wouldn't be unrealistic)	small break or valve (if any) opening: DBA				DBA
	P-B	o Primary pipe (down-stream pump). (one, more wouldn't be unrealistic)					DBA
	P-B	o IHX primary side.(one, more wouldn't be unrealistic)					DBA
	P-I	o IHX intermediate side, (intermediate pressure is high)					medium break : DBA pinhole : AOO
	I-B	o Intermediate pipe/HX (inside the buffer tank), (intermediate pressure is high, high risks in the IHX, due to thermal stresses)					break : DBA pinhole (HX): AOO
	P-B	o Primary loop extruding from core vessel to outside (inside the buffer tank) (chemistry control, pebbles injector)					DBA
	P-B	o PRACS (especially the PHX as thin tubes are used)					DBA
	P-B	o Core vessel.				This event is a beyond design basis event.	Neglected
	B-T	o DRACS (especially the DHX as thin tubes are used)					DBA
	P-T	o Primary loop extruding from core vessel to outside (outside the buffer tank, at the atmosphere) (chemistry control, pebbles injector)					DBA
	I-T	o Intermediate loop (at the atmosphere)	spurious opening of a valve: AOO				DBA
	B-T	o Buffer tank (in the argon filled cavity).				This event is a beyond design basis event.	Neglected
	B-T	o Buffer loop extruding to outside, at the atmosphere (chemistry control)					DBA
	T-T	o Other loops used for passive cooling (RCCS, DRACS)					DBA
	PIBT	Intrusion / Extrusion of gases via normal connections					AOO
	P	Failure of coatings in a fuel particle (small release)					AOO (misconception)
	T	Failure in the tertiary boundary (concrete containment, spurious opening of a valve or damper)				The failure of the concrete containment is a beyond design basis event. A spurious opening of a valve is common.	AOO

APPENDIX V

SCENARIO CONSTRUCTION

Sub-system impacted	Postulated Initiating Event (PIE)	Estimated Annual Occurency Frequency of the PIE	Issue of the following sequence	Initial conditions	Most interesting Single Failure Criterion	Comments / description	Safety criteria	Scenario retained
P	Reactivity insertion: withdrawal of one group of control rods.	AOO	Neutronics, Core heat-up	Power	SCRAM failure	We do not consider the case of the core start-up (no feedback, and not realistic, as it has a little probability). In the full power mode, the power increase is expected to be limited by the Doppler effect (the large amount of power available for temperature feedback is balanced by the important thermal inertia of the graphite). The parameter to be assessed here is the reactor ability to respond quickly to fast change in k.eff and shutdown (not to remove extra-decay heat). Thus a SCRAM failure is more interesting than a PRACS one. It has links with a power distribution anomaly.	k.eff, peak metal and fuel temperature	yes
P	Power distribution anomaly (pebbles position, fuel block motion, spurious CR insertion)	AOO	Hot point: local fuel temperature	Power	SCRAM failure	The total output power is not changed, so the decay heat to remove is not the main issue. We could have a neutronics flux pinching. Issues are similar to a partial flow blockage in the core.	peak fuel temperature	no
PIBT	Heating system failure when stand-by (P, I, B, T) during a loss of off-site power.	AOO	Freezing.	Shut-down state	Spurious increase of a DRACS efficiency (damper opens broadly).	Add aggravating conditions with low temperatures outside (extreme weather) and low decay heat. Diesel generators will supply reserve power after a conservative delay.	coolant temperature	yes
P	Spurious scram.	AOO	Fast drop in temperature	Power	/	This safe event drives no particular risk except thermal fatigue to materials. This would be aggravated by a late trip of the power conversion system and primary pumps (fast distribution of colder fluid). The phenomena induced are found in other transients with SCRAM.	metal temperatures	no
I	Load increase (off-normal)	AOO	Heat decay removal	Power	1 PRACS failure	The event should result in a initial steady decrease in average core temperature. Then an increase of the neutronic power (with temperature feedbacks), this power will have to be removed after the turbine trip. We have to assume a delay between the starting time of the event and the turbine-trip and SCRAM time. This turbine trip can be considered as a loss of load. We are interested in maximizing the peak primary temperature: by limiting the heat transferred from primary to buffer salt, we expect such phenomenon. Moreover, this event could result in an initial transitionnal increase of temperature difference through IHX and then greater thermal stresses.	peak metal temperature	yes
I	Total loss of cooling	DBA	Core heat-up, decay heat removal, neutronics	Power	1 PRACS failure	No cooling, no forced circulation. The primary temperature increases. SCRAM has to occur after delay, to remain realistic. The neutronic behavior of the core regarding the heat-up is also of interest in this transient. As for the load increase scenarion, we retain a PRACS failure. In reality, there would be a reserve way of heat removal on the intermediate loop (used for start-ups and shutdown, in order to prevent excessive heating of buffer salt). These assumptions are not used. The extra heat to be removed is due to the stored energy not an increase of core power (and then extra-decay heat).	k.eff, peak metal temperature	yes
P	Total loss of forced circulation.	AOO	Temperature distribution in primary system.	Power	SCRAM failure	This transient should not result in a dramatic increase of the heat to be removed (core power and stored energy in the primay system won't change as in a loss of cooling or reactivity transients). The interesting effect is the increase in temperature differences in the core, which could be maximized by a failure to scram. The ability to perform natural circulation when cooling is still active is assessed by assuming a late trip of the power conversion system.	peak metal temperature.	yes
P	Partial loss of forced circulation.	AOO	Flow disturbance, heat removal	Power	Other primary pumps don't trip	The beginning of this event is mild: the deltaT core will slightly increase (not relevant in this scenario, compared to a total loss of cooling). The important issue is that the other pumps still running prevent the PHX to remove heat. Scenario put aside because of its similarity with primary pump seizure.	peak metal temperature	no

Sub-system impacted	Postulated Initiating Event (PIE)	Estimated Annual Occurency Frequency of the PIE	Issue of the following sequence	Initial conditions	Most interesting Single Failure Criterion	Comments / description	Safety criteria	Scenario retained
P	Partial flow blokage in one or several IHX	several: DBA	Core heat-up, heat removal	Power	1 PRACS failure	It induces a decrease in both flow (more pressure drop) and a heat removal (less heat transfer area). These phenomena, considered separetely are respectively bounded by loss of circulation and loss of cooling. As we consider only one or few IHX (more won't be realistic), we except that these two combined phenomena will present limited consequences, compared to the two boundary scenarios.	peak metal temperature.	no
P	Flow blokage in PRACS (one)	total : DBA	Decay heat removal	Shut-down state	1 DRACS failure	PRACS are not used in Power. The ability to remove primary heat is threatened. Another PRACs failure would certainly be too unrealistic. One postulates a spurious closure of a damper on a DRACS system. Aggravating conditions are choosen with a high level of decay heat (sequence likely to happen just after reactor shutdown).	peak metal temperature	yes
B	Partial flow blokage around DHX (one)	DBA	Decay heat (or heat losses at full power) removal.	Shut-down state	1 DRACS failure	DRACS system is used to maintain the buffer salt at the lowest acceptable temperature at the Full Power state (but their are capable of a greater heat removal,up to 1% of the full power). However, this event is not relevant at this mode, because of the possibility to adjust the heat removed by the other DRACS systems (assumed to be enough reliable to not fail themselves). The interesting mode is during shutdown state (during a reactor shutdown won't be realistic). The risk is to reach a peak metal temperature (for buffer or primary salt). It is not clear to determine which failure to add: DRACs or PRACS... However, a blockage would remain only partial, so this event is bounded by a total failure of the tertiary side of the DRACS.	peak metal temperature	no
B	Partial flow blokage around PHX (one)	DBA	Decay heat removal	Shut-down state	1 DRACS failure	Similar to a flow blokage in PRACS	peak metal temperature	no
T	Flow blokage in RCCS	DBA	Cavity cooling.	Shutdow n state	1 DRACS failure	Most of the heat in the buffer salt is removed by the DRACS system (natural convection or radiation). Thus RCCS is taking an more important part at the lowest buffer salt temperatures (at full power or at the end of a long stand-by state, where DRACS aren't used at their plain capacity). However, RCCS is designed to cool the cavity, not to the buffer salt. Thus a RCCS failure would have significant consequences for hight buffer salt temperatures (heat-up in the cavity): hence during a early stage of shutdown state. An additionnal PRACS failure won't be realistic. A DRACS failure mades the buffer salt rise a bit.	cavity (concrete) temperatures.	yes
T	Flow blokage in DRACS	DBA	Decay heat (or heat losses at full power) removal.	Shut-down state	1 DRACS failure	This sequence bounds the event of flow blokage of buffer salt around DHX.	peak metal temperature	yes
P	Flow run-up. Primary pump speed increases anormally.	AOO	Neutronics	Power	SCRAM failure	This event will result in a steady decrease of average core temperature (reactivity feedback issue). The most aggravating condition, in a neutronic point of view (prumpt criticity) is at start-up (not considered, as it is more likely a BDBA). Reactivity feedbacks are expected to limit the increase of the neutronic power (hence the amount of decay heat). So the total heat to remove is not the issue, hence a ATWS is worth to study. This sequence presents similitudes with the reactivity insertion and load increase transients: the average core temperature is decreasing and feedbacks are expected; the interest of these sequences rely on the assessment of neutronic effect and ability to remove extra decay heat. Thus the choice of an adapted failure is arguable...	k.eff	yes
I	Flow run-up. Intermediate pump speed increases anormally. Cavitation occurs, or automatic shutdown, or breakdown.	AOO	Mixing, Neutronics	Power	/	This event is bounded by a load increase in terms of general core behavior (the temperature variation in core would remain inferior). However, mixing phenomena (between the cold streaks of the incriminated loop and the hotter others) are of interest in the inlet plenum. Unperfect mixing could result in local reactivity feedbacks in the core. As this event presents particular phenomena and is already bounded by another more severe scenario, no need of additionnal failure (a single action of the protection system will result in the end of the phenomenon: turbine or primary pump trip, SCRAM...). The consequences would be closed to the power distribution anomaly event.	peak fuel temperature	no

Sub-system impacted	Postulated Initiating Event (PIE)	Estimated Annual Occurency Frequency of the PIE	Issue of the following sequence	Initial conditions	Most interesting Single Failure Criterion	Comments / description	Safety criteria	Scenario retained
T	Flow run-up : spurious wide opening of a regulated valve or damper on the cooling systems.	AOO	Freezing.	Shutdown state	DRACS failure (another flow run up)	This event can be treated with electrical heating (their total failure would be unrealistic). This kind of sequence can be assessed with a loss of off-site power (when shut-down) scenario.	coolant temperature	no
P	Off-normal fuel or pipe motion-vibration.	AOO	Mechanical break (cycling), power distribution anomaly, hot point.	Start-up	SCRAM failure	Complex : need to list resonance frequencies of components and determine the amplitudes of these motions. Important, but local, changes in pebble packing factor may induce hot points in the core. These neutronics consequences are closed to the issues of power distribution disturbance. Thus a SCRAM failure is considered.	stresses, frequency, peak fuel temperatures	yes
I	Off-normal component vibration (pipe).	AOO	Core heat-up, mechanical break (cycling).	Start-up	/	Heat removal through IHX is still effective but modified. Thus this event is bounded by the scenarios of loss of cooling or load increase. The mecanical response of the intermediate components to this scenario is not directly of interest, as the most severe consequences are also adressed in a intermediate break scenario.	/	no
T	Off-normal component vibration (RCCS pipe).	AOO	Cavity cooling, mechanical break (cycling).	Start-up	RCCS trip failure	The break of RCCS is adressed in another scenario. Simple vibrations of the RCCS do not imply particular phenomena in term of heat transfer and core safety. These are bounded by a flow blockage. However, severe vibrations could alter the cavity integrity (e.g. insulation).	stresses, frequency	yes
P	LOCA : small (pinehole), moderate break, large break, spurious opening of a valve.							
P	o Primary pipe (up-stream pump).	DBA	Void reactivity, heat removal, mixture of different salts, hot point	Power	Primary pumps don't trip.	ATWS is in this case a BDBA. In this part of the primary loop, the pressure difference between the primary and buffer side is expected to remain limited, thus equilibrium might be reached before any gas might be sucked in and the amount of salt exchanged might be important. It is not clear that primary salt will leak into the buffer salt. 2 cases are proposed, depending on the values of these pressures: loss of primary coolant and buffer salt suction. The first scenario is bounded by breaks down-stream pump (loss of primary coolant is more important). The entrainment of gas might alter the heat transfer (flow blocked by trapped bubbles, gas insulating the fuel) and create local hot points (bad heat transfer and excess reactivity due to void). SCRAM is assumed to occur after a delay.	peak fuel / metal temperature	yes
P	o Primary pipe (down-stream pump).	DBA	Void reactivity, heat removal, core heat-up, mixture of different salts, hot point	Power	Primary pumps don't trip.	ATWS is in this case a BDBA. In this part of the primary loop, primary pressure is higher than buffer salt one (even down-stream IHX). The event starts with a loss of primary coolant, then inert gas is sucked. When pumps stop (cavitation), buffer salt is injected. Needs to study possibilities for buffer salt to be sucked (if any possibility of venturi effect). This scenario is closed to the previous one. They differ by the amount of salts injected and the sequence of injections (depend on pumps characteristics, levels of free surface, working temperatures). 2 more detailed scenarios need to be adressed: first: the case of a break in the cold leg (not highest pressure but high density) could imply a partial loss of circulation through core as flows of other cold legs could flow prefeentially through the break; second: break up-stream IHX (highest pressure but low density).	peak fuel / metal temperature	yes (2)

Sub-system impacted	Postulated Initiating Event (PIE)	Estimated Annual Occurency Frequency of the PIE	Issue of the following sequence	Initial conditions	Most interesting Single Failure Criterion	Comments / description	Safety criteria	Scenario retained
P	o IHX primary side.	DBA	Void reactivity, heat removal, mixture of different salts, hot point	Power	Primary pumps don't trip.	ATWS is in this case a BDBA. This event is similar to a leak on a pipe down-stream the pump and is half-way of the 2 proposed scenarios.	peak fuel / metal temperature	no
P	o IHX intermediate side	medium break : DBA pinhole : AOO	Void reactivity, heat removal, mixture of different salts, hot point	Power	SCRAM failure	The intermediate loop works at a higher pressure than the primary loop. Thus the primary inventory will be maintained. However, depending of the design, gas used for intermediate pressurization could be entrained in fixed amount. Considering the high probability of this initiating event, a SCRAM failure could be envisioned (we asses the ability to cope with a limited ingress of void).	k.eff, peak metal and fuel temperature	yes
I	o Intermediate pipe/HX (inside the buffer tank).	break : DBA pinhole (HX): AOO	Core heat-up, heat removal, mixture of different salts	Power	1 PRACS failure	Bounded by a loss of cooling. We assume that the increase in temperature of buffer salt before SCRAM is insignificent (low amount of intermediate salt compared to buffer salt), thus heat removal by buffer after SCRAM is not significantly hindered. Moreover, similar calculations would have been performed for leaks of primary salts into buffer.	peak fuel / metal temperature	no
P	o Primary loop extruding from core vessel to outside (inside the buffer tank) (chemistry control, pebbles injector)	DBA	Void reactivity, heat removal, mixture of different salts, hot point	Power	Primary pumps don't trip.	ATWS is in this case a BDBA. These loops are assumed to be taken out the cold leg. So this event is similar to a leak on a cold leg. However, we can assume that generally, the progression of the accident is slower than for a main primary pipe.	peak fuel / metal temperature	no
B	o PRACS	DBA	Void reactivity, heat removal, mixture of different salts, hot point	Power	Primary pumps don't trip.	ATWS is in this case a BDBA. As for a breach in primary pipes up-stream the pumps, it is not clear which salt will leak into the other as only static heads are to be taken into account (depends on temperature, inventory). In a neutronic point of wiew, this scenario is closed to the previous one. However, the effects of the breach will have a long-lasting impact. Contrary to the previous breaches, the failure is still concerning the loop active during the passive cooling.	peak fuel / metal temperature	yes
B	o DRACS (in buffer tank)	DBA	Decay heat (or heat losses at full power) removal.	Shut-down state	1 DRACS failure	This scenario has the same impact that a total flow blockage in a DHX. The heat properties of buffer salt are not altered.	peak metal temperature	no

Sub-system impacted	Postulated Initiating Event (PIE)	Estimated Annual Occurency Frequency of the PIE	Issue of the following sequence	Initial conditions	Most interesting Single Failure Criterion	Comments / description	Safety criteria	Scenario retained
P	o Primary loop extruding from core vessel to outside (outside the buffer tank, at the atmosphere) (chemistry control, pebbles injector)	DBA	Void reactivity, heat removal, hot point	Power	Primary pumps don't trip.	ATWS is in this case a BDBA. Here we consider a non-insulable leak on a loop without any auxiliary pump (otherwise, the leak consequence could be limited by the pump trip). Primary pressure is assumed to be superior to the atmosphere one. Hence, no air could be entrained (maybe by venturi effect if any). This scenario is similar to a leak on a cold leg, except the fact that no buffer salt is reinjected at the end of the accident. The speed of the accident depends of the diameter of the loop and the pressure in the pipe.	peak fuel / metal temperature	yes
I	o Intermediate loop (at the atmosphere)	DBA	Core heat-up, decay heat removal, neutronics	Power	Power conversion system doesn't trip.	Bounded by loss of cooling. Classical hazards (fire, toxicity) are not adressed here.	k.eff, peak metal temperature	no
	o Buffer loop extruding to outside, at the atmosphere (chemistry control)	DBA	Decay heat (or heat losses at full power) removal.	Shut-down state	1 DRACS failure	The matter of the buffer salt pool integrity (the inventory ensures the AHTR ability to cope with any transient) implies that such loop can't be just drained out of the tank. These loops use auxiliary pumps taking suction in the pool without creating a opening in the tank. Considering a late action of operator to trip the auxiliary pump (failures of alarms on level, pressure), a few amount of buffer salt, compared to the large inventory, will be lost. Thus, one may consider that appropriate design of this loop may result in a reasonnable loss after such accident, that doesn't affect much the heat removal during the first hours of a shut-down state (compared to one DRACS failure for instance).	peak metal temperature	no
T	o Other loops used for passive cooling (RCCS, DRACS)	DBA	Heat removal, cavity cooling	Shutdown state	1 DRACS failure	ATWS is in this case a BDBA. Leaks on DRACS is bounded in severety (in terms of core safety, not classical industrial hazards) by a flow blockage in one DRACS loop. Leaks on RCCS could also hamper radiation and generate cooling by boiling (if RCCS water is normally slightly pressurized). However, these scenarios present phenomena (oxydation, insulation degradation, hot points on buffer salt tank) that could be included in more complex BDB accidents (e.g. failure of buffer salt tank and RCCS). This event has some links with a flow blockage in RCCS event, as other ways of heat removal are still available.	cavity (concrete) temperatures.	no
PIBT	Intrusion / Extrusion of gases via normal connections (argon carried along by pebbles, spurious pressurization of inert cover)	AOO	Void reactivity, heat removal, hot point	Power	Primary pumps don't trip.	These events are similar to break events with gas suction (but salts it-selves are not modified). If CFD can adress every primary breach scenario, study of simple gas intrusion are useless. Mechanical stresses resulting of pressure increases are supposed to remain within the design basis values.	k.eff, peak metal temperature	no
P	Failure of coatings in a fuel particle (significant release)	AOO	Radioactivity release	Shut-down state	Opening in the tertiary boundary.	This event does not present any additionnal interresting phenomena in terms of PIRT. Coating failures are also adressed at the full power regime as a normal phenomenon. In terms of safety, failure of a significant number of particles could be challenging in a shut-down state in a refuelling operation or reflector replacement, when the primary boundary is open. A additionnal failure criterion would be a spurious opening in the tertiary boundary.	Activity	no
T	Failure in the tertiary boundary (spurious opening of a valve or damper)	AOO	Radioactivity release	Shut-down state	TRISO failure	This event is similar to the failure of TRISO when shut-down for refueling or reflector replacement. It does not present any additionnal interest.	Activity	no

APPENDIX VI

COMPONENT LEVEL ANALYSIS AT FULL POWER

We will adopt a sub-system approach, by grouping modules depictions in "sub-system paragraphs". The rankings proposed for each phenomena and module take already into account the corrections imposed by the system-level analysis.

1. Primary sub-system.

A) INLET PLENUM.

This component is composed of salt, graphite and steel of the reactor vessel. The lower reflector in the design is provided by the inlet flow of the beryllium-based salt. The following parameters are retained:

Table A.VI.1: Inlet plenum parameters.

Diameter (core diameter)	6.84
Plenum height (half block height) (m)	0.396
Salt volume (m^3)	14.5
Lower reflector thickness (formed by liquid salt for the pebble bed) (m)	1.2
Reactor vessel thickness (m)	0.1

Due to the proximity of the core, gamma heating of the constituents of the plenum is expected. This internal power generation would affect every phenomenon (heat transfer, pressure drop, stresses). However, the importance of convective heat transfer can be expected to be superior to the contribution of heat delivered by gamma heating.

Flow:

- The inlet plenum flow is multi-dimensional. For the prismatic core, the flow distribution is dominated by the effects of the flow channels and orificing in the graphite structure of the inlet plenum. For the pebble bed, the bottom reflector is formed by liquid salt and the flow structures may include jets directed toward the bottom of the pebble bed. The flow distribution is important since it affects the distribution of the working fluid that moves upward through the core, then the operational power profile.
- Pressure drop is estimated to be small compared to other primary loop components (IHX or core).

Heat transfer:

- For prismatic fuel heat is transferred to salt from the graphite lower reflector by forced convection. There is no heat source at lower plenum except gamma heating and temperature differences generated by the inlet flow are small, so heat transfer is not important in this region. A permanent temperature at the interface between graphite and salt, equal to the inlet temperature, is assumed for simple calculations.

- Heat is transferred by conduction through the lower reflector and reactor vessel to the buffer salt. The graphite-steel gap would be filled with liquid-salt bypass cooling flow.
- Heat transfer from reactor vessel to the buffer salt is developed latter in this chapter.
- Cooling of the radial reflector is performed by upward flow from the inlet plenum: cool primary salt is used (5 to 15 % of core flow, according to [36]). This salt comes initially into the reflector at the cold leg temperature and is slightly heated through the reflector. It is discharged in the outlet plenum to mix with hot flow exiting the core.

Stresses: Steady thermal stresses are generated by gradients of temperatures throughout components (graphite reflector and reactor vessel). However, the results of simple heat transfer calculations for the bottom of the core (developed in 3 B)) show that these phenomena can be mitigated. The stratification of the buffer salt and the use of insulation materials (to minimize steady-state heat losses from the buffer tank) result in a low temperature difference through the lower reflector and reactor vessel.

Table A.VI.2: Phenomena in the inlet plenum.

Rank	Phenomena	Criteria
H	Flow distribution	Fuel operational performance (FOP)
M	Forced convection	FOP
M	Pressure drop – forced convection	FOP – Pumping power
M	Jet discharge and mixing (depending on design)	FOP - Stresses
L	Conduction (including gaps)	Stresses
L	Gamma heating	All
L	Thermal stresses	Stresses

A) <u>CORE:</u>

Three possible designs are retained for the AHTR-MI core: prismatic blocks, pebble-bed and stringers (this stringer variation is not studied here, but is quite similar to prismatic fuel). For both designs, flibe primary salt is considered.
The following parameters are used for bulk calculations and take into account the particularities of each version of the AHTR-MI.

Table A.VI.3: General core parameters.

Total thermal power (MW)	2,400
Core power density ($MW.m^{-3}$)	10.2
Core height (m)	6.40
Core diameter (m)	6.84
Total cross-section area for core (m^2)	36.76
Core inlet temperature (°C)	600
Core outlet temperature (°C)	700
Mass flow ($kg.s^{-1}$) (Flibe)	9,140

Table A.VI.4: Prismatic core parameters.

Coolant channel diameter (m)	0.00953
Number of columns	325
Number of coolant channels per column	108
Average heat transferred per coolant channel (W)	68.4×10^3
Average surface heat transfer in coolant channel ($W.m^{-2}$)	357×10^3

Table A.VI.5: Pebble-bed parameters.

Pebble bed porosity	0.4
Pebble diameter (m)	0.06

Whatever the design finally retained, the following phenomena are encountered and are of high importance as they all combine to bring about the issue of fuel operational temperature and the peak coolant temperature:

- Power:
  - Steady state neutronics has to be accurately predicted to assess the fuel performance achievable (burn-up, k-effective, radioactive materials to be released in accidents conditions)
  - Gamma heating is expected to be the most important in the fuel zone, however, it is often neglected in steady-state calculations [31].
- Flow:
  - Flow distribution, linked to the pressure drop, convective heat transfer and power profile, drives the peak fuel temperature and the peak exit coolant temperature (that might creates hot jet impinging structures in the outlet plenum and also thermal striping that could affect critical components as IHX). In the particular case of prismatic core, it is considered as one-dimensional ($\frac{L}{D} >> 1$).
  - Pressure drop is a relevant phenomenon as it affects the pumping power and the flow distribution.

Rough values for the prismatic core:

The pressure loss by friction is estimated, assuming a constant flow speed and density through core and using the Blasius relation for friction factor. Liquid Salts don't wet graphite; therefore, even rough surface for salt is smooth, precise values for roughness are not relevant. Pressure drop calculations will assume smooth surfaces.

The regular pressure drop throughout a channel due to friction is given by:

$$\Delta P_{fc} = C_f \cdot \frac{\rho \cdot v_0^2}{2 \cdot D} \cdot L$$

Where:
- C_f is the friction coefficient, given by the Blasius relation
- D, L have been defined earlier
- v_0 is the average flow velocity
- ρ is the average coolant density
- L is the height of the channel

Hence,
$\Delta P_{f_c} = 8.4\ 10^4$ Pa

The singular pressure drop is given by the general relation:

$$\Delta P = K \cdot \frac{\rho \cdot v_0^{\ 2}}{2}$$

Where K is taken out a catalogue of geometries and the other parameters have been defined above.

At coolant channel entry, K = 0,5, we obtain ΔP = 1.7 10^3 Pa
At coolant channel outlet, K = 1, we obtain ΔP = 3.4 10^3 Pa

The total value is an order of 10^5 Pa, which represents the third of the IHX pressure drop (1J)).

Rough values for the pebble-bed core:

Different correlations to get the frictional pressure loss are available in literature. Rough calculations are done for 3 correlations, considering the simplification of a one-dimensional core (with theoretical power profile in sinus and a constant mass flow rate).

The pressure loss due to friction through a bed of packed spheres is given by:

$$\Delta P_{fc} = \int_0^{H_{core}} \frac{f_c \cdot \rho \cdot v^2}{d_{pebble}}$$

Where:
- f_c is the friction coefficient, given by:

$$f_c = \frac{1-\varepsilon}{\varepsilon^3} \cdot (a \cdot \frac{1-\varepsilon}{\mathrm{Re}} + b)$$

- d_{pebble}, Re, ε, v have been defined earlier
- a and b are defined in correlations (respectively 170 and 1.75 for the correlation by Van Acker and Mude [37] [38] or 180 and 1.80 for the correlation by Mac Donald [39])
- H_{core} is the height of the bed
- ρ is the coolant density
- L is the height of the bed

Another similar relation, by Kugeler and Schulten [40], cited in [33] could be used:

$$f_c = \frac{1}{2} \cdot \psi \cdot \frac{1-\varepsilon}{\varepsilon^3}$$

Where:

$$\psi = \frac{320}{\frac{Re}{1-\varepsilon}} + \frac{6}{\left(\frac{Re}{1-\varepsilon}\right)^{0.1}}$$

The correlation by Kugeler and Schulten shows significant differences, compared to the two others. Figure A.VI.1 and Figure A.VI.2 points out a difference of roughly 25 % in the pressure drop prediction. The validity of this very correlation should be discussed, since the source [40] deals with helium-cooled reactor. However, Achenbach presents it as the latest valid correlation available [32].

The resulting pressure drops are fairly reduced (order of 75 % of the prismatic core values) and show little dependency of the average porosity and working temperature.

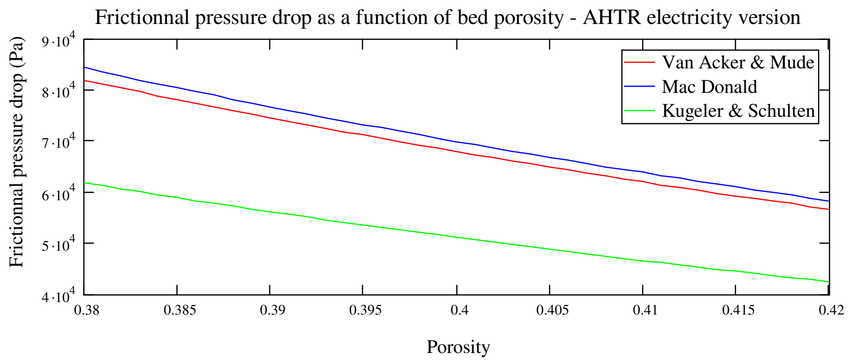

Figure A.VI.1: Influence of porosity on frictional pressure drop through the pebble-bed core (low temperature version).

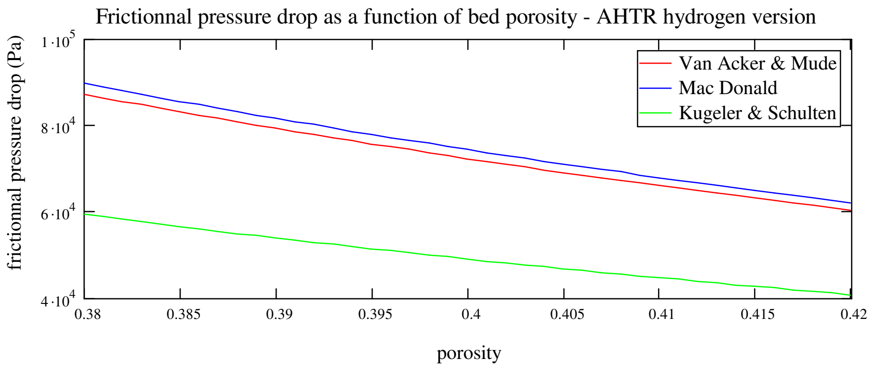

Figure A.VI.2: Influence of porosity on frictional pressure drop through the pebble-bed core (high temperature version)

- Heat transfer:
    - Conduction in fuel (spherical TRISO particles, cylindrical compacts, hexagonal graphite blocks or spherical pebbles). Graphite conductivity has been well studied and data are available. However, since AHTR works at a higher power density than gas-cooled reactors, fuel conductivity values have great importance to predict the peak fuel temperature. More detailed information (results of ORNL studies) is available concerning the graphite conductivity in [31]. TRISO conductivities are not clearly known, however, this is not particularly relevant due to the small size, leading to small temperatures differences within a TRISO particle (less than 5°C).

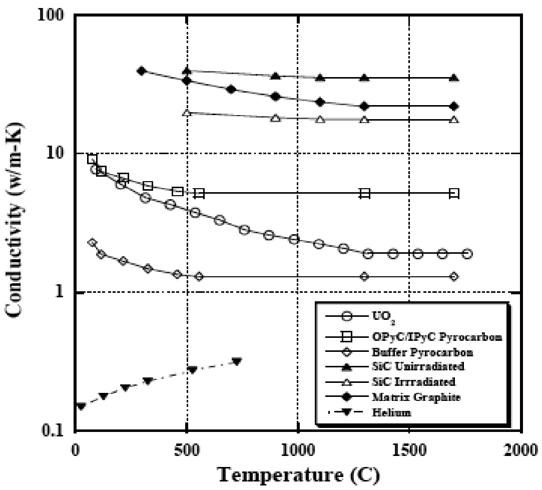

Figure A.VI.3: Conductivities in TRISO constituents

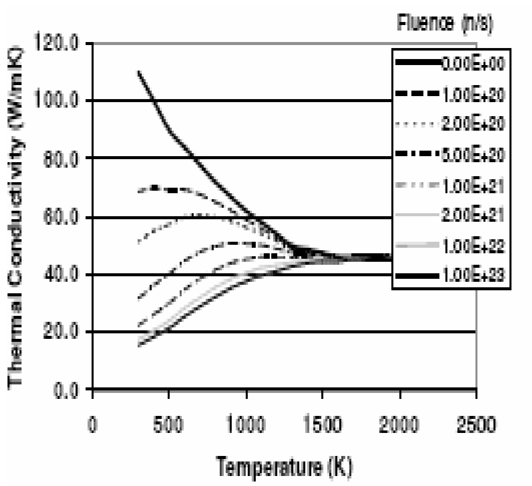

Figure A.VI.4: Conductivity in graphite matrix

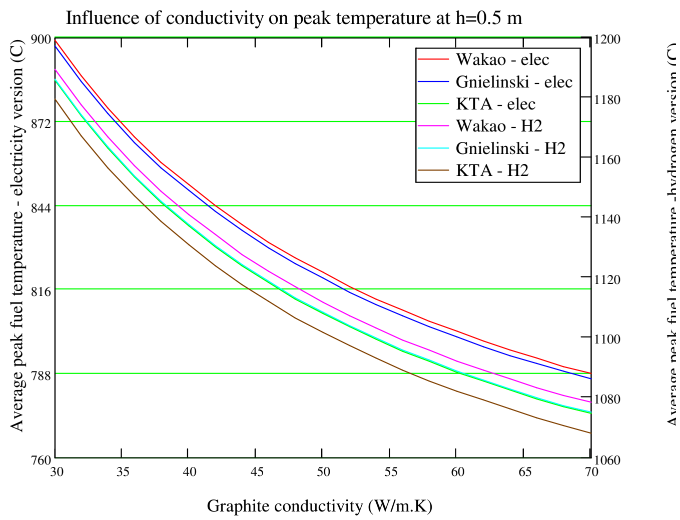

Figure A.VI.5: Fuel conductivity effect on peak temperature.

This importance is illustrated by estimations of peak fuel temperature in the pebble-bed AHTR. A one –dimensional calculation shows that, in the range we are interested in (fuel temperatures superior to 900 K, where conductivity is between 30 and 70 $W.m^{-1}.K^{-1}$), conduction modifies the peak core temperature of an order of 100 K, whatever the correlation used or the average core temperature.

For these calculations, the following assumptions are used:

- The porosity is taken to be 0.4,
- The packing factor of the TRISO particles 0.10,
- Salt temperature profile is given after a theoretical sinus power profile and a constant mass flow rate (1-D model),
- Power generation is assumed to be constant in the fuel zone of the pebble, gamma heating in the protective outer layer is neglected,
- No gap conductance is taken into account at the interfaces fuel/protective layer

The following relations, direct translations of Fourier laws in spherical coordinates (with constant heat generation within the fuel zone) are used:

- At the wall of the pebble: $T_{wallpebble} = \frac{q'''_{fuel} \cdot R_{fuel}^{3}}{3 \cdot R_{pebble}^{2}} \cdot \frac{1}{h_{wall}} + T_{bulksalt}$

- For $R_{fuel} \leq r \leq R_{pebble}$: $T_{pebble}(r) = T_{pebblewall} + \frac{q'''_{fuel} \cdot R_{fuel}^{3}}{3 \cdot \lambda_{outlayer}} \cdot \left[\frac{1}{r} - \frac{1}{R_{pebble}} \right]$

- For $0 \leq r \leq R_{fuel}$: $T_{pebble}(r) = T_{interface} + \frac{q'''_{fuel}}{6 \cdot \lambda_{fuel}} \cdot \left[R_{fuel}^{2} - r^{2} \right]$

Where,

- $q'''_{fuel} = q'''_{reactor} \cdot \frac{1}{1-\varepsilon} \cdot \left(\frac{R_{pebble}}{R_{fuel}} \right)^{3}$ is the average power density in the fuel zone
- $T_{wallpebble}$ is the temperature at the pebble wall
- $T_{bulksalt}$ is the bulk temperature of the coolant salt
- $T_{interface}$ is the temperature at the interface fuel zone and the outer protective layer
- ε porosity of the bed
- R_{pebble} is the radius of the pebble
- $\lambda_{outlayer}$ is the thermal conductivity of the outer protective layer
- R_{fuel} is radius of the fuel zone
- λ_{fuel} is the volume-averaged thermal conductivity of the fuel zone
- h_{wall} is the heat transfer coefficient, given by Nusselt
- $q'''_{reactor}$ is the average power density in the reactor

- Forced convection in coolant channels or around pebbles.

Rough values for the prismatic core:

Estimations have been done of the possibility of mixed convection. All calculations are done with an average heat flux. So, here is not taken into account a possible different heat transfer mechanism at the centre of the core, where power peaks, and then buoyancy forces might be more important.

The following correlations were used:

- Blasius relation:

$$C_f = 0.316 \cdot \mathrm{Re}_D^{-0.25}$$

Where:
- C_f is the friction coefficient, equal to $C_f = 4 \cdot f$
- Re_D is the Reynolds number considering the diameter D of the duct
- This correlation is valid for turbulent flow as long as 2500 < Re_D < 3.10^4.

- Gnielinski correlation ([41], page 394, equation (8.33)):

$$Nu_D = \frac{\left(\frac{f}{2}\right)\left(\mathrm{Re}_D - 10^3\right)\mathrm{Pr}}{1 + 12.7\left(\frac{f}{2}\right)^{\frac{1}{2}}\left(\mathrm{Pr}^{\frac{2}{3}} - 1\right)}$$

Where:
- Pr is the Prandlt number at the fluid bulk temperature
- f is the friction factor
- This correlation is valid in the range 0.5 < Pr < 10^6 and 2,300 < Re_D < 5 10^6. It can be used in both constant heat flux and wall temperatures cases.

- Dittus-Boelter correlation ([41], page 393, equation (8.31)):

$$Nu_D = 0.023 \mathrm{Re}_D^{\frac{4}{5}} \mathrm{Pr}^{0.4}$$

Where:
- This correlation is valid in the range 0.7 < Pr < 120 and 2500 < Re_D < 1.24 x 10^5 and L/D > 60 (where L is the length of the duct).

- The Rayleigh and Grashoff number are defined by ([41], page 210, equation. 4.92 and [42]):

$$Ra_D = \frac{g\beta D^3 \Delta T}{\alpha \nu}$$

$$Gr_D = \frac{g\beta D^3 \Delta T}{\nu^2} = \frac{Ra_D}{\Pr}$$

Where:

- g is the gravitational acceleration
- β is the volume expansion coefficient
- D is the inner diameter of the duct
- ΔT is the temperature difference between wall and bulk fluid.
- α is the thermal diffusivity
- ν is the cinematic viscosity
- these data are taken at the bulk temperature

Mixed convection is expected when the thickness of respective thermal layers for natural and forced convection are similar.

- Bejan in [41] gives the following criterion for Pr > 1 fluids by defining the ratio:

$$\frac{Ra_D^{\frac{1}{4}}}{\mathrm{Re}_D^{\frac{1}{2}} \Pr^{\frac{1}{3}}}$$

If this ratio is an order of magnitude superior to 1, natural convection drives the heat transfer, if this ratio is an order of magnitude inferior to 1, forced convection has to be considered.
We may note that this ratio is defined differently in [42]:

$$\frac{Ra_D^{\frac{1}{5}}}{\mathrm{Re}_D^{\frac{1}{2}} \Pr^{\frac{1}{3}}}$$

- A map by Metais and Eckert [43] gives the driving phenomenon, using two entries in the chart (Re_D and $Ra_D \frac{D}{L}$).

This map is valid as long as: $10^{-2} < \Pr \frac{D}{L} < 1$, which is valid, as $\Pr \frac{D}{L}$ is approximately equal to $2\ 10^{-2}$.

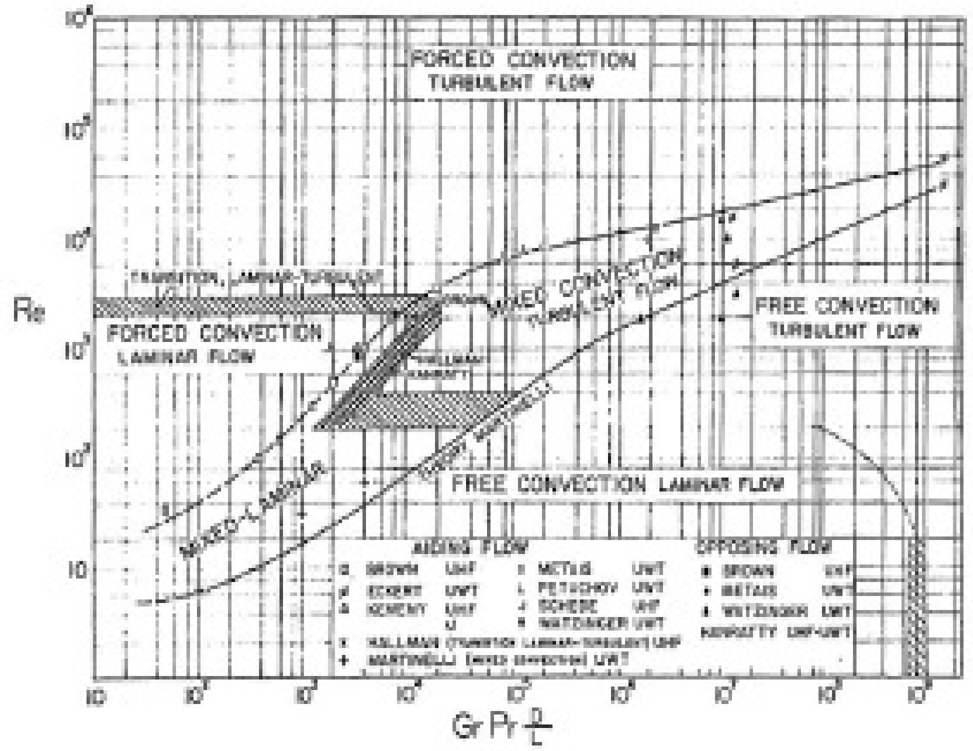

Figure A.VI.6: Metais and Eckert map of mixed convection heat transfer.

Table A.VI.6: Simple convective heat transfer results in prismatic core.

	600°C case		655°C case		710°C case	
Prandtl number	18,6		14,4		11,5	
Reynolds number	4060		5240		6580	
Flow speed (m.s^{-1})	1,84		1,86		1,89	
Friction factor	0,039 (Blasius relation)		0,037 (Blasius relation)		0,035 (Blasius relation)	
Correlation	Gnielinski	Dittus-Boelter	Gnielinski	Dittus-Boelter	Gnielinski	Dittus-Boelter
Nusselt number	44	57	54	63	63	69
Temperature difference in boundary layer (°C)	70	54	57	49	49	45
Rayleigh number	1.46 10^5	1,13 10^5	1.52 10^5	1,30 10^5	1.61 10^5	1,48 10^5
Bejan ratio	0,12	0,11	0,11	0,11	0,11	0,11
Metais-Eckert map entry	100	170	100	190	100	220

Table A.VI.6 shows that the flow is turbulent and forced convection is the heat transfer mechanism, rather than mixed convection. A similar calculation, assuming a local heat flux equal to 1.5 times the average heat flux, at 655°C, leads to:

- $Ra_D = 1.94\ 10^5$
- $Gr_D = 1.35\ 10^4$
- $Ra_D \frac{D}{L} = 300$

Here again, forced convection remains the main heat transfer mechanism, thus peaking power shouldn't affect this phenomenon.

Rough values for the pebble-bed core:

Convective heat transfer coefficients in beds are given by experimental and semi experimental correlations. Numerous studies have been conducted around heat transfer in packed bed of spheres, however the literature shows a great scattering in the available known reliable correlations, especially when it comes to high Prandtl fluids. Experiments have been mainly conducted with air and transcriptions of the results to high Prandtl fluids have been done through analogy with mass transfer experiments. Three correlations are used to assess the convection and have been selected because of the large experimental database they rely on.

- Correlation used in [33], referencing the VDI Warmatlas [37] and initially proposed by Gnielinski:

$$Nu = (1 + 1{,}5 \cdot (1 - \varepsilon)) \cdot Nu_{sphere}$$

Where:

- ε is the porosity of the bed
- $Nu_{sphere} = 2 + \sqrt{Nu_{lam}^{\ 2} + Nu_{turb}^{\ 2}}$
- $Nu_{lam} = 0{,}664\,\mathrm{Re}^{\frac{1}{2}} \cdot \mathrm{Pr}^{\frac{1}{3}}$
- $Nu_{turb} = \dfrac{0{,}037 \cdot \mathrm{Re}^{0{,}8} \cdot \mathrm{Pr}}{1 + 2.443 \cdot \mathrm{Re}^{-0{,}1} \cdot \left(\mathrm{Pr}^{\frac{2}{3}} - 1\right)}$
- Re is the Reynolds number, characteristic of the pebble bed, considering the diameter d_{pebble} of a pebble:

$$\mathrm{Re} = \frac{v_0 \cdot d_{pebble}}{\nu}$$

- ν is the cinematic viscosity, taken at the mean coolant temperature

- v_0 is given by: $v_0 = \frac{\dot{m}}{A}$, also called in literature superficial velocity
- $\dot{m}$ is the total mass flow through the core
- A is the total frontal area
- This correlation is valid for $0,1 < \text{Re} < 10^4$ and $0,6 < \text{Pr (or Sc)} < 10^4$, all thermal properties of the fluid are taken at the mean temperature (between inlet and outlet one)

- Correlation used in [33], referencing to the relation proposed by the German regulatory authority (KTA):

$$Nu = 1{,}27 \cdot \frac{\text{Pr}^{\frac{1}{3}}}{\varepsilon^{1{,}18}} \cdot \text{Re}^{0{,}36} + 0{,}033 \cdot \frac{\text{Pr}^{\frac{1}{2}}}{\varepsilon^{1{,}07}} \cdot \text{Re}^{0{,}86}$$

Where Re, Pr are defined in the same way than previously described. This correlation is valid for $10^2 < \text{Re} < 10^5$ and for Pr=0,71 (precised in [44]), as experiments have only been performed with air.

- The last correlation, by Wakao, is given by Kaviany [45]:

$$Nu = 2 + 1{,}1 \cdot \text{Pr}^{\frac{1}{3}} \cdot \text{Re}^{0{,}6}$$

One-dimensional calculations (Figure A.VI.9) show a maximum difference of 15°C in the prediction of the peak wall temperature of a pebble (hence peak fuel temperature of the pebble). This difference is obtained with the Wakao and KTA correlations. This uncertainty, that might be not relevant for a neutronics calculation (certain MCNP cross-sections libraries are not so accurate), would still be relevant in the prediction of initial conditions during transients (amount of stored heat in the graphite, instantly released in the salt).
The average temperature of the core does not modify this observation.

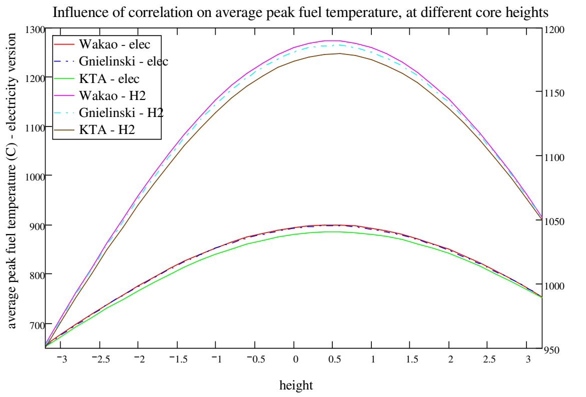

Figure A.VI.7: Radially-averaged peak fuel temperature as a function of height.

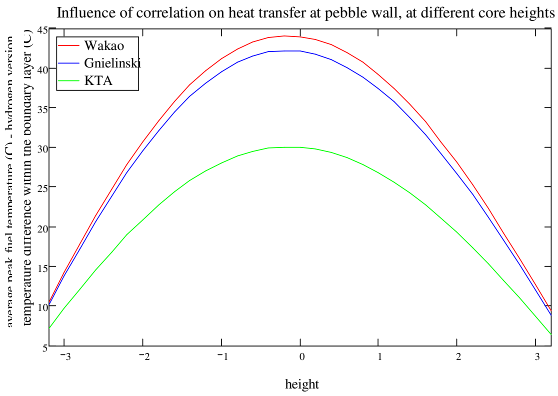

Figure A.VI.8: Heat transfer at the pebble wall.

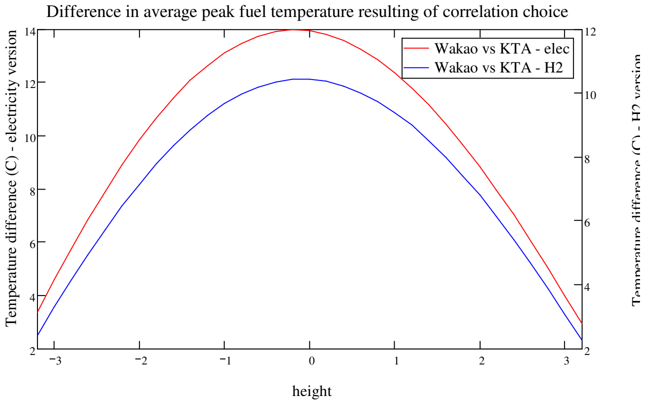

Figure A.VI.9: Difference in fuel temperatures prediction due to the choice of correlation.

Other phenomena of importance are expected:

- Thermal stresses generated by gradients of temperatures throughout components, especially in the TRISO particles (this has been intensively studied).
- Kernel migration due to over pressure of CO2 in the TRISO particle. This phenomenon is important at the edge of the core where the temperature gradient is steep. The cylindrical shape of the core is likely to amplify the temperature gradient, compared to annular cores.
- Pebbles distribution is not uniform through the bed. The average porosity of a randomly packed bed in gas-cooled reactor is given by the formula:

$$\varepsilon = 0.375 + 0.34 \cdot \frac{d_{pebble}}{D_{bed}}$$

where d_{pebble} and D_{bed} are respectively the diameters of a pebble and the bed. It gives the theoretical value: $\varepsilon = 0.378$. Buoyancy will alter these values.

Important porosity changes are also observed near the walls [32], on a 4 pebbles thick layer, as shown in Figure A.VI.11.

The flow velocity and so the pressure drop will certainly be lower near the walls than in the center (due to a higher porosity near the walls). However, the small buoyancy of pebbles and the limited friction (roughness becomes relative issue when it comes to liquid salts as a coolant) may limit the scattering in porosity distribution.

Finally, the influence of the total average porosity in a short range of values (around 0.4) on the peak fuel temperature is not important. However, porosity remains an important issue to predict the k effective and local distortions could also have significant local effects on the fuel temperature.

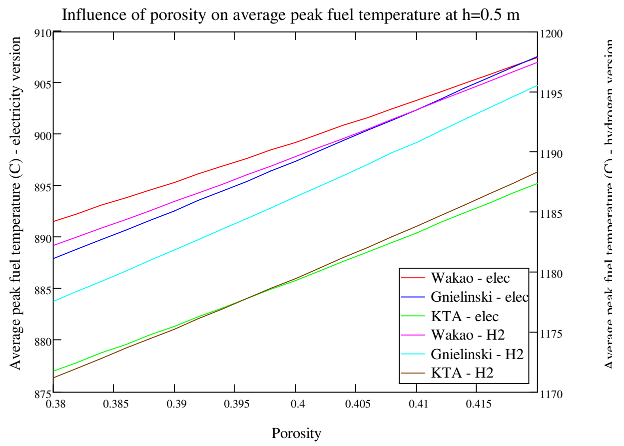

Figure A.VI.10: Influence of average porosity on peak fuel temperature (radially-averaged at h=0.5m)

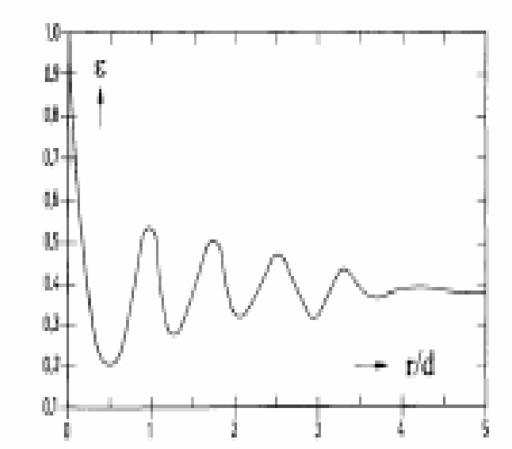

Figure A.VI.11: Porosity distribution as a function of radial position in the bed.

Table A.VI.7: Phenomena in the core.

Rank - PBR	Rank - PMR	Phenomena	Criteria
H	H	Flow distribution	Fuel operational performance (FOP)
H	H	Forced convection	FOP
H	H	Pressure drop – forced convection	FOP – Pumping power
H	H	Conduction (including gaps)	FOP - Stresses
H	H	Thermal stresses	Radioprotection
H	H	Kernel migration	Radioprotection
M	M	Gamma heating	All
H	/	Pebble distribution	FOP

B) <u>REFLECTOR</u>

This component is composed of graphite and salt (approximated to 5 % of the reflector volume).

Power: as for the plena, gamma heating is expected. The possibility of flexible heat removal by by-pass salt flow can mitigate this phenomenon and then reduce the temperature difference through the reactor vessel.

Flow:

- By-pass salt flow is cooling the reflector downwards (this choice is flexible) through vertical channels and/or an annulus. Thus the flow can be considered as one-dimensional. The distribution of the flow is relevant to determine the pressure drop and heat removal in the reflector.

- Flow resistance influences the heat removal but is not really relevant to the total pumping power (as only 15 % maximum of the total mass flow rate would pass through the reflector).

Heat transfer:

- Forced convection is a flexible and important phenomenon that drives the temperature gradient through reflector and reactor vessel, as it drives the average temperature in the reflector. A 5% by-pass flow exiting with a temperature increase of 1 °C corresponds to an amount of power removed of an order of one tenth of the total power transferred through radial conduction within the reflector. It influences also the temperatures at the edge of the active core, thus the operational fuel temperatures. An accurate prediction of fuel temperature everywhere in the core is of importance to optimize the fuel utilization. However, the phenomena in the reflector are expected to have a secondary influence in the core heat and temperature issues. One may keep in mind that the heat transferred radially through the reflector is an order of one thousand of the nominal thermal power.
- Heat is transferred by conduction through reflector and reactor vessel. At that point, no thermal resistance at the contact graphite-steel is available. This phenomenon is the most relevant in the graphite (compared to the thin reactor vessel), as it presents the more important heat resistance.
- Heat transfer from reactor vessel to the buffer salt is developed latter in this chapter.

Steady thermal stresses are generated by gradients of temperatures throughout the graphite and the reactor vessel. Insulation of the reactor vessel and cooling by-pass can mitigate this phenomenon. Results of simple heat transfer calculations are given in 3 B). The gradients are expected to be much lower than in other components, as for example the hot leg.

Table A.VI.8: Phenomena in the reflector.

Rank	Phenomena	Criteria
M	Flow distribution	Heat losses - **Stresses** – FOP
M	Forced convection	Heat losses - **Stresses** – FOP
M	Pressure drop – forced convection	Heat losses - **Stresses** – FOP – Pumping power
M-L	Conduction (including gaps)	Heat losses - **Stresses** – FOP
M-L	Gamma heating	All
L	Thermal stresses	Stresses

C) <u>OUTLET PLENUM</u>

For the prismatic version, the active core is toped by a thick layer of salt, itself topped by the upper reflector. The following characteristics are assumed:

Table A.VI.9: Outlet plenum parameters.

Diameter (core diameter)	6.48
Plenum height (half block height) (m)	0.396
Salt volume (m^3)	14.5
Upper reflector thickness (m)	1.2
Reactor vessel thickness (m)	0.1

The outlet plenum in the PB version will not follow these characteristics. The graphite reflector will directly top the pebbles bed and would be equipped with 4 de-fueling chutes for pebble circulation, located at the top of a smooth curved ceiling. Channels through the reflector will drive the coolant towards the 4 outlet nozzles.

Phenomena relevance is given by the issues arisen in the inlet plenum: stresses to the components and pressure drop (influence on pumping power and on the flow distribution in the core, hence on the fuel temperatures).

Power: as in the inlet plenum, gamma heating is expected to not take a significant part in heat issues.

The flow distribution prediction is a very challenging issue due to the complex geometry of the component (particularly for pebble-bed AHTR), as it presents array of obstacles (control-rods: diameter is 11cm and pitch ~ 80 cm). Flow distribution drives mixing efficiency and then the issue of thermal striping.

Heat transfer:

- Heat is transferred from salt to structures by forced convection. This mechanism is relevant for the prediction of flow distribution and the temperature gradients (stresses) through the structures, as the conduction phenomenon. However, it is not clear to define this as the main heat transfer mechanism, as side reflector may transfer heat to top reflector.
- Heat transfer from reactor vessel to primary pool is developed latter in this chapter.
- Hot streaks due to non-completely mixed flow from hot channels may result in structures failure due to periodic high temperature thermal cycles. This phenomenon was identified as one of very important issue for some GT-MHR components as control rods, turbine inlet (not relevant for AHTR) or IHX. However, the flow rates at stake are not comparable. The pebble-bed version presents the advantage of multi-dimensional flow, exiting directly into channels through the core top. This zone should see turbulent flows smoothing the issues of mixing and hot streaks. There is no issue of jet discharging in the upper plenum, like for the prismatic version.

The thermal stresses on the reactor vessel can be limited by the design of the primary pool (insulation over the reactor vessel and primary salt at the inlet plenum temperature, as described in 1 D)), and the design of the reactor cover (important thickness to enhance the heat resistance or adapted flow paths to prevent streaking and bad mixing). The true concern about thermal stresses is then focused on the constituents closed to the hot salt (control rods, de-fueling machines).

It might be emphasized that the high Prandlt and low velocities of flow may reduce the mixing issue, compared to the NGNP reactors, where temperature difference between the hot streaks can reach more than 100 K.

Table A.VI.10: Phenomena in outlet plenum.

Rank	Phenomena	Criteria
M	Flow distribution	Fuel operational performance (FOP) – Stresses
L	Forced convection	FOP – Stresses
L	Pressure drop – forced convection	FOP – Pumping power – Stresses – Heat losses
H	Mixing, including jets discharge (for prismatic), hot streaks.	FOP – Stresses – Heat losses
L	Conduction (including gaps)	Stresses – Heat losses
L	Gamma heating	All
M	Thermal stresses	Stresses

D) REACTOR VESSEL

The previous paragraphs showed that the reactor vessel is not a relevant component in terms of heat transfer issues, since other components with higher heat resistance (reflector) drive the characteristics of the problem.

The only concern that arises is the issue of thermal stresses in some local places: especially in the outlet plenum, where hot-streaks could create cycling fatigue or in the inlet plenum if no lower reflector is retained. The sides of the reactor vessel are quasi-isothermal, due to the thickness of the cooled reflector and the high temperature of the external buffer salt. Moreover, external insulation could minimize it.

Table A.VI.11: Phenomena in reactor vessel.

Rank	Phenomena	Criteria
L	Conduction (including gaps)	Stresses – Heat losses
L	Gamma heating	Stresses – Heat losses
L	Thermal stresses (especially close to the outlet plenum)	Stresses

E) REACTOR COVER AND PRIMARY SALT POOL

The reactor cover is topped by a pool of “cool” of primary coolant, at the inlet temperature. This is for two main reasons: it provides more thermal inertia during transient and it lowers the neutron radiation level towards the ground level, where workers are.

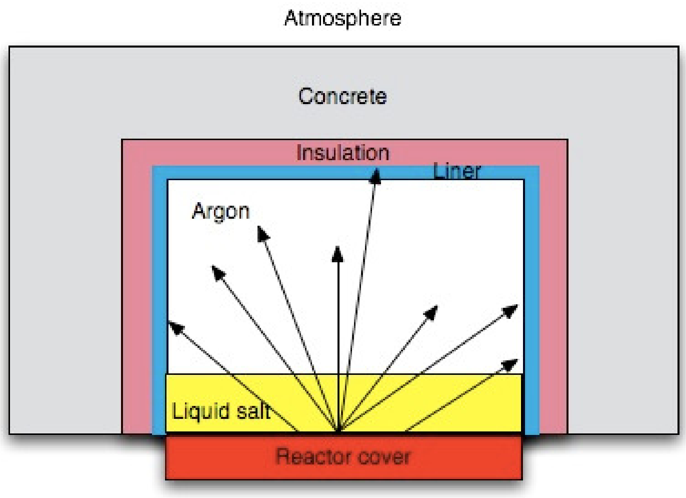

Figure A.VI.12: Schematic of the primary pool.

Rough calculations have been done (for electricity and hydrogen versions of AHTR) to assess the influences of some parameters on the expected phenomena. The following simplifications are used:

- Uniform temperature on each side of the cavity (top, side, top of reactor cover),
- Heat is transferred by radiation only from the top of the reactor cover, assumed at the inlet primary temperature. Radiation is not altered by the presence of control rods, and salt, assumed to be transparent.
- Heat is transferred by conduction through the liner, insulation and concrete to the outside.

The simple conclusions can be drawn:

- The protection of the concrete surroundings of the primary pool cavity requires the use of insulation materials. Without this, concrete temperatures reach failure threshold of 300 °C. Figure A.VI.13 to Figure A.VI.16 show this influence for the side insulation of the pool (similar values are found for the top insulation). This is more efficient than modify the emissivity coefficients of the walls of the pool (by using polished steels for instance). Typical furnace bricks are used for calculations, with a conductivity of λ=0.3 W.m^{-1}.K^{-1} [46]. For the lower temperature AHTR version, a thickness of 0.5 m is enough, whereas these values are doubled for the very high temperature version.

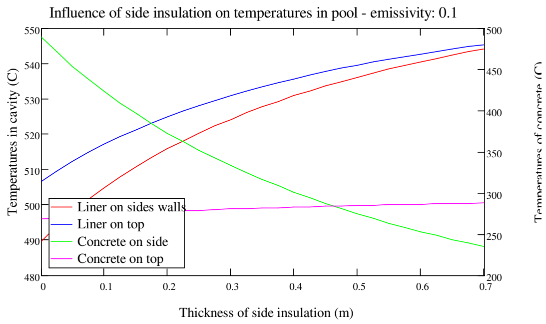

Figure A.VI.13: Influence of insulation on temperatures in the low temperature version of AHTR with low emissivity of walls.

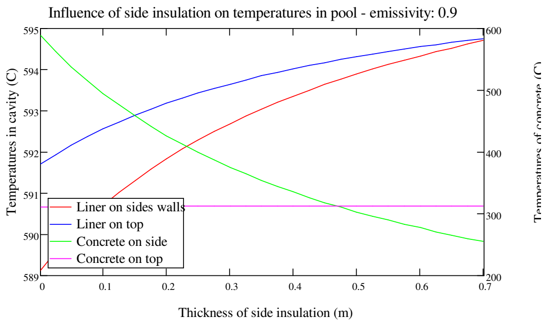

Figure A.VI.14: Influence of insulation on temperatures in the low temperature version of AHTR with high emissivity of walls.

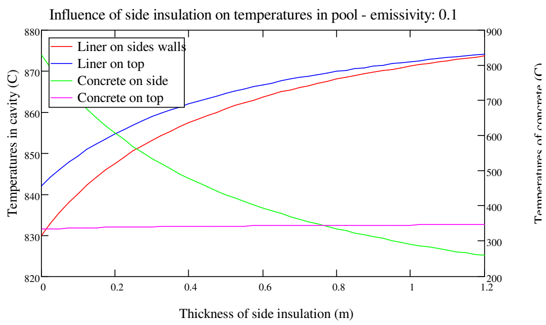

Figure A.VI.15: Influence of insulation on temperatures in the high temperature version of AHTR with low emissivity of walls.

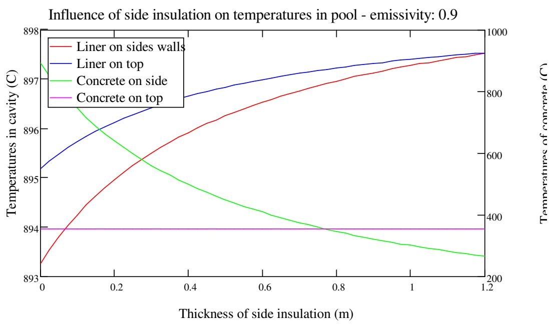

Figure A.VI.16: Influence of insulation on temperatures in the high temperature version of AHTR with high emissivity of walls.

- Heat losses are extremely reduced and very small temperature gradients are found through the sensitive constituents (metallic liner). Thermal stresses become thus a very secondary issue.

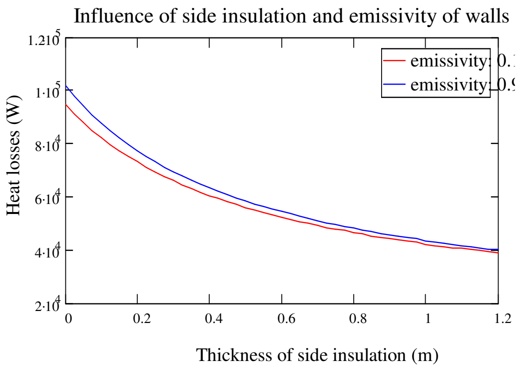

Figure A.VI.17: Heat losses in low temperature version of AHTR.

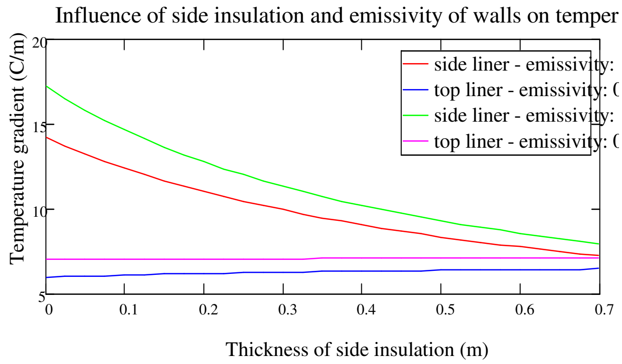

Figure A.VI.18: Temperature gradients through liner in low temperature version of AHTR.

- The use of standard-emissivity surfaces results in a quasi-uniform temperature distribution in the all cavity (few degrees of temperature difference). For radiations problems in argon filled cavity, typical values of 0.8 are taken for emissivity [36,37,31,47,48]. The small temperatures differences between the different sides of the pool imply that free convection phenomena through argon are not relevant, as no significant temperature difference may drive buoyancy flows (not to mention conduction). Heat is transferred by radiation. Stratification through argon is expected. Concerning the primary salt, natural (forced if a forced flow is created by design choice) convection over the reactor cover is planned to insure the cooling of this hot component.
- If low-emissivity materials are used for the walls, important temperatures differences will be found (order of 10°C, as shown in Figure A.VI.13 and Figure A.VI.15), and then natural free convections may become more relevant, particularly in salt as it presents better natural circulation ability than argon.
- Conduction through insulation constituents drives the temperature distribution.

Some uncertainties remain:

- Effects of the control rods and salt solid impurities on radiation heat transfers,
- Effective heat transfer coefficients in the liquid salt pool: free convection along the sides wetted by salt could occur and also Rayleigh-Benard heat transfers from reactor cover to argon (but the ratio H/L is not really characteristic). Moreover hot plumes exiting the interstices between the control rods and their ports are mixing in the pool, as well as cool salt injected at the inlet temperature.
- Gas contained in primary salt might get released in inert gas cover, and condensate or settle on “colder” walls, altering coefficient of heat transfer by radiation.

Table A.VI.12: Phenomena in the reactor cover and primary pool.

Rank	Phenomena	Criteria
L-**M**	Radiation (including emissivity, issues, effects of array of control rods)	Stresses – Heat losses
L-**M**	Conduction (including gaps)	Stresses – Heat losses
L-**M**	Natural convection (in primary salt mostly)	Stresses – Heat losses
L	Mixing, hot plumes.	Stresses – Heat losses
L	Stratification	Stresses – Heat losses
L	Thermal stresses (including control rods)	Stresses

F) <u>HOT LEG (UP-STREAM PUMP)</u>

The pressure drop is negligible in these components compared to the values of other components. The heat losses (through forced convection and conduction) can be reduced by wrapping the pipes with an insulating material. It limits also the thermal stresses, expected to be the most important in the primary loop. Thus the phenomena are not really relevant in terms of economics.
By the way, the value of initial buffer salt temperature is of interest for transients modeling. It is linked to the heat transferred from primary salt to the buffer salt. But, here again, this issue is not relevant, since the hot legs do not contribute significantly to the total heat transferred from the

primary sub-system to the buffer one (leakage flow through PHX is more relevant). It is shown in 3 D) and 1O).

The emphasis must be laid just mainly on conduction issues since insulation will regulate the whole temperature distribution and then the criteria associated (stresses, heat losses and determination of the buffer salt temperature).

Table A.VI.13: Hot leg parameters.

Legs number	4
Temperature (°C)	700
Inner diameter (m)	0.82
Flow speed ($m.s^{-1}$)	2.24
Reynolds number	6.71×10^5
Regular pressure drop (Pa)	$< 10^2$
Singular pressure drop (two 90°-elbows) (Pa) (K from 0,25 to 1,44)	$2.5 \times 10^3 << 1.4 \times 10^4$

Table A.VI.14: Phenomena in hot leg.

Rank	Phenomena	Criteria
L-M	Conduction of pipe and insulator	Stresses – Heat losses – **Initial conditions**
L	Forced convection	Stresses – Heat losses – **Initial conditions**
L	Pressure drop (regular and singular)	Pumping power
L	Thermal stresses	Stresses

G) PRIMARY PUMP

In terms of heat losses and temperature gradients, the primary pump presents the same characteristics than the hot leg. However, particular attention might be necessary on shaft stresses if a "long-shaft" pump is used, and the heat exchange surfaces are lower.

Table A.VI.15: Phenomena in primary pump.

Rank	Phenomena	Criteria
L-M	Conduction of pipe and insulator	Stresses – Heat losses – **Initial conditions**
L	Forced convection	Stresses – Heat losses – **Initial conditions**
M	Thermal and Mechanical stresses	Stresses

H) PRIMARY PUMP SEAL BOWL AND LEVEL EQUALIZING LINE

The "primary pump" component is separated from the "seal bowl" component by the shaft bearing. This cylindrical-shaped component presents a reduced heat exchange area, compared to the others "hot" components (hot and cross-over legs, reactor vessel), thus the only issue that

arises is thermal stresses and heat losses are not relevant. Moreover, as for the other components, insulation can be used and thus reduce constraints.
Primary salt flow is only driven by natural circulation in the bowl, itself driven by free convection along the inner walls cooled by the buffer salt.
Inert gas is contained in the upper part of the seal bowl: bottom is heated (salt free surface) and sides walls partly (up to the height corresponding to buffer salt level). Free natural convection will occur (no Rayleigh-Bénard phenomena as the ratio H/L is too high).
Heat is radiated from the hot bottom towards the more cool walls (through both transparent argon and salt).
Low temperatures differences between the different constituents (argon, salt, walls) are expected, since high temperatures and insulations will surround this component. Hence heat transfer to the outside will be mainly by radiation and convection mechanisms might be of secondary importance (small temperature differences, then small buoyancy forces).
Important temperature difference is expected between the ends of the equalizing line: pump side at hot leg temperature and pool side at the inlet temperature. However, the high ratio of length over diameter may lead to stratification of temperature and a low flow circulation rate (no important buoyancy-driven flow). Important temperatures gradients are expected in these no-flow regions. Insulations are required.
As for the previously described components, conduction phenomena is the relevant issue.

Table A.VI.16: Phenomena in Primary pump seal bowl.

Rank	Phenomena	Criteria
L	Radiation (including emissivity)	**Stresses** – Heat losses
L-M	Conduction of pipe and insulation	**Stresses** – Heat losses
L	Natural convection (in primary salt and argon)	**Stresses** – Heat losses
L	Stratification	**Stresses** – Heat losses
L	Thermal stresses	Stresses

I) <u>CROSS-OVER LEGS</u>

The phenomena are similar to one occurring in hot legs. Singular pressure drop are higher as the flow coming from one primary pump divides in several cross-over legs towards currently 28 IHX. Even if the design of these legs is not yet defined, it is reasonable to consider the pressure drop as an important phenomenon (still inferior to the IHX or core values).

Table A.VI.17: Phenomena in cross-over legs.

Rank	Phenomena	Criteria
L-M	Conduction of pipe and insulator	Stresses – Heat losses – **Initial conditions**
L	Forced convection	Stresses – Heat losses – **Initial conditions**
M	Pressure drop (regular and singular)	Pumping power
L	Thermal stresses	Stresses

J)
K)

L) IHX MODULES

The design of IHX is modular and can evolve with AHTR requirements (higher temperatures for hydrogen production, for instance). Compact exchangers are used but their type (with off-set fins, zig-zag channels,…) is not finalized. The pressure drop is the most important in the primary loop and important additional pressure drops in the manifolds must be taken into account. The flow in the IHX channels is laminar and 3-Dimensional (but can be approximated as 1-D for sizing). The prediction of temperatures, pressures, flow and stresses distributions is a combined work. Porous media modelisation can be used to take into account the combined effects of forced convection and conduction. As the main heat sink of the reactor at steady state, these phenomena are ranked of high importance.

Simple calculations have been made for an outlet temperature of 700°C and show that a slow, laminar flow passes through the component.

Table A.VI.18: IHX main characteristics.

Average velocity ($m.s^{-1}$)	0.79
Reynolds number	103
Pressure drop (Pa)	20 to 30x 10^4
LMTD (°C)	24.6
Differential pressure between hot and cold side (Pa)	Up to 1 x 10^6

Table A.VI.19: Phenomena in IHX.

Rank	Phenomena	Criteria
H	Flow distribution	Pumping power - Stresses
H	Forced convection	Pumping power - Stresses
H	Pressure drop – forced convection	Pumping power - Stresses
H	Conduction	Pumping power - Stresses
H	Thermal and Mechanical stresses	Stresses

M) COLD LEG (DOWN-STREAM PUMP)

The characteristics of flow depend on the design retained (if pebble-bed design is selected, the number of legs may vary from 16 to 32). The phenomena in cold legs are strictly the same than in the hotter pipes and are granted the same ranking. But, here, thermal stresses will be reduced. Here are some results (Pipe diameters are taken to keep flow speed constant).

Table A.VI.20: Cold leg parameters.

	4 legs	**16 legs**	**32 legs**
Diameter (m)	0.81	0.41	0.29
Reynolds number	4.25 x 10^5	2.07 x 10^5	1.47 x 10^5
Regular linear pressure drop ($Pa.m^{-1}$)	< 100		
Singular pressure drop (Pa) (one 90° elbow: K from 0.25 to 1.44)	1.2 x 10^3 < < 7.2 x 10^3		

Table A.VI.21: Phenomena in cold leg.

Rank	Phenomena	Criteria
L-M	Conduction of pipe and insulator	Stresses – Heat losses – **Initial conditions**
L	Forced convection	Stresses – Heat losses – **Initial conditions**
L	Pressure drop (regular and singular)	Pumping power
L	Thermal stresses	Stresses

N) PRACS PIPES

The flow coming from the cold leg encounters at PRACS actual outlet an important resistance, due to the fluidic diode (entrance by the tangential port). However, a leakage flow through PRACS can be determined.

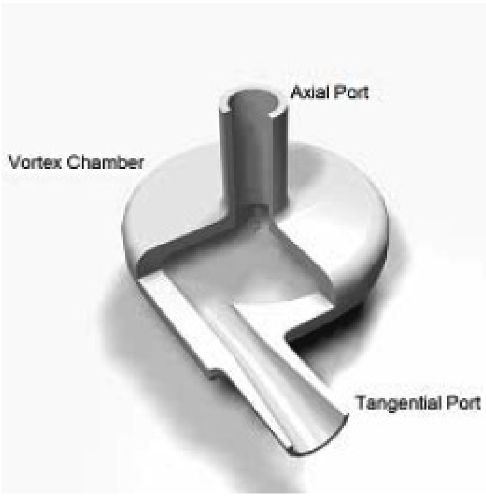

Figure A.VI.19: Picture of a vortex diode (taken out a vendor's brochure) [49].

Data given by a vendor of Vortex diode are given [49]:
- Friction factor K in the forward sense is equivalent to two 90° elbows. Taking K maximum (1.44), we choose K=2,88 for the downward flow.
- Pressure loss in the reverse flow is up to 150 times higher than in the downward flow. So, K=430 is chosen.

These data are arguable: C. Forsberg proposes a three time smaller value of K [50].

Assuming that:
- Pressure drop (regular and singular) in PRACS, down-stream diode, is negligible.
- Pressure drop through core is taken for a prismatic core
- Singular pressure drop at the nozzle in inlet plenum is negligible

We have the following relation:
Total pressure drop in core = Pressure drop in fluidic diode

$$\Delta P = K \cdot \frac{\rho \cdot v_0^{\ 2}}{2}$$

Thus:

$$\dot{m}_{leak} = \rho \cdot S \cdot v_0 = S \cdot \sqrt{\frac{2 \cdot \rho \cdot \Delta P}{K}}$$

Where ρ, v_0, S are respectively the density, velocity of the coolant at the inlet pipe and the flow area. K and S are important parameters to determine the leakage trough PRACS (compared to ρ and ΔP.

Table A.VI.22: PRACS pipes parameters.

K	430	145
Diameter of PRACS pipes (Alain Griveau data) (m)	0.1	0.1
Pressure drop in fluidic diode (Pa)	8.9×10^4	8.9×10^4
Mass flow in one PRACS module ($kg.s^{-1}$)	7	12
Flow speed in a PRACS hot pipe (600°C) ($m.s^{-1}$)	0.45	0.77
Reynolds number in hot pipe	$10.4\ 10^3$	$17.8\ 10^3$
Flow speed in a PRACS cold pipe (500°C) ($m.s^{-1}$)	0.44	0.75
Regular linear pressure drop on 2 m (Pa)	< 100	
Singular pressure drop (Pa) (two 90° elbows, K = 1.44)	$< 10^3$	

The pressure drops down-stream fluidic diodes are negligible.

The importance of the component relies only on the issue of the determination of the singular pressure drop through the fluidic diode. Otherwise, the low temperatures (roughly the inlet temperature), the small flow rate and the small heat exchange area (compared to the PHX bundles) lead to consider the other phenomena, similar as those of the cold leg, as not important. The pressure drop is a high-ranked phenomenon as it drives the main source of heat in the buffer tank, as shown in 3 C).

Table A.VI.23: Phenomena in PRACS pipes.

Rank	Phenomena	Criteria
H	Pressure drop – fluidic diode	Heat losses – Stresses – **Initial conditions**
L	Forced convection	Heat losses - Stresses
L	Conduction	Heat losses - Stresses
L	Thermal stresses	Stresses

O) <u>PHX TUBES</u>

The final design of PRACS has not yet been definitely defined. The diameter of the tubes, the geometry of the bundles (square or staggered rows) and the total number of tubes are variable parameters. These parameters are designed, according to the conditions of the natural circulation wanted the system to achieve when the reactor is shut down: mean temperatures of the core, buffer salt, value of decay power, LMTD on PRACS.

Using the previous preliminary studies, different sizing of PRACS are done, with the following constant features:

- Reactor inlet temperature of 700°C (a 100°C temperature increase is assumed at the beginning of a LOFC transient).
- Tube thickness is taken to be 0.1 of the tube diameter

- Salt is Flibe

Table A.VI.24: Sizing of the DHX.

Value of decay heat (%)	1		2	
Buffer salts temperatures (°C)	550	600	550	600
Tube diameter: 2. cm	1600	2180	2940	4050
Tube diameter: 2.5 cm	1530	2150	2880	3950

The minimal and maximal exchange area are obtained respectively for 1600 tubes/diameter 2cm (643 m^2) and 3950 tubes/diameter 2.5cm (1,985 m^2)
The minimal and maximal flow areas are obtained respectively for 1600 tubes/diameter 2cm (0.32 m^2) and 3950 tubes/diameter 2.5cm (1.24 m^2)

Assuming that 8 PHX are used and taking Flibe properties at 600°C, the flow remains laminar.

Table A.VI.25: Average flow characteristics in PHX pipes.

K	430	145
Diameter of PHX pipe (cm)	2.5	2
Number of PHX pipes	3950	1600
Flow speed in a PHX pipe ($m.s^{-1}$)	0.022	0.15
Reynolds number	102	556

There is almost no friction pressure drop, compared to the effects of the vortex (previous assumptions are verified).

The phenomena expected here are identical to those in PRACS pipe. However, one may notice that:

- Heat is transferred from salt to pipe walls by a forced convection, but here we are not in a case of aided flow mechanism, as for other vertical pipes. No mixed convection is achievable because of counter-flow. The very reduced thickness of the pipes result in a quasi-transparency to heat transfer and they will be isothermal (radially).
- We can expect that the most important thermal stresses are not radial but axial. Outlet primary temperature is expected to be very low, as the heat exchange surface is important. Thus temperature difference through walls may become rapidly small, whereas the inlet end of the PHX pipes may experience a fairly high temperature difference (until the transition to laminar flow zone). Moreover, tubes thickness is very small: thermal stresses are a high ranked phenomenon in this component.

Estimations of heat losses and temperatures differences through pipe walls are given in 3 A). These losses are expected to be important compared to the other components (hence must be assessed accurately). However, the very large heat transfer area and the very small flow speed may result in an outlet temperature equal to the buffer salt one (whatever the knowledge on convective heat transfer). Hence the following proposed ranked phenomena:

Table A.VI.26: Phenomena in the PHX tubes.

Rank	Phenomena	Criteria
H-**M**	Flow distribution	Heat losses – **Stresses – Initial conditions**
H-**M**	Forced convection	Heat losses – **Stresses – Initial conditions**
H-**M**	Pressure drop – forced convection	Heat losses – **Stresses – Initial conditions**
L	Conduction	Heat losses – **Stresses – Initial conditions**
H	Thermal stresses	**Stresses**

P) CHEMISTRY, VOLUME CONTROL AND PEBBLE INJECTION SYSTEMS

This component gathers many different complex systems that are not precisely designed yet.
The main comments can be expressed:

- Two phases and two fluid constituents are at stake: primary salt and inert gas, as argon in an volume control tank or in a pebble injection system (especially in the system where fresh or recycled pebble are re-inserted in the liquid salt loop)
- Flow can be driven by pumps (chemistry control loop for instance) or stagnant (volume control tank).
- Heat can be transferred in various ways: radiation through argon cover (for instance in the volume control tank) or forced convection in the chemistry control loop. Stratification mechanism is found in volume control tank.

Finally, the variety of phenomena is not relevant for the full-power PIRT since the volumes at stake are negligible compared to the other components. Heat losses are reduced. The main parts of these systems are at the atmosphere (where maintenance is easily achievable) and insulation can reduce the stresses induced by the high primary temperatures.
Moreover, these systems do not play any role during transients, thus, the estimation of their working parameters are not relevant for finding initial conditions in transients modelisations.

An attempt to provide a complete table of phenomena in this component would be unnecessary, as the numerous phenomena are found to be not important.

However, the pebble injection system could be the source of some very particular concerns:

- Fouling of salt by graphite dust or steel particles may be important: friction and bumps of pebbles against the steel pipes in the injection system,
- Inert gas entrainment with pebbles, as it could lead to local peak power increase, if void reactivity coefficient is positive.

2. Intermediate sub-system.

The intermediate sub-system is a key element of the whole system at full power since it provides the main heat sink. However, as detailed earlier, this sub-system is not precisely defined and a PIRT proposal would not be relevant.
Meanwhile, preliminary works have been performed on IHX: the intermediate side of this component shares the same issues than its primary counterpart.

Table A.VI.27: IHX intermediate side parameters.

Inlet temperature (°C)	570
Outlet temperature (°C)	630
Reynolds number	190
Pressure drop (Pa)	20 to 30x 10^4
LMTD (°C)	24.6
Differential pressure between hot and cold side (Pa)	Up to 1 x 10^6

Table A.VI.28: Phenomena in IHX intermediate side.

Rank	Phenomena	Criteria
H	Flow distribution	Pumping power - Stresses
H	Forced convection	Pumping power - Stresses
H	Pressure drop – forced convection	Pumping power - Stresses
H	Conduction	Pumping power - Stresses
H	Thermal and Mechanical stresses	Stresses

3. Buffer salt sub-system.

A) PHX REGION

A small forced circulation occurs in PHX pipes due to leakage through fluidic diode. Hence some heat is transferred to buffer salt in PHX region, driving some natural circulation, aided by baffles. Cold salt coming downwards along DHX pushes salt upwards through PHX.
The heat is transferred to the buffer salt by convection (natural circulation in baffles), however the effect of buoyancy must be checked in order to determine the adequate correlation: mixed or forced convection.

Simple calculations have been done, considering:

- Uniform buffer salt temperature at 500°C (the effect of natural circulation is ignored)
- Different PHX geometries, working temperatures and pressure drop through fluidic diode.
- 8 inlet PRACS pipes
- For calculation, the flow is assumed to be one-dimensional and laminar fully developed (the ratio $\frac{L}{D} = 250$ drives to this assumption), Nusselt=4.36.
- The conductivity has been taken to be 20 $W.m^{-1}.K^{-1}$ (Incolloy® 800 at 500°C)

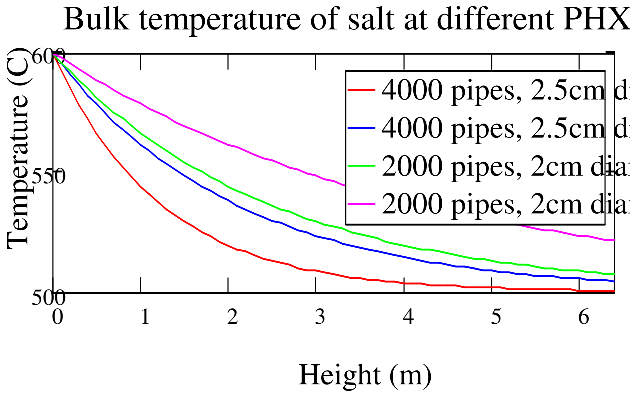

Figure A.VI.20: Flibe temperature in PHX, AHTR low temperature version.

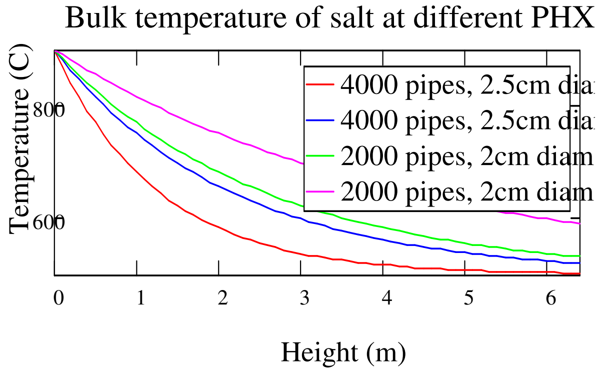

Figure A.VI.21: Flibe temperature in PHX, AHTR high temperature version.

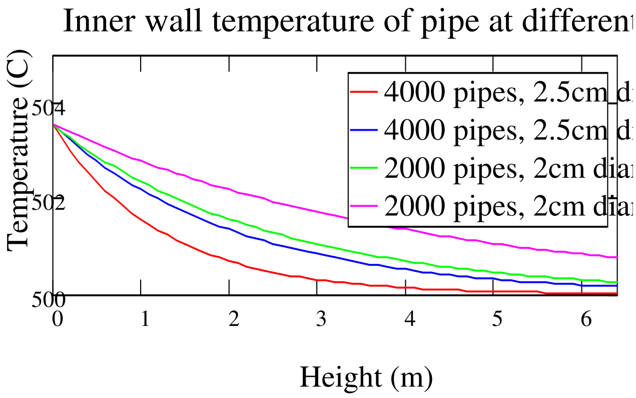

Figure A.VI.22: Inner wall temperature in PHX tube, AHTR low temperature version.

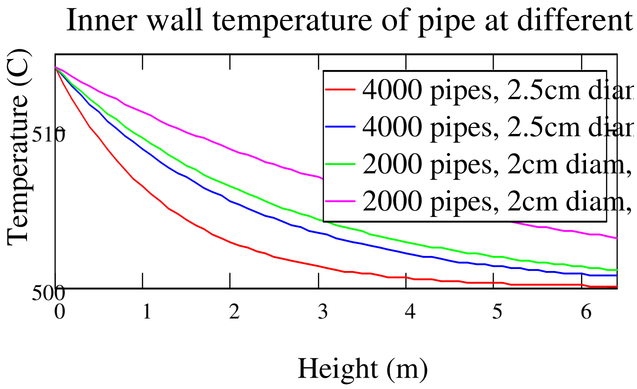

Figure A.VI.23: Inner wall temperature in PHX tube, AHTR high temperature version.

Table A.VI.29: Heat losses (MW) through PHX, for different cases.

	Electricity version		H2 version	
	K=430	K=150	K=430	K=150
Tubes number: 4000- diameter: 2.5 cm	**12**	**19**	**49**	**79**
Tubes number: 2000- diameter: 2.0 cm	**11**	**16**	**46**	**64**

The total heat losses are important, compared to the other primary components: the high temperature difference in the hydrogen version of AHTR lead to a rough loss of 3 % of the total output. The value of the pressure drop through the diode is extremely important: thus the determination of the K-factor is a key parameter, as well as the pressure drop through the bed (but, already judged important for other reasons). It has been already discussed in 1O).

Figure A.VI.20 and Figure A.VI.21 show that, whatever the design (diode or PHX), the outlet temperature is very closed of the buffer salt one. The slow laminar flow results in a quasi equilibrium between buffer salt and Flibe at the PHX outlet. Hence the convection mechanisms (and phenomena associated such as pressure drop) are slightly less important that the driving phenomena, upstream the PHX: the diode effect and the core pressure drop.

Radial thermal stresses are expected to be important in the beginning of the tube (especially in the hydrogen version and the designs with small PHX cross-section area, as speed increases), as shown in Figure A.VI.22 and Figure A.VI.23. However, it would be reduced by the effect of the external boundary layer in the buffer salt, imposed by the convection mechanism.

The axial temperature gradient is reduced, however, the transition zone from the inlet turbulent flow (coming from the PHX plenum) to the laminar flow, would modify this.

Using these values, simple calculations have been done to characterize the buffer salt flow:

- The single case of 4000 tubes, with a 5 cm pitch (squared) is considered
- Natural circulation is assumed (buoyancy forces are balanced by the regular and outlet singular pressure drop)
- Heat transfer values are taken from
- Table A.VI.29: Heat losses (MW) through PHX, for different cases..

Table A.VI.30: Buffer salt general characteristics in PHX.

Cases	80 MW transferred	10 MW transferred
Reynolds number	50,000	50,000
Flow speed ($m.s^{-1}$)	0.4	0.2
Outlet temperature (°C)	508	502

It can be noted that the assumption of a constant buffer salt temperature is reasonable. The flow would be turbulent. It may result in an actual lower temperature difference through the PHX tubes, due to the thickness of the boundary layer.

Table A.VI.31: Phenomena in buffer salt PHX region.

Rank	Phenomena	Criteria
H-**M**	Flow distribution	Heat losses – **Stresses – Initial conditions**
H-**M**	Forced (or mixed) convection	Heat losses – **Stresses – Initial conditions**
H-**M**	Pressure drop – forced (or mixed) convection	Heat losses – **Stresses – Initial conditions**

B) REACTOR VESSEL REGION

Considering the geometry, one may assume two different regions:

- Along the sides of the reactor vessel
- On the bottom of the reactor vessel.

Along the reactor vessel, cool buffer salt flows upwards, along the hot walls of the vessel. Heat is removed by external free convection. Heat losses and temperature gradient through the metallic vessel have been estimated. Of course, an insulation layer can mitigate the results.

The following simplifications are used:

- Buffer salt bulk temperature is taken constant (no stratification)
- Constant temperature in the reactor
- We consider that heat transfer from reactor vessel to buffer salt is similar to a vertical flat wall heated constantly, as curvature does not have a particular influence. So we use the following correlation (4.112), valid for all Prandtl and Rayleigh, by Churchill and Chu, taken out Bejan [41], page 216, assuming that:

$$\overline{Nu_y} = \left(0.825 + \frac{0.387 \cdot Ra_y^{1/6}}{\left(1 + (0.437/\Pr)^{9/16}\right)^{8/27}} \right)^2$$

Where

- ○ $\overline{Nu_y}$ is the Nusselt number averaged on a y length height.
- ○ Ra_y is the Rayleigh number, calculated with y as a characteristic length

- No gap conductance between reflector and reactor vessel
- Cooling through graphite reflector is simulated by reducing the radial conductivity of graphite.

The following parameters are used:

Table A.VI.32: Reactor vessel and reflector parameters.

Characteristic height (m)	8
Core diameter (m)	6.84
Graphite reflector thickness (m)	0.9
Reactor vessel thickness (m)	0.1
Reactor vessel outer diameter (m)	9
Steel conductivity	21.5

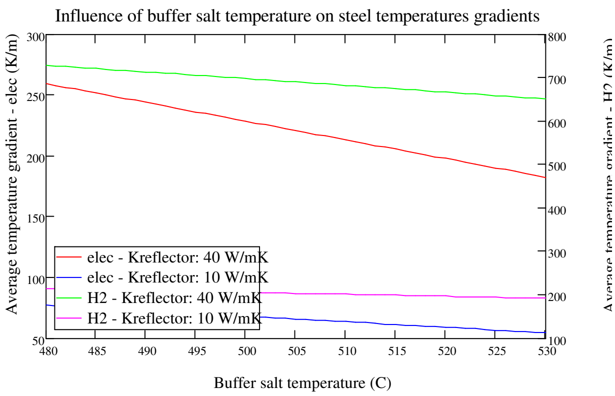

Figure A.VI.24: Effect of buffer salt temperature on temperature gradient through reactor vessel, for different versions of AHTR.

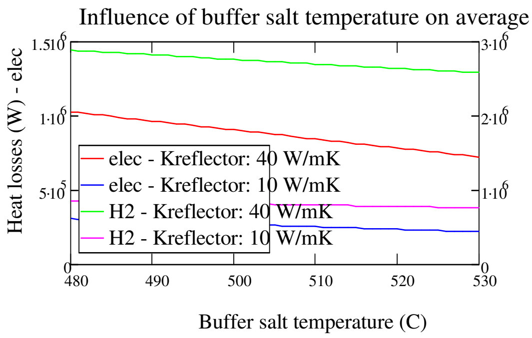

Figure A.VI.25: Effect of buffer salt temperature on heat losses, for different versions of AHTR.

The cooling by the by-pass flow in the reflector drives the heat losses and temperatures distribution in the reactor vessel (Figure A.VI.24 and Figure A.VI.25). It is reasonable to model the effect of by-pass on the effective radial conductivity by a decrease of a factor at least 4 (which roughly corresponds to a 5% by-pass flow exiting with 5 to 10 °C of temperature increase). The effect of a reasonable change in the conductivity has more impact than an important change of the average buffer salt temperature. Moreover the values found for temperature gradients and heat losses are low (same order than the all insulated legs for instance). Finally it could be concluded that phenomena occurring along the reactor vessel are not important, even if for buffer salt initial temperature prediction. In addition, it is found that the heat losses through PHX are the main heat source for buffer salt.
The presence of PHX baffles closed to the reactor vessel should not alter significantly these heat transfer as they remain at temperatures closed to the average buffers salt one.

The bottom region will mainly see stratification phenomena, as it can be modeled as a zone heated from the top and cooled from the side. The curved shape of the bottom would induce flows created by external free convection.
In this planar heat transfer model, the problem is ruled by two important heat resistances: the buffer salt layer and the insulating layer (other materials become negligible, as for instance the presence or not of a thick lower graphite reflector).
As boundary temperatures are fixed (RCCS and inlet plenum), a minimum amount of insulation is needed to prevent buffer salt from freezing (order of one meter for the electricity version of AHTR, as shown in Figure A.VI.26). It results in very small temperature gradients through metal components (reactor vessel and buffer salt tank), no heat losses and negligible impact of boundary temperature changes (Figure A.VI.27 and Figure A.VI.28).
No phenomenon is judged as important in this region of the component.

Data used to describe the problem:

Table A.VI.33: Parameters of materials for heat transfer from the bottom of reactor vessel.

Bottom area (m^2)	63.7
Buffer salt conductivity ($W.m^{-1}.°C^{-1}$)	0.5
Graphite reflector inner temperature (°C)	600
Graphite reflector thickness if any (m)	1.2
Reactor vessel thickness (m)	0.1
Buffer salt thickness (m)	1
Buffer salt tank thickness (m)	0.15
Graphite insulating thickness (m) (We can choose high temperature thermal insulation material to prevent heat loss through bottom tank wall, there is a layer of Argon gas)	0.5
Liner thickness	0.02
Steel conductivity	21.5
Graphite conductivity (600°C – 50°C)	30

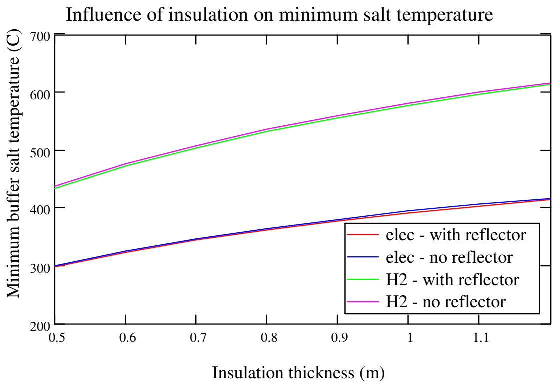

Figure A.VI.26: Effect of insulation on the minimum temperature of the buffer salt.

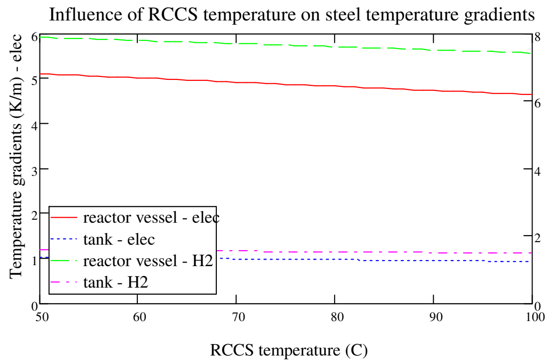

Figure A.VI.27: Temperature gradients through the metallic constituents and effect of RCCS temperature (with consistent insulation).

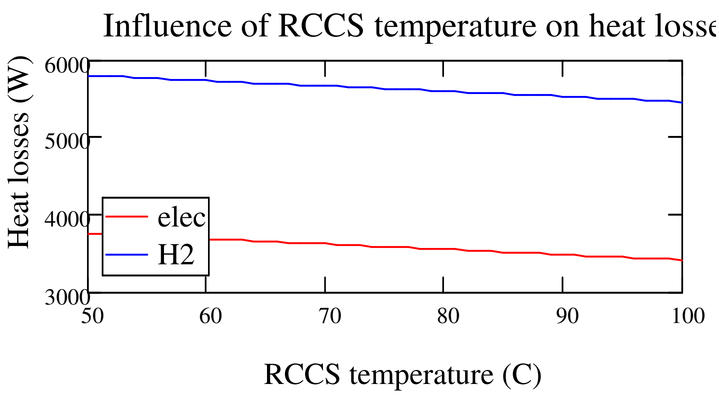

Figure A.VI.28: Heat losses as function of RCCS temperature.

Table A.VI.34: Phenomena in the reactor vessel region.

Rank	Phenomena	Criteria
L	Free convection	Stresses – Heat losses **– Initial conditions**
L	Stratification (relevant along the reactor vessel side).	Stresses – Heat losses – **Initial conditions**

C) <u>DHX REGION</u>

The same mechanisms than for PHX are involved. DHX heat transfer is an important issue as it provides the main heat sink for buffer salt. Because of the need to maintain in normal operations its temperature to the lowest possible value (highest thermal inertia), heat transfers have to be predicted accurately. However, contrary to the DHX, the temperature difference will be fairly reduced, as Flinak is likely to be used as DRACS coolant, thus stresses are not the driving criterion here.

Table A.VI.35: Phenomena in the DHX region.

Rank	Phenomena	Criteria
H	Flow distribution	**Initial conditions**
H	Forced (or mixed) convection	**Initial conditions**
H	Pressure drop – forced (fixed) convection	**Initial conditions**

D) REACTOR FREE SPACE

This module features the space enclosed by the reactor vessel, the buffer salt tank and the PHX/DHX and is composed of two constituents and two phases, as inert gas (argon) at atmospheric pressure covers the buffer salt free surface.

Natural circulation of buffer salt, induced by external free convection occurs along:

- Horizontal pipes (hot and cold legs),
- Vertical pipes (cold leg, primary pump tanks)
- IHX

On the other hand in the large obstacle-free space, stratification of the large amount of buffer salt is expected (which could influence heat transfer prediction along reactor vessel, buffer salt tank and primary pipes).
Since insulation would be used to minimize the temperature gradients within the buffer salt tank, the temperature distribution would be roughly uniform in the whole space enclosed by the buffer tank, especially even in the argon cover (as for the primary salt pool). Thus natural circulation of argon would remain limited, as temperatures differences would be too small to drive significant internal free convection (Rayleigh-Bénard cells if the argon layer is thin enough). Hence radiation is expected to be the main heat transfer mechanism through argon (as for primary salt free surfaces, gas released through free surface may condensate on tank colder walls and modify radiation characteristics).

Rough calculations have been conducted to estimate the heat losses along the primary pipes plunged in the buffer salt. The relative influence of insulation and buffer salt temperature are assessed, regarding their consequences on the temperature gradients and total heat transferred. It yields to ranking propositions for phenomena (Table A.VI.14, Table A.VI.15, Table A.VI.17 and Table A.VI.21). The average working temperature is taken into account (hydrogen or electricity version of AHTR), as well as the possibility of multiple colds legs in the pebble-bed version.

Assumptions:

- The pipes are considered as totally horizontal or vertical.
- Total length is assumed to be 13 meters: 2 horizontal pipes of 3 meter long and 1 vertical pipe 1 meter long.
- Pipe thickness is assumed to be one tenth of the radius.
- To assess the inner convection, we used the correlation by Gnielinski ([41], page 394, equation (8.33)). The friction factor is given by the correlation by Karman-Nikuradse (Bejan page 387, (8.14)), valid for $2\ 10^4 < Re_D < 10^6$

$$f = 0.046 \cdot \mathrm{Re}_D^{-1/5}$$

This is more suitable than the Blasius relation.

- To assess the external convection along horizontal pipes (parts of hot and cold legs), we used the following correlation by Churchill and Chu, taken out Bejan, page 221 (4.122):

$$Nu_D = \left(0.6 + \frac{0.387 \cdot Ra_D^{1/6}}{\left(1 + (0.559/\Pr)^{9/16}\right)^{8/27}} \right)^2$$

This is valid for an isothermal cylinder and all range of Pr and $10^{-5} < Ra_D < 10^{12}$. In our case, we assumed that this relation is still valid, as the Ra are superior at less on order of magnitude to 10^{12}.

- To assess the external convection along vertical pipes, we used the correlation by Churchill and Chu for a vertical wall, taken out Bejan, (4.112). This assumption is valid as long as the boundary layer thickness is much smaller than the cylinder diameter. When Pr >1, the thermal boundary layer thickness δ_T can be approached by:

$$\delta_T = H \cdot Ra_H^{-1/4}$$

The hot leg is subject by far to the highest temperature gradient (Figure A.VI.32) in the whole reactor. Insulation must be used and reduces very efficiently this gradient (Figure A.VI.34), whereas the influence of buffer salt temperature is very secondary as shown in Figure A.VI.29 and Figure A.VI.30. Hence, the need to model the effective buffer salt temperature is not relevant for thermal stresses issues in the leg.

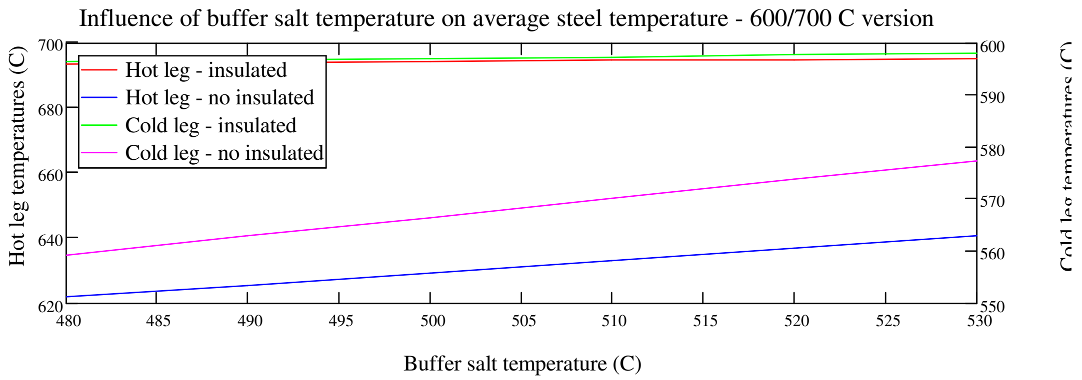

Figure A.VI.29: Average legs temperatures as functions of buffer salt temperature in low temperature version of AHTR.

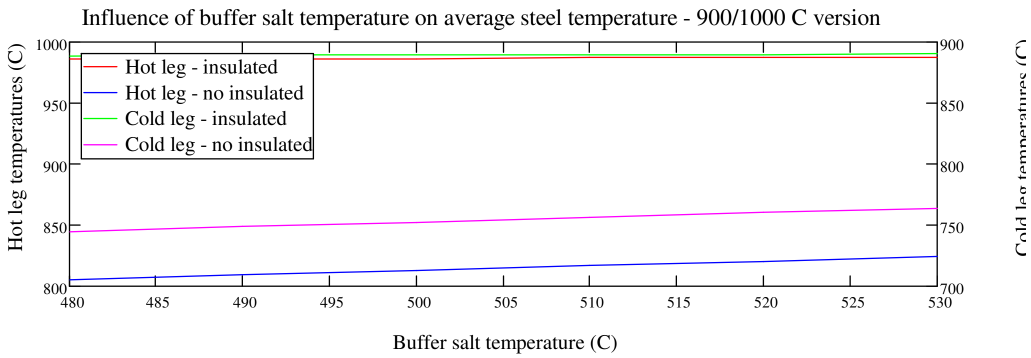

Figure A.VI.30: Average legs temperatures as functions of buffer salt temperature in high temperature version of AHTR.

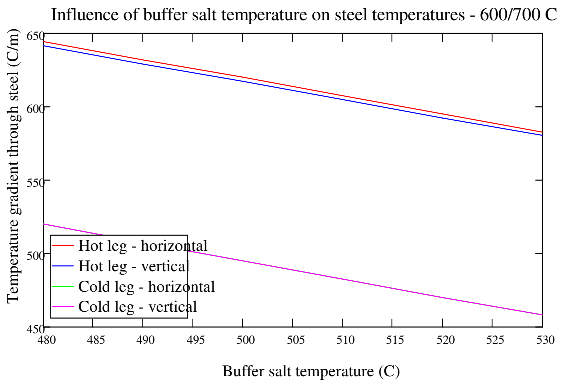

Figure A.VI.31: Temperature gradients in insulated legs as functions of buffer salt temperature in low temperature version of AHTR.

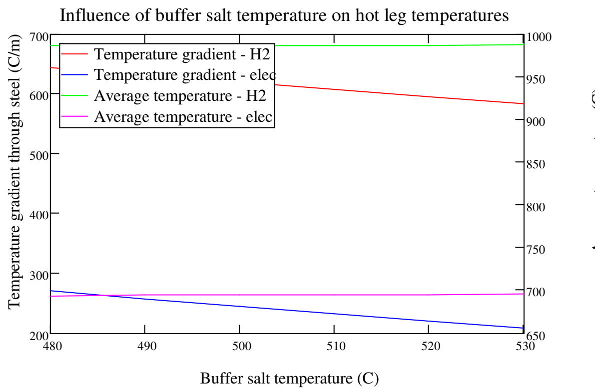

Figure A.VI.32: Average temperatures and temperature gradients in the insulated hot leg, as functions of buffer salt temperature, in different AHTR versions

The efficiency of insulation reaches a threshold, beyond which extra-insulation is not useful. This approximate threshold value (2 cm) is used in calculations in insulated legs (Figure A.VI.29 and Figure A.VI.30). This effect is shown in Figure A.VI.34 and Figure A.VI.36.
Heat losses for the total length of primary pipes are calculated. Insulation reduces dramatically these losses as shown in Figure A.VI.34.

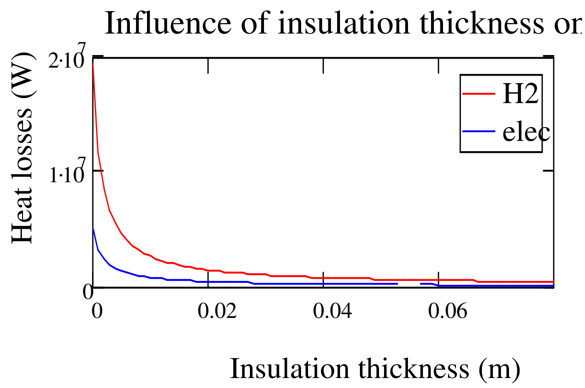

Figure A.VI.33: Effect of insulation on total heat losses (4 cold legs).

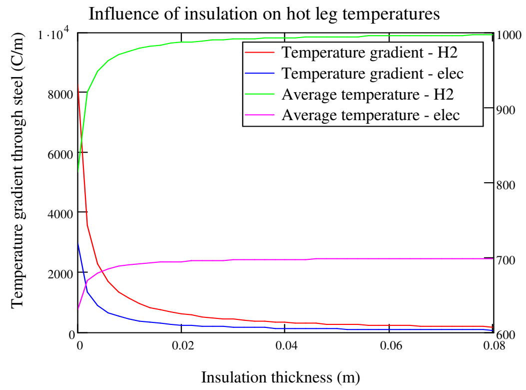

Figure A.VI.34: Effect of insulation on temperatures distribution within the hot leg.

Calculations done for a larger number of cold legs show similar effects. The flow speed has been kept constant to size the cold legs diameter. Insulation thickness is taken to be equal to the steel thickness (itself one tenth of the radius).
Even if the values of heat losses are multiplied by up to four, by using insulation, these values become negligible regarding the total thermal output of the reactor (economics criteria).

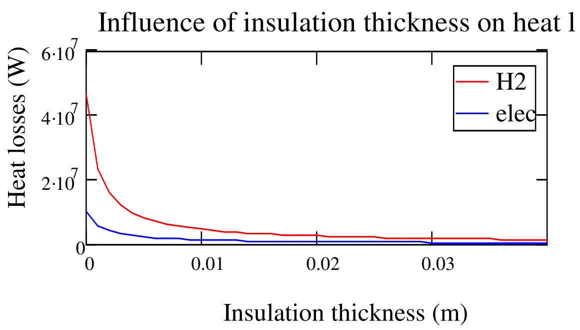

Figure A.VI.35: Effect of insulation on total heat losses (16 cold legs)

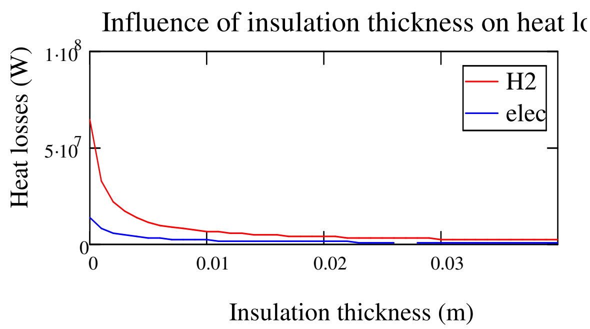

Figure A.VI.36: Effect of insulation on total heat losses (32 cold legs)

The absolute need to insulate the legs implies that in terms of heat losses and thermal stresses, the phenomena occurring in the buffer salt become not really relevant (free convection or buffer salt temperature distribution due to stratification), since their influence become minor (as shown in Figure A.VI.37), related to the importance of conduction through insulation.

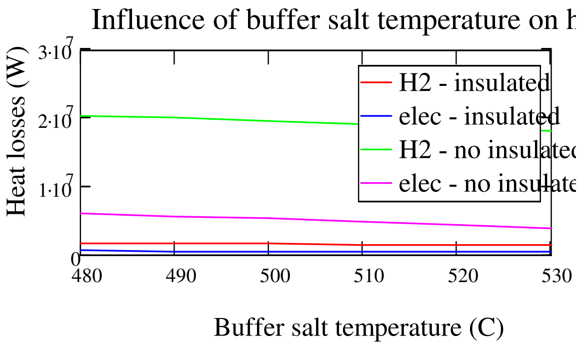

Figure A.VI.37: Effect of average buffer salt temperature on heat losses, in different cases.

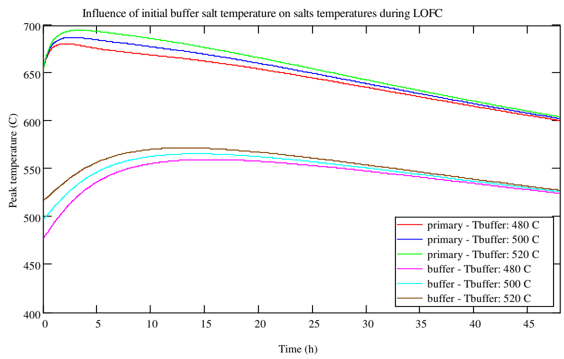

Figure A.VI.38: Effect of initial buffer salt temperature on the peak salt temperatures during LOFC (electricity version of AHTR).

As mentioned earlier, buffer salt temperature must be correctly assessed to ensure that decay heat is removed efficiently by the buffer salt during transients (however, the resulting difference in the peak primary temperature is inferior to the difference in the initial buffer salt temperature, as shown in Figure A.VI.37). This temperature is driven by the heat source in the buffer salt (the primary heat losses) and the heat sink (DRACS and heat losses through the buffer salt tank). Finally, the amount of power lost through the insulated primary pipes is of the same order of magnitude (few MW) than the free convection along the reactor vessel (Figure A.VI.28).
This is still inferior to the heat transferred through PHX (order of 10 MW).

Table A.VI.36: Phenomena in the free space.

Rank	Phenomena	Criteria
L	Free convection	Stresses – Heat losses – **Initial conditions**
L	Stratification	Stresses – Heat losses – **Initial conditions**

E) <u>TANK REGION</u>

The previous phenomena observed in the free space are expected locally (except the fact that a permanent downwards flow will exist). Heat transferred by free convection then by conduction through the tank itself is strongly linked to the phenomena in tertiary sub-system and is assessed in 4 A). This latter paragraph will show that temperature gradients through buffer salt tank, as well as heat losses, are driven by the conduction mechanisms through insulation and radiation issues in the gap. Influence of the boundary buffer salt temperature plays then a secondary role.

Table A.VI.37: Phenomena in the tank region.

Rank	Phenomena	Criteria
L	Conduction	**Stresses** – Heat losses – Initial conditions
L	Natural convection (in buffer salt)	**Stresses** – Heat losses – Initial conditions
L	Stratification	**Stresses** – Heat losses – Initial conditions
L	Thermal stresses	**Stresses**

4. Tertiary system.

A) LINER/GRAPHITE/CAVITY

The buffer tank is located in a cooled cavity. Argon is likely to be the gas retained to fill the cavity (avoid corrosion of buffer tank and oxidation of graphite during severe accidents where temperatures may rise if air leaks from this space). The bottom of the buffer salt tank lays on an insulation layer.

Following the baseline design, the parameters described in Table A.VI.38 are used.

Table A.VI.38: Cavity parameters.

Buffer tank inner diameter (m)	14.5
Buffer tank thickness (m)	0.15
Gas space thickness (m)	0.25
Liner insulator thickness (m)	0.5
Liner thickness (m)	0.01
Height (m)	12
Cavity diameter (at RCCS) (m)	16

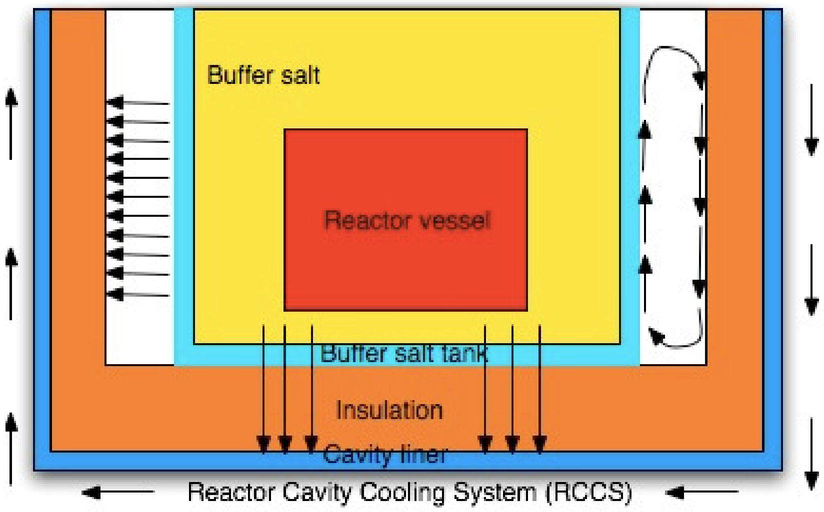

Figure A.VI.39: Schematic of the cavity.

The argon gas, the only fluid constituent, of this component can flow in its cavity, driven by a natural circulation, created along the inner hot and outer cold walls by external free convection mechanisms. The gas far from these zones could stratify vertically.
Heat is transferred by conduction through buffer salt tank, argon (expected to be negligible), graphite insulation, liner and then RCCS tubes. In the argon filled gap, radiation and convection compete to transfer heat.

The temperatures distribution and the heat losses are estimated for the sides of the buffer tank (for the bottom this simple work has been done in 3 B).

Convective heat transfer is estimated by considering that the situation in argon gap is similar to a situation with two plates at different temperatures (the curvature of the large tank allows this simplification). We used a correlation dedicated to tall enclosures, taken out of Bejan (5.40), page 256:

$$\overline{Nu} = 0.364 \cdot \frac{L}{H} \cdot Ra_H^{1/4}$$

Where

- $\overline{Nu}$ is the Nusselt number averaged on a H height.
- Ra_H is the Rayleigh number, calculated with H as a characteristic length
- L is the width of the enclosure

Radiation is calculated by:

$$q'' = \frac{\sigma \cdot \left((T_{in})^4 - (T_{out})^4\right)}{\left(\frac{1}{\varepsilon_{in}} + \frac{1}{\varepsilon_{out}} - 1\right)}$$

Where:
- q'' is the heat flux by area unit.
- σ is the Stefan Boltzmann constant
- T is the temperature of one side of the cavity (the suffix "in" for inner side, "out" for outer side)
- ε is the emissivity of one side of the cavity.

The main issues arisen are the heat losses and the temperature gradient though the buffer salt tank. Two parameters can be used to minimize this: insulation and emissivity of the walls of the gap. In some high temperature reactors designs, the cavity is one of the main systems used for heat removal, thus cavity design is optimized for radiation heat transfer (emissivity of 0.4 for air or 0.8 for argon are commonly used [33], [34] and [31]). In AHTR, emissivity can be reduced to help to insulate the buffer tank and then reduce temperature differences, as other systems are used for heat removal.

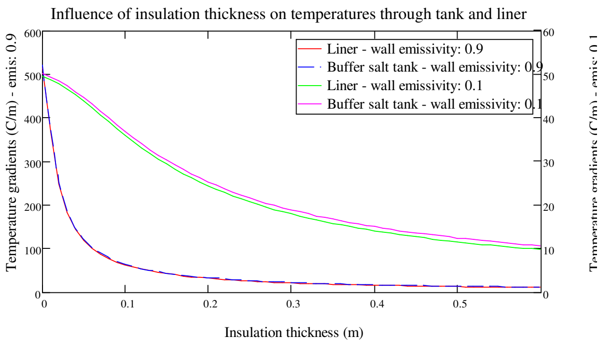

Figure A.VI.40: Effect of insulation on temperature gradients through buffer salt tank and cavity liner (high and low emissivity cases).

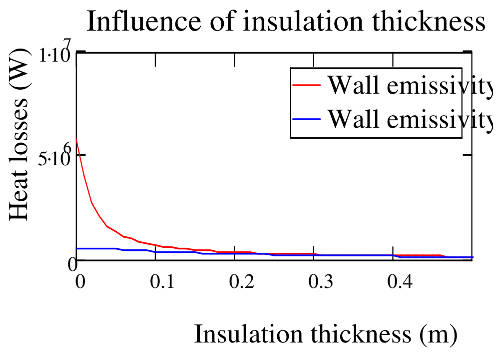

Figure A.VI.41: Effect of insulation on heat losses (high and low emissivity cases).

The use of low emissivity surfaces has the same consequences in terms of heat losses and temperature gradient than an insulating layer of 0.3m. Heat losses (order of several hundreds of kW) become inferior by far to the estimated primary heat losses (several MW) and temperature gradients are inferior of those within the reactor vessel.

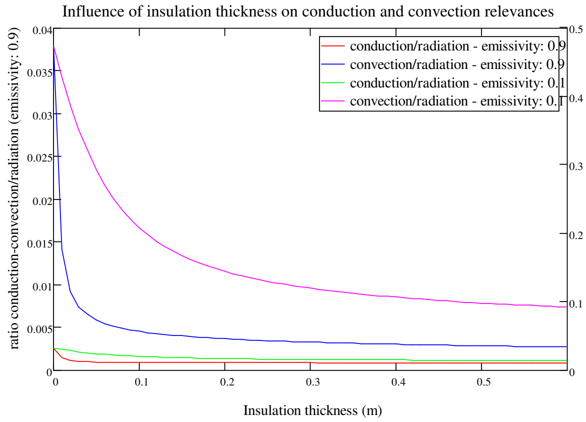

Figure A.VI.42: Ratios of heat transferred by conduction (or convection) over heat transferred by radiation, as functions of insulation thickness. Effect of emissivity on these ratios.

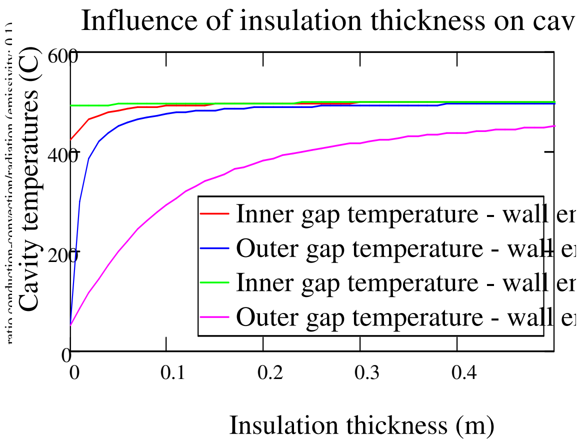

Figure A.VI.43: Main temperatures as functions of insulation thickness. Effect of emissivity on these temperatures.

Low emissivity surfaces induce a higher temperature difference through the argon gap, thus increasing the internal free convection mechanisms. This phenomenon is reduced by the insulation. Then, convection mechanisms are found to transfer up to 50 % of the heat transferred by radiation, in low emissivity walls cases, with little insulation (still 10 % with important insulation layer).

Conduction through insulation and radiation through argon are the most important phenomena. Changes in the boundary conditions (linked for instance to free convection mechanisms of the buffer salt along the tank, or forced circulation of water in the RCCS) don't affect much the temperature gradients (Figure A.VI.44 and Figure A.VI.45) and the heat losses (Figure A.VI.46 and Figure A.VI.47). The values obtained remain in the same range of results: very low temperature drops and heat losses inferior of an order of magnitude to the primary losses. Thus DHX will play the most important role in buffer salt temperature regulation.

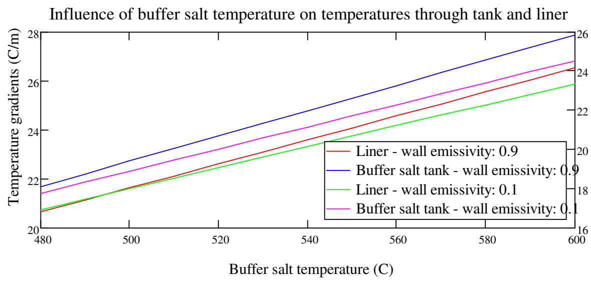

Figure A.VI.44: Influence of buffer salt temperature on temperature gradients through metallic constituents (insulated cavity).

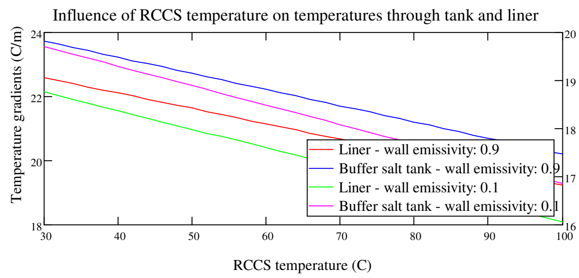

Figure A.VI.45: Influence of RCCS temperature on temperature gradients through metallic constituents (insulated cavity).

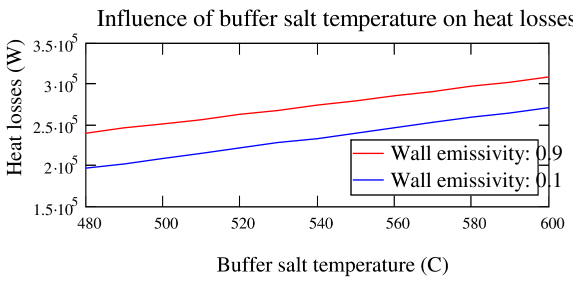

Figure A.VI.46: Influence of buffer salt temperature on heat losses (insulated cavity).

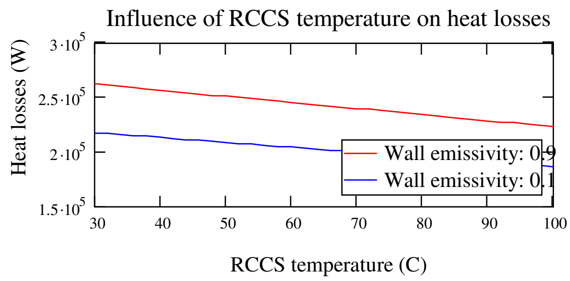

Figure A.VI.47: Influence of RCCS temperature on heat losses (insulated cavity).

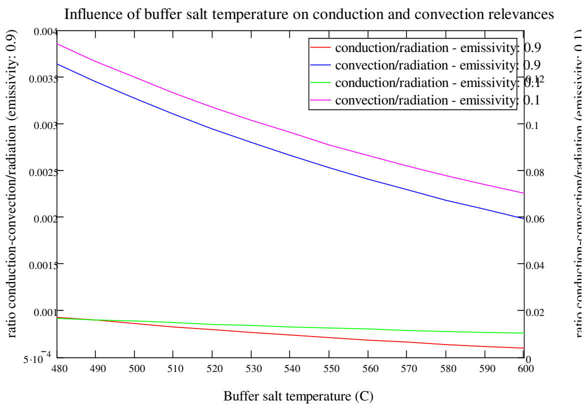

Figure A.VI.48: Influence of average buffer salt temperature on the relevance of convection and conduction phenomena, compared to radiation.

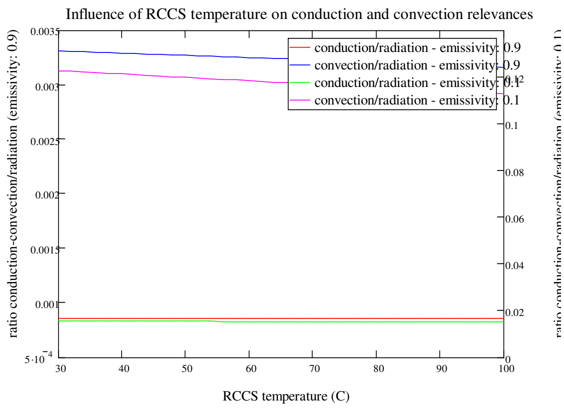

Figure A.VI.49: Influence of RCCS temperature on the relevance of convection and conduction phenomena, compared to radiation.

The importance of conduction and convection, compared to radiation is not altered by large variations of the boundary temperatures (Figure A.VI.47 and Figure A.VI.48). For instance, the amount of heat transferred by convection is still of an order of 10 % in transients conditions (LOFC where buffer salt temperature may rise 600°C, even if radiation importance would increase as the 4th power.

Table A.VI.39: Phenomena in the cavity.

Rank	Phenomena	Criteria
M-L	Radiation (including emissivity issues)	**Stresses** – Heat losses – Initial conditions
M-L	Conduction (including gaps)	**Stresses** – Heat losses – Initial conditions
L	Natural convection (in argon)	**Stresses** – Heat losses – Initial conditions
L	Stratification (in argon)	**Stresses** – Heat losses – Initial conditions
L	Thermal stresses	**Stresses**

B) DHX

The actual design has retained an intermediate salt for heat removal in DHX. This salt, presumably Flinak, would flow by loop natural circulation mechanism. Heat will removed in the

DHX by forced or mixed convection mechanisms, as well as conduction through pipe walls. The distribution of the flow within the bundle of pipes is a relevant phenomenon to estimate the efficiency of the exchanger. The pressure drop assessment is a relevant phenomenon as it is linked to the flow and heat transfer.
The DRACS systems have been found to be important components for regulation of buffer salt temperature and the prediction of initial conditions for transient modelisations.
Thermal stresses through walls should be reduced as Flinak works with a high freezing temperature of 450°C [51].

Table A.VI.40: Phenomena in the DHX.

Rank	Phenomena	Criteria
H	Flow distribution	Initial conditions
H	Forced (or mixed) convection	Initial conditions
H	Pressure drop – forced (or mixed) convection	Initial conditions
H	Conduction	Initial conditions
L	Thermal stresses	Stresses

C) DRACS OUTSIDE EXCHANGERS

The liquid coolant would release heat through different possible passive heat exchangers (water, air). No PIRT is proposed here as phenomena are very dependent of the design. However, those linked to heat transfer would be ranked of the highest importance since they regulate the buffer salt temperature.

D) DRACS HOT/COLD LEGS

Natural circulation is driven by buoyancy forces: thus pressure drop is an important issue in this loop since it determines the heat transfer in the sensitive components: the heat exchangers.
The legs, in the open air, are insulated, thus reducing heat losses and temperature gradients through pipe walls. Convection or conduction mechanisms are essential to estimate these latter phenomena (expected to be limited due to insulation) that influence also the temperature distribution within the loop (hence the natural circulation mechanism).

Table A.VI.41: Phenomena in the DRACS legs.

Rank	Phenomena	Criteria
M - L	Forced (or mixed in vertical cold leg) convection	Heat losses - Stresses
H	Pressure drop (regular and singular)	Initial conditions
M - L	Conduction (through pipe and insulator)	Heat losses - Stresses
L	Thermal stresses	Stresses

E) RCCS

The Reactor Cavity Cooling System (RCCS) is composed of a stack of tubes, wherein water flow is forced. It covers the whole surface of cavity. Heat is transferred first by conduction through tubes walls and then by forced (possibly mixed) convection.
As shown in 4 A), variations of RCCS temperature don't affect much global values as heat losses and temperatures gradients, as long as proper design is retained (insulation for instance). Thus the mechanisms that drive the temperature distributions are considered of low importance.

Table A.VI.42: Phenomena in the RCCS.

Rank	Phenomena	Criteria
L	Forced (or mixed if any) convection	**Stresses** – Heat losses – Initial conditions
L	Pressure drop (regular and singular)	**Stresses** – Heat losses – Initial conditions
L	Conduction	**Stresses** – Heat losses – Initial conditions
L	Thermal stresses	Stresses

F) CONCRETE SILO/CONFINEMENT

This module groups a fairly important number of different elements. To simplify, one may retain:

- Concrete silo surrounding the cavity
- Concrete structures topping the primary pool and buffer salt tank.
- Ambient atmosphere in the hall toping the reactor
- Concrete containment over this hall.

Residual heat losses are transferred to the ground by conduction and external free natural convection to the atmosphere of the hall.

As shown in the previous paragraphs, insulations or low emissivity walls are retained in the design to minimize the temperature differences in the sensitive components. Hence, the choice of the surrounding materials and the estimation of the phenomena becomes secondary, as this component will show little influence on the all criteria found to be affected by the other components.

Table A.VI.43: Phenomena in the silo-confinement.

Rank	Phenomena	Criteria
L	Free convection	Stresses – Heat losses – Initial conditions
L	Conduction	Stresses – Heat losses – Initial conditions

APPENDIX VII

DETAILED FULL POWER PIRT

		Primary															Buffer					Tertiary				
		Inlet plenum	Core	Reflector	Outlet plenum	Reactor vessel	Reactor cover and primary pool	Hot leg	Pump	Seal bowl	Cross-over leg	IHX	Cold leg	PRACS pipe	PHX tubes		PHX region	Reactor vessel region	DHX region	Free space	Tank	Liner / Graphite / Cavity	DHX	DRACS leg	RCCS	Silo / Confinement
Power	Steady state neutronics		H																							
	Gamma heating	L	M	M-L	L	L																				
Flow	Flow distribution	H	H	M	M							H			H-M	H	H-M		H				H			
	Pressure drop	M	H	M	L			L			M	H	L	H	H-M	H	H-M		H				H	H	L	
Heat transfer	Jet discharge, hot streaks, hot plumes and mixing				H		L																			
	Forced (or mixed)convection	M	H	M	L			L	L		L	H	L	L	H-M	H	H-M		H				H	M-L	L	
	Stratification						L			L								L		L	L	L				
	Conduction	L	H	M-L	L	L	M-L	M-L	M-L	M-L	M-L	H	M-L	L	L	H					L	M-L	H	M-L	L	L
	Radiation						M-L			L												M-L				
	Natural free convection						M-L			L								L		L	L	L				L
Others	Thermal stresses	L	H	L	M	L	L	L	L	L	L	H	L	L	H	H					L	L	L	L	L	
	Kernel migration		H																							
	Pebble distribution		H																							
	Mechanical stresses								M			H				H					H	H				
	Fouling	x	xxx	x	xx		x	xx	xx	x	xx	xx	x	x	x	xx	x	x	x	x	x		x	x	x	
	Condensation						x													x	x					
	Irradiation damage	x	x	x	x	xx	x																			

SIMPLIFIED LOFC PIRT

	Core			**Plenum**			**Reflector**			**Pracs pipe**			**PHX**			**Buffer salt - PHX region**			**Buffer salt - DHX region**			**Dracs**		
Stage	1	2	3	1	2	3	1	2	3	1	2	3	1	2	3	1	2	3	1	2	3	1	2	3
Decay heat	M	H	H																					
Convection	L	H	H	L	L	L	L	M	L	L	L	L	L	M	H	L	M	H	L	L	L	L	L	L
Conduction – stored energy	L	H	L-M	L	H	H	L	H	L	L	H	L	L	H	H	L	M	H	L	L	L	L	L	L
Pressure loss	L	L	L	L	L	L	L	L	L	L	H	H	L	L	L	L	L	L	L	L	L	L	L	L
Pebble distribution	L	M																						

APPENDIX VIII

LITERATURE REVIEW ON HEAT TRANSFER THROUGH PACKED BED OF SPHERES

A literature review has been performed to find the most relevant correlations to determine the heat transfer in a packed bed of spheres. Reports on pebbles-beds cite sometimes very different sources that are not consistent. As the AHTR deals with extremely different fluids (high Prandlt number compared to helium), the adequacy of the known correlations has to be questioned.

1. Review.

Here is a chronological list of the work in this field.

1952

Ranz [52] gives the following correlations:

- For 1 single sphere:

$$Nu = 2 + 0{,}6 \cdot \mathrm{Pr}^{\frac{1}{3}} \cdot \mathrm{Re}^{\frac{1}{2}} \quad (1),$$

(cited in [51]), where Re is calculated with the superficial velocity and the range of validity is 1< Re <70000 and 0,6 < Pr < 400

- For a bed of packed spheres:

$$Nu = 2 + 1{,}8 \cdot \mathrm{Pr}^{\frac{1}{3}} \cdot \mathrm{Re}^{\frac{1}{2}} \quad (2)$$

Where Re is calculated with the superficial velocity. Experimental data are found to match this correlation within the range: 100< $\mathrm{Pr}^{\frac{2}{3}} \cdot \mathrm{Re}$<1000. According to [53], this is valid for Re > 100. Here, Nu is the overall bed Nusselt number (different from a local, particle Nusselt number (Kunii & Levenspiel give additional informations on that topic in [64] and expect that a local Nusselt will lie between the 2 correlations)

1956

Chu [61] gives values for heat transfer in beds, but correlations rely only on solid/gas experiments.

1961

Kunii & Smith performed heat transfer experiments with small particles and water. They proposed a correlation giving Nu, function of Re, Pr and effective and measured thermal conductivities… They refer to experiments by Satterfield with copper and water.

1962

Kunii & Levenspiel [53] give the correlation for a pebble-bed:

$$Nu = 0{,}664 \cdot \mathrm{Pr}^{\frac{1}{3}} \cdot \left(\frac{\mathrm{Re}}{\varepsilon}\right)^{\frac{1}{2}} (3)$$

Gupta & Todos [60] gave 2 correlations (apparently valid for gas) valid for a range of 1-20 < Re < 2400

1965

Rowe & Claxton [63] establish a correlation for Nusselt, for a single heated sphere among a packed bed, for various arrangements.

$$Nu = A + B \cdot \Pr^{\frac{1}{3}} \cdot \mathrm{Re}^n$$

Where, Re is superficial Reynolds number (1< Re < 100,000), Nu is a local quantity (and can be extended to a bed). Pr is the Prandlt number for water and ranges from 6.04 to 7.18.

- $A = \dfrac{2}{1-(1-\varepsilon)^{\frac{1}{3}}}$
- $B = \dfrac{2}{3 \cdot \varepsilon}$ for air, and is 15% higher for water
- $\dfrac{2-3 \cdot n}{3 \cdot n - 1} = 4{,}65 \cdot \mathrm{Re}^{-0{,}28}$

1966

Baldwin [69] proposes the following correlations for **local** Nusselt numbers:

- Regular cubic packed bed: $Nu = 0{,}99 \cdot \Pr^{\frac{1}{3}} \cdot \mathrm{Re}^{\frac{2}{3}}$
- Dense packed bed: $Nu = 0{,}94 \cdot \Pr^{\frac{1}{3}} \cdot \mathrm{Re}^{0{,}7}$

Where fluid is pressurized water at 115 C and 3000 < Re < 70000. Re is calculated with superficial velocity. He refers to Gupta & Todos work [60].

1967

Suzuki & Kunii [56] re-expressed (2), by:

$$Nu = 2 + 0{,}6 \cdot \Pr^{\frac{1}{3}} \cdot \mathrm{Re}^{\frac{1}{2}}$$

Assuming that Re is calculated with a real velocity, 9 times higher than the superficial velocity, it matches with (2), but this expression is bit confusing…
Their work focuses on finding another correlation for low Peclet number (calculated with superficial velocity) (Pe < 20), which is not relevant in our case. However, this study gives an overview of all the experiments realized at that time, especially the working fluids: Kunii & Smith [58].

1969

Kunii & Levenspiel [53] state equations (1) and (2) for fixed beds and refer to experimental data. No other experiments in the field of liquid/bed heat transfer than those cited by Suzuki & Kunii are referenced. Equation (3) is no more cited, nor in the latest edition of the book [64]…

1971

Karabelas [67] proposes correlations for mass transfer at low Reynolds. He also gives an overview of heat and mass transfer correlations in packed beds. He states numerous correlations existing at that time. But only one correlation in the range we are interested in (for a large range of Pr and Re > 3000) is given. It has been established by Baldwin [69].

<u>1972</u>

Whitaker [65] proposes a correlation for gas flows in spheres-packed bed, after the experimental data of six series experiments (air and nitrogen).

$$Nu = (0{,}5 \cdot \mathrm{Re}^{\frac{1}{2}} + 0{,}2 \cdot \mathrm{Re}^{\frac{2}{3}}) \cdot \mathrm{Pr}^{\frac{1}{3}} \quad (4)$$

Here, Nu and Re are defined with unusual characteristic lengths and speeds. This case is not relevant for us. This is valid for the approximate following range: 20 < Re < 10000

<u>1973</u>

Sorensen & Steward [66] propose computational methods for calculate Nu, in:

- Slow flows at low Pe number
- Slow flow (Re < 20) and high Pe (Pe >> 1)

$Nu = c \cdot Pe^{\frac{1}{3}}$, where *c* is calculated with different simple and dense cubic geometries

Re and Pe are calculated with superficial velocity. These correlations are compared with results from 2 other studies: Karabelas [67] and Wilson [68]. Analogies are used between heat and mass transfer coefficients mechanisms.

<u>1974</u>

Gupta [60] gives an overview of the different experimental data existing at that time and proposes the following correlation:

$$Nu = 2{,}876 \cdot \frac{1}{\varepsilon} \cdot \mathrm{Pr}^{\frac{1}{3}} + 0{,}3023 \cdot \frac{1}{\varepsilon} \cdot \mathrm{Pr}^{\frac{1}{3}} \cdot \mathrm{Re}^{0{,}65} \quad (5)$$

We may note that the original correlation is defined by J_h as a function of Re and ε, where J_h is the heat transfer factor ($J_h = Nu \cdot \mathrm{Pr}^{-\frac{1}{3}} \cdot \mathrm{Re}^{-1}$). This correlation is supposed to match with past experiments (experiments by Rowe [63] are the only one with a Prandtl over 1 among all), for 10 < Re < 10,000 where Re is the superficial Reynolds number.

<u>1978</u>

Gunn [71] starts from a mathematical model to propose a correlation. It is compared to few experiments (he highlights the limited amount of work done at this stage in the liquid-solid heat and mass transfer in beds and the large scattering in results… especially those by Rowe and Claxton [63]). This correlation is supposed to match a very broad field of validity (from a creeping flow to high Reynolds, and single sphere and beds).

$$Nu = \left(7 - 10 \cdot \varepsilon + 5 \cdot \varepsilon^2\right) \cdot \left(1 + 0.7 \cdot \mathrm{Re}^{0.2} \cdot \mathrm{Pr}^{\frac{1}{3}}\right) + \left(1.33 - 2.4 \cdot \varepsilon + 1.2 \cdot \varepsilon^2\right) \cdot \left(\mathrm{Re}^{0.7} \cdot \mathrm{Pr}^{\frac{1}{3}}\right)$$

<u>1978</u>

Martin [57], as Kunii & Suzuki, focuses his study on low Pe, but gives a summary of correlations and precisions:
For Pe (superficial velocity) > 100

$$Nu = (1 + 1{,}5 \cdot (1 - \varepsilon)) \cdot Nu_{sphere} \quad (6)$$

where

$$Nu_{sphere} = 2 + F \cdot \mathrm{Pr}^{\frac{1}{3}} \cdot \left(\frac{\mathrm{Re}}{\varepsilon}\right)^{\frac{1}{2}}$$

Re is calculated with the superficial velocity
In laminar region, F=0,6 (Ranz [16]) or F=0,664 (Gnielinski work in 1975)

In turbulent $F = 0{,}664 \cdot \sqrt{1 + \left(\dfrac{0{,}0557 \cdot \left(\frac{\mathrm{Re}}{\varepsilon}\right)^{0{,}8} \cdot \mathrm{Pr}^{\frac{2}{3}}}{1 + 2.44 \cdot \left(\frac{\mathrm{Re}}{\varepsilon}\right)^{-0{,}1} \cdot \left(\mathrm{Pr}^{\frac{2}{3}} - 1\right)}\right)^2}$, valid for Pr > 0,6 (Gnielinski work in 1975)

Martin produces the Kunii & Suzuki chart, more detailed.

Martin refers to Sorensen [66] work for specials values of Pe.

<u>1978</u>

The KTA authority delivers for its reference correlation for German HTR [43]

$$Nu = 1{,}27 \cdot \frac{\mathrm{Pr}^{\frac{1}{3}}}{\varepsilon^{1{,}18}} \cdot \mathrm{Re}^{0{,}36} + 0{,}033 \cdot \frac{\mathrm{Pr}^{\frac{1}{2}}}{\varepsilon^{1{,}07}} \cdot \mathrm{Re}^{0{,}86} \quad (7)$$

<u>1978</u>

Gnielinski [54] modifies its 1975 work and uses a large number of different experimental data (assuming links between mass and heat transfer correlations):

- $Nu = (1 + 1{,}5 \cdot (1 - \varepsilon)) \cdot Nu_{sphere}$ (8)
- $Nu_{sphere} = 2 + \sqrt{Nu_{lam}^{\ 2} + Nu_{turb}^{\ 2}}$
- $Nu_{lam} = 0{,}664\,\mathrm{Re}^{\frac{1}{2}} \cdot \mathrm{Pr}^{\frac{1}{3}}$
- $Nu_{turb} = \dfrac{0{,}037 \cdot \mathrm{Re}^{0{,}8} \cdot \mathrm{Pr}}{1 + 2.443 \cdot \mathrm{Re}^{-0{,}1} \cdot \left(\mathrm{Pr}^{\frac{2}{3}} - 1\right)}$

He concludes by giving the following range of validity:

- $0,7 < Pr$ (or Sc) $< 10^4$
- $Re < 2x10^4$
- $Pe > 500\text{-}1000$

Note that here, Re and Pe are calculated with the real velocity and not the superficial one.

1982

Wakao and Kaguei [70] proposed two semi-empirical correlations, after a selection of relevant experimental results:

Mass transfer (liquid phases -mainly water- and high Schmidt number), excellent consistence with experimental results, for 3< Re < 3,000 (lower Re numbers have been skipped because of the influence of natural convection which would alter results) and for Sc > 1-200

$$Sh = 2 + 1{,}1 \cdot Sc^{\frac{1}{3}} \cdot \mathrm{Re}^{0,6}$$

By analogy, they propose the following correlation for heat transfer. However, it has been 'benchmarked' after only air experiments.
The interval of confidence is getting very large when Re decreases (because of the difficulty to conduct heat transfers measurements at low Re and the difference between the diffusivity coefficients between mass and heat, up to 1.5 ratio whether the sources…).
When Re < 100, one can observe this difference. However, the authors consider that this correlation is still valuable (regarding the ratios cited above).
The asymptote value (for Re<10 as Gunn [71] points out, Re tends to 0, creeping flow) for Nusselt is here 2, but literature show a great scattering in this results (up to 10). This issue is considered as negligible by the authors as heat transfer will be dominated by conduction in this area.

$$Nu = 2 + 1{,}1 \cdot \mathrm{Pr}^{\frac{1}{3}} \cdot \mathrm{Re}^{0,6}$$

Here Re is based on the superficial velocity.

1983

The KTA organization [48] gives the correlation (7) for an helium (Pr=0,7) cooled PB reactor with the following precisions:
100 < Re < 100 000, 0,36 < ε < 0,42 and Re is calculated with the superficial velocity.

1993

The VDI heat atlas [36] states Gnielinski results [54] and [55].
The range of validity is slightly modified:

- $0,6 < Pr$ (or Sc) $< 10^4$
- $0,1 < Re < 10^4$

It also references to Kunii & Suzuki [56] and Martin [57] studies to address the situations where Pe < 500-1000.

1995

Achenbach [32] makes a survey of the field of investigation in heat and mass transfers in porous media. He describes the pros and cons of the different techniques used to determine the correlations.
He extends the validity of (8) to Re<7,7 x 10^5
He gives also another correlation, which matches (8) and has only been checked with Air and helium (Pr=0,71).

$$Nu = \mathrm{Pr}^{\frac{1}{3}} \cdot \left[\left(1{,}18 \cdot \mathrm{Re}^{0{,}58}\right)^4 + \left(0{,}23 \cdot \mathrm{Re}^{0{,}75}\right)^4 \right]^{0{,}25} \quad (9)$$

Where Re is calculated with the real velocity. Nu is an average Nusselt number. A local $\mathrm{Nu_h}$ is given by: $Nu \cdot \frac{\varepsilon}{1-\varepsilon}$

<u>2001</u>

The MIT and INEEL made for the PBMR a literature review [51] and refers to equations (1), (2), (3) and (7).

<u>2005</u>

Delft University [33] used the VDI results with a typo

$$Nu_{turb} = \frac{0{,}037 \cdot \mathrm{Re}^{0{,}8} \cdot \mathrm{Pr}}{1 + 2.443 \cdot \mathrm{Re}^{0{,}1} \cdot \left(\mathrm{Pr}^{\frac{2}{3}} - 1 \right)}$$

One may note that here Re is the calculated with the superficial velocity, that would mean that the correlation is not properly used, under-estimating the heat transfer.

In this report is also used the KTA correlation (7) (with the superficial Reynolds, consistent with the KTA precisions)

and a third relation for the HEAT code
$Nu = 2 + 0{,}66 \cdot \mathrm{Pr}^{\frac{1}{3}} \cdot \mathrm{Re}^{\frac{1}{2}}$, no validity range is précised and here Re is calculated with the real velocity. It is closed to (2) and (3)

<u>2006</u>

Kaviany [44] states the relation by Wakao [70] as reliable, because it is based on:
- An accurate cell modeling of energy equations
- For low Re, it follows the asymptote
- A rigorous selection and adaptation of relevant experimental data

$$Nu = 2 + 1{,}1 \cdot \mathrm{Pr}^{\frac{1}{3}} \cdot \mathrm{Re}^{0{,}6} \quad (10)$$

2. Conclusions.

6 correlations are selected regarding:
- The variety of experiments conducted (especially with liquids),
- The consistence with other correlations,
- The occurrence of reference in design papers.

These correlations are the one proposed by Gupta, Gnielinski, Achenbach, Wakao, Gunn and the KTA organization.
Below are displayed two plots of these correlations for two Prandlt numbers (0.71: helium and 15: liquid salts), within the range of superficial Reynolds number we are interested in (from the laminar values of 20 in natural circulation to 2,000 in steady state).
The scattering in the results becomes important (30 %) for liquid salts, at full power, and the KTA correlation is likely to produce wrong results, as it mainly rely on gas experience. Experiments would be needed to reduce this uncertainty.
In this project, the correlation by Wakao is mainly used, considering its simple form and its accuracy.

Particular attention is drawn on the very low Peclet numbers (inferior to 500) situations (loss of forced circulation in AHTR for instance), as the quality of experimental data is poor and the uncertainty of the relevant correlations high.

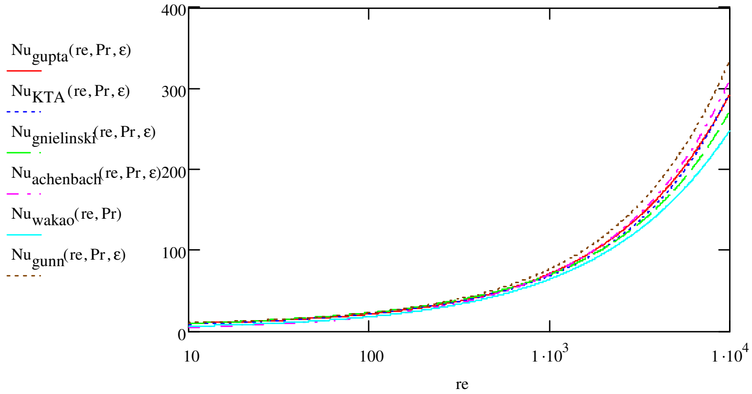

Figure 1: Nusselt number as a function of superficial Reynolds (Prandtl = 0.71).

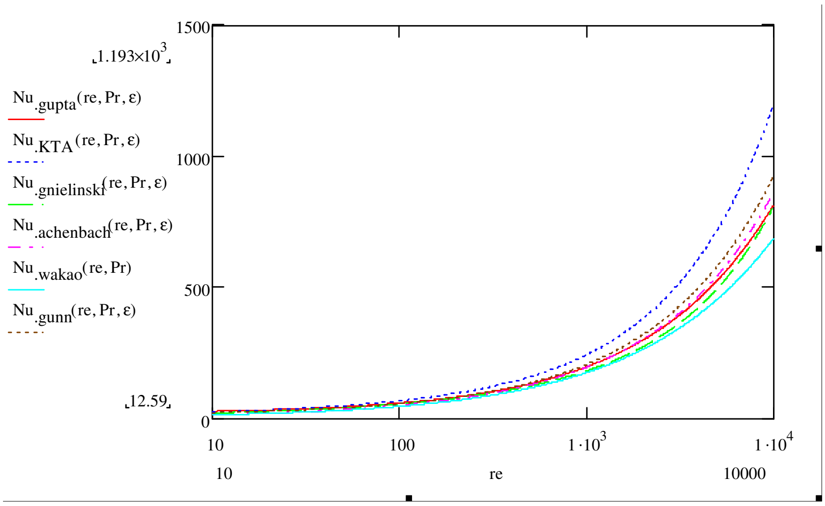

Figure 2: Nusselt number as a function of superficial Reynolds (Prandtl = 15).

APPENDIX IX

INFLUENCE OF PRIMARY INITIAL TEMPERATURES ON NATURAL CIRCULATION

Two cases are considered for the initial primary temperature distribution in the loop formed by the core, PRACS pipes and the PHX bundles.

- Case 1: outlet temperature of the core of 700°C and a PHX temperature distribution ranging from 600°C to 500°C. It is a mild case since the outlet temperature is reduced.
- Case 2: outlet temperature of the core of 750°C and PHX temperatures more hot, up to 580°C.

The final peak temperatures are still around 770°C and change from 10°C. This peak is reached after the same order of time an hour, as shown in Figure A.IX.1 and Figure A.IX.2.

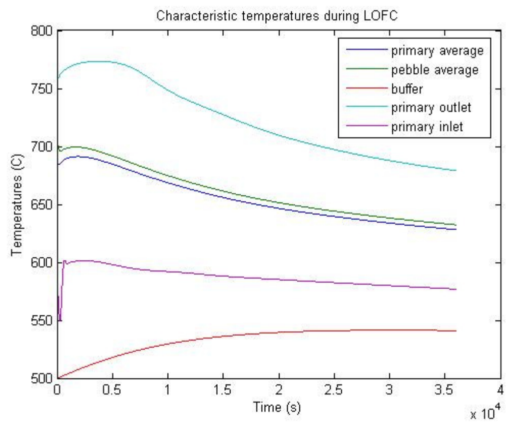

Figure A.IX.1: Relevant temperatures during LOFC, in the 750°C outlet temperature case

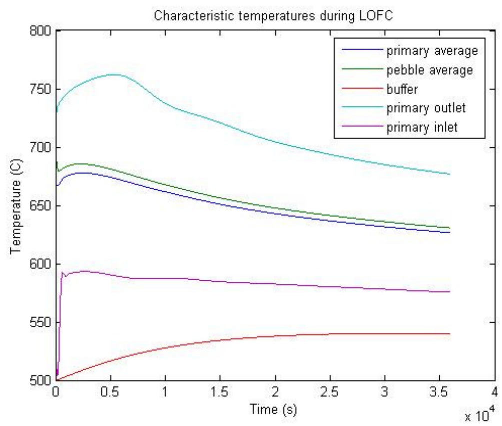

Figure A.IX.2: Relevant temperatures during LOFC, in the 700°C outlet temperature case

The mass flow rate reaches is quasi-steady value after the same order of time of 10 minutes, as shown in Figure A.IX.3 and Figure A.IX.4.

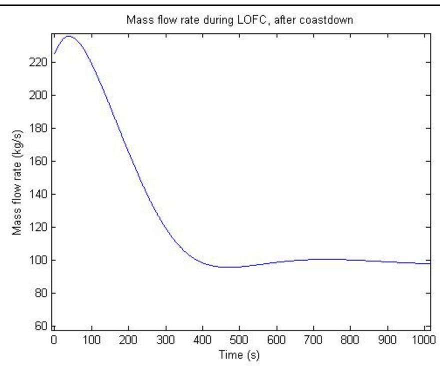

Figure A.IX.3: Mass flow rate during LOFC, in the 750°C outlet temperature case

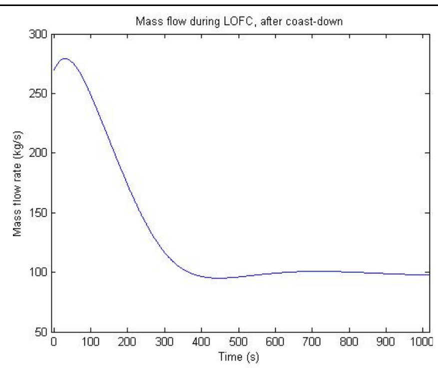

Figure A.IX.4: Mass flow rate during LOFC, in the 700°C outlet temperature case

Thus it can be concluded that the initial stage of coast-down does not impact significantly the safety criterion chosen, the peak coolant temperature.

APPENDIX X

EXAMPLE OF MATHCAD FILE: COAST-DOWN MODELING

This appendix provides an example of a calculation completed with the Mathcad application. This software allows performing simple calculations (such as solving systems of partial differential equations) in a comprehensive way.

Calculations of coast-down effects in core

1- References used:

Physical properties of the constituents:

Reference:C:\Documents and Settings\FP\My Documents\pfe\mathcad\properties.x

Design parameters of the core:

Reference:C:\Documents and Settings\FP\My Documents\pfe\mathcad\design-references.x

Steady-state temperature profiles in the core:

Reference:C:\Documents and Settings\FP\My Documents\pfe\mathcad\Core\core1D-fullpower.x

ANS 79 decay heat function:

Reference:C:\Documents and Settings\FP\My Documents\pfe\mathcad\actual\Copy of decay_heat_function.

2- Useful parameters for the steady state calculations:

Inlet, outlet and average (profile assumed linear to simplify) temperatures of flibe

$$Tinlet\_steady := 600$$

$$Toutlet\_steady := 700$$

$$Tcore\_steady := \frac{Tinlet\_steady + Toutlet\_steady}{2}$$

$$m_{core\_init} := \frac{Power}{(Toutlet\_steady - Tinlet\_steady) \cdot c_{pflib}}$$ Steady mass flow rate in core (mCp delta T)

$$S_{reflector} := (\pi \cdot 7 \cdot 6.5) + 36$$ Wetted surface of the reflector

$$k_{reflector} := k_{graphite}(Tcore\_steady)$$ Conductivity of reflector

$$\varepsilon := 0.4$$ Porosity of the bed

$$P_f := 0.10$$ Packing factor

$$q_{v\_steady} := \frac{Power\_density}{1 - \varepsilon}$$ Power density in pebble

$$q_{f\_steady} := \frac{q_{v\_steady}}{\left(\frac{R_f}{R_p}\right)^3}$$ Power density in the fuel zone of pebble

$c_{ps}(T) := c_{p\_graphite}(T)$

$c_{pf}(T) := c_{p\_graphite}(T)$

Heat capacities of the pebble constituents (shell and fuel), assumed to be equal to the graphite one.

$\rho_f := P_f \cdot \rho_T + (1 - P_f)\rho_{c2}$

Density of fuel zone in pebble (TRISO + matrix)

$\rho_s := \rho_{c2}$

Density of shell in pebble

$\lambda_f := (1 - P_f)\lambda_g + P_f \cdot \lambda_T$

Conservative fuel conductivity

$\lambda_s := \lambda_g$

Conservative shell conductivity

$Nu_{steady} := Nu_{1D}(Tcore\_steady, \varepsilon, 1)$

Wakao correlation is retained for Nusselt

$Nu_{steady} = 290.958$

$h_{steady} := Nu_{steady} \cdot \frac{k_{flib}}{d_p}$

Definition of heat transfer coefficient in core

3- Steady state temperature distribution in one average pebble

Guessed initial values for Mathcad needs :
- Temperature at the surface of pebble (Twall)
- Temperature at the center of pebble (Tpeak)
- coefficients used for expression of T(r) within the fuel and shell zones (A2 and B2)

$Twall\_steady := 700$ $Tpeak\_steady := 800$ $A_2 := 100$ $B_2 := 100$

We solve the following system of equations, knowing the solutions profiles of the heat equation in spherical coordinates in the pebble (parabolic profile):

Given

$$Tpeak\_steady - \frac{q_{f\_steady} \cdot R_f^2}{6 \cdot \lambda_f} = A_2 + \frac{B_2}{R_f}$$

Temperatures equality at the interface between the fuel zone and the shell (r=Rf)

$$A_2 + \frac{B_2}{R_p} = Twall\_steady$$

Temperatures equality at the surface of pebble (r=Rp)

$$-\lambda_f \cdot \left(\frac{-q_{f\_steady} \cdot R_f}{3 \cdot \lambda_f}\right) = -\lambda_s \cdot \left(\frac{-B_2}{R_f^2}\right)$$

Heat flux equality at the interface between fuel zone and shell

$$-\lambda_s \cdot \left(\frac{-B_2}{R_p^{\;2}} \right) = h_{steady} \cdot (Twall\_steady - Tcore\_steady)$$

Heat flux equality at the surface of pebble (Newton law for convection)

We solve the system...

$$\begin{pmatrix} Twall\_steady \\ Tpeak\_steady \\ A_2 \\ B_2 \end{pmatrix} := \mathrm{Find}(Twall\_steady, Tpeak\_steady, A_2, B_2)$$

The 4 solutions are:

$$\begin{pmatrix} Twall\_steady \\ Tpeak\_steady \\ A_2 \\ B_2 \end{pmatrix} = \begin{pmatrix} 681.87 \\ 827.142 \\ 511.87 \\ 5.1 \end{pmatrix}$$

We obtain the following profiles:

$$Tf\_steady(r) := Tpeak\_steady - \frac{q_{f\_steady} \cdot r^2}{6 \cdot \lambda_f}$$

Temperature profile in fuel zone of pebble

$$Ts\_steady(r) := A_2 + \frac{B_2}{r}$$

Temperature profile in shell zone

$$Tpeb\_steady(r) := \begin{cases} Tf\_steady(r) & \text{if } 0 \le r \le R_f \\ Ts\_steady(r) & \text{if } R_f \le r \le R_p \\ Tcore\_steady & \text{otherwise} \end{cases}$$

Temperature profile in whole average pebble

Plot of the temperature distribution in steady-state within a pebble:

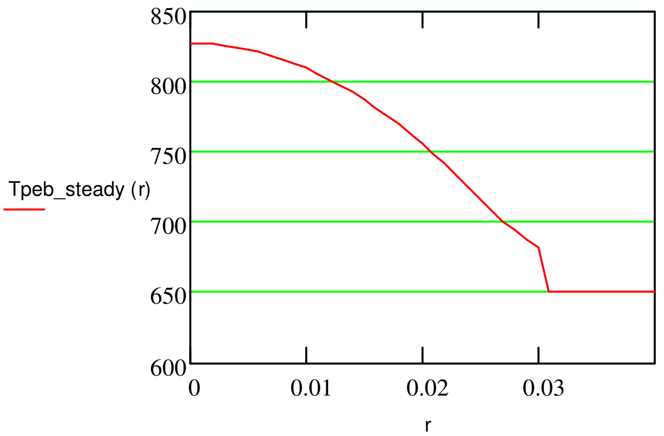

4-Calculation of the coastdown effect:

$\text{Time}_{scram} := 3$ Scram 3 seconds after the coast-down beginning

$$f_{transient}(t) := \begin{cases} 1 & \text{if } t \le \text{Time}_{scram} \\ f_{decay}(t \cdot s - 1s) & \text{otherwise} \end{cases}$$

Normalized decay heat shape (ANS 79 data)

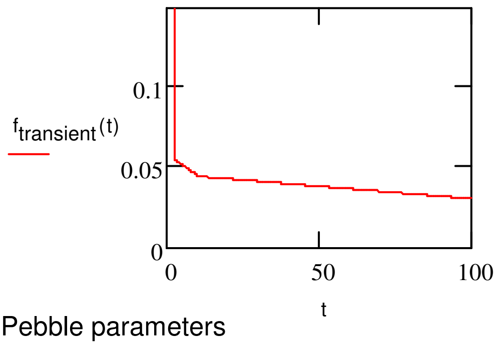

Pebble parameters

$$\lambda(r) := \begin{cases} 25 & \text{if } 0 \le r < R_f \\ 30 & \text{if } R_f \le r \le R_p \end{cases}$$

Conductivity

$$q_{p\_steady}(r) := \begin{cases} q_{f\_steady} & \text{if } 0 \le r < R_f \\ 0 & \text{if } R_f \le r \le R_p \end{cases}$$

Steady-state power generation in pebble

$$\rho(r) := \begin{cases} \rho_f & \text{if } 0 \le r < R_f \\ \rho_s & \text{if } R_f \le r \le R_p \end{cases}$$

Density

$$c_p(r) := \begin{cases} c_{pf}(750) & \text{if } 0 \le r < R_f \\ c_{ps}(690) & \text{if } R_f \le r \le R_p \end{cases}$$

Heat capacity

Coastdown of pumps: linear decrease of mass flow rate

$\text{Time}_{coastdown} := 10$ 10 seconds coast-down

$m_{core\_nat} := 200$ a 200 kg/s mass flow rate is assumed to be achieved at the end of the transient

Mass flow as a function of time in one primary loop (out of 4)

$$m_{pump}(t) := \begin{cases} \frac{1}{4} \cdot m_{core\_init} & \text{if } t \le 0 \\ \frac{1}{4} \left[m_{core\_init} - \left(m_{core\_init} - m_{core\_nat}\right) \cdot \left(\frac{t}{Time_{coastdown}} \right) \right] & \text{if } 0 \le t \le Time_{coastdown} \\ \frac{m_{core\_nat}}{4} & \text{otherwise} \end{cases}$$

$m_{core\_cd}(t) := 4 \cdot m_{pump}(t)$ Mass flow through core, we neglect the leak through PHX

$$Re_{core\_cd}(t) := \frac{m_{core\_cd}(t) \cdot d_p}{A_{core} \cdot \mu_{flib}(Tcore\_steady)}$$

Superficial Reynolds number in core, with viscosity considered constant

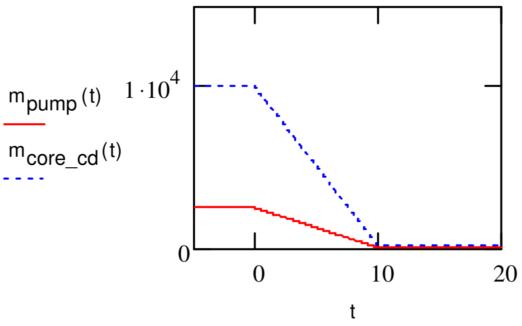

Plot of mass flow

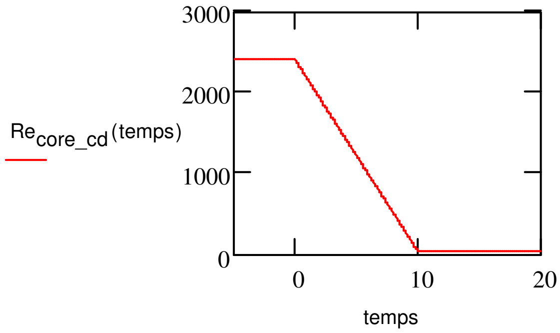

Plot of Reynolds

Heat transfer coefficient

$$h_{cd}(t) := \frac{Nu_{wakao}\left(Re_{core\_cd}(t), Pr_{flib}(Tcore\_steady)\right) \cdot k_{flib}}{d_p}$$

Simplification : Prandlt number considered constant

Wetted area in core

$$S_{Wcore} := \frac{6 \cdot A_{core} \cdot H_{core} \cdot (1 - \varepsilon)}{d_p}$$

Energy conservation in the salt enclosed in the core yield to (considering T.inlet constant at the beginnig of the transient, valid considering the long path in the primary loop, until T=Time CL) :

Mass of flibe enclosed between the IHX and the inlet of core:

$$\left(V_{CL\_single\_loop} + \frac{V_{inlet\_plenum}}{4}\right)\cdot\rho_{flib}(Tinlet\_steady) = 1.772\times 10^{4}$$

Mass pumped during the coastdown:

$$\int_{0}^{Time_{coastdown}} m_{pump}(t)\,dt = 1.278\times 10^{4}$$

Time during which the inlet temperature in core remains constant (cold leg and inlet plenum totally pumped)

$Time_{CL\_1} := Time_{coastdown}$

Given

$$\int_{0}^{Time_{CL\_1}} m_{pump}(t)\,dt = \left(V_{CL\_single\_loop} + \frac{V_{inlet\_plenum}}{4}\right)\cdot\rho_{flib}(Tinlet\_steady)$$

$Time_{CL\_1} := Find(Time_{CL\_1})$

$Time_{CL\_1} = 108.845$

This volume is ot totally emptied at the end of the coastdown...

$Tinlet\_1 := Tinlet\_steady$

5- Calculation of temperature distribution in pebble during the coastdown

We search 3 variables, functions of space and time:
- Temperature distribution in a average pebble
- Average temperature of salt in core
- Average temperature in reflector

We use the variable change U = r x Temp (skipp division by zero issue).

Because of the constraints of Mathcad format (can solve only a system of only partial differential equations), the salt temperature (Tcore) is artifically calculated as Tcore (r,t), the actual Tcore is Tcore(Rp,t)

Given

3 initial conditions at t=0, for the 3 variables

$U\_1(r,0) = r\cdot Tpeb\_steady(r)$ The pebble temperature distribution is the steady-state one, calculated above.

The average salt temperature is a function of T inlet and the amount of heat transfered by convection in steady state.

$$Ucore\_1(r,0) = \frac{S_{Wcore}\cdot h_{cd}(0)\cdot r\cdot Tpeb\_steady(r) + 2\cdot m_{core\_cd}(0)\cdot c_{pflib}\cdot r\cdot Tinlet\_1}{2\cdot m_{core\_cd}(0)\cdot c_{pflib} + S_{Wcore}\cdot h_{cd}(0)}$$

$Ureflector\_1(r,0) = r\cdot\left(\frac{Tcore\_steady + 550}{2}\right)$ The initial temperature in the reflector is assumed to be 600 C.

Heat equation in the pebble:

$$U\_1_t(r,t) = \frac{\lambda(r)}{\rho(r)\cdot c_p(r)}\cdot U\_1_{rr}(r,t) + \frac{r}{\rho(r)\cdot c_p(r)}\cdot\left(q_{p\_steady}(r)\cdot f_{transient}(t)\right)$$

Energy conservation in the salt in the core (simplification by considering the average salt temperature and the surface temperature of an average pebble, it corresponds to a 1-D model with uniform heat generation):

$$Ucore\_1_t(r,t) = \left(\frac{1}{c_{pflib}\cdot V_{core}\cdot\varepsilon\cdot\rho_{flib}(Tcore\_steady)}\right)\cdot\left[2\cdot m_{core\_cd}(t)\cdot c_{pflib}\cdot(r\cdot Tinlet\_1 - Ucore\_1(r,t)) + h_{cd}(t)\cdot S_{Wcore}\cdot(U\_1(r,t) - Ucore\_1(r,t))\right]$$

Energy conservation in the reflector with conduction heat transfer through the reflector thickness. Reflector temperature is assumed linearly distributed within the reflector.

$$Ureflector\_1_t(r,t) = \left(\frac{S_{reflector}\cdot k_{reflector}}{M_{reflector}\cdot c_{p\_graphite}(Tcore\_steady)}\right)\cdot\left(\frac{2}{e_{reflector\_side}}\right)\cdot(Ucore\_1(r,t) - Ureflector\_1(r,t))$$

Boundary conditions at r=0 to solve the system

$U\_1(0,t) = 0$

$Ucore\_1(0,t) = 0$

$Ureflector\_1(0,t) = 0$

Boundary conditions at r=Rp (convective heat transfer at the wall of pebble)

$$U\_1_r(R_p,t) = \frac{U\_1(R_p,t)}{R_p} - \frac{h_{cd}(t)}{\lambda(R_p)} \cdot \left(U\_1(R_p,t) - Ucore\_1(R_p,t)\right)$$

Solve the system of 3 partial differential equations and 3 variables...

$$\begin{pmatrix} U\_1 \\ Ucore\_1 \\ Ureflector\_1 \end{pmatrix} := \text{Pdesolve}\left[\begin{pmatrix} U\_1 \\ Ucore\_1 \\ Ureflector\_1 \end{pmatrix}, r, \begin{pmatrix} 0 \\ R_p \end{pmatrix}, t, \begin{pmatrix} 0 \\ Time_{CL\_1} \end{pmatrix}, 100, 200\right]$$

We come back to the original variables: temperatures...

$$Tpeb\_1(r,t) := \frac{U\_1(r,t)}{r}$$ Temperature distribution, as a function of the radius r

$$Tpeb\_av\_1(t) := \frac{1}{\left(\frac{4}{3}\right)\cdot\left(\pi \cdot R_p^{\,3}\right)} \cdot \left(\int_0^{R_p} 4 \cdot \pi \cdot r^2 \cdot Tpeb\_1(r,t)\,dr\right)$$ Average pebble temperature

$$Tcore\_1(t) := \frac{Ucore\_1(R_p,t)}{R_p}$$ Average salt temperature

$$Treflector\_1(t) := \frac{Ureflector\_1(R_p,t)}{R_p}$$ Reflector temperature

$$Toutlet\_1(t) := 2\,Tcore\_1(t) - Tinlet\_1$$ Outlet temperature

We plot the temperatures in the pebble at different times

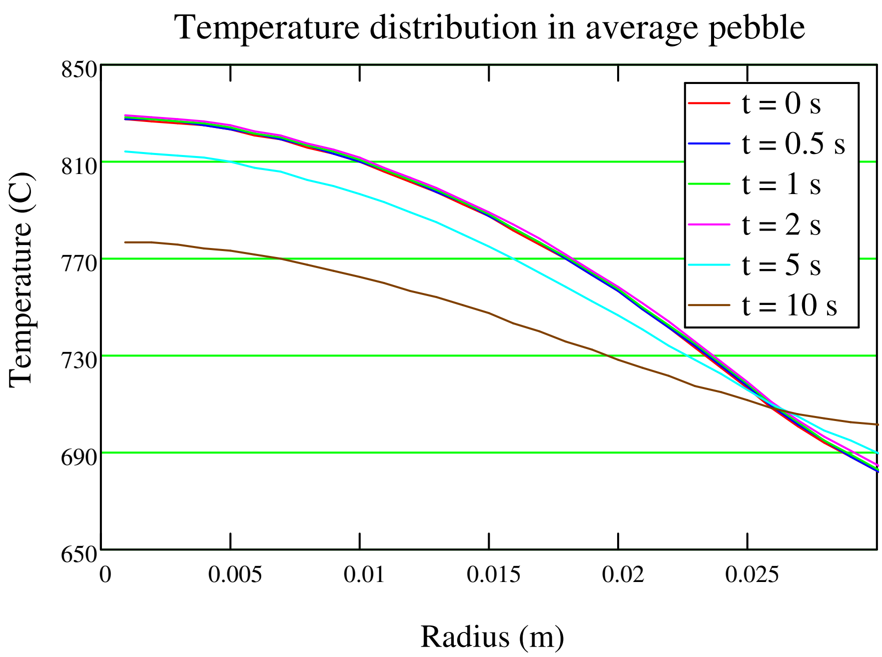

We plot the characteristic temperatures evolutions in the core

temps := $0, 0.01 .. \text{Time}_{CL\_1}$

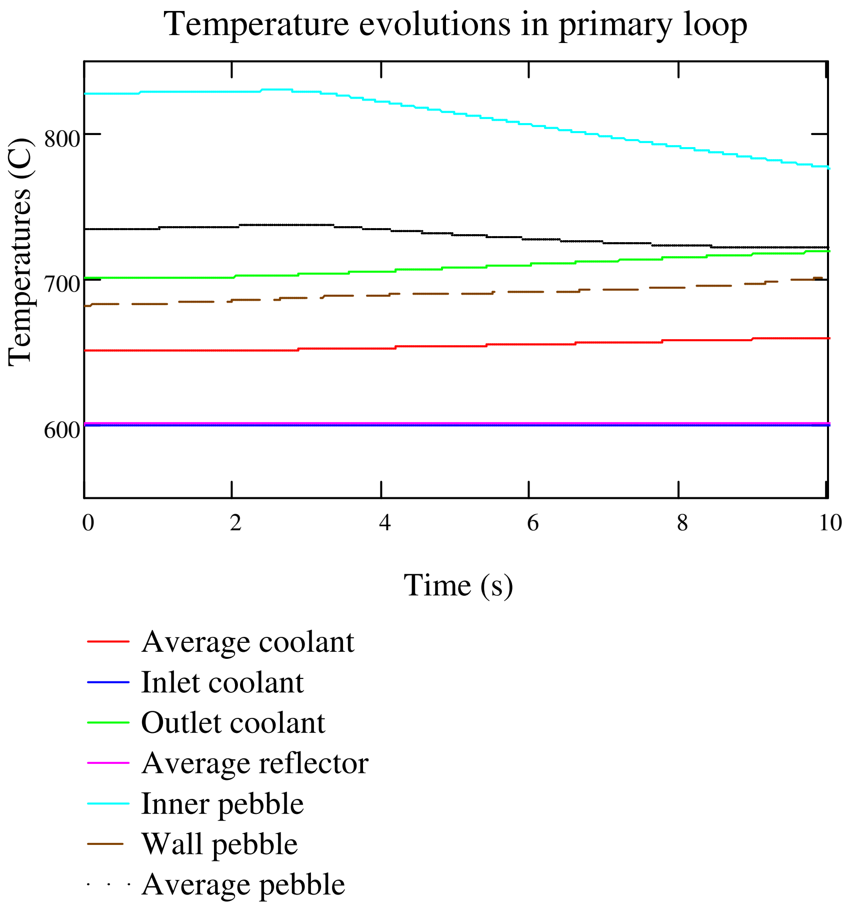

Power transferred from the core to the salt by convection:

$$\text{Power}_{core\_to\_salt}(t) := h_{cd}(t)\cdot S_{Wcore}\cdot\left(\text{Tpeb\_1}\left(R_p,t\right) - \text{Tcore\_1}(t)\right)$$

Power removed by the flow (mCpdelta T)

$$\text{Power}_{removed\_from\_core}(t) := 2\cdot m_{core\_cd}(t)\cdot c_{pflib}\cdot\left(\text{Tcore\_1}(t) - \text{Tinlet\_1}\right)$$

Power stored in pebble (thermal inertia)

$$\text{Power}_{absorbed\_by\_fuel}(t) := \frac{(1-\varepsilon)\cdot V_{core}}{\left(\frac{4}{3}\right)\cdot\pi\cdot R_p^{\,3}}\cdot\int_0^{R_p} 4\cdot\pi\cdot r^2\cdot\rho(r)\cdot c_p(r)\cdot\left(\frac{d}{dt}\text{Tpeb\_1}(r,t)\right)dr$$

Power stored in salt (thermal inertia)

$$\text{Power}_{absorbed\_by\_salt}(t) := c_{pflib}\cdot V_{core}\cdot\varepsilon\cdot\rho_{flib}(\text{Tcore\_steady})\cdot\frac{d}{dt}\text{Tcore\_1}(t)$$

Power stored in reflector (thermal inertia)

$$Power_{absorbed\_by\_reflector}(t) := c_{p\_graphite}(Tcore\_steady) \cdot M_{reflector} \frac{d}{dt} Tcore\_1(t)$$

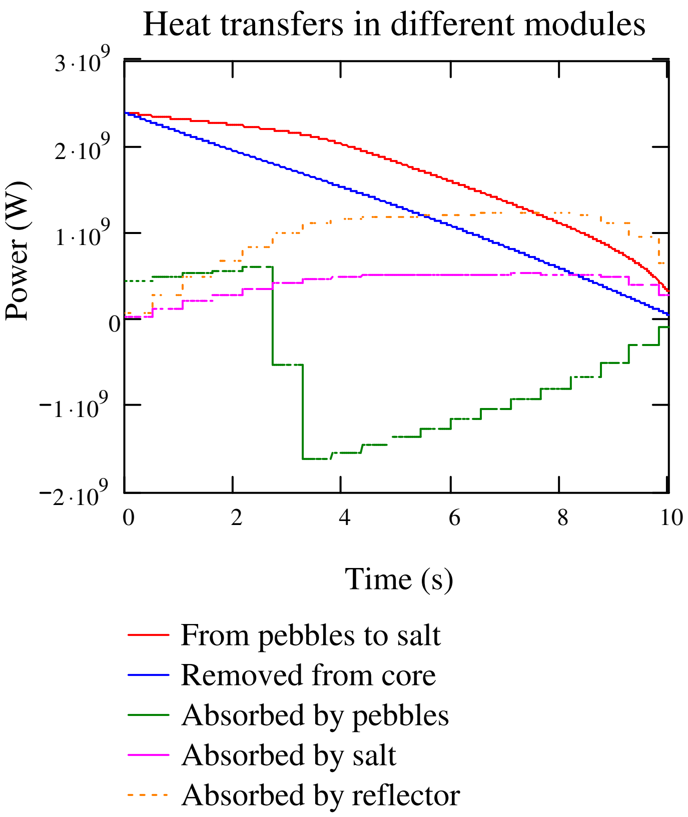

BIBLIOGRAPHY – PIRT study

[1] **Technical Program Group**, "*Quantifying reactor safety margins: Application of CSAU to a LBLOCA*", NUREG/CR-5249, EG&G Idaho, Inc (December 1989)

[2] **G.E. Wilson and B.E. Boyack**, 1998, "*The role of PIRT process in experiments, code development and code applications associated with reactor safety analysis*", Nuclear Engineering and Design, Vol.186, pp. 23-37.

[3] **G.E. Wilson and B.E. Boyack**, "*Lessons learned in obtaining efficient and sufficient applications of the PIRT process.*", (2006)

[4] **Mailliat**, et al., EURSAFE Project – "*The Status of the European Severe Accident PIRTs*", EUROSAFE 2002, International Forum for Nuclear Safety, Berlin, Germany (November 4-5, 2002)

[5] **R.B. Vilim** et al., "*Initial VHTR Accident Scenario Classification: Models and Data*", Status Report, Argonne National Laboratory, (September 2004)

[6] **R.P. Martin,** "*AREVA's activities related to VHTR thermal-hydraulics analysis using RELAP5-3D*", RELAP5-3D Users Seminar, Sun Valley, Idaho, USA, August 25-27, (2004)

[7] **U.S. Office of Nuclear Regulatory Commission,** *Policy Issue Information*, 2004, SECY-04-0001

[8] **U.S. Office of Nuclear Regulatory Commission**, 2002, *Advanced Reactor Research Plan*, ML021760135

[9] **U.S. Office of Nuclear Regulatory Commission**, "*Transient and accident analysis methods*", Regulatory Guide 1.203 (December 2005)

[10] **P.F. Peterson and H. Zhao**, "*A flexible baseline design for the Advanced High Temperature Reactor using Metallic Internals (AHTR-MI)*", Proc., 2006 International Congress on Advances in Nuclear Power Plants (ICAPP '06), Embedded International Topical Meeting 2006 American Nuclear Society Annual Meeting, Reno, NV, USA, June 4-6, (2006)

[11] **C. Forsberg**, "*Alternative Passive Decay Heat Systems for the Advanced High Temperature Reactor*", Proc., 2006 International Congress on Advances in Nuclear Power Plants (ICAPP '06), Embedded International Topical Meeting 2006 American Nuclear Society Annual Meeting, Reno, NV, USA, June 4-6, (2006)

[12] **G.E. Wilson** et al., "*Phenomena-based thermal-hydraulic modeling requirements for systems analysis of a Modular High Temperature Gas-Cooled Reactor*", Nuclear Engineering and Design, Vol. 136, pp. 319-333 (1992)

[13] **S. Levy**, "*Two-phase flow in complex systems*", Ch. 2, Wiley-Interscience (1999).

[14] **International Atomic Energy Agency**, "*Incorporation of advanced accident analysis*

methodology into safety analysis reports", TECDOC-1351, (May 2003)

[15] **International Atomic Energy Agency**, "*Safety Assessment and Verification for Nuclear Power Plants*", NS-G-1.2, Safety Standards series, (2001)

[16] **International Atomic Energy Agency**, *Safety related terms for Advanced Nuclear Plants*, IAEA TECDOC-626, Vienna, (1991)

[17] **International Project on Innovative Nuclear Reactors and Fuel Cycles (INPRO)**, *"User's Manual for the Area of safety of Innovative Nuclear Reactor Systems*", IAEA, Vienna, Austria, November 11, (2005)

[18] **U.S. Nuclear Regulatory Commission,** *Policy Issue Information* (includes Draft for new licensing Policy Guide), SECY-05-0006, (2005)

[19] **U.S. Nuclear Regulatory Commission**, *Policy Issue Information*, SECY-02-0139, (2002)

[20] **U.S. Nuclear Regulatory Commission**, "*Staff Requirements Memorandum to W.D. Travers, Executive Director of Operations*, Re: SECY-03-0047 - Policy Issues related to licensing Non-Light Water Reactor Designs", June 26, (2003)

[21] **R.B. Vilim**, "*Designing for a Safe Response to Operational and Severe Accident Initiators in the Integral Fast Reactor*", International Topical Meeting on Advanced Reactor Safety, Pittsburgh, PA, pp 353-364, Vol. 1, (April 1994)

[22] **U.S. Nuclear Regulatory Commission**, "*Application of the Single-Failure Criterion to Safety Systems*", Regulatory Guide 1.53, Revision 2, (November 2003)

[23] **International Atomic Energy Agency**, "Accident *Analysis for Nuclear Power Plants*", No. 23, Safety Reports series, (2002)

[24] **F.A. Silady, E.G. Wallace, K.N. Flemming**, "*Selection of Licensing Basis Events for the U.S. Design Certification for the PBMR*", Proc., 2006 International Congress on Advances in Nuclear Power Plants (ICAPP '06), Embedded International Topical Meeting 2006 American Nuclear Society Annual Meeting, Reno, NV, USA, June 4-6, (2006)

[25] **U.S. Nuclear Regulatory Commission**, "*A prioritization of Generic Safety Issues*", Staff report, NUREG-0933, (November 2005)

[26] **J.M. Lanore**, "*Les etudes probabilistes de surete*", Institut de Radioprotection et de Surete Nucleaire (IRSN), Presentation at the "Genie Atomique" course, Cherbourg, (2006)

[27] **B.F. Laurenty and al**., "*Inhibiting Corrosion by Molten Fluoride Salts: Investigations on Flinak*", UCB report, (November 2005).

[28] M. **Simpson and al.,** "*Recent Advances in Redox-Based Corrosion in Molten Salts Suitable for use in High Temperature Heat Transfer*", INEEL report, (November 2005).

[29] **D.F. Williams and al**., "*Assessment of Candidate Molten Salt Coolants for the Advanced High-Temperature Reactor*", Report ORNL/TM-2006/12, (March 2006).

[30] **D.A. Powers**, "*Travel by D.A. Powers to attend the High-Temperature Gas-Cooled Reactor Safety and Research Issues Workshop*", Advisory Comitee on reactor safeguards, Trip report, Rockville, MD, USA, October 10-12, (2001).

[31] **H.D. Gougar**, "*Advanced Core Design and Fuel management for Pebble-Bed reactors*", Thesis, (2004).

[32] **E. Achenbach**, "*Heat and Flow characteristics of Packed Beds*", Experimental Thermal and Fluid Science, Vol. 10, pp 17-27, (1995).

[33] **S.J. de Zwann**, "The *Liquid Salt Pebble Bed Reactor, a new high temperature reactor*", M.Sc. thesis, Report PNR-131-2005-008, (November 2005).

[34] **J. Wang and al**., "*TIMCOAT: an integrated fuel performance model for coated particle fue*l", Second International Topical Meeting on High temperature reactor Technology, Beijing, China, September 22-24, (2004).

[35] **D.T. Ingersoll and al**., "Status of Physics and Safety Analyses for the Liquid-Salt-cooled Very High-Temperature Reactor (LS-VHTR)", Report ORNL/TM-2005/218 (December 2005).

[36] **VDI-Warmeatlas (Heat atlas)**, Springer Verlag Berlin Heidelberg, (2002).

[37] **S. Rinkevicius, and al**., "*Experimental results of Pebble-Beds Thermal Hydraulics characteristics*", 2006 International Congress on Advances in Nuclear Power Plants (ICAPP '06), Reno, NV, June 4-8, (2006).

[38] **I.F. Macdonald**, "*Flow through Porous Media – the Ergun Equation Revisited*", Ind. Eng. Chem. Fundam., Vol. 18, No. 3, p. 199 (1979).

[39] **K. Kugeler and R. Schulten**, "*Hochtemperaturreaktortechnik*", Springer-Verlag, (1989)

[40] **A. Bejan**, "*Convection Heat transfer*", third edition, Wiley, (2004).

[41] **F.P Hauk**, "*Design and Set-up of a high temperature flow loop for the investigation of heat transfer and pressure loss in a mixed convection regime flow of higher Prandtl number molten salt simulants*", Diplomarbeit, (March 2006).

[42] **B. Metais and E.R.G. Eckert**, "*Forced, mixed and free convection regimes*", J. of Heat transfer, vol. 86, pp 295-296 (1964).

[43] **Geschaftsstelle des Kerntechnischen Ausschusses (KTA)**,"*Core Design of High-Temperature Gas-Cooled Reactors, Part 2, Heat transfer in Spherical Fuel elements*", Safety Standards of KTA, KTA 3102.02, (June 1983).

[44] **M. Kaviany,** "*Principles of Convective heat transfer*", second edition, Springer, (2001).

[45] Consolidated Refractories Australasia PTY.LTD vendor's brochure, http://www.consolidatedrefractories.com.au/insulating.htm

[46] **S. Ball**, "*Sensitivity Studies of Modular High-Temperature Gas-Cooled Reactor (MHTGR) Postulated Accidents*", Second International Topical Meeting on High temperature reactor Technology, Beijing, China, September 22-24, (2004).

[47] **Idaho**, **Oak Ridge and Argonne National Laboratories**, "*Next Generation Nuclear Plant, Research and Development Program Plan*", Report INEEL/EXT-05-02581, (January 2005).

[48] **AEA Technology**, Power Fluidics, vendor's brochure, http://www.aeatech.com/uploads/vortex_diode.pdf

[49] **C. Forsberg**., "*Alternative Passive Decay Heat Systems for the Advanced High Temperature Reactor*", 2006 International Congress on Advances in Nuclear Power Plants (ICAPP '06), Reno, NV, June 4-8, (2006).

[50] **D.F. Williams and al.**, "*Assessment of properties of candidate liquid salt coolant for the advanced high temperature reactor (AHTR)",* Report ORNL/GEN4/LTR-05-001, (June 2005).

[51] **W.K. Terry and al.**, "*Modular pebble-bed reactor project*", Report INEEL/EXT-01-01623, (December 2001).

[52] **W.E. Ranz and al.**, "*Evaporation from drop*", Chem. Eng. Progr., vol 48, pp. 141, (1952)

[53] **D. Kunii and al.**, "*Fluidization engineering*", John Wiley & Sons, (1962)

[54] **V. Gnielinski**, "*Gleichungen zur Berechnung desWarme und Stoffaustausches in durchstromten ruhenden Kugel-schuttungen bei mittieren und grossen Plecletzahlen*", Verfahrentechnik, vol. 12, 6, pp. 363/66, (1978),

[55] **V. Gnielinski**, "*Berechnung des Warme und Stoffaustauschs in durchstromten ruheneden Schuttungen*", Verfahrentechnik, vol. 16, 1, pp. 36/39, (1982)

[56] **D. Kunii, M. Suzuki**, "*Particle to fluid heat and mass transfer in packed beds of fine particles*", Int. Journal of H&M transfer, vol. 10, 7, pp. 840/52, (1967)

[57] **H. Martin**, "Low *Peclet number particle to fluid heat and mass transfer in packed beds*", Chem. Eng. Sciences., vol. 33, 6, pp. 913/19, (1978).

[58] **D. Kunii and al.**, "*Heat transfer characteristics of porous rocks*", American Institute of Chemical Engineering journal, vol. 7, pp. 29, (1961)

[59] **W.E. Ranz**, "*Friction and transfer coefficients for single particles and packed beds*", Chem. Eng. Progress, 46, pp. 247, (1952)

[60] **S.N. Gupta**, "*Fluid-particle heat transfer in fixed and fluidized beds*", Chem. Eng. Sciences, vol. 29, pp. 839, (1974)

[61] **J.C. Chu**, "*Heat and mass transfer in solid fluidization*", in "Fluidization", pp. 20, Reinhold, New-York, (1956)

[62] .**D.W. Gamson**, "*Heat and mass transfer in fluid-solid systems*", Chem. Eng. Progress, vol. 47, pp. 19, (1951)

[63] **P.N. Rowe and al**., "*Heat and mass transfer from a single sphere to fluid flowing into an array*", Transactions of Institution of Chemical Engineers of London, vol. 43, T 321, (1965)

[64] **D. Kunii and al**., "*Fluidization engineering*", second edition, Butterworth & Heinemann, (1991)

[65] **S. Whitaker**, "*Forced convection, heat transfer correlations for flow in pipes, past flat-plates, single cylinders, single spheres, and for flow in packed beds and tube bundles*", American Institute of Chemical Engineering journal, vol. 18, 2, pp. 361, (1972).

[66] **J.P. Sorensen**, "*Computations of forced convection in slow flow through ducts and packed beds*", Chem. Eng. Sciences, vol. 29, pp. 827/37, (1974)

[67] **A.J. Karabelas and al**., "*Use of asymptotic relations to correlate mass transfer data in packed beds*", Chem. Eng. Sciences, vol. 26, pp. 1581/89, (1971)

[68] **E.J. Wilson**, "Liquid *mass transfer at very low Reynolds numbers in packed beds*", Industrial Engineering Chemistry Fundamentals, vol. 5, 1, pp. 9, (1966)

[69] **D.E. Baldwin**, "*Heat transfer in beds of oriented spheres*", Ind. Eng. Chem. Des & Dev, vol. 5, 3, pp. 281, (1966)

[70] **N. Wakao S. Kaguei**, "*Heat and Mass transfer in packed beds*", Gordon and Breach Sciences Publishers, New-York, (1982)

[71] **D.J. Gunn**, "*Transfer of heat or mass to particles in fixed and fluidized beds*", Int. Journal of H&M Transfer, vol. 21, pp. 467/476, (1978).

[72] **S. Ball and al**., "*Advanced-High Temperature Reactor (AHTR) loss of forced circulation accidents*", Second International Topical Meeting on High temperature reactor Technology, Beijing, China, September 22-24, (2004).

[73] **A. Griveau**, "*Scaling of AHTR Pilot Plant*", University of California, Berkeley report, (July 2006).

PART II :
NEUTRONIC STUDY

A. MODELING of a PEBBLE for MCNP5

I. COMPONENTS DESCRIPTION

The PB-AHTR combines several existing technologies in a new way. In order to set a proper model of the core, its main components have to be modeled accurately in order to reproduce reliably their neutronic behavior. The first step is to study their physical description: it can help further to model them and understand the results that will be obtained with the code.

I.1. FLIBE salt

The Flibe is the primary salt, extracting the power from the pebbles. We will not discuss its thermal hydraulic properties. Our concern here is its neutronic characteristics and implications of the design.

It consists of LiF and BeF_2 at nearly a 2-to-1 molar ratio, and this composition is assumed fixed anywhere, any time in the core. However, the isotopic composition of Li will change due to the ^{6}Li (n,α) reaction. It will have different ^{7}Li enrichment level during a cycle, starting from a "low" level that is affordable to a steady high level made possible by the irradiation inside the core. We are considering here only a steady high level of purity, fixed at 99.995% of ^{7}Li molar fraction, since more design details are required to determine the "real" amount of ^{6}Li that can be tolerated in the core. A lower enrichment level in ^{7}Li might be a safety issue if it gives a positive coolant void coefficient. It will also have an adverse effect on the neutron economy by wasting neutrons through the ^{6}Li(n,α) reaction. Figure A-1 shows that the neutron capture by ^{6}Li should not be neglected.

Shall it be activated, the excited isotopes (^{8}Li, ^{9}Li and ^{11}Li) would decay with a very short half-life (less than a second). Thus ^{7}Li is interesting since it has poor neutronic properties, especially compared to the other isotope of the salt.

Beryllium has good scattering properties and a little absorption cross section on the whole spectrum, making it interesting on the neutronic prospective (Figure A-2). We naturally find only ^{9}Be. It has however two drawbacks that have to be considered:

- it can turn into ^{10}B by (n,α) reaction. It is decaying with a half life of $1.52.10^{6}$ year, producing a 555 eV energy gamma and a ^{10}B. The activated beryllium is thus to be taken into account for the disposal of the salt. Note that other activated isotopes of Be can be obtained trough various reactions, as beta decay of ^{8}Li into ^{8}Be. But they all decay with short half-life (53 days for ^{7}Be, less than a minute for the other isotopes);
- Beryllium salts are very toxic, making them hazardous material even before being activated into the core.

Fluorine also shows mainly scattering properties. However it also has four absorption resonances at 27, 49, 98 and 359 keV (see Figure A-2). The activated isotope will then quickly decay (half life shorter than 15 seconds) to Neon. The gas should be removable at the free surface of the primary loop: in the primary pump tank. Besides, it should not have any problem of compatibility with the different materials of the primary loop.

After discharge from the core, Flibe should not represent an hazard since it is slightly activated. It remains to be determined the required enrichment level of lithium, that may have an important impact on the coolant price.

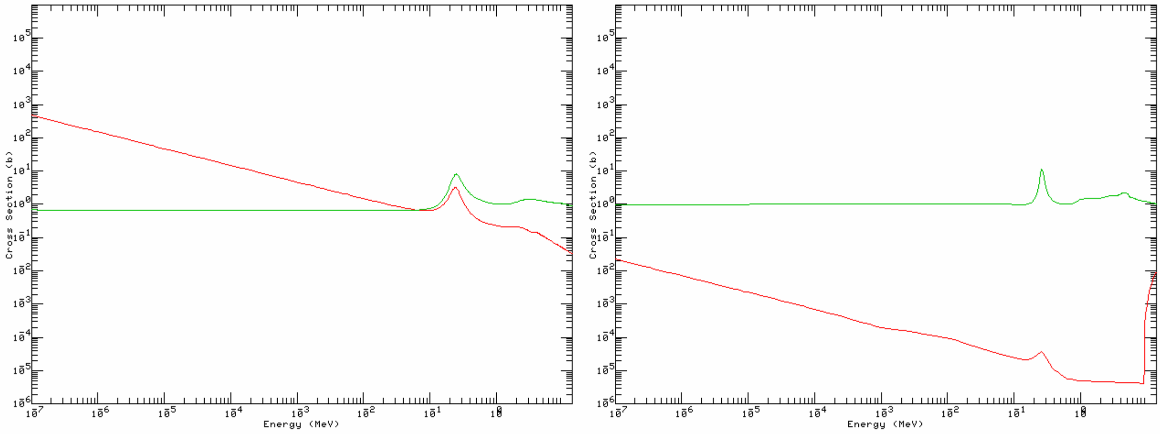

Figure A-1 ^{6}Li (left) and ^{7}Li (right) absorption (red) and scattering (green) cross sections

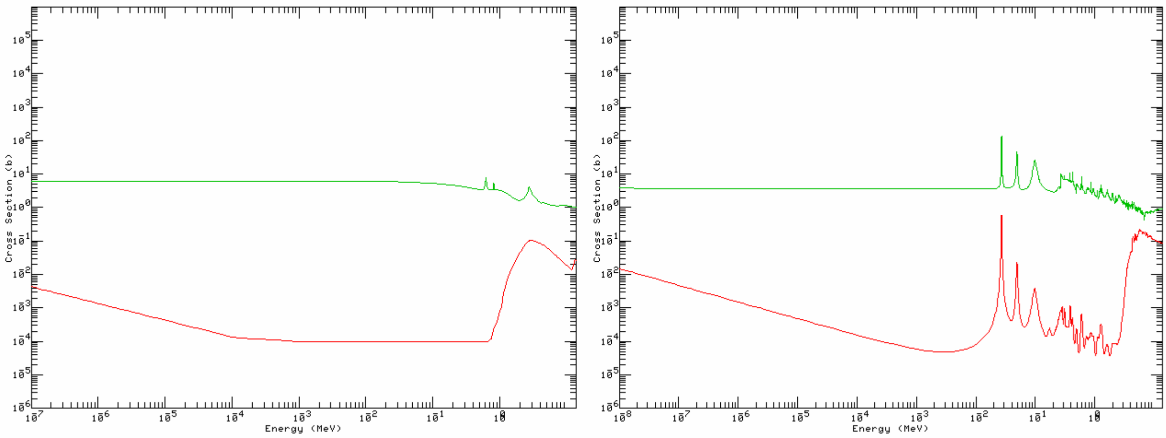

Figure A-2 ^{9}Be (left) and ^{19}F (right) cross section for scattering (green) and absorption (red) cross section

The range of temperature we consider is 500 to 1000°C; this allows dealing with all the different reactor conditions, from hot stand-by to steady full power, including small transients. Though never used in full scale power plant, Flibe has been widely studied and has been tested in numerous experiments [1]. Table A-1 summarizes the characteristics of Flibe.

Table A-1 Flibe characteristics

Salt (mol %)	Molar weight (g/mol)	Melting point (°C)	Density (g/cc), T (°C)	700°C heat capacity (cal/g/°C)	Viscosity (cP), T(K)	700°C thermal conductivity
LiF-BeF2 (66-34)	33.1	458	2.28-4.884e-4*T	0.57	0.116*exp(3755/T)	0.011

It is believed that material compatibility for primary loop components used with Flibe at high temperature is an issue that can be handled.

I.2. TRISO particle

The TRISO particle carries the heavy metal load. It is made of a kernel of the fuel material coated by several graphite and silicon-carbide layers. The particle radius does not exceed 1 mm and is made as shown in Figure A-3. The particle guarantees integrity for high burn-up and can sustain a temperature outing during transient accident up to 1400$^{\circ C}$ for a short period of time.

Table A-2 shows the TRISO physical characteristics.

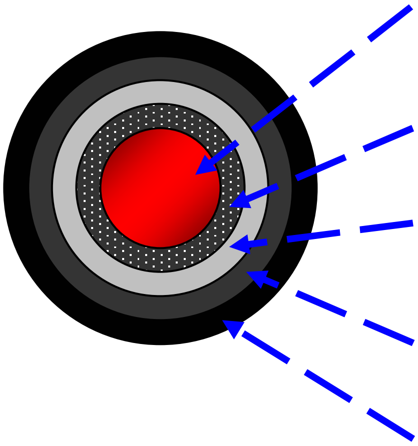

Kernel: matrix of U_2CO_3.
Other fissile or fertile material can be used.

Carbon buffer: attenuates the fission recoils and provides void volume for the fission gases and the kernel swelling.

Inner Pyrocarbon (IPyC): retains the fission gases and provides structural support for the SiC

Silicon Carbide: primary load bearing and leak tight barrier for fission products.

Outer PyroCarbon (OPyC): provides structural support for SiC, fission product barrier with a defective SiC layer.

Figure A-3 TRISO particle description

Table A-2 TRISO particle specification

Data	Kernel	Carbon buffer	IPyC	Silicon Carbide	OPyC
Composition	U_2CO_3	C	C	SiC	C
Density	10.5	1.	1.9	3.18	1.9
Radius (cm)	0.025	0.0345	0.0385	0.042	0.046
% TRISO volume	16.05%	26.13%	16.44%	17.49%	23.88%
Temperature (°C)	815	780	780	780	780

I.3. Pebble fuel element

The pebble is the fuel element of the AHTR. It is made of two parts:

- the fuel volume, made of a matrix of graphite holding the TRISO particles; the graphite density is set at 1.6. It can be adjusted if the pebble density does not allow positive buoyancy (the pebble mass ranges from 193 to 215 grams depending on the number of TRISO kernels used). However tests should be done to determine the characteristics of a new fuel design. It is assumed that the TRISO particles are spread homogeneously inside the pebble. The temperature is set uniformly at 705°C.
- the external protective layer, 0.5 cm thick, made of high density graphite (1.9 g/cm^3).

Figure A-4 describes the pebble. Its buoyancy is always positive whatever the salt density is (under normal operating conditions).
The graphite is used as structural material and moderator, while allowing heat transfer to the primary salt. A pebble is defined by its radius and density, but also by its packing factor. The packing factor (PF) is the volume of TRISO particles over the inside volume of the pebble.

$$PF = \frac{\text{TRISO particle volume}}{\text{Fuel area volume}} \quad \text{(A.I.1)}$$

However, the irradiation damage and the buoyancy of the pebble are to remain acceptable during all the pebble's life, so the PF upper limit is around 25%. The density of the pebble then ranges roughly from 1.35 to 1.82 g/cc. The packing factor is a parameter that will be studied further.

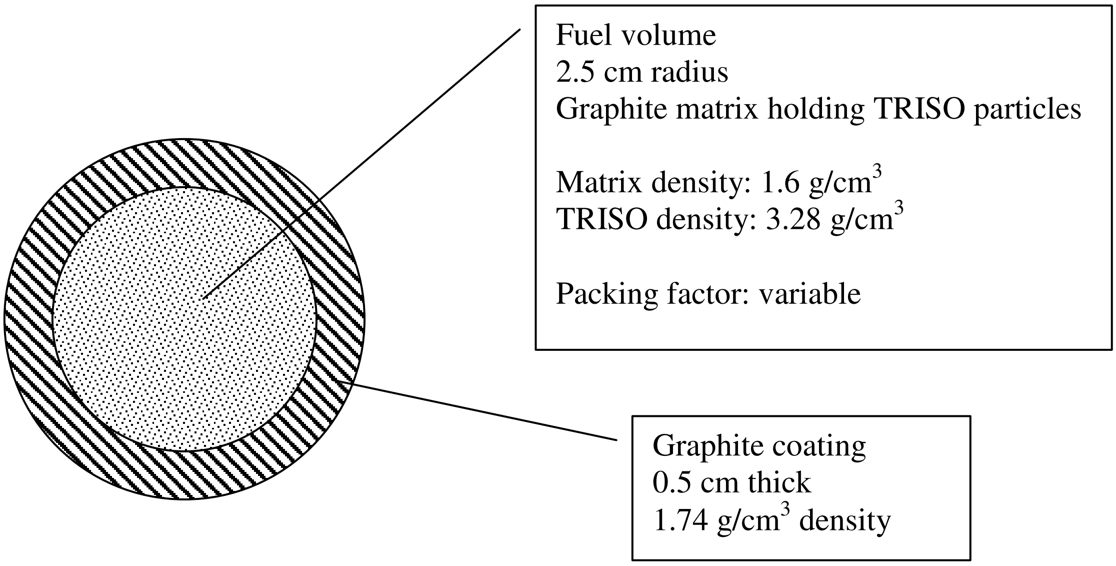

Figure A-4 Pebble scheme

These differences in the packing factor give a number of TRISO particles per pebble ranging from 8000 to 40,000, and the mass of heavy metal ranges from 4.9 to 19.6 grams.
Note that the primary salt does not wet the graphite; therefore, the heat transfer at the surface can be strongly reduced if gas bubbles are stuck at the surface of the pebble. Gas entrainment can also be feared in the core. All cares should therefore be taken to prevent the gas from "sticking" to the pebble's surface by keeping an excellent slick surface and by controlling the pebble before its injection in the core.
In the continuous refueling design, a pebble goes through the core several times during its life. After each cycle, its burn-up will be measured and it will be either discarded or reloaded in the core.
When placed in the core, the pebbles will pack in the top of the core due to the buoyancy force. We will consider that they group in a homogenous way. The ratio of space filled by pebble over the space studied will be called pebble bed compactness (PBC). The space that is not occupied by a pebble is filled with Flibe salt. We will assume a constant PBC in the core and neglect any side effect that might occur.

II. PEBBLE DESCRIPTION FOR MCNP5

Once their description known, the components have to be translated into an MCNP input file. The geometry has to be reproduced precisely; the materials have to be simulated by choosing the best nuclear data tables among all the available tables. The user also has to enter the tallies for the result he is looking for. The model has to be relevant by giving results that are as accurate as possible, meaning that a calculated $\bar{x}$ value is close to the true physical quantity being estimated. Therefore a good precision (the statistical fluctuation around $\bar{x}$ of the x_i's sampled) is not showing the quality of the result since it is not related to the physical meaning of the quantity that is calculated.

II.1. Models description

The pebble bed reactor core can be reproduced in full details with the MCNP code but the more accurate is the model the more the computational time increases. In order to decrease the machine time without losing accuracy different simplified model have been considered:

- the heterogeneous model;
- the coating homogenized model;
- the fuel area homogenized model;
- the reactivity equivalent physical transformation model.

The pebble used to test the model has the same properties as described in §1.3. It is placed in an infinite medium by using reflective boundary conditions. The void is filled with Flibe salt, the pebble bed compactness is set to 49.8%. Accurate temperatures for the different materials are given so that the cross sections can be calculated while considering the thermal motion of the carbon nuclei when scattering thermal neutrons. A gain of energy is thus possible for a thermal neutron. The materials do not contain impurities, and the pebble is "fresh": it does not contain any fission products.
The different parameters were set as follow:

- ^{235}U enrichment : 10%;
- packing factor: 10% to 25% per step of 5%, giving a maximum number of 40,132 TRISO particles per pebble.

The runs were made with 4000 particles and 600 cycles were done. The first 100 cycles were skipped in order to reach the fundamental distribution of sources in the pebble. The results are shown in Table A-3 for the first three models. Models are described and discussed later, with their results. The cross sections are averaged over the whole spectrum (0 to 20 MeV), the flux is averaged over the whole fuel area for a power of 1908 W, which is the expected average power per pebble for the core. The reactivity equivalent physical transformation model will be discussed at the end.

Table A-3 Pebble models results

Packing factor	Pebble model	K_∞ and standard deviation	Δk_∞ with reference	Flux at 1908 W (n/cm²-s)	ΔFlux with reference	σ_f (barn)	
						^{235}U	^{238}U
10%	Heterogeneous	1.319 ±0.00041	0%	2.931E+14	0%	108.5	18E-3
	Fuel area homogenized	1.24935 ±0.00042	-5.28%	2.825E+14	-3.62%	105.1	19E-3
	TRISO coatings homogenized	1.31804 ±0.00042	-0.07%	2.937E+14	+0.21%	108.2	18E-3

Table A-3 Pebble models results (continuation)

Packing factor	Pebble model	k_∞ and standard deviation	Δk_∞ with reference	Flux at 1908 W (n/cm^2-s)	ΔFlux with reference	σ_f (barn)	
						^{235}U	^{238}U
15%	Heterogeneous	1.3109 ±0.00068	0%	2.468E+14	0%	85.5	22E-3
	Fuel area homogenized	1.24602 ±0.00069	-4.95%	2.394E+14	-2.99%	82.4	22E-3
	TRISO coatings homogenized	1.31049 ±0.00062	-0.03%	2.477E+14	+0.37%	85	22E-3
20%	Heterogeneous	1.28326 ±0.00069	0%	2.208E+14	0%	69.9	24E-3
	Fuel area homogenized	1.22594 ±0.0007	-4.47%	2.155E+14	-2.41%	67.5	24E-3
	TRISO coatings homogenized	1.28244 ±0.00066	-0.06%	2.222E+14	+0.63%	69.4	25E-3
25%	Heterogeneous	1.25115 ±0.00027	0%	2.039E+14	0%	58.8	26E-3
	Fuel area homogenized	1.20122 ±0.00029	-3.99%	2.000E+14	-1.93%	56.8	26E-3
	TRISO coatings homogenized	1.24932 ±0.00029	-0.15%	2.056E+14	+0.82%	58.3	27E-3

II.1.a. Heterogeneous model

In this model, each TRISO particle in the fuel area is individually and fully described (Figure A-5). Although as precise as the code can be, this model is also expensive in computer time since a pebble can hold up to thousands of particles. Each coating is described by an individual cell containing the atomic fraction of materials the coating is made of. Temperature is set for each cell from the kernel to the OPyC and the material cards are chosen in the library according to these temperature.

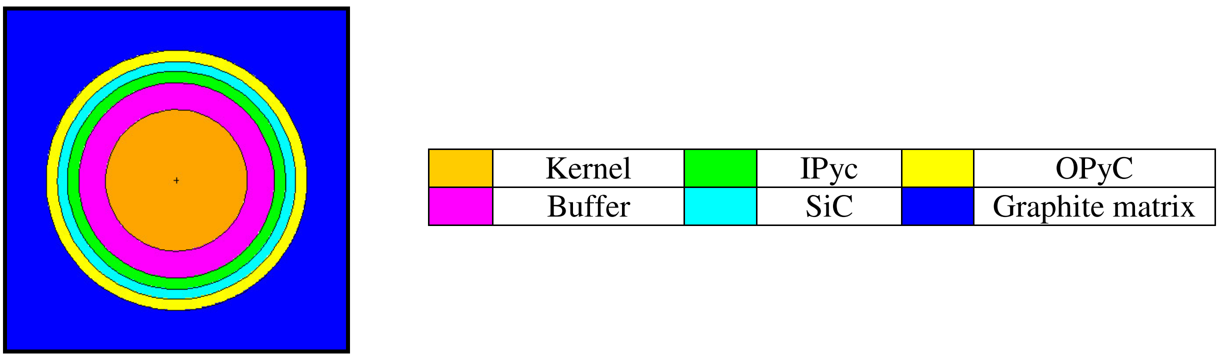

Figure A-5 TRISO particle model

In the MCNP5 model, the TRISO particles are disposed according to a deterministic lattice. Two options are available, as shown in Figure A-:
- columnar hexagonal lattice;
- cubic centered lattice.

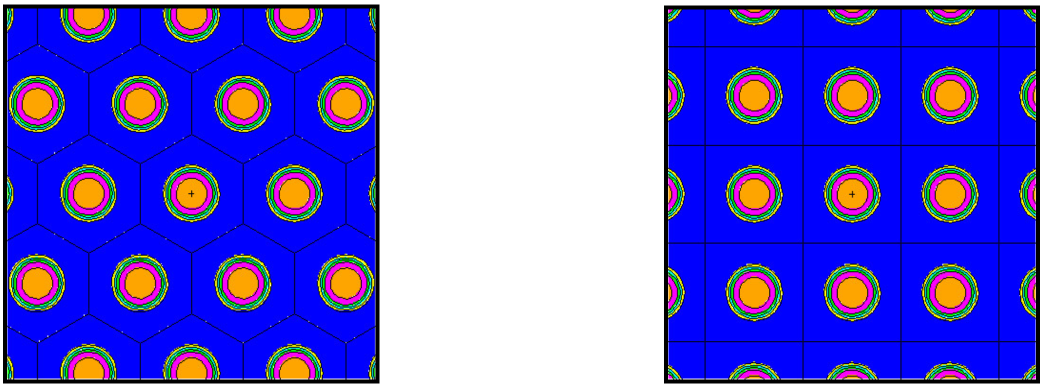

Figure A-6 Columnar hexagonal (left) and cubic centered (right) lattice for TRISO distribution inside the fuel area

According to L. Massimo [1], such a deterministic placement does not greatly impact on the neutronic behavior of the pebble. Tests performed showed a negligible difference (less than 10^{-5}, as shown in Table A-) on the k_∞.

Table A-4 Influence of lattice choice on results for a 10% packing factor

Model full detail pebble	Hexagonal columnar lattice	Cubic centered lattice	Delta
K∞	1.32988 ± 0.00047	1.32965 ± 0.00052	0.018%
Average time/cycle (second)	15’	14’	1’

The choice between the two lattices was then made on computational time required. The computational times between the two types of lattice were in the same order of magnitude, but the cubic lattice is simpler to input and therefore it will be used as the reference model.
One can notice that the latest release of MCNP5 allows one to randomly place particles inside a volume; thus it would be interesting to study the impact of a deterministic versus a stochastic positioning.

The results obtained with this model are defined as “reference”: we do not intend to consider these results as an exact prevision of the real pebble, but we want others models to get as close as possible to these results. Figure A- shows the influence of the packing factor over k_∞. We can notice that while PF is increasing, the C/HM ratio is quickly decreasing as well as neutron moderation: the reactivity goes down, and the spectrum thermal peak is reduced, as illustrated on Figure A-. Smaller C/HM ratio increases the probability of capturing neutron in the resonances of uranium, thus the fission cross section of U^{235} decreases and the thermal over total fission ratio for U^{235} goes down from 91% to 80%. Meanwhile there is a very small increase in U^{238} fast fissions.
Table A- gives the ratio of thermal versus total flux, and the percentage of thermal fission. This ratio F_r is defined as:

$$Fr = \frac{\int_{Thermal} dE \int_V dV \cdot \phi(\vec{r}, E)}{\int_{Total} dE \int_V dV \cdot \phi(\vec{r}, E)} \quad \text{(A.I.2)}$$

Where : $\phi(\vec{r}, E)$ is the neutron flux;
Thermal is the thermal spectrum [0.01;1] [eV];
Total is the fast spectrum [0.01; 20E+6] [eV];
V is the volume of the cell considered.

Table A-5 Thermal versus fast spectrum ratio and C/U ratio

PF	10%	15%	20%	25%
$C/^{235}U$	2853	2481	1849	1113
Fr	0.43	0.34	0.28	0.23
% thermal fission (<0.625 eV)	90.74	86.92	83.07	79.23

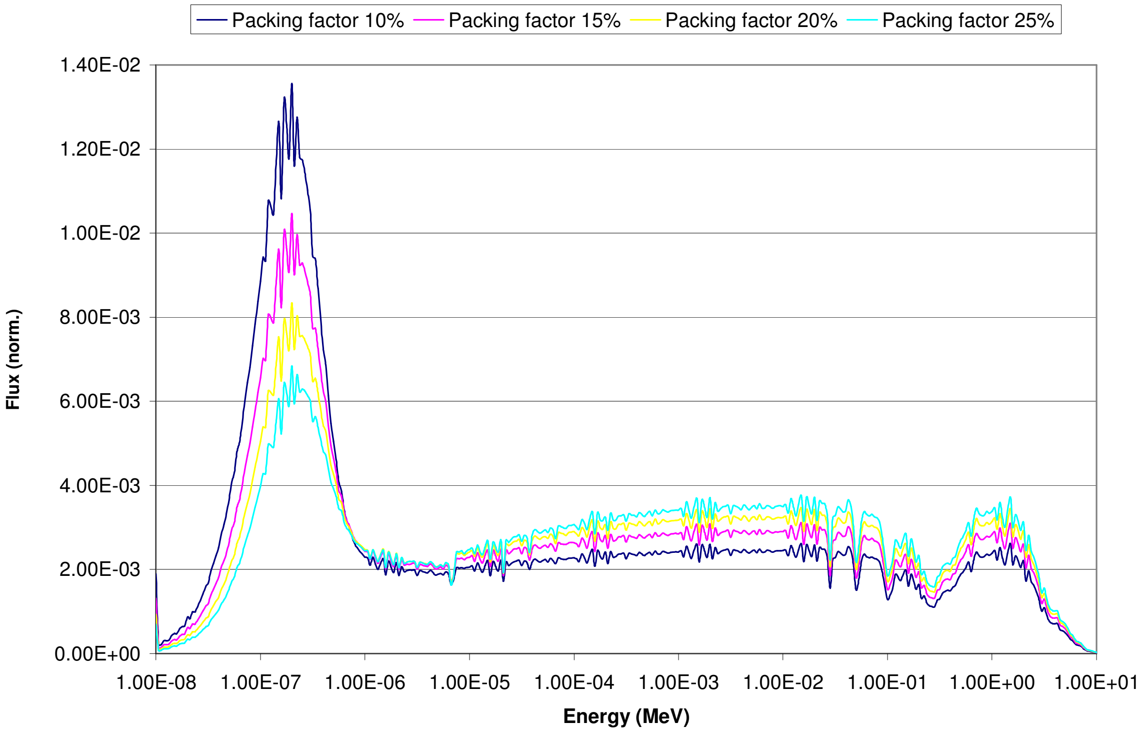

Figure A-7 Flux in the fuel kernel of an infinite bed of pebbles, ^{235}U enrichment 10%, pebble bed compactness 49.83%

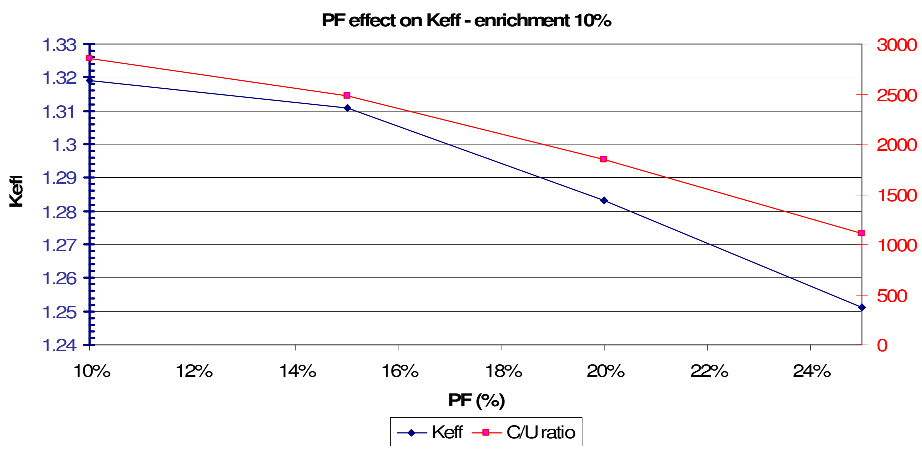

Figure A-8 Effect of the PF on k_∞ and the C/U ratio

II.1.b. Homogenized model

Different approaches have been considered in order to simplify the model and save computational time.
The first method used is called Volume Weighted Homogenization. In that model, we homogenized the TRISO particles inside the graphite matrix according to their volumetric fraction: the materials are blended, the atomic densities of the isotopes are recalculated by keeping the volumetric fractions. The temperature of the new cell is set to an average temperature from the heterogeneous model but nuclides cross sections are kept at the original temperature according to their volumetric fraction. This model is called the fuel area homogenized model (FHM). The composition of the homogenous fuel area is described in Table A-.

Table A-6 Material concentrations for homogenization

Material	Density (g/cm^3)	% volume of the fuel area	Concentration (atoms/b-cm)	Homogenous concentration (atoms/b-cm)
Fuel kernel U_2CO_3	10.5	1.61%	U 2.36153E-02	3.790875E-04
			O 3.54229E-02	5.686313E-04
			C 1.18076E-02	1.895438E-04
Buffer	1.	2.61%	C 5.26442E-02	1.375850E-03
IPyC	1.9	1.64%	C 9.52610E-02	1.566185E-03
SiC	3.18	1.75%	Si 4.77543E-02	8.350910E-04
			C 4.77543E-02	8.350910E-04
OPyC	1.9	2.39%	C 9.52610E-02	2.275240E-03
Graphite matrix	1.6	90.00%	C 8.02198E-02	7.219782E-02

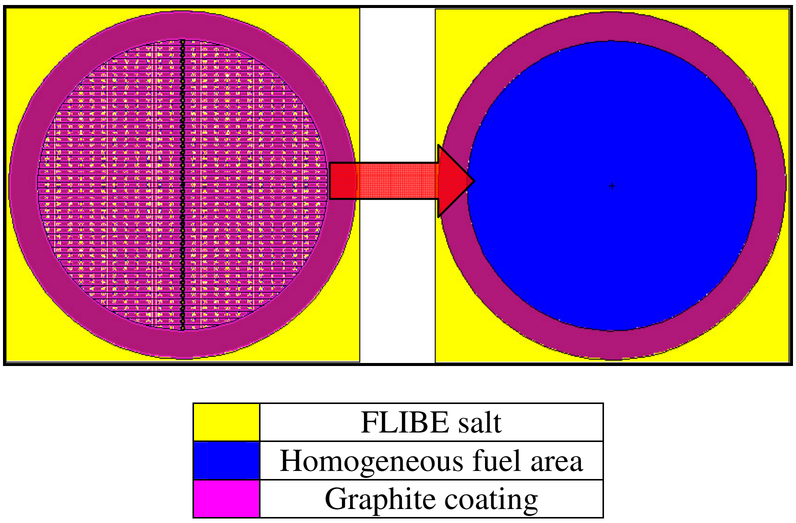

Figure A-9 Pebble fuel area homogenization

In the second model only the different coatings of the TRISO particles are homogenized, leaving the kernel intact so to preserve part of the spatial heterogeneity of the fuel area. It is called homogenized coating model (HMC).

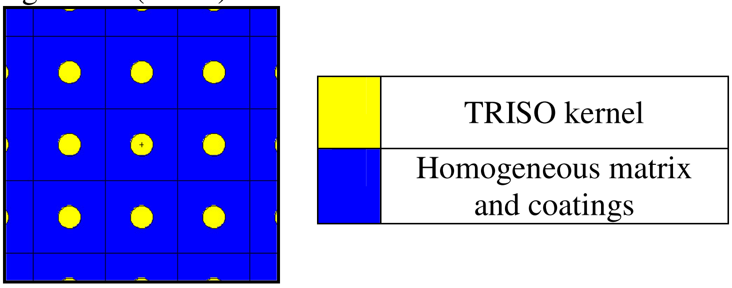

Figure A-10 Homogenized TRISO coatings - only the TRISO kernels are described

The table of material concentration in that case is:

Table A-7 Material concentration in the homogenous coating model

Cell	Material	% volume of the fuel area	Concentration (atoms/b-cm)	Note
Kernel	Fuel kernel U_2CO_3	1.61%	U 2.36153E-02	Same as in heterogeneous model
			O 3.54229E-02	
			C 1.18076E-02	
Homogenous TRISO coatings and graphite matrix	C and Si	98.39%	C 6.052366E-03	Material card for 780°C
			C 7.21978E-02	Material card for 705°C
			Si 8.350910E-04	Material card for 780°C

Figure A- and Figure A- plot the relative difference for k_∞ and for the flux found for each model compared to the reference.

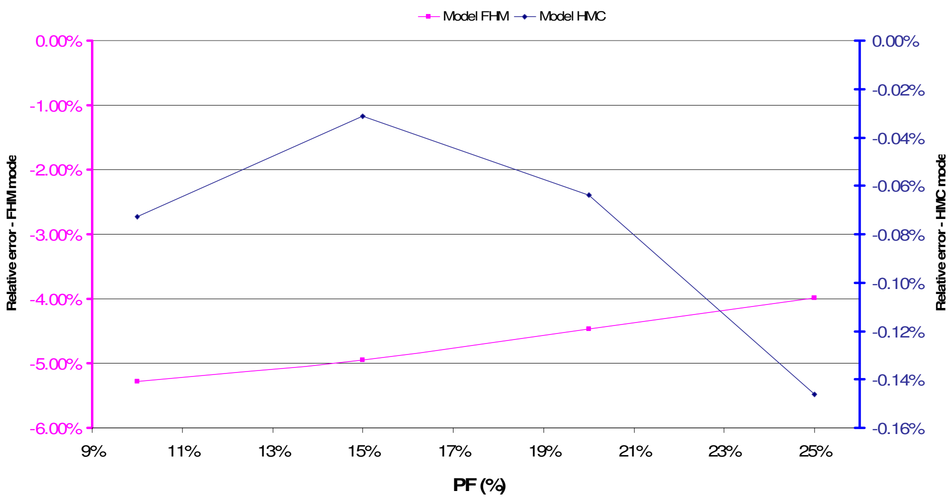

Figure A-11 Relative error of k_∞ versus packing factor

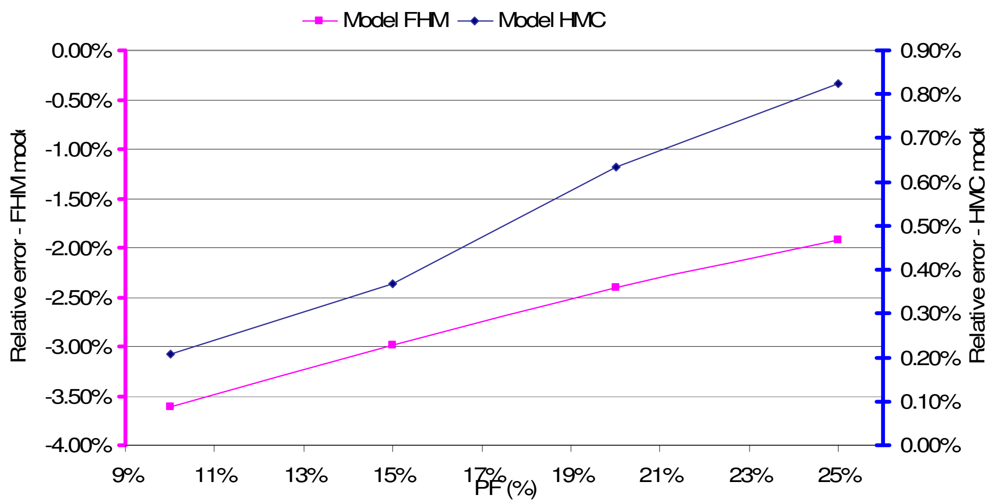

Figure A-12 Relative error of flux versus packing factor

II.1.b.1. Fuel area homogenized model

Although very efficient for computational time purpose, the results were not very satisfying. An average -4.5% differences in k_∞ was found compared to the full detail model. The homogenous pebble was found to be much less reactive. This difference is due to the fact that we removed a level of heterogeneity in the pebble by changing the spatial distribution of the different elements: the fuel area homogenized does not give the same environment for a neutron. Likely, in the homogenized model the resonances capture probability is increased, casing a drop in reactivity.

It is also interesting to see that a neutron born inside a pebble will certainly have the time during his life to move into other pebbles. Also one can notice that the more we pack the pebble, the bigger is the mean free path. This is due to the faster flux that allows a neutron to travel more before being absorbed or scattered. Besides, the error is also getting smaller, as shown on Figure A-. Indeed, the more we add kernel in the matrix, the smaller the change is visible for a neutron when we blend the materials as we smoother the spatial heterogeneity. However we can conclude that simple volumetric homogenization does not take adequately into account the complex neutron interactions that take place in the pebble.

We can underline the impact the homogenization has on the neutronic behavior of the pebble when we plot the spectrum in the epithermal area where self-shielding of the resonance of capture can have a big impact on the overall neutron balance. Figure A- show that the flux is not reproduced accurately between 1 and 100 eV. Firstly over predicted in the homogenous model, it is then under predicted below 6.68 eV, after the biggest capture resonance. In this area of the flux, each TRISO kernel is shadowing its neighbors in the double heterogeneous model, therefore limiting the captures and making the pebble more reactive. In the homogeneous fuel however, self-shielding is under-estimated and more neutrons cannot make it through the resonances.

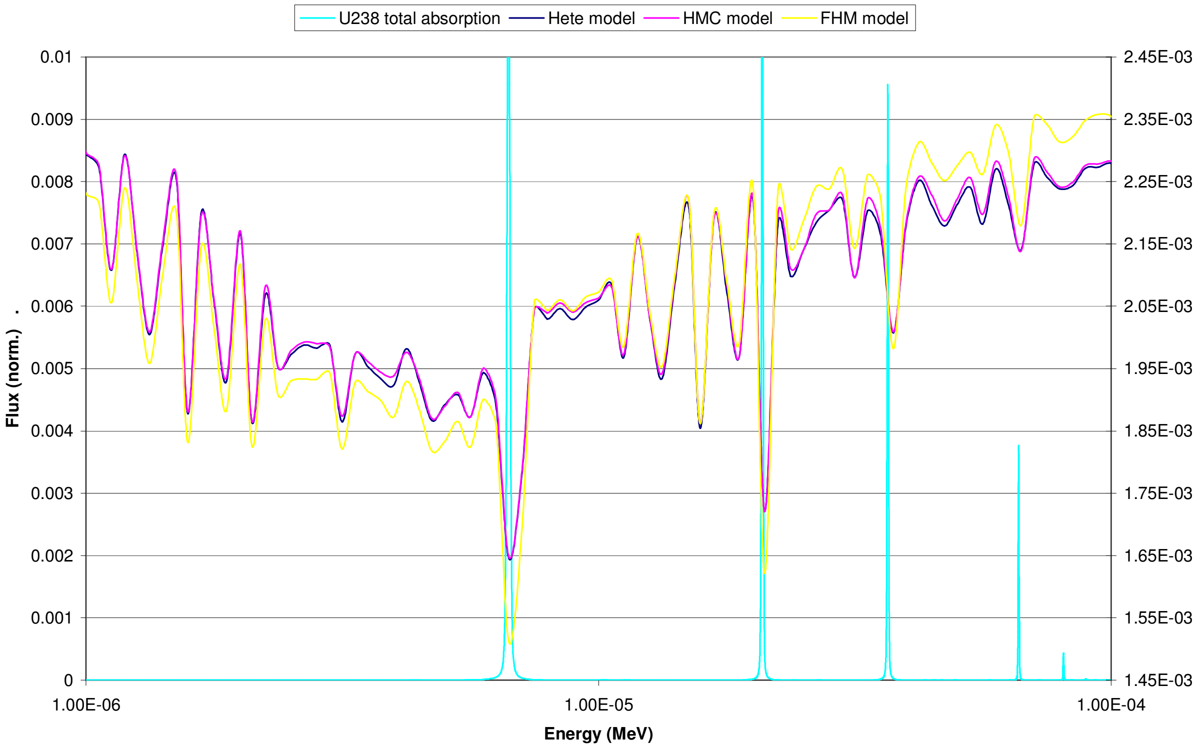

Figure A-12 Plot of the flux for different model in the epithermal region [1; 100 eV], with U^{238} resonance of absorption (blue picks)

To investigate the importance of this phenomenon, we ran calculations with different ^{235}U enrichments. The results in Table A- show that the capture by ^{238}U is indeed the main source of the difference between the volumetric homogenization (FHM) model and the realistic (heterogeneous) model. Other elements may also contribute to the difference. Indeed, Silicon has few small resonances of absorption in the high epithermal and in the fast energy ranges. Oxygen shows also small resonance of absorption in the fast energy range. To investigate the impact of these resonances, one could remove numerically these absorption cross sections in the two models and see if the results are affected.

Table A-8 Models comparison for various ^{235}U enrichment, packing factor of 10%

	^{235}U enrichment	**10%**	**50%**	**80%**	**90%**	**99%**
k_∞ and standard deviation	**Heterogeneous**	1.319 ±0.00041	1.60542 ±0.00039	1.68164 ±0.00039	1.71509 ±0.00039	1.76174 ±0.00035
	FHM	1.24935 ±0.00041	1.56026 ±0.00046	1.66525 ±0.00038	1.70645 ±0.00037	1.75713 ±0.00037
	Δ k_∞	-5.28%	-2.81%	-0.97%	-0.50%	-0.26%

Figure A-1 below shows the spatial distribution of the flux in the pebble. The flux is obtained by cutting the pebble in several spherical shells of the same volume. The HMC has a local increase of flux close to the outer limit of the fuel area. This is due to the external graphite coating; it is acting as a reflector for the fuel area and is strengthening the thermal flux amplitude; thus we get more fission for the outside TRISO kernels. Then the flux is decreasing towards the center of the pebble: thermal neutrons are captured in the fuel kernels so that the fission rate is also decreasing near the center. The FHM model shows an almost constantly decreasing flux towards the center.

We can expect the fission rate to do the same, as every spherical sell contains the same amount of fissile material. The uniform distribution of uranium increases the probability of capturing neutrons in the external layers of the pebble then the flux peak does not appear in the homogenized model.

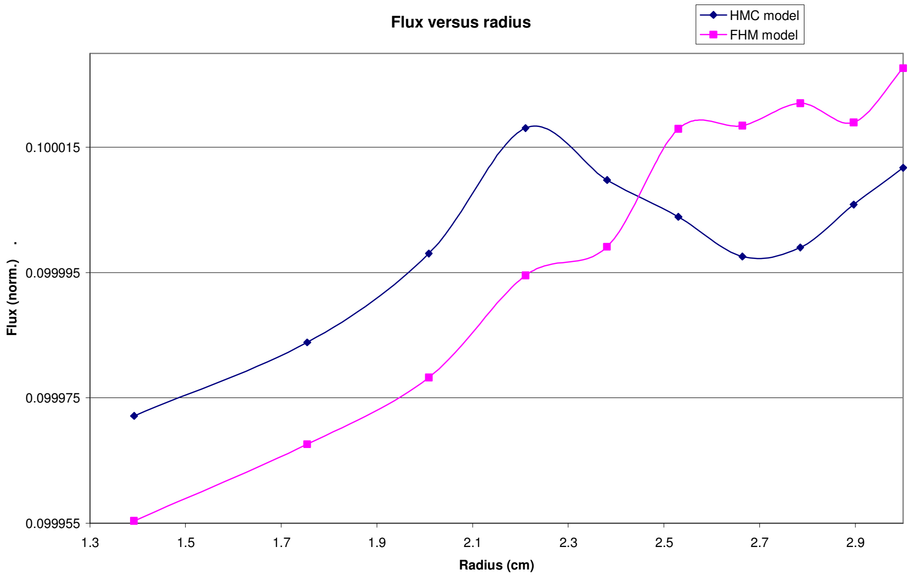

Figure A-1 Spatial distribution of the flux versus fuel area radius: HMC model (blue) and FHM model (pink)

If we plot the flux for fast, epithermal and thermal flux in the pebble, we obtain Figure A-2 .

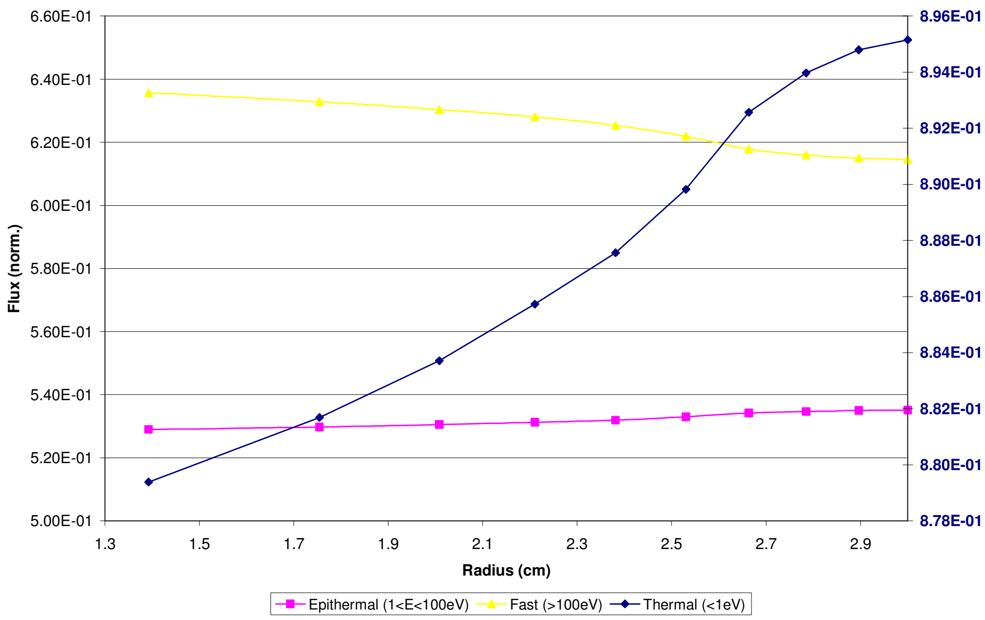

Figure A-2 Flux in the pebble versus radius for different spectrum – the scale for the thermal flux (on the right) is changed to underline the flux shape – HMC model

The thermal flux maximum is found in the graphite coating of the pebble, where there is no capture. The closer we get to the center, the more the thermal flux is decreasing because of the TRISO kernels. Like a pressurized water reactor fuel element, we can expect a radial distribution of the burn-up in the fuel kernels.

The fast flux has an opposite behavior. Fast neutrons born from fission have enough energy to escape from the pebble before having their first interaction, as shown in Table A-. They are then scattered (or captured) either in a neighboring pebble or in the primary salt that has good scattering properties thanks to the Beryllium. Table A- presents the mean free path (MFP) of neutron from different energy group in the graphite and in Flibe. MFP is calculated with MCNP according to the following equation:

$$\lambda = \frac{1}{\overline{\Sigma_T}} \quad \text{(A.II.1)}$$

where: λ is the mean free path [cm] ;

$\overline{\Sigma_T} = \frac{\int_{E\min}^{E\max} \phi(E) \cdot \Sigma(E) \cdot dE}{\int_{E\min}^{E\max} \phi(E) \cdot dE}$; total cross section [cm^{-1}], condensed on the energy group considered.

Neutron energy group	Thermal (E<1eV)	Fast (100eV<E)
Graphite	2.93	4.93
Flibe	7.5	11.3

Table A-9 Neutron mean free path (cm)

II.1.b.2. TRISO external coatings homogenized

Here we just homogenized the OPyC, SiC, IPyC and buffer. Two reasons call for this solution:

- first we homogenized mostly graphite with graphite, so that the neutronic properties are conserved. Only the Si is blended with graphite. Since it has almost the same neutronic properties – mainly scattering, very few capture (Figure A-3 - the total cross sections are almost pure scattering) - and it represents less than 2% of the volume in the fuel area, the average behavior of the homogenous material does not noticeably change; besides we reduce the distortion in temperature, although it has a secondary effect;

- second by keeping the kernel of fissile material, we keep the heterogeneous shape of the flux, taking into account any kind of shadowing effect we might have between kernels: this effect called double heterogeneity cannot be reproduced with a simple volumetric homogenization. This has been found to be the preferred method for studying HTR fuel elements [2].

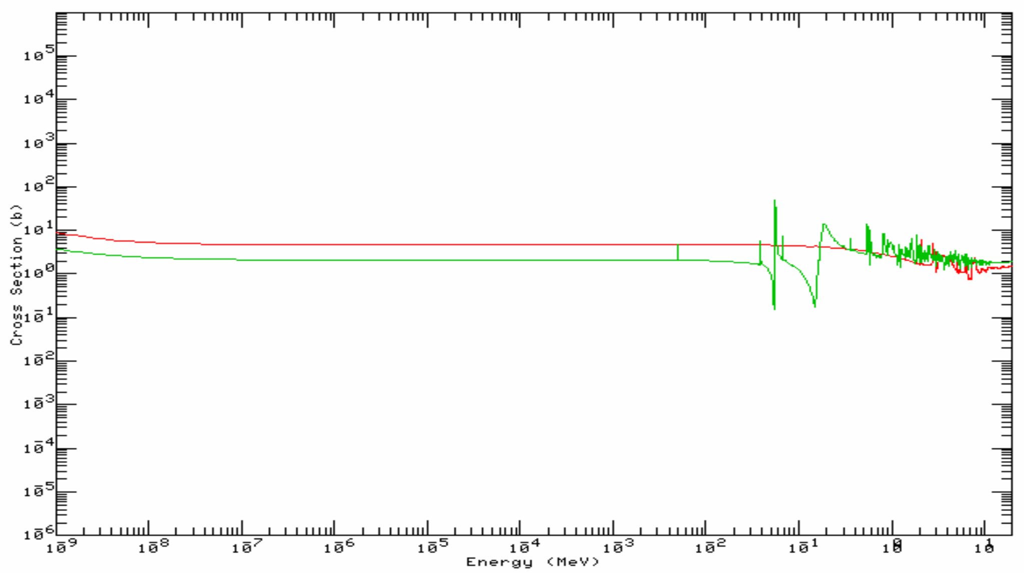

Figure A-3 C (in red) and Si (in green) total cross sections

The results were found to be extremely satisfying: the difference between the two models was less than 0.08%, the homogeneous pebble being less reactive. The spectrum matches precisely the reference spectrum. To illustrate this improvement, we plot the relative error between the normalized flux of the different models. The relative error is defined as:

$$\text{Relative error for bin i} = \frac{\left(\frac{1}{\int_{Ecut}^{E\max}\phi(E)\cdot dE}\left(\int_{Ei}^{Ei+1}\phi(E)\cdot dE\right)\right)_{\hom ogeneous} - \left(\frac{1}{\int_{Ecut}^{E\max}\phi(E)\cdot dE}\left(\int_{Ei}^{Ei+1}\phi(E)\cdot dE\right)\right)_{ref}}{\left(\frac{1}{\int_{Ecut}^{E\max}\phi(E)\cdot dE}\left(\int_{Ei}^{Ei+1}\phi(E)\cdot dE\right)\right)_{ref}} \quad \text{(A.II.3)}$$

Figure A-4 shows the excellent behavior of the HMC model on the whole spectrum, while the FHM model is found to be far from the reference, especially in the ^{238}U resonance of absorption area. We can notice that close from the borders of the spectrum, the error is increasing. This is due to the fact that these extreme areas have a very low flux. Therefore the statistical uncertainty is growing, spreading randomly the results and so the error.

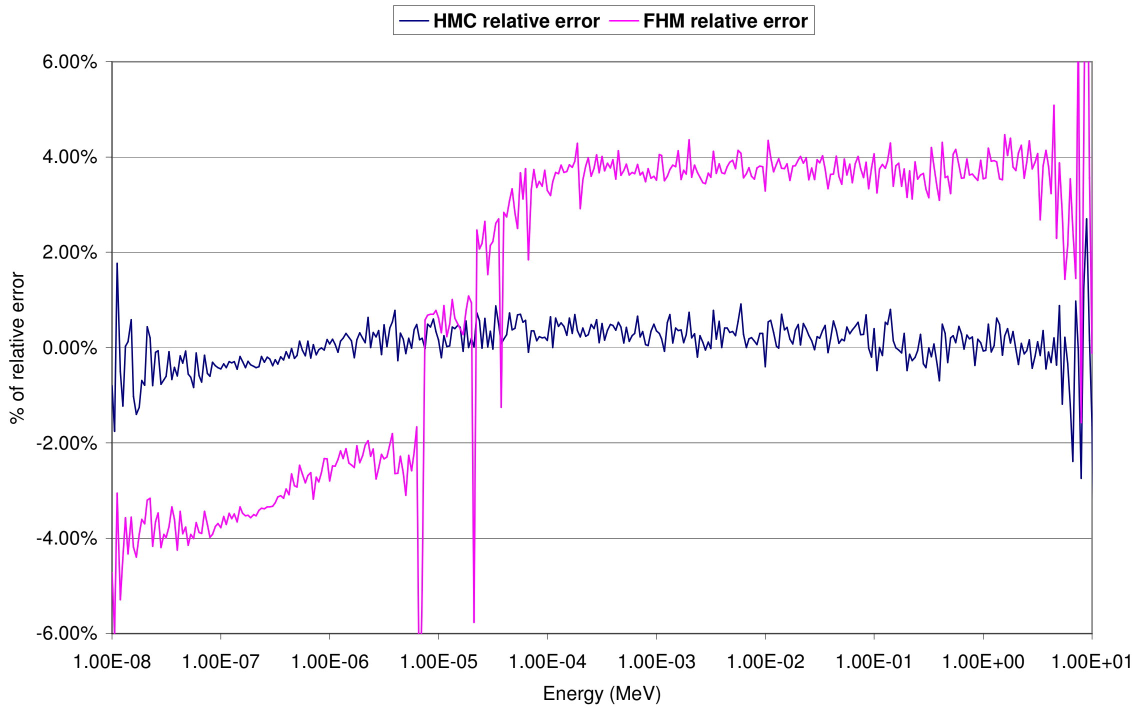

Figure A-4 Relative error of the neutron flux in the fuel area predicted by the homogenized model

The flux is also well reproduced, the error being only 0.51% but this time it is over predicted. Finally, we approximately reduce the computational time from a factor two.

The difference of results between the two models cannot be reduced further, but are acceptable. However, the computational time still remain significant. Besides, we should also check that these two types of model behave in the same way when we reproduce the core. We finally searched in literature to find other methods that could be used.

II.2. Reactivity equivalent physical transformation (RPT) model

This method was suggested by Yonghee Kim and Jae Man Noh from the Korea Atomic Energy Research Institute. The original double heterogeneous problem is transformed to a conventional single-heterogeneous one: fuel particles are dispersed in a smaller fuel zone with a higher packing fraction and the new fuel region is smeared like in the volume weighted homogenization. The fuel radius (RPT radius) is determined such that the neutron multiplication factor is equivalent to the reference value. Figure A-5 illustrate the method.

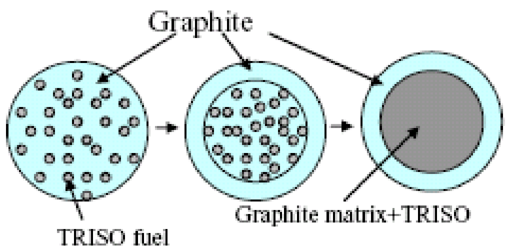

Figure A-5 Picture of the RPT concept

RPT looked very attractive since it gave very fast results. We tested it for an original packing factor of 10%. We were able to get an excellent k_∞ reproduction, with less than 0.04% of relative error as shown in Table A-. However, if we take a close look at the flux, we can see that it is not well reproduced, especially in the fast and the thermal area. Therefore we can expect the cross sections and the reaction rates to be different. Thus matching the reactivity is not sufficient to have a useful model. Figure A-6 shows the two spectrums and the relative error. One has to notice that in this method, the graphite to heavy metal ratio is not conserved. We made a test with a RPT model conserving this ratio by changing the density of the graphite used in the matrix. We were unable to reproduce k_∞ in that case. Indeed, it has been used originally for a pebble that does not have a high density external coating, and therefore it does not have a change in the graphite to heavy metal ratio.

Table A-10 Test of the RPT model, original PF 10%, enrichment 10%

RPT radius (reference radius = 2.5 cm)	k_∞ and standard deviation	Relative error with reference (k_∞=1.319)
1.85	1.31542 ±0.00078	-0.27%
1.825	1.31775 ±0.0042	-0.095%
1.8125	1.31950 ±0.00042	-0.038%
1.8	1.32132 ±0.00039	+0.17%

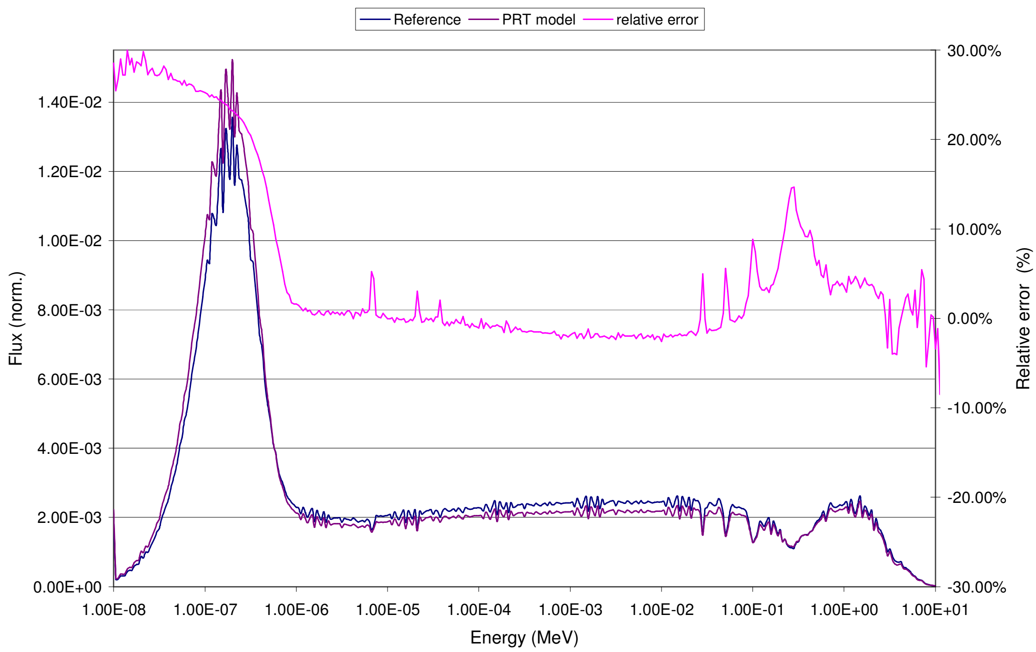

Figure A-6 RPT model results – flux predicted in fuel area – infinite core, ^{235}U enrichment 10%

II.3. Limited Chord Length Sampling method

Research in literature showed that the homogenization problem we face brought a lot of attention from many universities. A very promising method has been under research and tests with MCNP version 4C2 [5]. However, it requires a "calibration" for each problem it is used in, and we have not been able to find out if it was still under research. The LCLS method was designed for the simulation of pebbles loaded with spheres randomly spread inside, making the whole a stochastic mixture. These spheres could be TRISO particles in our case. The spheres are supposed to be homogenously spread. Thus, if excluding boundary effect, the chord length (λ_1) distribution between TRISO spheres for such a mixture can be represented by the exponential form:

$$p(\lambda_1) = \frac{1}{\overline{\lambda_1}} \cdot \exp(-\frac{\lambda_1}{\overline{\lambda_1}}) \quad \text{(A.II.4)}$$

Where: $\overline{\lambda_1}$ is the average chord length in the matrix material.

$\overline{\lambda_1}$ is determined empirically for a given mixture, thus a "calibration" process is required. Once known, it is used in the transport subroutine of MCNP to test if a particle reaches a stochastic interface. In this case, the particle is actually transported inside a fully described TRISO particle, until it exits it or gets killed. Each particle reaching a stochastic interface will be transported into this TRISO cell, and then if required, reintroduced inside the fuel area where the LCLS method is used to transport. Figure A-7 illustrates the LCLS model.

The results were focused on surface current and flux, and were better than any other method. However we were not able to find tests performed on k_∞ or the spectrum. This is simply underlining the complexity of homogenization process. It shows that one should take great care with homogenization method and always study its results on a benchmark model. However powerful the computers are, Monte-Carlo codes remain time consuming. When using them, experience does matter, and the first things the user should learn about the code are its limits.

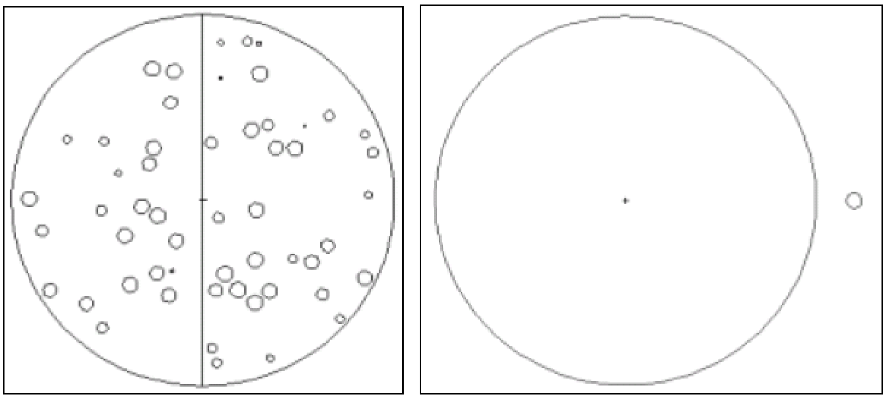

Figure A-7 The stochastic model (left) and its equivalent using the LCLS method; note the single TRISO particle for the LCLS

II.4. Annular pebble design

In order to limit the temperature variation inside a pebble after a scram, a new pebble design has been proposed. The aim is to smoothen the temperature profile in the fuel area in order to limit reactivity oscillation induced by Doppler effect after a scram. To do so, the fuel area is reduced to a spheroid zone surrounding a kernel of graphite. This design is described in Figure A-.

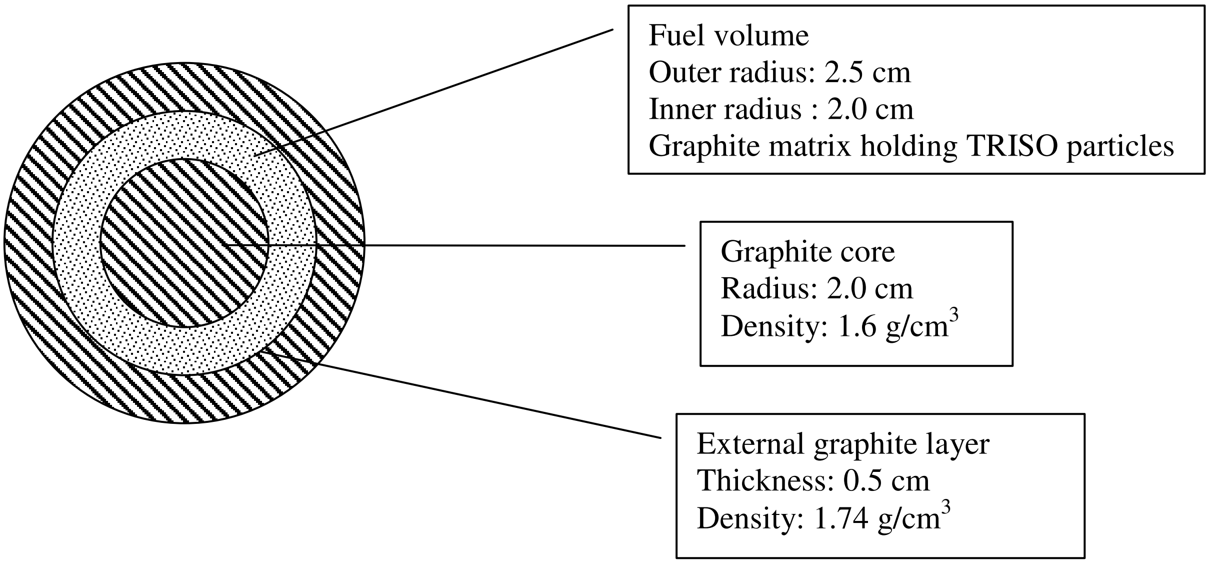

Figure A-20 Annular pebble design

The kernel is therefore acting as a heat tank that will prevent a quick cooling of the fuel area in case of a SCRAM. Therefore the high temperature inside the fuel area will provide a strong negative Doppler coefficient, thus allowing to passively shut-down the reactor.

In order to compare this design with the "classic" one, we made computations with the same number of TRISO particle inside a pebble: thus the amount of heavy metal is conserved from one design to the other. The heterogeneous and the FHM models were used in order to assess the impact of this new design on the homogenized results. In this design, the fuel area is representing only 28% of the pebble volume while it is 58% in the classic design. Therefore the annular pebble has a higher PF for an equivalent mass of ^{235}U. We can notice that in our test, we almost reach the maximal PF achievable. No other parameter is modified in the model. Table A-1 Results of the annular pebble design reports the results and compares them with the equivalent classic design.

Table A-1 Results of the annular pebble design

Model	Pebble PF (%)	Equivalent PF in classic pebble (%)	k_∞	Classic pebble k_∞	Std dev	% delta / hetero model
Annular heterogeneous pebble	20.49	10	1.32112	1.319	0.00041	-4.82%
	30.7	15	1.31489	1.3109	0.00043	-4.30%
	40.10	20	1.28702	1.28326	0.00047	-3.66%
	51.20	25	1.25665	1.25115	0.00046	-3.15%

There is a small increase in k_∞, while the relative error between the heterogeneous and HMC model is slightly reduced. While we increase the PF in the fuel area, the spatial double heterogeneity is decreased, therefore reducing the error between the two models.
The effect on the k_∞ can be explained by the impact the new design has on the spatial distribution of the flux. The fuel area being surrounded by graphite, all the kernels are placed in a thermal spectrum of high amplitude, contrary to the classic design where the thermal spectrum is higher close to the outer limit of the fuel area and weakened at the center.
The spectrum itself is lightly affected. It is enhanced in the fast energy range, while a little bit reduced in the thermal area.
This annular design does not seem to represent any problem for the control of the reactivity. However, a depletion analysis would be necessary to assess the potential burn-up performance. The technical feasibility of a very high packing factor region, shaped as a spherical shell, is also to be considered.

III. PB-AHTR CORE MODEL FOR MCNP5

III.1. Overview

The core is modeled as a cylindrical shape and is bounded by the graphite reflector on the side, top and bottom. We consider the graphite with a density of 1.74 g/cc. We want a power of 2400MWth, with a volumetric power 10.2MW/m^3. In order to minimize the neutron leakage, we take a diameter over length ratio of 0.924. We come to a core radius of 3.435 m and a core height of 6.35m.
The core is filled with Flibe salt and pebbles. The pebble bed is assumed to be ordered in columnar hexagonal lattice geometry, creating a pebble bed that has a packing factor of 60% (so that 40% of the bed is salt). This packing factor is close to the one found in the current pebble bed reactors and we assume that the packing mechanism is the same, whether it is driven by gravity or buoyancy. The bed is supposed to be homogeneous: there is no "crystallization" effect close to the wall that might rearrange locally the bed and lower the packing factor. These boundary effects are reasonably neglect at the side and top of the core in a first approach, as the pebble radius over core radius (height) is less than 1% (0.5%).
We set an area free of pebble in the salt of 1m height. The sides of the core are made of graphite (density 1.74) and are used as reflectors. Primary salt is circulating inside. The amount of volume filled with salt is:

- 10% for the upper reflector (outlet plenum)
- 5% for the bottom reflector (inlet plenum);
- 5% for the side reflector (to cool down the reflector);

The salt and graphite in the reflector are homogenized inside the reflectors, since the shape of the coolant channels is not yet known yet. The effect of such a simplification should be however of the secondary order. Besides, the amount of salt circulating in the reflectors is set arbitrarily, the values are not known at the time of the computation.

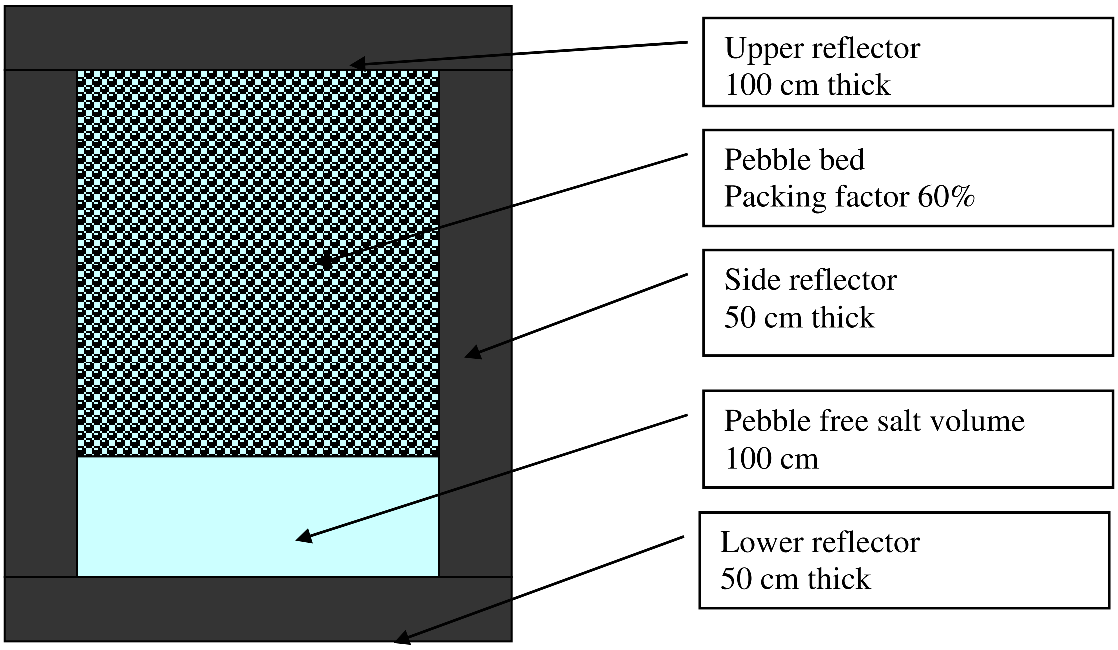

Figure A-21 Scheme of the core

III.2. Model test

Due to the difference of behavior between the two models of pebble, we tested also two models of core: one with the pebbles fully described, one with the pebbles homogenized as in §II.1.ii. The composition of the pebbles is the same as in the pebble study. However the k_{eff} cannot be compared since:

- the pebbles are not in an infinite lattice, therefore we have neutron leakage; the single pebble was placed in an universe with reflective boundary conditions;
- the lattice is of the hexagonal columnar type with a compactness of 60%; the single pebble was studied in a cubic centered lattice with a compactness set to 50%.

Again the results were very good with the TRISO external coating homogenized. The models with the TRISO kernel homogenized showed a difference of 5%. Note that with a packing factor of 60.46%, we will find around 1.2 millions pebbles in the core, each including up to 40,000 TRISO particles. Thus the homogeneous model is important for the study, but only the HMC model gives acceptable results.
The results are shown in Table A-. The test calculations were made with a 10% ^{235}U enrichment, a pebble packing factor ranging from 10% to 25% per 5% step, and a 60.46% pebble bed compactness. The salt temperature was set to 655°C, while the reflectors were at 680°C. 600 cycles were run with 4000 particles per cycle.

Table A-12 Comparison of the different core models

Packing factor	Core model	Keff and standard deviation	ΔKeff with reference	Flux at 1908 W (n/cm²-s)	ΔFlux with reference	σ_f (barn)	
						U5	U8
10%	Heterogeneous	1.32128 ±0.00049	0%	3.164E+14	0%	101.8	18E-3
	Fuel area homogenized	1. 24144 ±0.00052	-6.04%	3.172E+14	0.24%	98	19E-3
	TRISO coatings homogenized	1. 31935 ±0.00054	-0.15%	3.042E+14	-3.9%	101.4	18E-3
15%	Heterogeneous	1.28584 ±0.00055	0%	2.668E+14	0%	69	19E-3
	Fuel area homogenized	1.21643 ±0.00055	-5.4%	2.619E+14	-1.86%	76	19E-3
	TRISO coatings homogenized	1.28382 ±0.0005	-0.16%	2.681E+14	+0.48%	68.9	19E-3
20%	Heterogeneous	1.24242 ±0.00061	0%	2.390E+14	0%	50	19E-3
	Fuel area homogenized	1.17948 ±0.00061	-5.07%	2.329E+14	-2.54%	61.3	19E-3
	TRISO coatings homogenized	1.24094 ±0.00066	-0.12%	2.409E+14	0.79%	50	19E-3
25%	Heterogeneous	1.20151 ±0.00054	0%	2.212E+14	0%	38.8	19E-3
	Fuel area homogenized	1.14982 ±0.00053	-3.99%	2.169E+14	-1.91%	36.8	19E-3
	TRISO coatings homogenized	1.19915 ±0.00055	-0.15%	2.232E+14	0.93%	38.7	19E-3

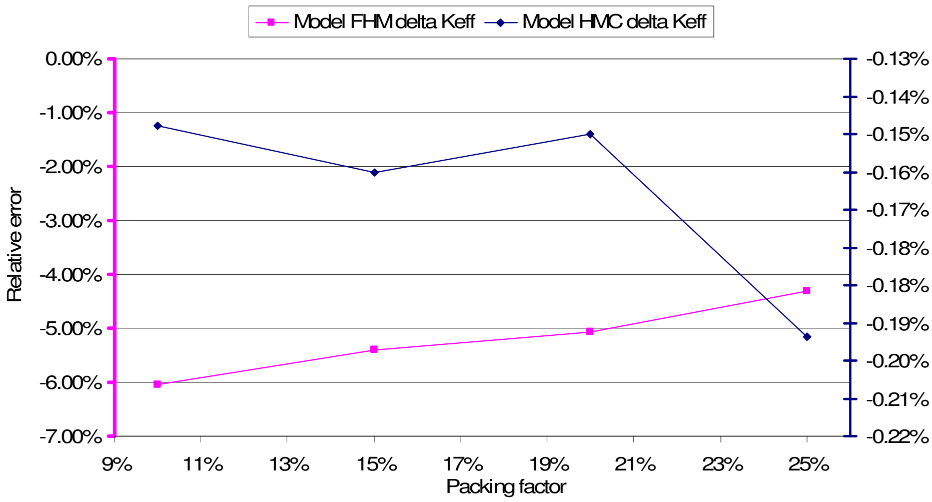

Figure A-21 Relative error on Keff with the reference model versus PF - HMC model error increases with PF but remain very reasonable

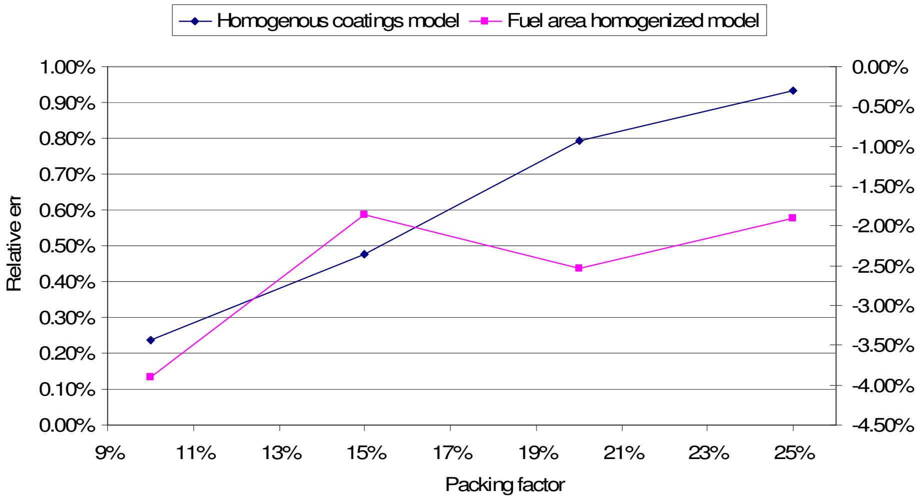

Figure A-22 Relative error on flux with the reference model versus PF - HMC model error increases almost constantly with PF

The flux in core keeps the same shape than the pebble model in the infinite lattice: we cannot notice any strong spectral effect from the permanent reflector. This is certainly due to the large size of the core and the already high heavy metal to graphite ratio. To correctly assess it, we should perform a calculation of the pebble bed place in a core with reflective boundary conditions. Thus we could have an idea of the effect of the reflectors on the reactivity.

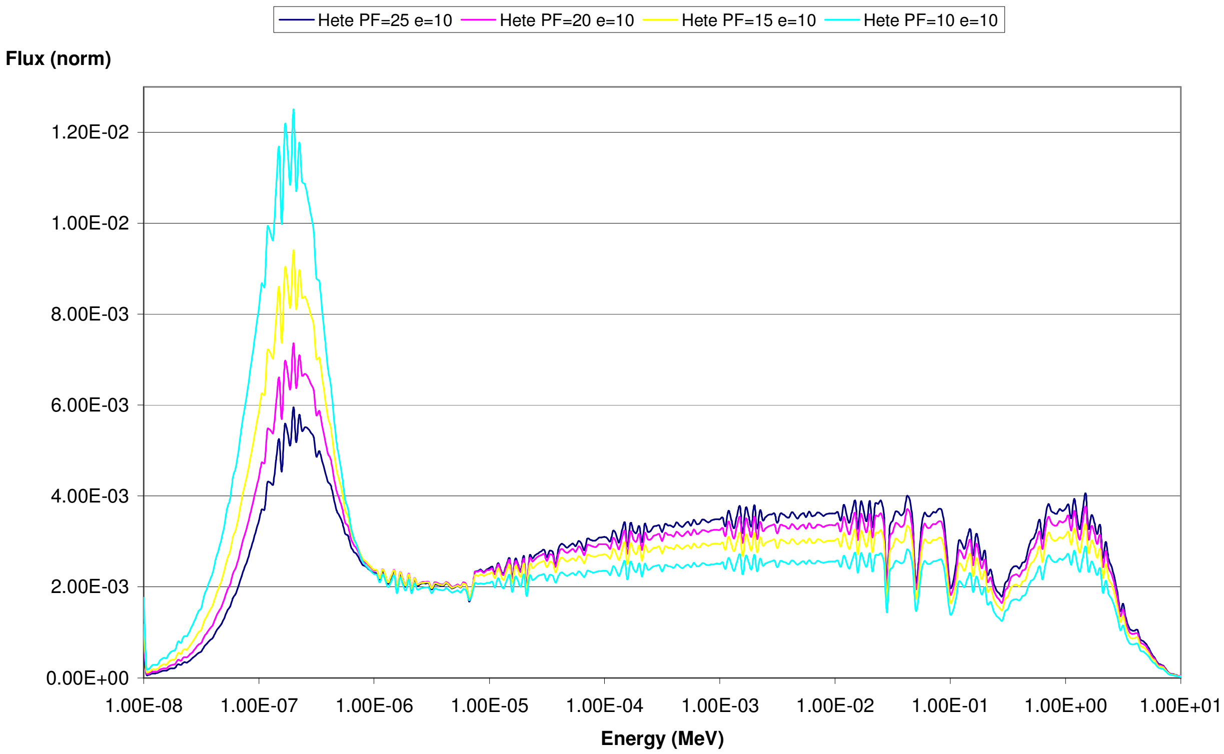

Figure A-23 Flux in core (normalized) versus PF – ^{235}U enrichment 10%, pebble bed compactness 60%

B. PB-AHTR CORE NEUTRONIC STUDY

I. PEBBLE DEPLETION ANALYSIS

The AHTR will be used on a base load mode, with continuous feeding. Therefore, after a start-up period, the core should reach an averaged, stable composition. Once known, we can input this equilibrium composition in the pebbles and obtain a fair reproduction of the neutronic behavior of the core. To do so, we are going to use the MCNP code coupled with the ORIGEN code through MOCUP. The MCNP core model used for the study is described in Appendix I; we will briefly present here the ORIGEN and MOCUP codes that were used.

I.1. ORIGEN2 code

Fission, generation and decay of isotopes can be calculated by ORIGEN2. The equation used to follow each nuclide *i* concentration is of the form [6]:

$$\frac{dX_i}{dt} = \sum_{j=1}^{N} l_{ij} \cdot \lambda_j \cdot X_j + \phi \cdot \sum_{k=1}^{N} f_{ik} \cdot \sigma_k \cdot X_k - (\lambda_i + \phi \cdot \sigma_i - r_i) \cdot X_i + F_i \quad \text{(B.I.1)}$$

Where: $i = 1,\ldots,N$ number of nuclides;
X_i is the atomic concentration of nuclide i [atoms/barn.cm];
l_{ij} is the fraction of radioactive disintegration by other nuclides, which leads to formation of species i;
λ_i is the radioactive decay constant [s^{-1}]
ϕ is the position and energy averaged neutron flux [n/cm².s];
f_{ik} is the fraction of neutron absorption by other nuclides which leads to formation of species i;
σ_k is the one group neutron absorption cross section of nuclide k [barn];
r_i is the continuous removal rate of nuclide i [s^{-1}];
F_i is the feeding rate of nuclide i [atoms/barn.cm.s].

We obtain N simultaneous equations that will be integrated over a time step, giving the concentration of each nuclide at the end of that step.
The input required for ORIGEN2 will be provided through MOCUP by MCNP and the user. In MCNP, when a criticality calculation is done, the tallies must be scaled to the steady state power level of the critical system in unit of fission neutrons per unit time. So the flux in the fuel kernels will be calculated with:

$$\phi = F4 \cdot \bar{\nu} \cdot \frac{P}{\overline{E}} \quad \text{(B.I.2)}$$

Where: Φ is the volume and energy integrated neutron flux [n/cm².s];
$F4$ is the MNCP particle flux averaged over all the TRISO kernel [part/cm²];
$\bar{\nu}$ is the average number of neutrons produced per fission in the core;

$\overline{E}$ is the average recoverable energy per fission [J/fission];
P is the total core power [J/s]

The recoverable energy per fission for each nuclide is obtained with equation I.3:

$$E_i = 1.29927 \cdot 10^{-3} \cdot \left(Z^2 \cdot A^{0.5}\right) + 33.12 \quad \text{(B.I.3)}$$

Where: Z is the atomic number of nuclide i;
A is the atomic mass of nuclide i;

The values calculated with equation B.I.3 are known to be within 1% of experimental data for nuclides between ^{232}Th and ^{242}Pu [8].

The averaged parameter $\overline{x}$ like $\overline{\nu}$ or $\overline{E}$ are obtained with equation B.I.4:

$$\overline{x} = \frac{\sum_i x_i \cdot \sigma_{f,i} \cdot N_i}{\sum_i \sigma_i \cdot N_i} \quad \text{(B.I.4)}$$

Where: i is the number of nuclides present in the fuel kernel;
x_i is the parameter x for nuclide i;
$\sigma_{f,i}$ is the one-group effective fission cross section of nuclide i [barn];
N_i is the atomic concentration of nuclide i [atoms/b.cm].

This equation allows to average parameter x according to the spectrum of the neutron flux present in the kernel.

I.2. MOCUP code

The MOCUP code (**M**CNP-**O**RIGEN2 **C**oupled **U**tility **P**rogram) is made of several external processors that operate MCNP and ORIGEN2 input and output to provide a time dependant composition of coupled nuclides. MCNP computes the spatial distribution of the flux and the one group cross section for each nuclide considered. Once treated through MOCUP processors, these data are used by ORIGEN2 to compute the isotopes generation/depletion and therefore their new concentrations. These concentrations are then updated to MCNP that recalculates the cross section and the flux, and so on. For the pebble depletion analysis, we developed a novel methodology. This process uses our core model in MOCUP and requires several assumptions:

- the pebbles are re-circulated several times during their life, thus the axial fuel composition can be assumed uniform;
- the pebbles are injected through multiple injection points with limited mixing in the pebble bed: the radial composition is assumed uniform;
- therefore we assume that the whole bed is homogeneous;
- the neutron flux is through a pebble is supposed to be constant (constant power due to the base load mode) during the entire residence time and averaged on the whole core volume.

The depletion methodology proceeds as follows:

1. a guess equilibrium composition is considered for the core and with that the overall core average flux level inside a pebble is calculated;
2. a second model is considered where all the pebble have the guessed fuel composition but a small fraction (less than 1%); the composition of this small fraction of pebbles is initially the fresh pebble composition and it is depleted assuming:
    a. the flux is constant and equal to that calculated at step 1;
    b. cross sections are calculated at each depletion step for the small fraction of pebbles depleted while the rest of the pebbles in the core have the equilibrium composition; the scope of analyzing a limited distribution of pebbles is to obtain a space average of the cross sections while keeping unperturbed the over all spectrum. The assumption here is that the probability of finding a pebble at a given burn-up level in any point in the core is the same.
    c. The total residence time is guessed;
3. Point 2 provides the time dependent fuel composition of each pebble; from this the average core composition can be calculated as the average over time of the single pebble composition; once again it is assumed the homogeneous distribution of pebble with different burn-up levels in the core.
4. the average composition of the core calculated at step 3 is assumed as the new core average composition and a new iteration can be started; the composition is the equilibrium one when it is unchanged from one iteration to the next.
5. once the equilibrium composition is reached it must be verified that k_{eff} is the one at which the core is operated (it was assumed 1.03, a small excess of reactivity being kept for power transient and the possible Xe pike); if it is smaller/greater then the residence time must be reduced/increased and the equilibrium composition recalculated.

Depletion calculation with Monte Carlo based code also shows oscillations from one time step to the other. In this case where depletion is performed with constant power a predictor/corrector methodology was applied in order to cancel these oscillations in the power level. Then for each time step:

1. first cross section are calculated for the initial composition of the step and depletion is performed;
2. the composition obtained at each fraction of the total time step is averaged over time;
3. cross sections corresponding to the time average composition are calculated;
4. depletion is performed again starting from the step initial composition but using cross sections calculated at step 3.

Note that one "loop" represents several hours of calculation, especially because the MCNP calculations are using 20,000 particles. To reduce the number of cycle, we always use the latest source file computed. Therefore, with an already treated source file, MCNP can start its calculation with a source that has already reached its fundamental distribution mode.

The equilibrium composition is searched for different pebble packing factor. The ^{235}U enrichment is set to 10%.

Figure B-1 and Figure B-2 illustrate the flow chart of MOCUP and the depletion analysis, Figure B-3 shows the position of the pebbles used for the depletion analysis.

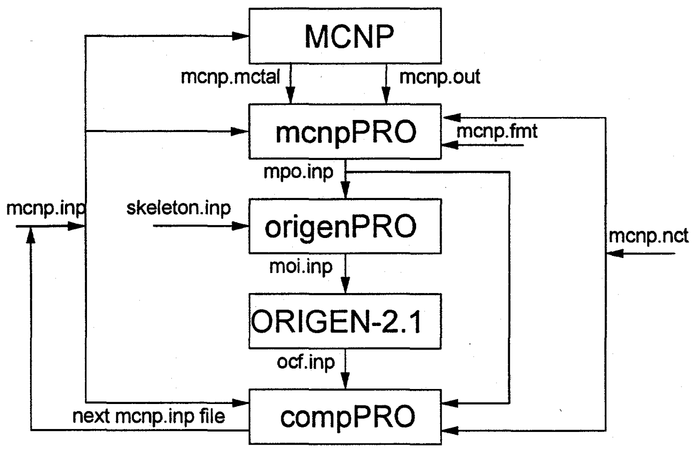

Figure B-1 MOCUP flow chart

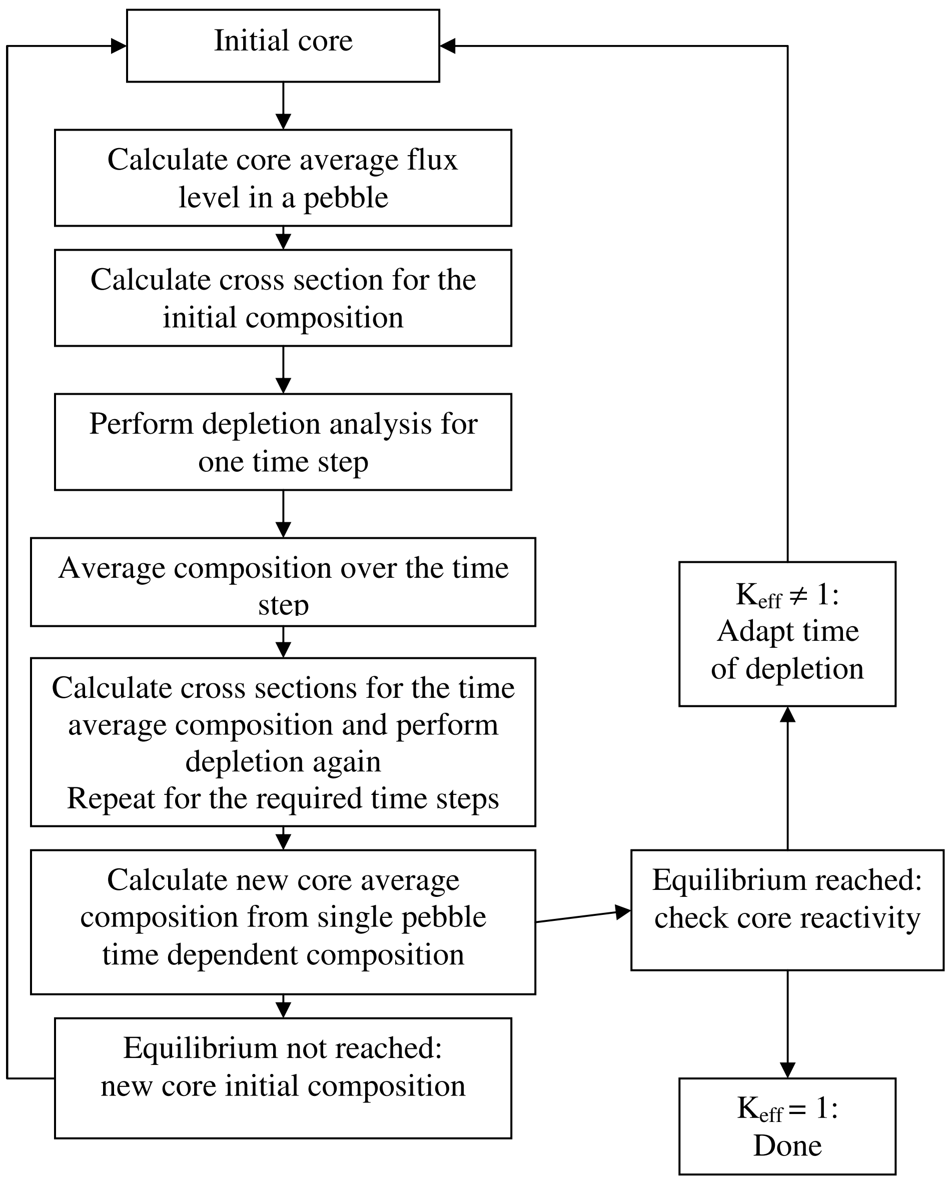

Figure B-2 Depletion analysis flow chart

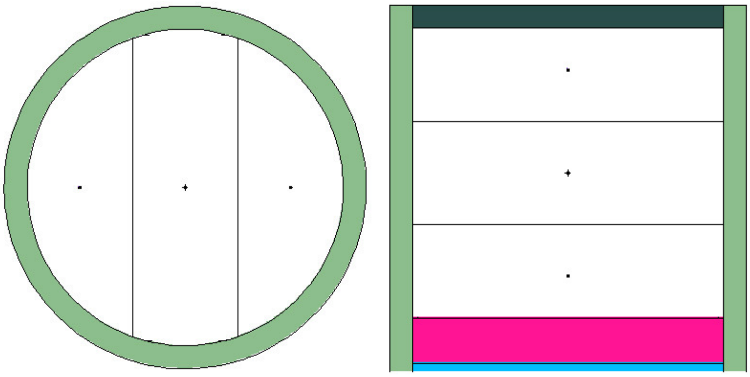

Figure B-3 Position of the pebbles (black spots) used for the depletion analysis
Top view (left) and side view (right) of the core

I.3. <u>Depletion analysis issues</u>

The main issue in setting the depletion analysis methodology is to determine the number of pebbles that should be tallied. The trade off must consider many factors:

1. the pebble distribution must guarantee a good sampling over the space;
2. the number of pebbles selected must be such that the over all neutron spectrum is not modified during depletion;
3. for a given uncertainty, the computational time increases when decreases the number of pebbles tallied.

First the depletion was run considering 9 pebbles, but after a dozen iterations a problem occurred: the equilibrium seemed to be not reachable; the resulting isotopes concentrations were oscillating around the solution as shown on Figure B-4. Therefore the flux was also oscillating, since the cross sections could not be the same.

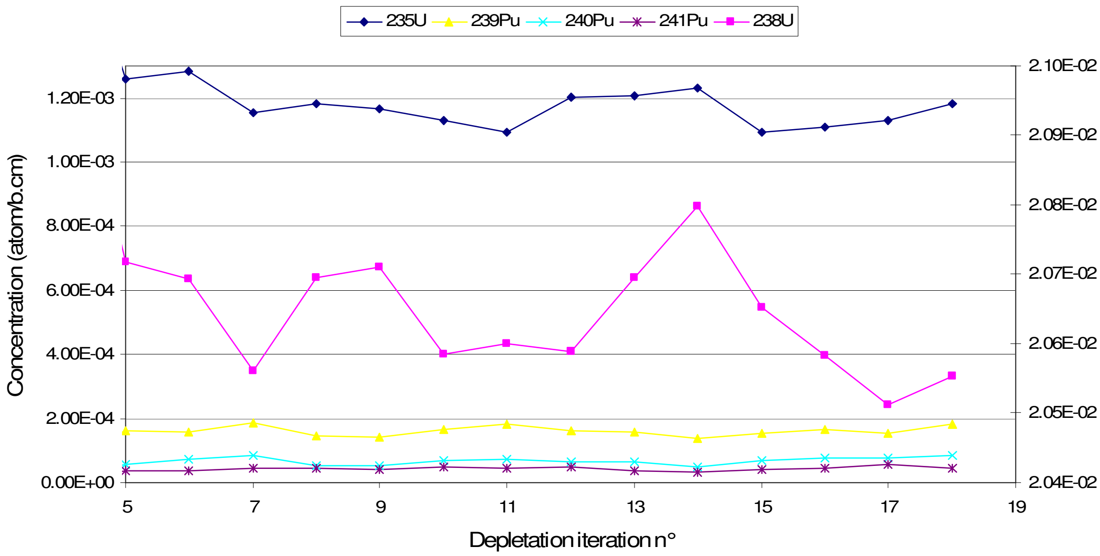

Figure B-4 Concentration of different isotope inside a TRISO kernel

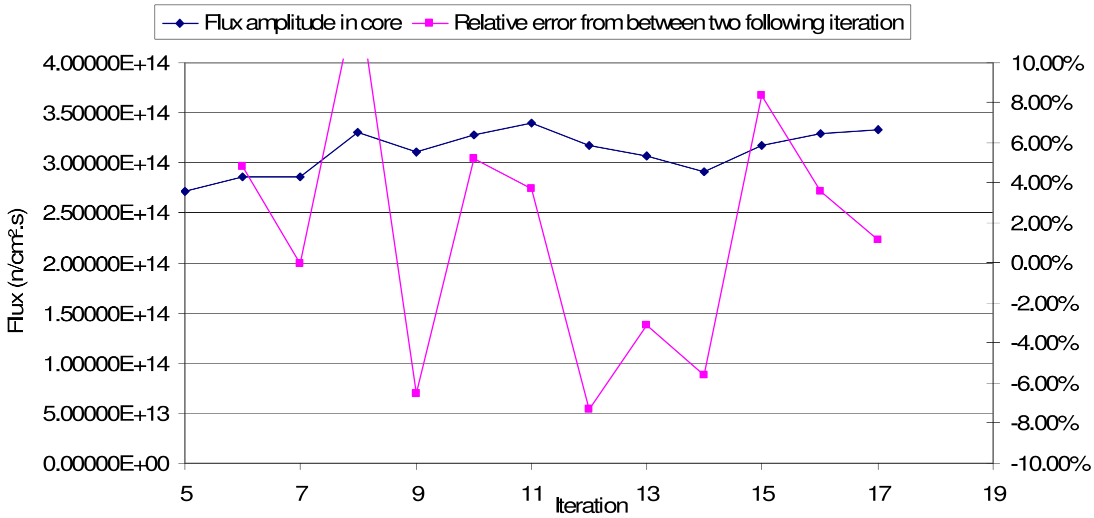

Figure B-5 Flux oscillations during depletion analysis – the pink curve is the relative difference of flux from one iteration to the next one

These oscillations were not satisfying, since the reactivity and the burn-up were significantly different between two iterations. The origin of that problem was searched for and the one group cross sections for fission and n,gamma reactions were plotted for several isotopes. The standard deviation of each cross section was associated to each point. Figure B-6 shows a sample of the results. This should have been done at the very first iterations, in order to assess the reliability of the data that were produced in the analysis. It must be underlined here that no matter how many kind of tallies are produced, each one should be checked. Indeed, some of them might appear of excellent precision; but others calculated in other cells of the model, or with different libraries, can show poor precision. If these tallies are then used elsewhere, like cross sections used as input for ORIGEN2, then the accuracy of the final result can become quickly quite irrelevant.

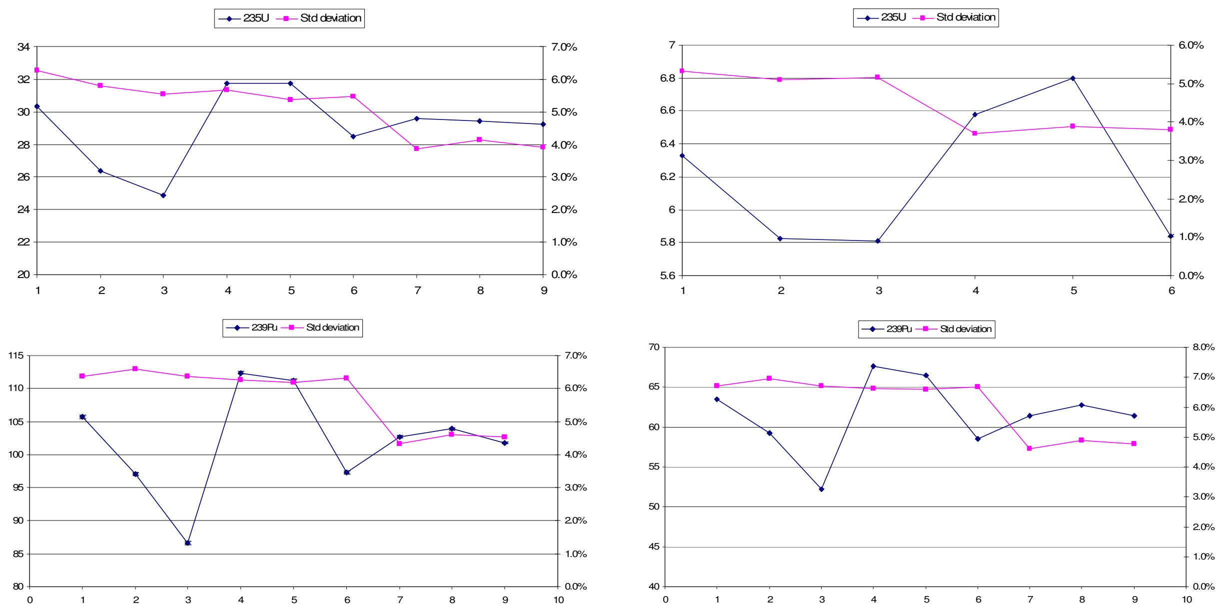

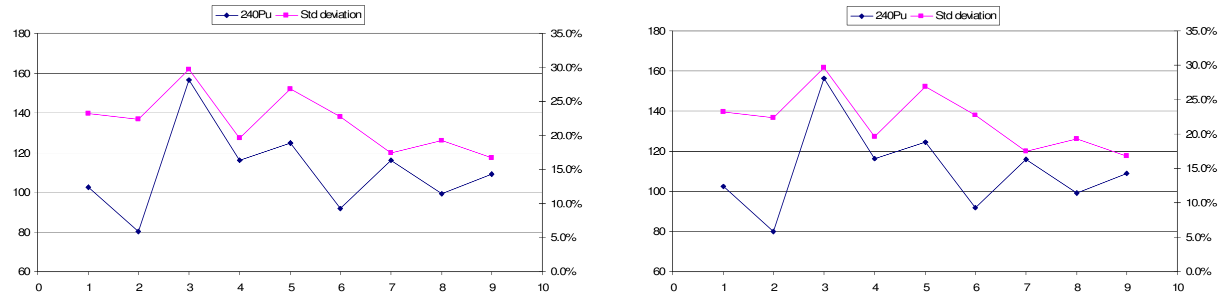

Figure B-6 Fission (left) and n,gamma (right) cross sections computed during depletion iteration – note that the last three points are computed with 50,000 particles, while the others are computed with 20,000

We can notice that for some isotopes, the results are absolutely not stable. Besides, the standard deviation associated is often so big that it makes the result very questionable. The n,gamma cross sections for a lot of isotopes are presenting very bad results. They are nonetheless as important as the fission cross section since they impact the neutronic behavior of the core and the depletion calculation.

Therefore the quality of the output has to be improved and the statistical uncertainty strongly reduced if we want to reach an equilibrium solution. One can notice here that only 20,000 particles were used. The code transports them in a complex and huge environment: millions of pebbles packed in the core, each one holding thousands of fuel kernels. However, only 9 pebbles were used to get the statistical data required to compute the cross sections. Therefore, the model was improved by updating two things:

- First the number of particles was increased from 20,000 to 50,000 particles. Even if it is more than doubling the computation time, it will also improve the statistical quality of the cross sections. This improvement is not sufficient by itself;
- Second we set the number of “fresh” pebbles used to compute the cross sections to 7700. By this change, we are able to get much more information to compute the cross sections, and by doing so we get better statistics. Besides, it is representing less than one per cent of the total amount of pebbles, therefore we can assume that the flux in the core is not strongly affected by this “heterogeneity”. This number is imposed by the lattice function that obliges the user to cut cells on one of its axis of symmetry in order to keep a continuous shape from one cell of the lattice to the other. Figure B-7 illustrates this new model.

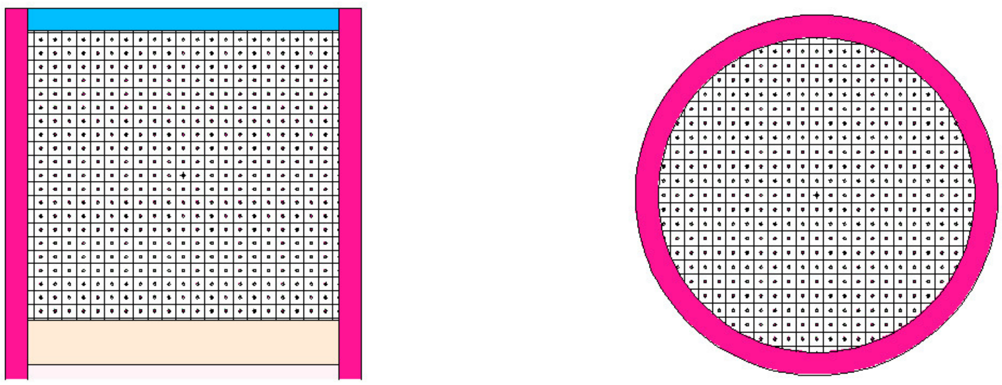

Figure B-7 Core model with the pebbles used to compute the cross sections for the depletion

After the first iteration, the statistical quality of the output was greatly improved. Besides, after only three iterations, the equilibrium was reached, the fourth iteration confirming it. Figure B-8 shows the same results than Figure B-6, this time with the improved model.

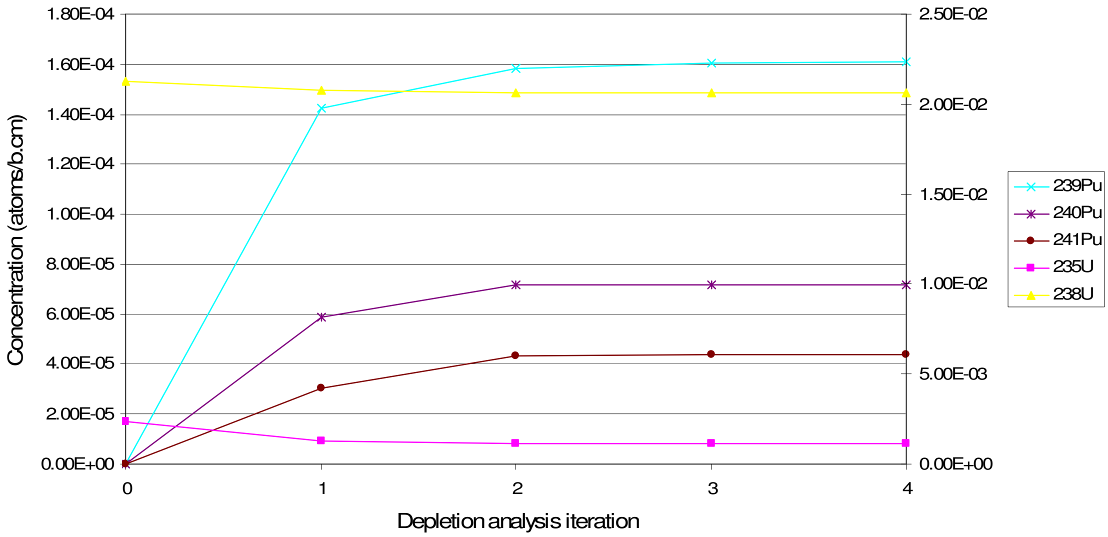

Figure B-8 A few isotopes during the equilibrium analysis

The concentrations of the different fission products and actinides are plotted for each iteration in Figure B-9. It clearly shows an excellent improvement of the quality of the output provided by MCNP.

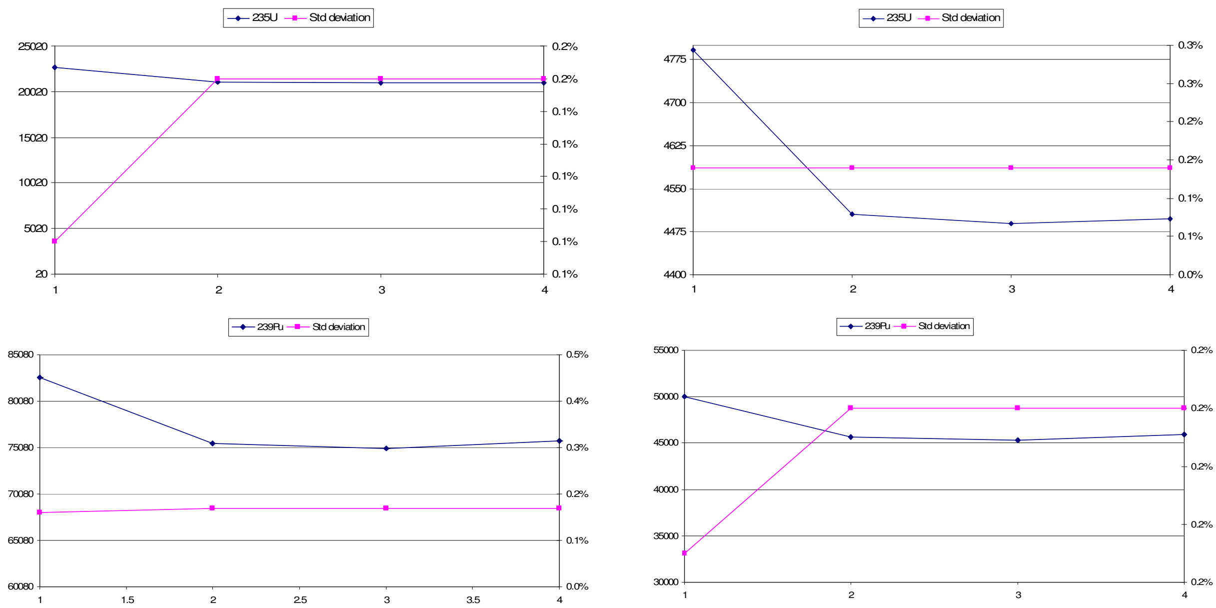

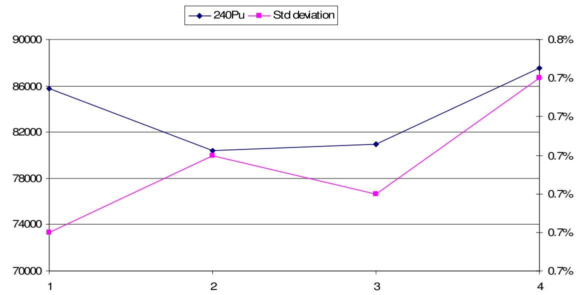

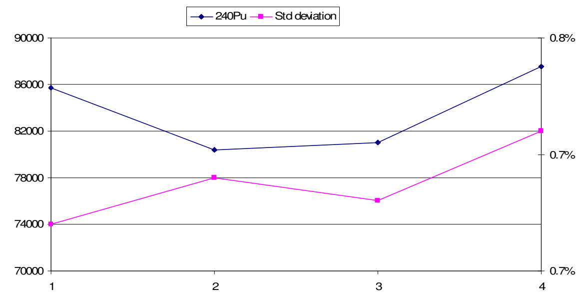

Figure B-9 Fission (left) and n,gamma (right) one group cross sections computed during depletion iteration – note that the scale of the standard deviation is in each case very small, the variation between two iterations are greatly reduced

Once the depletion analysis is done, we have an equilibrium core. It allows us to obtain several data, such as:

- average pebble burn-up and pebble burn-up over time;
- average flux in core, and the related fluence for the pebbles and the permanent graphite reflectors.

For the analysis of the fluence in the permanent reflectors, we "sliced" the side reflector and the upper reflector in several cells to have a spatial distribution of the fluence. The fluence was calculated for a spectrum of 0.01MeV and above. The maximum tolerable fluence is set to 3.10^{22} n/cm² for that spectrum. However, this value is set "arbitrarily". Indeed, the graphite high temperature in the PB-AHTR is at least half of its fusion temperature; therefore, we can expect recombination of the irradiation damages. The maximum fluence could then be increased. Figure B-10 shows the different cells used for the reflectors, Table B-1,Table B-2, Figure B-11 report the results obtained.

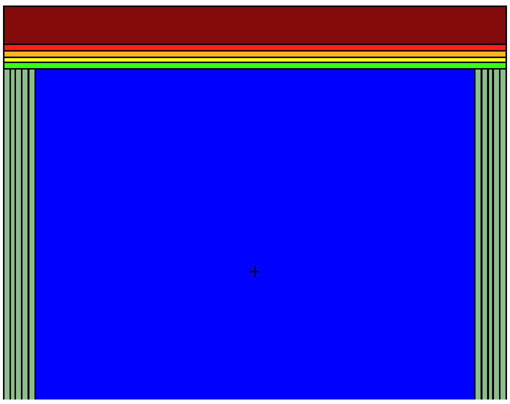

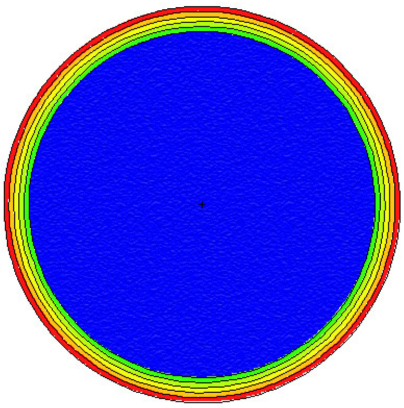

Figure B-10 Top (left) and side (right) reflector discretized in several cells (pictured here in different colors) for fluence analysis

Table B-1 Neutronic analysis results for 10% packing factor, 10% ^{235}U enrichment

Core reactivity	Average residence time (days)	Average burn-up (MWd/tHM)	Average flux at full power (2400MW) (n/cm².s)	Pebble fast fluence [0.01; 20 MeV] at discharge (n/cm²)
1.01605 ±0.00022	310	61.7	3.2E+14	8.56E+21

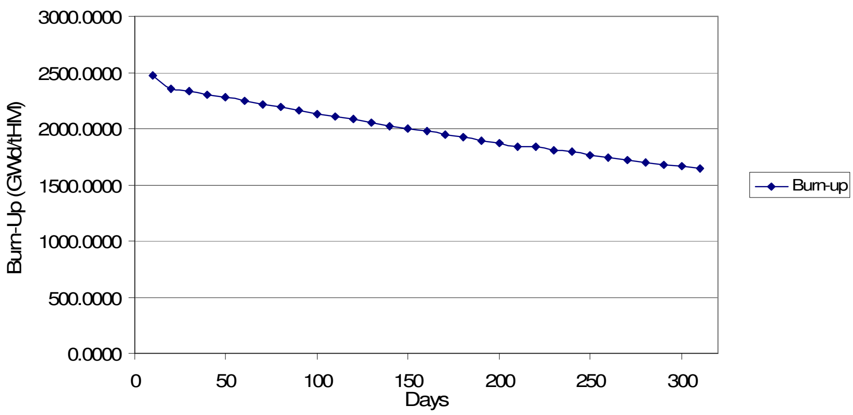

Figure B-11 Burn-up achieved for 10% packing factor, 10% ^{235}U enrichment

Table B-2 Fast fluence [0.01; 20 MeV] calculation for the permanent reflectors on a duration of one year at steady state power (maximum limit 3.10^{22} n/cm²)

Side reflector penetration	Fluence (n/cm²) normalized per cm^3	% of side reflector fluence	Top reflector penetration	Fluence (n/cm²) normalized per cm^3	% of top reflector fluence
0 to 10 cm	3.19E+19	65.4%	0 to 10 cm	2.18E+19	65.8%
10 to 20 cm	1.13E+19	23.2%	10 to 20 cm	7.54E+18	22.8%
20 to 30 cm	3.88E+18	8%	20 to 30 cm	2.55E+18	7.7%
30 to 40 cm	2.31E+18	2.7%	30 to 40 cm	8.07E+17	14.6%
40 to 50 cm	3.70E+17	0.8%	40 to 100 cm	4.15E+17	1.3%

From Table B-2, we assume an exponential alleviation of the flux in the reflectors. Therefore we extrapolated the flux to the boundary of the cells, were the fluence will be maximum. The result of that extrapolation is given in Figure B-12.

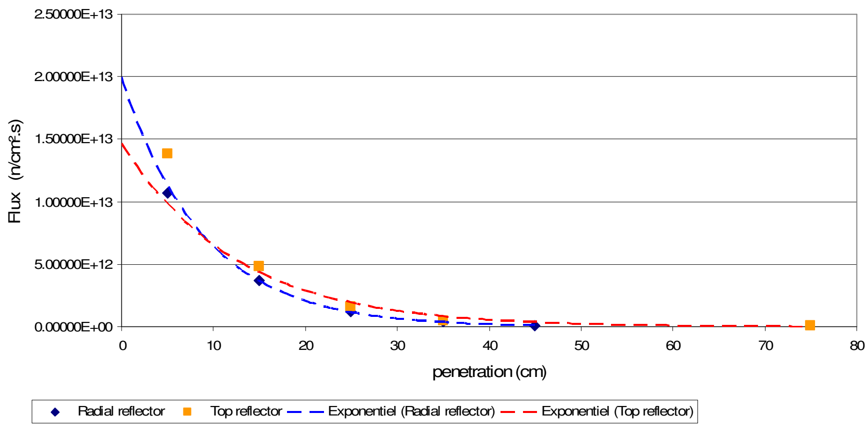

Figure B-12 Fluence per unit of volume extrapolated in side and top reflector

This gives a maximum fluence per unit of volume of 6.28E+20 n/cm² for the side reflector and 7.7E+20 n/cm² for the top reflector. The top reflector will certainly be a component very sensitive to the irradiation damage for several reasons:

- it will carry out of the bed the depleted pebbles and so will be irradiated in some parts all along its height;
- it will be a highly complicated component with a lot of channels, for the liquid salt circulation, the control rods insertion as for the pebbles extraction.

Therefore a change in the geometry due to high dose could lead to different kind of issues: impossibility to insert a control rod, coolant channel cross section reduction.

The result of the depletion also provides the pebble the composition of the pebble at each time step. Appendix II shows the distribution of the different actinides significantly present at the end of life of a pebble or of particular interest. It can be noticed that in this case, the fuel is less proliferant than a Light Water Reactor: the balance of Pu produced, with more ^{240}Pu produced, is less favorable for weapons grade Pu production. Besides, the higher amount of ^{241}Pu makes more difficult to handle due to alpha decay.
No further conclusion can be drawn from these results; they just give an idea of the different kind of parameters that can be studied.

II. CORE NEUTRONIC ANALYSIS

II.1. Power map

The spatial distribution of the power generated inside the core (also called power map) is an important parameter of the core. The power at a point is basically the image of the fission rate at that point. The more homogenous the distribution is, the better it is. The coolant will be heated equally. Therefore, the risk of coolant boiling is highly reduced, since there should be no "hot spot". Besides, there should be no difference of reactivity between two areas due to a difference of temperature.
The power map is evaluated with the power peaking factor, defined as:

$$F_{\varphi} = A_z \cdot A_r \quad \text{(B.II.1)}$$

Where: A_z is the axial power peaking factor;

A_r is the radial power peaking factor.

A_z and A_r are both calculated using a simple assumption: only the fission of ^{235}U is providing power in the core. Thus we obtain them by calculating the fission rate of ^{235}U on a cylindrical mesh that is dividing the core into several cells. We therefore have:

$$A_z = \max\left(\frac{\frac{1}{V_{\text{axial cells}}}\cdot\sum_i^{\text{axial cell}}\varphi_i\cdot\Sigma_{f,i}\cdot V_i}{\frac{1}{V_{\text{core}}}\cdot\sum_i^{core}\varphi_i\cdot\Sigma_{f,i}\cdot Vi}\right) \quad \text{(B.II.2)}$$

$$A_r = Max\left(\frac{\frac{1}{V_{\text{radial cells}}}\cdot\sum_i^{\text{radial cell}}\varphi_i\cdot\Sigma_{f,i}\cdot V_i}{\frac{1}{V_{\text{core}}}\cdot\sum_i^{core}\varphi_i\cdot\Sigma_{f,i}\cdot V_i}\right) \quad \text{(B.II.3)}$$

Where: φ_i is the particle flux in cell *i* calculated by MCNP [particle/cm²]
$\Sigma_{f,i}$ is the fission cross section of cell *i* [cm^{-1}];
V_i is the volume of cell *i* [cm^3].

Fφ was found to be equal to 2.7. This a very high value; it is due to the cylindrical shape of the core. Thus the center of the core, where leakage is minimized, is subject to a very strong thermal flux, increasing at the same time the fission rate and so the power released. However, the high radial peaking factor (1.9) is not as critical as in other reactors design. Indeed, thanks to the liquid salt and its high thermal capacity and boiling temperature, we benefit from a good temperature margin before boiling the primary coolant and creating void in the core. Besides, in a real core, the power might be flattened by using a two-zone core where fresh pebbles would be fed on the side, while "used" pebbles would be fed at the center in order to flatten the power map and achieve a high burn-up. Besides, a central reflector could be used to flatten the radial power distribution. It could also be used as a guide for control rods and would prevent the risk of impossible or partial rod insertion in the bed. This design has to be further explored since it offers several attractive options.

Figure B-13 pictures A_z, A_r. Note that A_z is shifted towards the top reflector (z=0 cm), where the thermal spectrum is stronger. There is a slight increase of A_r at the outer limit of the core (r=350 cm), also due to the side reflector.

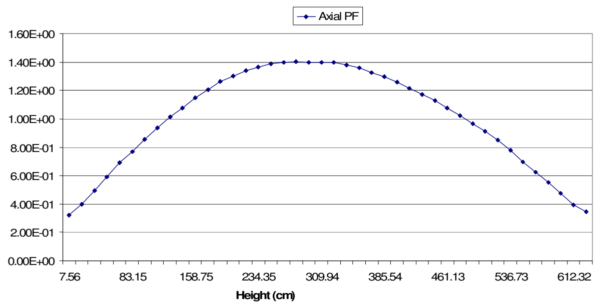

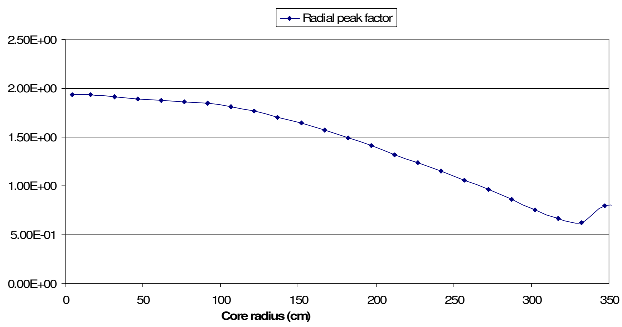

Figure B-13 A_z (left) and A_r (right)

II.2. Neutronic coefficient

The equilibrium composition allows use to calculate several neutronic coefficients to assess the core neutronic safety and response in reactivity to a transient. Each coefficient related to parameter X is calculated as in equation B.II.4:

$$C_X = \frac{1}{k} \cdot \frac{dk}{dX} \cdot 10^5 \quad \text{(B.II.4)}$$

Where: C_x is the coefficient [pcm/unit of parameter X];
k is the core reactivity (k_{eff});
X is the parameter.

Each parameter was evaluated versus a "reference" calculation. In order to maximize the precision of the evaluation, 50,000 particles were used and the same precise source file was used for each calculation. The standard deviation on k_{eff} for each output was then 0.00022. It makes the uncertainty bigger than most of the coefficient that we are looking for, but remains reasonable for a first evaluation. Note that the value found are relevant only close to the reference configuration: the linearity of these coefficients is not demonstrated.
The coefficients in Table B-3 are valid for the equilibrium core found before, at 2400MW. Five coefficients have been calculated, listed below.

- Fuel temperature coefficient: this coefficient is set by the TRISO kernel temperatures. When the different isotopes of the fuel experience a change of temperature, their cross sections are changed; resonances are broadened by the increase of temperature. For absorption resonance, the effect is safe because an increase in temperature is increasing the neutron capture, therefore decreasing the reactivity. For fission resonance, the effect will be positive, increasing the reactivity. The fuel coefficient is therefore related to the composition of the kernel and will evolve with the burn-up for a single pebble. Note that fresh pebble should have the strongest Doppler coefficient due to their composition of ^{235}U and ^{238}U only. On the other hand, a depleted pebble loaded with Pu will have a lower Doppler coefficient because these isotopes can make fission in the fast area. This coefficient does effect instantly.
- Moderator temperature coefficient: this coefficient is related to the pebble graphite temperature (fuel area matrix + external shell). It is a spectral effect: a shift of the "Maxwell-like" thermal spectrum will happen for neutrons if the moderator is increasing in temperature. Cross sections of fission and capture are reduced, but not in the same way. Depending on the fuel composition, the effect can be positive or negative. It can even go from negative at the beginning of life of the pebble to positive. It affects the reactivity of a pebble in a few minutes, the time it takes to the graphite to heat up in case of reduced heat decay by the primary salt.
- Reflector coefficient: it is the same effect than the pebble coefficient, but this time it is due to the temperature of the reflectors. Considering the mass of graphite that we have in these elements, this effect takes about an hour to impact the reactivity.
- Coolant coefficient temperature: this effect is representative of three factors. First the change of density of the LS related to the change of temperature. This is by far the main contributor of the LS coefficient. A reduction in density leads directly to a reduction in the cross sections. Second, the change of the nuclides' kernels properties that are linked together. The binding force in the molecule is affecting directly the cross sections and is dependant of the temperature. Third the broadening of the resonance of captures of each

nuclide (Doppler Effect). This effect can take a minute to an hour considering the dynamic of the transient that impact the LS temperature.

- Coolant void coefficient: this effect is representative of an accidental transient. The primary loop design can lead to a gas ingress that would be entrained in the core by the primary pumps. This effect is instantaneous. The boiling of the primary salt is not considered, since the boiling temperature is 1400°C, giving a sufficient margin.
- Pebble bed compactness coefficient: this coefficient is a very first approach of the impact of the pebble bed compactness on the reactivity. In case of decrease of bed compactness (due to a seismic event or a local change of salt density for example), the core geometry is changed. A decrease in volume is a decrease in the bed compactness and should reduce the reactivity. A rearrangement of the pebbles in the bed could also have an impact, but this cannot be studied here. The effect is very simply simulated by expanding the cell of the lattice of the pebble bed. It is formulated in pcm per % of pebble bed fraction.

Table B-3 Neutronic coefficients for equilibrium core

Coefficients	Value (pcm/°C or pcm/%)	Cells parameters updated for calculation
Fuel temperature	-2.02	TRISO kernel
Moderator	0.32	Graphite matrix + pebble external coating
Reflector	0.63	Top + side reflector
Coolant temperature	1.70	Temperature and density changed
Coolant void	16.1	LS density updated, temperature constant
Pebble bed compactness	-60	Bed compactness changed in the whole core

Several trends come out from this table. Firstly this equilibrium core can be expected to be stable: the coefficients are negative and of small amplitude, keeping the reactivity in a safe area during functional transient with “smooth” response.
The Doppler Effect is similar to the one experienced in LWR.
The liquid salt coefficient is positive. Highly enriched Flibe is not only a good coolant but also a good moderator. Therefore, depending on the moderating ratio, its voiding can conduct to an increased in reactivity due to less frequent parasitic neutronic capture in the salt; this happens in the over moderated area. In the same way, gas ingress is giving a positive response on reactivity. The void coefficient obtained is pretty big. However the method used to calculate it must be reminded in order to understand its sense. The liquid salt density is multiplied everywhere in the core by the void value. That means that the whole volume of salt is voided. In real gas ingress, we can expect a local increase of reactivity and an associated distortion of the flux; but considering the mechanism creating the void, we can hardly have a full and uniform voiding in the core as in the model. Besides, a pebble placed in a voided region will have a reaction that might help to reduce reactivity. First it might sink in the low density salt, giving it a chance to escape the pebble bed and reach a low flux region. Second the heat removal should be significantly reduced in a voided area; the temperature of the pebble would then increase, leading eventually to a negative Doppler Effect response that will limit, if not reduce, the increase of reactivity. But it must be also reminded that the voiding coefficient depends on the composition of the liquid salt and on the pebble packing factor which impact the moderator ratio.

In that model, a theoretical, highly ^{7}Li enriched salt (^{7}Li enrichment is set for the model at 99.995%) is used. Any reduction of that enrichment will have a negative effect. Since ^{6}Li is a neutron absorber, removing it will let more neutrons available for fission, therefore increasing reactivity.
The pebble graphite coefficient is almost equal to zero. It is slightly positive. This is not surprising since the average pebble already contains a significant amount of Pu. The reflector coefficient is also close to zero, extremely similar to the pebble coefficient.
Finally the bed coefficient is found to be very strong. This is not good for the core behavior since a bed experiencing variation in his compactness will have huge variation of reactivity. It is too early to conclude. Here we just found that the dynamic of a pebble bed has to be deeply understood in order to assess the risk of a bed motion.

A last kind of calculation was done: the balance of reactivity between the core in hot zero power and full power was evaluated. This shows the minimum worth required for the control rods in order to handle the restart of the reactor. It is the restart that is considered here since the core is filled with the equilibrium composition. The hot zero power status was modeled by changing all temperatures to 550°C in all cells. The materials cards were updated in consequence. Another assumption is that the pebbles are at the restart as they were under power: no decay calculations have been done, so there is no ^{149}Sm accumulation for example, which is a stable neutronic poison. The balance of reactivity was found to be 3080 pcm. Considering the fact that the core is used without much excess of reactivity and that no decay was calculated, the figure is reasonable.

II.3. Neutronic study proposition

The depletion analysis, using MOCUP, has shown after improvement the possibility to reach the equilibrium composition. In order to appreciate the behavior of the core versus different parameter and to assess its characteristics, a complete parametric study should be completed. For now, no conclusion can be draw. The parameters to be studied should be, in order of priority:

- Impact of the pebble packing factor; it can be increase or decrease and play directly on the fuel to moderator ratio;
- Impact of the ^{235}U initial enrichment; it should strongly affect the burn-up achievable;
- Impact of the pebble bed compactness (or porosity) and geometry
- Impact of the ^{7}Li enrichment on the core safety;
- Hot stand-by to full power balance of reactivity; this should give the efficiency required for the control rods for normal operations.

Also, a two zone core, if not more, should be set in the depletion analysis in order to keep the heterogeneity of the flux and assess the possibility of a dual zone core.

APPENDIX I

This appendix describes the core used for the depletion and neutronic analysis of the PB-AHTR. The figures show the model of the core used plus a model prepared that was including control rods (as a test). The rods were inserted throughout the upper reflector, Flibe salt was placed in the rod channels when they were removed.

Table Appendix.1 PB-AHTR core model characteristics

CORE CHARACTERISTICS					
Radius (m)	**Height (m)**	**Volume (m^3)**	**Height of pebble bed (m)**	**Volume of pebble bed (m^3)**	**Pebble bed porosity**
3.43	6.35	267	6.35	235	57.4%
Pebble bed lattice	**Number of pebbles in core**	**Pebble radius (cm)**	**Pebble density (g/cm^3)**	**Fuel area radius (cm)**	**Fuel area matrix density**
Columnar hexagonal	≈1 200,000	3	1.75 to 1.9	2.5	1.6
Pebble PF range	**Fuel load (g)**	**TRISO number**	**TRISO kernel**	**^{235}U enrichment**	**TRISO lattice**
10 to 25%	10 to 24	16,053 to 40,132	U_2CO_3	10%	Cubic centered

Liquid salt	**^7Li enrichment**	**In bed salt temperature**	**Free salt height (m)**	**Free salt volume (m^3)**
$LiF\text{-}BeF_2$ (66-34%)	99.995%	655°C	1	37

Side reflector thickness (m)	**Fraction of salt in side reflector**	**Top reflector thickness (m)**	**Fraction of salt in top reflector**
0.5	5%	1	10%

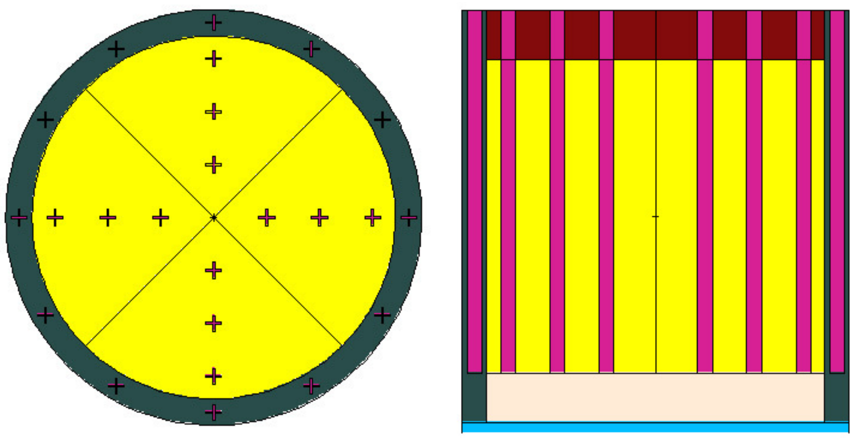

Figure Appendix.1 A PB-AHTR model with control rods (pink), pebble bed (yellow)

APPENDIX II

This appendix describes the composition of the equilibrium pebble and of the discharged pebble. Only the heavy elements are shown, fission products are not listed here. The spent fuel is simply compared to a Light Water Reactor in terms of proliferation resistance, considering the Pu isotopic vector.

Table A.1 Fuel composition for a discarded pebble, burn-up 61.7 GWd/tHM

Isotope	% of isotopic vector	% of spent fuel
234U	0.00%	0.00%
235U	3.65%	3.59%
236U	1.21%	1.19%
237U	0.00%	0.00%
238U	95.13%	93.44%
239U	0.00%	0.00%
236Np	0.00%	0.00%
237Np	62.06%	0.07%
238Np	0.38%	0.00%
239Np	37.56%	0.04%
236Pu	0.00%	0.00%
237Pu	0.00%	0.00%
238Pu	0.94%	0.02%
239Pu	47.55%	0.78%
240Pu	25.67%	0.42%
241Pu	18.19%	0.30%
242Pu	7.65%	0.13%
243Pu	0.00%	0.00%
244Pu	0.00%	0.00%
241Am	18.04%	0.00%
242Am	0.14%	0.00%
243Am	81.46%	0.01%
244Am	0.11%	0.00%
242Cm	29.10%	0.00%
243Cm	0.36%	0.00%
244Cm	67.91%	0.00%
245Cm	2.48%	0.00%
246Cm	0.14%	0.00%
247Cm	0.00%	0.00%
248Cm	0.00%	0.00%
249Bk	0.00%	0.00%
249Cf	8.83%	0.00%
250Cf	91.17%	0.00%

The Pu isotopic vector is not favorable for proliferation since it is containing a lot of ^{240}Pu and some ^{241}Pu. The ^{239}Pu is not the main form of Pu. A light water reactor, in comparison, can have 56.5% of ^{239}Pu and 26.6% of ^{240}Pu in spend fuel, a higher proportion of ^{239}Pu. Besides, the 18.2% of ^{241}Pu makes the PB-AHTR spend fuel "hot" by alpha decay, making it more difficult to reprocess than a usual light water reactor spend fuel.

Table A.2 Fuel composition for an equilibrium pebble, burn-up 61.7 GWd/tHM

Isotope	% of isotopic vector	% of spent fuel
234.04	0.00%	0.00%
235.04	5.18%	5.11%
236.05	0.93%	0.92%
237.05	0.00%	0.00%
238.05	93.88%	92.57%
0.00	0.00%	0.00%
236.05	0.00%	0.00%
237.05	49.60%	0.04%
238.05	0.30%	0.00%
239.05	50.10%	0.04%
236.05	0.00%	0.00%
237.05	0.00%	0.00%
238.05	0.56%	0.01%
239.05	54.88%	0.72%
240.05	24.59%	0.32%
241.06	15.08%	0.20%
242.06	4.88%	0.06%
243.06	0.00%	0.00%
244.06	0.00%	0.00%
241.06	21.34%	0.00%
242.06	0.16%	0.00%
243.06	78.11%	0.00%
244.06	0.11%	0.01%
242.06	32.40%	0.00%
243.06	0.36%	0.00%
244.06	64.86%	0.00%
245.07	2.25%	0.00%
246.07	0.12%	0.00%
247.07	0.00%	0.00%
248.07	0.00%	0.00%
249.07	0.00%	0.00%
249.07	8.76%	0.00%
250.08	91.24%	0.00%

BIBLIOGRAPHY – Neutronic study

[1] LUIGI MASSIMO
Physics of High-Temperature Reactors
ISBN 0-08-019616-0, 1976

[2] PAUL REUSS
Précis de Neutronique
ISBN 2-86883-637-2, 2003

[3] FORREST B. BROWN
Monte-Carlo Advances and Challenges
Topic at the Frederic Joliot / Otto Hahn Summer School, Karlsruhe, Germany, 2005

[4] X-5 MONTE-CARLO TEAM
MCNP – A General Monte-Carlo N-Particle Transport Code, Version 5
Volume I (LA-UR-03-1987), April 24, 2003
Volume II (LA-CP-03-245), April 24, 2003
Volume III (LA-CP-03-0284) April 24, 2003

[5] T. J. DONOVAN and Y. DANON
HTGR Unit Fuel Pebble k-infinity Results Using Chord Length Sampling

[6] ALLAN G. CROFF
ORIGEN2: A Versatile Computer Code for Calculating the Nuclide Compositions and Characteristics of Nuclear Materials
ANS Nuclear Technology Vol. 62, September 1983

[7] PER F. PETERSON and HAIHUA ZHAO
A Flexible Baseline Design for the Advanced High Temperature Reactor Using Metallic Internals (AHTR-MI)
Proceedings of ICAPP '06, Reno, NV USA, June 4-8, 2006, Paper 6052

[8] A. G. CROFF.
ORIGEN2 - A Revised and Updated Version of the Oak Ridge Isotope Generation and Depletion Code
ORNL-5621, Oak Ridge National Laboratory (1980)

CONCLUSION

Neutronic study

The work required first to set a model. The complexity of the neutronic in a fuel element made of TRISO particles prevented us to afford quick calculation; an approximate yet reliable method has to be used. Once a pebble model was found, another issue raised for the core model, related to the continuous feeding mode of the core. Using MOCUP, a method was set to find the equilibrium core fuel composition. The precision required for the depletion analysis and the complexity of the core model were found to be the source of problems that have been solved. We now have a tool available to complete a full parametric study of the core that will draw out the main parameters required to optimize the core design. It should also define the fields that are to be investigated more intensely, like the pebble bed dynamics, due to the reactivity sensitivity to it. Finally the model itself should be either compared to others models or improved (by adding a heterogeneous pebble bed and taking into account a spatial distribution of the flux).
The PB-AHTR shows a great potential that should be precise. However we have seen that it is a highly complex system. Therefore the methodology and the tools associated to the study have to be clearly defined in order to assess the precision of any results.

PIRT study

This project has cleared the way for the further detailed work that will be part of the AHTR licensing process. First, events sequences have been proposed for more comprehensive investigations that will require computational fluid dynamics or risk assessment codes. Then, preliminary studies of basic scenarios highlighted the relevance of some phenomena that would need experiments to improve the current knowledge in the impacted domains.
However, adapted tools will be needed to confirm the validity of the previous preliminary conclusions, such as models of the AHTR using the RELAP5-3D code (this activity has already begun at UCB).
Concerning the complementary work of setting reliable experimental database in heat transfer and fluid dynamics, facilities have recently been built and will soon be able to provide the missing information.

We both have seen the necessity of a preliminary study to have a relevant knowledge that allows improvement and advance in the design of a complex system such as the PB-AHTR. Besides, our stay in a foreign university has made us experience new ways of working and new approaches on nuclear reactor design. This cultural discovery is a unique chance to get the best of the different systems we have been working with.